

**Delivery and efficacy  
of targeted therapeutics  
and imaging agents for brain tumors**

**A DISSERTATION  
SUBMITTED TO THE FACULTY OF  
UNIVERSITY OF MINNESOTA  
BY**

**MINJEE KIM**

**IN PARTIAL FULFILLMENT OF THE REQUIREMENTS  
FOR THE DEGREE OF  
DOCTOR OF PHILOSOPHY**

**WILLIAM FREDERICK ELMQUIST**

**NOVEMBER 2018**



## ACKNOWLEDGEMENTS

This Ph.D. dissertation became possible with kind support of many individuals:

I am deeply grateful to my Ph.D. advisor, Dr. William Elmquist, for his guidance and support. Without his advice and encouragement, this dissertation would not have been possible.

My special appreciation goes to my Ph.D. dissertation committee members, Drs. Jann Sarkaria, Richard Brundage, and Ronald Siegel for their advice and comments to my thesis. I have greatly benefited from their expertise, insight, and support.

I would like to thank the members of Dr. Sarkaria's group at Mayo Clinic: Ann Mladek (Tuma), Katrina Bakken, Brett Carlson, Drs. Shiv Gupta, Danielle Burgenske, and Daniel Ma, for their help and contribution to the thesis. Special thanks to the former and current members of Dr. Elmquist's group at University of Minnesota: Janice Laramy, Surabhi Talele, Gautham Gampa, Jessica Griffith, Bryanna Wilken-Resman: Drs. Afroz Mohammad, Karen Parrish, Shuangling Zhang, and Sani Kizilbash, for their support and help.

My special thanks extend to Dr. Ronald Sawchuk for his special training in pharmacokinetics and the SAAMII software, Jim Fisher for his technical support and professional advice in the development of the LC-MS/MS assays.

I would like to thank the faculty and administrative staff in the Department of Pharmaceutics, who provided a great training and support throughout my graduate education. This dissertation is supported by the National Institutes of Health [Grants RO1 CA138437, RO1 NS077921, U54 CA210181, U01 CA227954 and P50 CA108960], the Ronald J. Sawchuk Fellowship in Pharmacokinetics. Other funding sources, including the Brain Tumor Program (BTP), PS-ON Investigators Meeting, and BBB Consortium Meeting, provided funds to travel and present my research at various conferences.

Collectively, I would like to express my gratitude to those who have directly and indirectly helped me throughout my Ph.D. training. Last but not least, I owe a very important debt to my friends and family.

## **ABSTRACT**

The treatment of both primary and secondary brain tumors is a serious unmet medical need in the field of neuro-oncology. Despite advances in developing molecularly-targeted anti-cancer therapeutics in treating peripheral tumors, there is no effective therapeutic for brain tumors that demonstrated dramatic improvement in patient survival. One of the major reasons of having lack of efficacy in central nervous system may be related to the delivery of therapeutic agents across the blood-brain barrier (BBB). The BBB expresses various transporters as well as unique junctional proteins that selectively permeate molecules into the brain from systemic circulation. Many molecularly-targeted therapeutic agents are found to be substrates of these efflux transporters at the BBB including P-glycoprotein (P-gp) and Breast cancer resistance protein (Bcrp). The current dissertation examined the multiple challenges in the treatment of brain tumors including non-specific protein binding, brain distributional kinetics, and role of efflux transporters on the distribution of various molecules such as molecularly-targeted anti-cancer drugs and tumor imaging agents.

# TABLE OF CONTENTS

<b>ACKNOWLEDGEMENTS</b> .....	i
<b>ABSTRACT</b> .....	iii
<b>LIST OF TABLES</b> .....	xi
<b>LIST OF FIGURES</b> .....	xiv
<b>LIST OF ABBREVIATIONS</b> .....	xx
<b>CHAPTER 1 Introduction</b> .....	22
1.1 Glioblastoma.....	23
1.2 Statement of problem .....	23
1.3 Research objectives .....	24
1.4 Research approaches .....	25
1.5 Specific aims .....	26
<b>CHAPTER 2 Barriers to Effective Drug Treatment for Brain Metastases: A Multifactorial Problem in the Delivery of Precision Medicine</b> .....	30
2.1 INTRODUCTION .....	31
2.1.1 Clinical presentation of Brain Metastases.....	33
2.1.2 Current therapy for brain metastases .....	36
2.1.3 Barriers to effective treatment .....	38
2.1.4 Mechanisms that limit drug delivery across the BBB .....	45

2.1.5	Impact of transporters on the treatment of brain metastases	48
2.2	Common types of brain metastases	49
2.2.1	Lung cancer	49
2.2.2	Melanoma	53
2.2.3	Breast cancer	58
2.2.4	Renal cell carcinoma	62
2.3	Conclusion	63
<b>CHAPTER 3 The potential for profound efficacy of the MDM2 inhibitor SAR405838 in glioblastoma is limited by poor distribution across the blood-brain barrier</b>		
	<b>blood-brain barrier</b>	<b>81</b>
3.1	INTRODUCTION	82
3.2	MATERIALS AND METHODS	83
3.2.1	Cell culture, drugs, and apoptosis	83
3.2.2	TP53 gene Sequencing	83
3.2.3	MDM2 Amplification and RNA expression	84
3.2.4	Real-Time PCR assays	84
3.2.5	Efficacy studies <i>in vivo</i>	84
3.2.6	Brain-to-plasma ratio for SAR405838	85
3.2.7	VEGFA over-expression	86

3.2.8	VEGFA ELISA .....	86
3.2.9	TUNEL Staining.....	86
3.2.10	Texas Red Imaging to Evaluate BBB Integrity.....	87
3.2.11	Preclinical MRI acquisition and analysis.....	87
3.2.12	MALDI MSI .....	88
3.2.13	Immunohistochemistry and quantitative analysis .....	88
3.2.14	Statistical analyses.....	89
3.3	RESULTS .....	90
3.3.1	<i>In vitro</i> efficacy of SAR405838 .....	90
3.3.2	<i>In vivo</i> efficacy of SAR405838.....	91
3.3.3	Imaging of BBB integrity .....	92
3.3.4	Effect of SAR405838 brain penetration on efficacy .....	94
3.4	DISCUSSION .....	96
	Figure 3.1 Characteristics of selected PDX GBM lines.....	100
<b>CHAPTER 4 Brain distributional kinetics of a novel MDM2 inhibitor</b>		
	<b>SAR405838: Implications for use in brain tumor therapy .....</b>	<b>108</b>
4.1	INTRODUCTION .....	109
4.2	MATERIALS AND METHODS .....	112
4.2.1	Chemicals and reagents.....	112
4.2.2	Animals.....	113



4.2.3	In vitro cell accumulation .....	113
4.2.4	Free fraction in mouse plasma and brain homogenate ....	114
4.2.5	Systemic and distributional pharmacokinetics Concentration-time profile after a single oral or intravenous administration of SAR405838 .....	115
4.2.6	Pharmacological inhibition of efflux transporters .....	116
4.2.7	LC-MS/MS bioanalysis .....	117
4.2.8	Pharmacokinetic data analysis .....	117
4.2.9	Statistical analysis .....	121
4.3	RESULTS .....	121
4.3.2	In vitro cell accumulation assay .....	121
4.3.3	SAR405838 disposition following IV dose .....	123
4.3.4	SAR405838 absorption and disposition following single oral dose .....	124
4.3.5	Plasma and brain unbound fraction .....	125
4.3.6	Pharmacological inhibition of efflux on the brain distribution of SAR405838 .....	126
4.3.7	Brain distributional kinetics of SAR405838 using BBB modeling.....	127
4.4	DISCUSSION .....	132

AUTHORSHIP CONTRIBUTIONS .....	139
<b>CHAPTER 5 Brain distribution of a panel of EGFR inhibitors using cassette-dosing in wild-type and <i>Abcb1/Abcg2</i> deficient mice.....</b>	<b>158</b>
5.1 INTRODUCTION .....	159
5.2 MATERIALS AND METHODS .....	162
5.2.1 Chemicals and reagents.....	162
5.2.2 Animals.....	163
5.2.3 Discrete Dosing Pharmacokinetic Study .....	163
5.2.4 Cassette Dosing Pharmacokinetic Study .....	164
5.2.5 Protein Binding Study in Plasma and Brain Homogenate	164
5.2.6 Analytical LC-MS/MS analysis to determine drug concentrations .....	166
5.2.7 Pharmacokinetic Calculations .....	167
5.2.8 Statistical Testing .....	168
5.3 RESULTS .....	168
5.3.1 Comparison of brain-to-plasma ratios from cassette and discrete dosing studies.....	168
5.3.2 Pharmacokinetic parameters and metrics of 8 EGFR inhibitors following cassette dosing in wild-type and <i>Mdr1a/b</i> <sup>-/-</sup> <i>Bcrp1</i> <sup>-/-</sup> FVB mice. ....	169

5.3.3	Brain penetration of EGFR inhibitors within an individual animal.....	170
5.3.4	Determination of Kp and Kpuu for brain .....	171
5.3.5	Correlation between physicochemical properties and the brain partition coefficients.....	173
5.4	Discussion .....	174
	AUTHORSHIP CONTRIBUTIONS .....	181
	<b>CHAPTER 6 Factors Influencing Luciferase-Based Bioluminescent Imaging in Preclinical Models of Brain Tumor.</b> .....	196
6.1	Introduction.....	197
6.2	Materials and Methods.....	201
6.2.1	Chemicals and reagents.....	201
6.2.2	<i>Lentiviral vector and cell transduction</i> .....	202
6.2.3	<i>In vivo</i> tumor xenograft mouse model .....	202
6.2.4	<i>In vivo</i> bioluminescent tumor imaging .....	203
6.2.5	Pharmacokinetic studies in vivo .....	203
6.2.7	Transporter inhibitor studies .....	204
6.2.8	In vitro trans-well permeability assay.....	204
6.2.9	Free fraction in mouse plasma and brain homogenate ....	206
6.2.10	Analytical LC-MS/MS bioanalysis.....	208

6.2.11	Pharmacokinetic data analysis .....	209
6.2.12	Statistical analysis .....	210
6.3	Results.....	210
6.3.1	Comparisons of bioluminescence imaging with D-luciferin and CycLuc1 in flank and intracranial tumors.....	210
6.3.2	Apparent permeability and efflux ratios of D-luciferin and CycLuc1 .....	212
6.3.3	Comparisons of pharmacokinetic parameters and metrics of D-luciferin and CycLuc1 in wild-type and <i>Bcrp1</i> <sup>-/-</sup> FVB mice following a single intravenous dose.....	213
6.3.4	Pharmacokinetic parameters and metrics of D-luciferin and CycLuc1 following a single intraperitoneal dose.....	215
6.3.5	Tissue distribution of D-luciferin and CycLuc1 following a single intraperitoneal dose.....	216
6.3.6	Influence of co-administration of transporter inhibitors on the systemic clearance and the brain partition coefficients of D- luciferin and CycLuc1 .....	217
6.4	Discussion .....	218
	<b>RECAPITULATION</b> .....	240
	<b>Bibliography</b> .....	246

## LIST OF TABLES

<b>Table 2.1</b> Incidence rate of brain metastases .....	75
<b>Table 2.2</b> Brain and transporter related features of molecularly targeted therapy for lung cancer. (ND, not determined; NA, not available.) .....	76
<b>Table 2.3</b> Brain and transporter related features of molecularly targeted therapy for melanoma. (ND, not determined; NA, not available.) .....	78
<b>Table 4.1</b> Pharmacokinetic/metric parameters and brain partition coefficients determined by non-compartmental analysis following a single intravenous dose of SAR405838 (5 mg/kg) in wild-type and <i>Mdr1a/b</i> <sup>-/-</sup> <i>Bcrp1</i> <sup>-/-</sup> FVB mice.....	151
<b>Table 4.2</b> Pharmacokinetic/metric parameters determined by non-compartmental analysis following a single oral dose of SAR405838 (25 mg/kg) in wild-type, <i>Mdr1a/b</i> <sup>-/-</sup> , <i>Bcrp1</i> <sup>-/-</sup> , and <i>Mdr1a/b</i> <sup>-/-</sup> <i>Bcrp1</i> <sup>-/-</sup> FVB mice.....	152
<b>Table 4.3</b> Free fraction (fu) values, partition coefficient of brain ( $K_{p, \text{brain}}$ and $K_{p_{uu, \text{brain}}}$ ), and distribution advantage. Data presented as mean + standard deviation (S.D.).....	153
<b>Table 4.4</b> Pharmacokinetic parameters estimated from one-compartment model that describes the total concentration-time profile from each genotype following a single intravenous bolus (5 mg/kg) administration.....	154

<b>Table 4.5</b> Pharmacokinetic parameters estimated from one-compartment model that describes the total concentration-time profile from each genotype following a single oral (25 mg/kg) administration.....	155
<b>Table 4.6</b> The changes in tissue transfer rate and clearance values with the total concentration model. ....	156
<b>Table 4.7</b> The $K_p$ and $K_{p,uu}$ values predicted from the compartmental BBB model describing the brain and plasma concentration-time profile following either intravenous or oral administration of SAR405838. ....	157
<b>Table 5.1</b> Physicochemical properties of EGFR inhibitors used in the study ...	189
<b>Table 5.2</b> PK parameters in wild-type mice.....	190
<b>Table 5.3</b> PK parameters in TKO mice.....	191
<b>Table 5.4</b> The partition coefficients and free partition coefficients of brain for EGFR inhibitors. ....	192
<b>Table 5.5</b> The calculated scores based on physicochemical properties and the partition coefficients of brain.....	193
<b>Table 5.6</b> Summary of clinical information on the studied 8 EGFR inhibitors...	194
<b>Table 6.1</b> Summary of physicochemical properties and structures of D-luciferin and CycLuc1.....	234

**Table 6.2** Summary of pharmacokinetic parameters and metrics following a single intravenous dose of either D-luciferin or CycLuc1 in wild-type and Bcrp knockout FVB mice..... 235

**Table 6.3** Summary of pharmacokinetic parameters and metrics following a single intraperitoneal dose of either D-luciferin or CycLuc1 in wild-type FVB mice.  
..... 236

# LIST OF FIGURES

**Figure 2.1** The expression and localization of transporters in the brain endothelial cell in the context of the overall composition and structure of the neurovascular unit (NVU). Important drug transporters include: SLC, solute carrier; MRP, multidrug resistance protein; LAT, L-type amino acid transporter; OATP, organic anion transporting polypeptide; MCT, monocarboxylate transporter; ENT, equilibrative nucleoside transporter..... 67

**Figure 2.2** Primary tumors that preferentially metastasize to the brain and the occurrence of brain metastases from each of these primary tumors. Examples of key tumor driving oncogenes are represented for each tumor type..... 68

**Figure 2.3** Depiction of the most common treatment options for brain metastases. .... 69

**Figure 2.4** Mechanisms of resistance development against drug in brain metastases due to inherent tumor heterogeneity or acquired resistance. .... 70

**Figure 2.5** Multiple equilibria in different compartments in the brain, blood, and cerebrospinal fluid. .... 71

**Figure 2.6** Signaling pathways and oncogenic targets of molecularly-targeted therapeutics for melanoma. .... 72

**Figure 2.7** Heterogeneity of blood-brain barrier disruption and drug concentration in the experimental model (mice) of breast cancer brain metastases (from reference (Taskar et al., 2012)). <sup>14</sup>C-lapatinib was measured in normal brain and



different brain metastases by quantitative autoradiography at 2 hours (a-c) and 12 hours (d-f) following the oral administration of 100 mg/kg <sup>14</sup>C-lapatinib. Signal from metastatic cells labelled with EGFP (a,d), Texas Red 3kD dextran (b,e), and <sup>14</sup>C-lapatinib (c,f) indicate the location of tumor cells, the integrity of the BBB, and the concentration of drug, respectively. The concentrations of lapatinib, as well as disruption of BBB, were highly variable within and between the metastatic breast cancer lesions in the brain. .... 73

**Figure 3.1** Characteristics of selected PDX GBM lines..... 100

**Figure 3.2** *In vivo* efficacy of SAR405838 in heterotopic and orthotopic models of GBM108 ..... 102

**Figure 3.3** BBB permeability and distribution of SAR405838 in GBM108-Vector and GBM108-VEGFA ..... 103

**Figure 3.4** Improved pharmacodynamic response and orthotopic survival in GBM108-VEGFA ..... 106

**Figure 4.1** Chemical structure of SAR405838..... 140

**Figure 4.2** A compartmental blood-brain barrier (BBB) model in order to describe a concentration-time profile in the central (plasma) and brain compartment after a single intravenous bolus or oral dose. (A) A one compartment model to describe the total concentration-time profile in plasma and to get systemic parameters for a forcing function. (B) A compartmental BBB model to describe the total concentration-time profile in brain. Cp, concentration in plasma; Vc, the volume

of distribution in central compartment;  $K_e$ , the elimination rate constant from the central compartment;  $K_a$ , absorption rate constant;  $K_{in}$ , tissue transfer rate constant into the brain;  $K_{out}$ , tissue transfer rate constant out of the brain;  $C_b$ , concentration in brain;  $V_b$ , the apparent volume of distribution in brain. .... 141

**Figure 4.3** Cell accumulation of SAR405838. (A) The intracellular accumulation of vinblastine (positive control) and SAR405838 in MDCKII vector control and MDR1-transfected cells in the presence and absence of P-gp inhibitor, LY335979 (1  $\mu$ M). (B) The intracellular accumulation of prazosin (positive control) and SAR405838 in MDCKII vector control and Bcrp-transfected cells in the presence and absence of Bcrp inhibitor, Ko-143 (0.2  $\mu$ M). Data presented as mean + standard deviation (S.D.) where  $N = 3$  for all groups. \* $P < 0.05$ , \*\* $P < 0.01$ , \*\*\* $P < 0.005$ , \*\*\*\* $P < 0.001$ ..... 143

**Figure 4.4** Pharmacokinetic profile of SAR405838 following a single intravenous administration. (A) Concentration-over-time in plasma, (B) concentration-over-time in brain, and (C) brain-to-plasma ratio over time in wild-type and *Mdr1a/b*<sup>-/-</sup> *Bcrp1*<sup>-/-</sup> mice. Data presented as mean + standard deviation (S.D.) where  $N = 3$  to 5 for each time point. .... 145

**Figure 4.5** Pharmacokinetic profile of SAR405838 following a single oral administration. (A) Concentration-over-time in plasma, (B) concentration-over-time in brain, and (C) brain-to-plasma ratio over time in wild-type, *Mdr1a/b*<sup>-/-</sup>, *Bcrp1*<sup>-/-</sup>, and *Mdr1a/b*<sup>-/-</sup>*Bcrp1*<sup>-/-</sup> FVB mice. Data presented as mean + standard deviation (S.D.) where  $N = 3$  to 5 for each time point. .... 146

**Figure 4.6** The effect of a pharmacological inhibitor of efflux transport, elacridar, on the plasma and brain concentration of SAR405838. (A) Concentrations in plasma and brain at 2-hr and 6-hr post dose with co-administration of either vehicle control or inhibitor, either LY335979 or elacridar. (B) Brain-to-plasma ratio at 2-hr and 6-hr post dose. Data presented as mean + standard deviation (S.D.) where  $N = 3$  to 5 for each group.  $**P < 0.01$ ,  $***P < 0.005$  ..... 147

**Figure 4.7** Observed (squares and circles) and model predicted (solid line and dotted line) plasma (red) and brain (blank) concentrations of SAR405838 following a single intravenous bolus administration (5 mg/kg) in wild-type (A) and *Mdr1a/b<sup>-/-</sup>Bcrp1<sup>-/-</sup>* (B) FVB mice. The observed data are presented as the mean standard deviation (S.D.) where  $N = 3$  to 4 for each time point. .... 148

**Figure 4.8** Observed (squares and circles) and model predicted (solid line and dotted line) plasma (red) and brain (blank) concentrations of SAR405838 following a single oral administration (25 mg/kg) in wild-type (A), *Bcrp1<sup>-/-</sup>* (B), *Mdr1a/b<sup>-/-</sup>* (C), and *Mdr1a/b<sup>-/-</sup>Bcrp1<sup>-/-</sup>* (D) FVB mice. The observed data are presented as the mean standard deviation (S.D.) where  $N = 3$  to 4 for each time point..... 149

**Figure 5.1** Structures of EGFR inhibitors used in the current study. .... 182

**Figure 5.2** Comparison of brain-to=plasma ratios between cassette and discrete dosing in wild-type and triple-knockout (*Mdr1a/b<sup>-/-</sup>Bcrp1<sup>-/-</sup>*) FVB mice. (A) Brain-to-plasma ratios at 1-hour post dose in wild-type FVB mice. (B) Brain-to-plasma ratios at 8-hour post dose in wild-type FVB mice. (C) Brain-to-plasma ratios at 1-

hour post dose in triple-knockout ( $Mdr1a/b^{-/-}Bcrp^{-/-}$ ) FVB mice. (D) Brain-to-plasma ratios at 8-hour post dose in  $Mdr1a/b^{-/-}Bcrp^{-/-}$  FVB mice. .... 183

**Figure 5.3** Rank order of the brain distribution of EGFR inhibitors in a single animal. Rank order was based on the brain-to-plasma ratio at a single time point after dosing in individual animal..... 185

**Figure 5.4** Correlation between  $K_p$  and  $\text{clogD}/\sqrt{\text{MW}}$  or MPO (multiparameter optimization) scores. (A) Correlation between  $K_p$  or  $K_{puu}$  in wild-type FVB mice and  $\text{clogD}/\sqrt{\text{MW}}$  (R square for  $K_p = 0.04895$ , R square for  $K_{puu} = 0.224$ ). (B) Correlation between  $K_p$  or  $K_{puu}$  in triple-knockout ( $Mdr1a/b^{-/-}Bcrp^{-/-}$ ) FVB mice and  $\text{clogD}/\sqrt{\text{MW}}$  (R square for  $K_p = 0.137$ , R square for  $K_{puu} = 0.0386$ ). (C) Correlation between  $K_p$  or  $K_{puu}$  in wild-type FVB mice and MPO score (R square for  $K_p = 0.108$ , R square for  $K_{puu} = 0.0000911$ ). (D) Correlation between  $K_p$  or  $K_{puu}$  in triple-knockout ( $Mdr1a/b^{-/-}Bcrp^{-/-}$ ) FVB mice and MPO score (R square for  $K_p = 0.557$ , R square for  $K_{puu} = 0.433$ )..... 187

**Figure 6.1** Schematic depiction of various factors influencing the bioluminescent light signal intensity. .... 228

**Figure 6.2** Bioluminescent imaging of GBM6 in flank tumor (A) and intracranial tumor (B) models. Cross-over imaging was performed for both substrate D-luciferin and CycLuc1 on different days..... 229

**Figure 6.3** *In vitro* trans-well experiment results to examine the apparent permeability of D-luciferin and CycLuc1 with MDCKII-wildtype vector control and

Bcrp overexpressing cell lines in the absence of Ko-143 (A) or in the presence of Ko-143 (B). ..... 230

**Figure 6.4** Concentration-time profiles of D-luciferin and CycLuc1 following a single intravenous dose in wild-type and Bcrp knockout FVB mice. .... 231

**Figure 6.5** Concentration-time profiles of D-luciferin and CycLuc1 following a single intraperitoneal dose in wild-type FVB mice. .... 233

**Figure 6.6** Tissue partition coefficients of D-luciferin and CycLuc1 following an intraperitoneal injection (A). Each partition coefficient values were determined by the ratios of AUC in tissue from time zero to infinity to AUC in plasma from time zero to infinity (B). ..... **Error! Bookmark not defined.**

**Figure 6.7** Plasma and brain concentrations and brain-to-plasma ratios of D-luciferin and CycLuc1 at two time points with a co-administration of Ko-143. .... **Error! Bookmark not defined.**

**Figure 6.8** Plasma and brain concentrations and brain-to-plasma ratios of D-luciferin and CycLuc1 at two time points with a co-administration of probenecid. .... **Error! Bookmark not defined.**

## LIST OF ABBREVIATIONS

ADME, absorption, distribution, metabolism, and elimination

AR, accumulation index

AUC, area under the curve

BAT, brain-around-tumor

BBB, blood-brain barrier

BCRP, breast cancer resistance protein

*Bcrp1*, gene encoding the murine breast cancer resistance protein

BEV, bevacizumab

bECF, brain extracellular fluid

CL/F, apparent clearance

C<sub>max</sub>, maximum drug concentration

CNS, central nervous system

DA, distribution advantage

DDI, drug-drug interactions

ERL, erlotinib

FDA, Food and drug administration

f<sub>u</sub>, free (unbound) fraction

FVB, Friend leukemia virus strain

GBM, glioblastoma

GFP, green fluorescent protein

IC, intracranial

IC<sub>50</sub>, the half maximal inhibitory concentration

K<sub>p</sub>, total brain or tissue-to-plasma ratio

K<sub>p,uu</sub>, unbound (free) brain-to-plasma ratio

LC-MS/MS, liquid chromatography–tandem mass spectrometry

*Mdr1*, gene encoding the murine p-glycoprotein

MTT, mean transit time

NCA, non-compartmental analysis

PDGFR-alpha, platelet-derived growth factor receptor-alpha

PDX, patient-derived xenograft

P-gp, p-glycoprotein

RED, rapid equilibrium dialysis

RET, REarranged during Transfection

TKI, tyrosine kinase inhibitor

T<sub>max</sub>, time at the maximum drug concentration

TMZ, temozolomide

V<sub>d</sub>/F, apparent volume of distribution

**CHAPTER 1**  
**INTRODUCTION**



## **1.1 GLIOBLASTOMA**

Glioblastoma (GBM) is the most common malignant brain tumor, which is reported to be 47.1% of malignant primary brain and CNS tumors and 16% of all primary brain and central nervous system neoplasm (Thakkar et al., 2014). GBM is an aggressive tumor with poor survival outcome (Minniti et al., 2009). A median survival of GBM is approximately 14 to 15 months from the diagnosis ((Thakkar et al., 2014). According to the classification system by World Health Organization (WHO), glioma is classified in to grade I to IV based on the level of malignancy determined by histopathological criteria (Furnari et al., 2007; Jovcevska et al., 2013). Grade I gliomas are low proliferative and can be curable, whereas, grade II to grade IV are highly malignant and invasive. GBM is the most aggressive and invasive tumor, which is categorized as grade IV glioma (Jovcevska et al., 2013).

## **1.2 STATEMENT OF PROBLEM**

Brain delivery of exogenous compounds, including the therapeutics and imaging agents, is challenging due to a highly selective barrier, the blood-brain barrier (BBB). Many of molecularly-targeted agents have failed to demonstrate significant efficacy in patients with the tumors located in the brain including primary and metastatic tumors, despite of their success in other non-brain tumors. There are two critical challenges related to the problem; First, the limited drug delivery to the brain across the blood-brain barrier (BBB), and Second, the

drug potency challenges to have a proper target for the treatment. Therefore, there are critical needs of discovering a potent target for the brain tumors and developing brain penetrant therapeutics. MDM2 inhibitors are recently developed as a potent molecularly-targeted anticancer agents in various solid tumors, but their efficacy in brain tumors has not been investigated. In addition, the understanding of brain distribution and pharmacokinetics of the common imaging agents in preclinical cancer research, luciferase substrates can elucidate the importance of selecting right imaging agents considering their tissue distribution.

### **1.3 RESEARCH OBJECTIVES**

The main research objective of this dissertation is to investigate the drug delivery challenges of exogenous compounds including the treatments of brain tumors and the imaging agents in preclinical research. Novel molecularly-targeted therapeutics, including MDM2 inhibitors and epidermal growth factor receptor (EGFR) inhibitors, are examined focusing on their potential efficacy in GBM and their brain penetrability. The bioluminescent imaging agents for brain tumors in preclinical research, firefly luciferase substrates, are studied to understand their biodistribution for better interpretation of the results and to select a proper imaging agent for cancer research. The long-term goal of this dissertation is to improve the outcome of patients with brain tumors through understanding drug delivery-potency challenges and our understanding on the brain imaging agents to choose a right drug for the treatment of brain tumors. The research objectives of this dissertation are the following:

**CHAPTER 2.** Review on the challenges of treating the metastatic brain tumors focusing on the role of efflux transporters

**CHAPTER 3.** Determine the relationship between the preclinical efficacy and the drug delivery in a patient-derived xenograft (PDX) animal model

**CHAPTER 4.** Quantitative understanding of the role of efflux transporters on brain penetration of a novel MDM2 inhibitor, SAR405838

**CHAPTER 5.** Examine the brain distributional kinetics of EGFR inhibitors by using cassette dosing approach and the prediction of brain distribution based on the physicochemical properties of compounds

**CHAPTER 6.** Investigate the factors influencing luciferase-based bioluminescent imaging in preclinical models of brain tumors focusing on the brain distribution and pharmacokinetic properties of luciferase substrates

## **1.4 RESEARCH APPROACHES**

### ***Central hypothesis***

The central hypothesis of this dissertation is that both delivery and potency of compounds need to be integrated to properly understand the efficacy of molecularly-targeted therapeutics (including MDM2 inhibitors and EGFR inhibitors) and tumor imaging agents (including luciferase substrates).

## 1.5 SPECIFIC AIMS

### *Specific Aim 1. (CHAPTER 3 and 4)*

*Determine the relationship between the preclinical efficacy and the drug delivery in a patient-derived xenograft (PDX) animal model*

- **Rationale:** Delivery is a major barrier in the treatment of brain tumors. The assumption is that preclinical efficacy of a novel MDM2 inhibitor, SAR405838, is dependent on the drug distribution at the target in the brain.
- **Working hypothesis:** The working hypothesis for this specific aim is that drug distribution would contribute to efficacy in the PDX model of glioblastoma. The limited delivery of SAR405838 to the brain would be due to efflux transporters at the blood-brain barrier.
- **Approach:** This hypothesis will be tested through creation of tumors that have different blood-brain barrier integrity by using the expression of vascular endothelial growth factor A (VEGFA). In vivo efficacy and a spatial distribution of SAR405838 will be examined in the intracranial GBM108 tumors with or without the expression of VEGFA. To understand the role of efflux transporters on the limited brain delivery of SAR405838, pharmacokinetics and a brain distributional kinetics will be examined in wild-type and transporter knockout FVB mice.

## ***Specific Aim 2. (CHAPTER 5)***

***Examine the brain distributional kinetics of EGFR inhibitors by using cassette dosing approach and the prediction of brain distribution based on the physicochemical properties of compounds***

- **Rationale:** Cassette dosing approach could be useful tool to determine the brain distributional kinetics of multiple compounds with reduced number of animal usage. The prediction of brain distribution of compounds based on the physicochemical properties would have a limitation to rely on.
- **Working hypothesis:** The working hypothesis of this specific aim is that a cassette dosing approach can be useful tool to understand the brain distributional kinetics of a panel of therapeutics that share the same target and prioritize a compound in a drug discovery.
- **Approach:** This hypothesis will be tested by obtaining the brain partition coefficients of a panel of EGFR inhibitors selected to have a range of brain distribution by using a cassette dosing strategy. To validate the cassette dosing method, the results from a cassette dosing will be compared with the results from a discrete dosing. Correlation between the prediction based on the physicochemical properties of compounds and the brain partition coefficients will be examined.

### ***Specific Aim 3. (CHAPTER 6)***

***Investigate the factors influencing luciferase-based bioluminescent imaging in preclinical models of brain tumors focusing on the brain distribution and pharmacokinetic properties of luciferase substrates***

- **Rationale:** The concentration of luciferase substrate and the expression level of luciferase are not only factors that determine the signal intensity of bioluminescent light that is commonly used to measure the tumor size in orthotopic model. It has been reported that a synthetic luciferase substrate, CycLuc1, produces much stronger and more stable light signal from intracranial tumor when compared to D-luciferin, possibly due to its better brain penetration.
- **Working hypothesis:** The working hypothesis of this specific aim is that CycLuc1 would have favorable pharmacokinetic and distributional properties over D-luciferin, especially when it is used for bioluminescent imaging of intracranial tumor.
- **Approach:** This hypothesis will be tested by quantification of luciferase substrate, D-luciferin and CycLuc1, by LC-MS. Pharmacokinetic properties and brain distributional kinetics will be examined following different routes of administration of both compounds. To investigate the role of efflux transporter, Bcrp, on the distribution and pharmacokinetics of D-luciferin and CycLuc1, in vitro experiments using MDCKII-Bcrp overexpressing

cells and in vivo animal experiments using Bcrp knockout FVB mice will be performed.

**CHAPTER 2**

**BARRIERS TO EFFECTIVE DRUG TREATMENT FOR  
BRAIN METASTASES: A MULTIFACTORIAL PROBLEM  
IN THE DELIVERY OF PRECISION MEDICINE**

The content of this chapter has been published in:

Kim, M., Kizilbash, S. H., Laramy, J. K., Gampa, G., Parrish, K. E., Sarkaria, J. N., & Elmquist, W. F. (2018). Barriers to Effective Drug Treatment for Brain Metastases: A Multifactorial Problem in the Delivery of Precision Medicine. *Pharmaceutical research*, 35(9), 177.



## 2.1 INTRODUCTION

Metastatic spread of tumor cells from primary lesions to distant organs is a significant concern in the management of patients suffering from cancer (Gaspar et al., 1997; Sperduto et al., 2012). The formation of tumor metastases in vital organs, particularly the brain, can lead to a dismal quality of life and ultimately organ failure and death. Brain metastases are difficult to detect and diagnose, especially early in the disease course (Bruzzone et al., 2012). Even after diagnosis, metastases to the brain are difficult to effectively treat due to various challenges associated with their treatment. While limited numbers of discrete metastases can be effectively treated with focal radiation and/or surgery, these patients have a high risk of subsequent metastases developing from pre-existing sub-clinical 'micrometastases' that are not detectable at the time of focal therapy. Patients with advanced brain disease (>10 metastases), or otherwise at high risk for micrometastases, are typically treated with whole brain irradiation, which is associated with an adverse effect on neuro-cognitive function (Brown et al., 2003; Brown et al., 2013). Thus, in light of the significant morbidity associated with radiation, efficacious small molecules that could effectively replace whole brain radiation therapy could have a significant positive impact on patients requiring treatment for brain metastases.

There has been important progress in the development of anti-cancer therapeutics, including molecularly-targeted agents (Druker, 2002; Becker et al., 2006; Reungwetwattana et al., 2012; Bayraktar and Gluck, 2013) and novel immunotherapies (Scott et al., 2012). Both of these modalities are clearly

efficacious towards tumors at the primary site (Druker, 2002; Becker et al., 2006; Reungwetwattana et al., 2012; Scott et al., 2012; Bayraktar and Gluck, 2013), however, it remains a struggle to deliver these therapeutics across an intact BBB to many metastatic sites in the brain (Lockman et al., 2010). The capillaries and associated cellular components in the brain have a highly specialized structure called the blood-brain-barrier (BBB) or neurovascular unit (NVU) that keeps many solutes, especially water-soluble solutes and large molecules, out of the brain (Abbott, 2013). The tight junctions between the endothelial cells in the BBB in conjunction with multiple transport systems, both influx and efflux, regulate selective movement of molecules across the BBB into the brain (Abbott, 2013) (Figure 1 - a depiction of the NVU with transporters). Such mechanisms prevent the entry of various drugs, intended for the treatment of CNS diseases, into the brain. Specifically, many small molecule anti-cancer targeted agents have been shown to be substrates of active efflux transporters at the BBB, resulting in limited brain penetration of such therapies (Table 2, 3, 4) (Agarwal et al., 2011b; Gampa et al., 2017).

Another key issue for the treatment of brain metastases is the difference in gene expression profiles in tumor cells growing in the brain microenvironment compared to the peripheral (non-brain) lesions (Brastianos et al., 2015). The local tumor microenvironment between the brain and peripheral tumor lesions can potentially dictate that such differences will ultimately result in the development of resistance to therapies. This is a critical issue that needs to be tackled along with brain drug delivery to effectively treat tumors in the brain. While we recognize the

importance of microenvironment in the context of resistance, the main focus of this review is to discuss aspects related to the delivery of targeted agents to the brain. We will give a brief overview on the clinical presentation of brain metastases as well as the currently available therapeutic options, before describing the difficulties encountered in the treatment of brain metastases.

### **2.1.1 Clinical presentation of Brain Metastases**

Brain metastases, a devastating complication of systemic malignancies, substantially raise the burden of cancer morbidity and mortality (Gaspar et al., 1997; Sperduto et al., 2012). They typically stem from hematogenous spread that seed at the distal fields of the main cerebral arteries (the “anatomic watershed areas”) (Delattre et al., 1988). Consequently, approximately 80% of brain metastases are localized in the cerebral hemispheres (Delattre et al., 1988). Initial symptoms at diagnosis range from headaches and seizures to focal neurological deficits and cognitive dysfunction; however asymptomatic brain metastases are also commonly found during initial staging exams. The symptoms presented by the patients often depend on the location of lesions and extent of metastatic disease burden (Delattre et al., 1988).

Population studies underestimate the true incidence rates of brain metastases because of issues related to diagnosis and underreporting. The incidence of brain metastases, observed in 8.5-9.6% of cancer patients, is estimated to be approximately ten times higher compared to primary brain tumors that represent 1.4% of cancer patients (Schouten et al., 2002; Barnholtz-Sloan et

al., 2004; Siegel et al., 2016; Kromer et al., 2017). Lung cancer, breast cancer, melanoma and renal cancer have a high propensity to metastasize to the brain and account for up to 80% of brain metastases (Table 1 and Figure 2) (Nayak et al., 2012). Patients with lung cancer are likely to develop brain metastases during the course of the disease (reported to be 16.3-19.9% of lung cancer patients (Schouten et al., 2002; Barnholtz-Sloan et al., 2004)). This incidence can be as much as 50-60% in other reports, depending on individual study methods and analyses (Newman and Hansen, 1974; Chamberlain et al., 2017). Small cell lung cancer (SCLC) is known to be associated with a slightly higher occurrence of brain metastases than non-small cell lung cancer (NSCLC) at 5 years after the diagnosis, but the incidence rates of brain metastases for both subtypes tend increase over the course of the disease (Newman and Hansen, 1974; Chamberlain et al., 2017). The treatment of SCLC patients with prophylactic intracranial radiation following completion of definitive radio/chemotherapy markedly reduces subsequent risk of brain metastases and is associated with a survival benefit (Auperin et al., 1999; Zhang et al., 2014). Incidence of brain metastases from breast cancer is second to that of lung, even though only 5% breast cancer patients develop brain metastases, due to the high overall incidence of breast cancer (Lin et al., 2004; Weil et al., 2005; Nayak et al., 2012). Autopsy series reveal brain metastases in about 30% of patients dying from breast cancer (Rostami et al., 2016). Melanoma accounts for 6-11% of all metastatic brain lesions, and is the third most frequent cause of brain metastases. The observations from clinical and autopsy series estimate that the incidence of brain metastases in patients with

malignant melanoma ranges from 10-70% (Sampson et al., 1998; McWilliams et al., 2003; Zakrzewski et al., 2011; Gorantla et al., 2013). While lung cancer is reported to have the largest proportion of incidence of brain metastases, melanoma has the highest predilection to metastasize to the brain (Nayak et al., 2012).

Several reasons contribute to the rising incidence of brain metastases. Advanced imaging techniques have improved the detection of occult brain metastases. Preliminary MRI screening for brain lesions is now routinely practiced for patients with newly diagnosis advanced lung cancer even in the absence of neurologic symptoms (Auperin et al., 1999; Nayak et al., 2012). Another possible reason for the increased incidence of brain metastases is that the median survival of patients with peripheral (non-brain) tumors is prolonged due to the novel therapeutic agents, that introduces the time it can take for the peripheral tumor cells to spread to the brain and thus, cause metastatic lesions in the brain (Davis et al., 2012; Kromer et al., 2017). The restricted entry of systemically active therapeutic agents into the brain is another contributor to the increasing incidence of brain metastases because it creates pharmacological sanctuary that nurtures and protects the tumor cells to thrive in the brain (Agarwal et al., 2011b; Gampa et al., 2017). Thus, to advance drug therapies that are effective for controlling brain metastases, the field needs to consider that the BBB is likely intact in some regions of the tumor, especially in early non-contrast enhancing micrometastases, and can compromise the penetration of anti-cancer agents across the BBB (Essig et al., 2006; Osswald et al., 2016; Gampa et al., 2017).

### 2.1.2 Current therapy for brain metastases

The initial treatment of brain metastases involves the management of acute symptoms. For instance, the use of glucocorticoids to alleviate symptoms secondary to brain edema, and anti-epileptic drugs (AEDs) to treat seizures. However, co-administration of AEDs and anti-cancer agents can increase the potential risk of clinically significant drug-drug interactions because of the shared metabolic pathways or transport systems across these different drug regimen (Yap et al., 2008; Cheung et al., 2010). Some AEDs can modulate the hepatic cytochrome (P450) enzymes and/or expression of drug transporters, causing an increase or decrease of systemic drug exposures, each of which can have consequences on resulting efficacy or toxicity. Such a complex interplay between transporters and drug-metabolizing enzymes (Pang et al., 2009; Shi and Li, 2014), along with reduced drug delivery to the brain, can result in undesirable therapeutic outcomes in patients with brain metastases.

Surgical resection is the preferred treatment option, in part because as yet only surgery can drastically reduce the tumor mass in the brain (Patchell et al., 1990) and improve survival outcome (Figure 3. Treatment options). In cases where surgical resection is not feasible due to multiple low-volume metastases or inaccessible or eloquent locations where tumor cannot be surgically resected, alternative approaches such as stereotactic radiosurgery (SRS) and whole brain radiation therapy (WBRT) are considered. SRS delivers high-dose of radiation to a specific region, whereas WBRT delivers to the whole brain. While surgery or SRS can provide a high rate of durable local tumor control, both of these strategies

do not reduce the significant risk of developing additional brain metastases. In contrast, WBRT can reduce the risk of intracranial relapses, but the lower dose applied to the entire brain associated with this treatment failed to improve overall survival and is associated with a risk of neuro-cognitive impairment (Kocher et al., 2011).

Systemic therapies have historically been considered ineffective against brain metastases. However, examples of limited success with systemic therapies have been reported in patients with brain metastases. For example, in patients with chemotherapy-naive brain metastases, the combination of cisplatin and etoposide achieved an overall objective response rate of 38% in breast cancer and 30% in NSCLC (Franciosi et al., 1999). Also, treatment with a combination of carboplatin and pemetrexed exhibited an overall response rate of 40% in patients with chemotherapy-naive brain metastases from NSCLC (Bailon et al., 2012). In addition to these studies, several clinical trials also report limited efficacy from using a combination therapeutic approach in order to treat various types of cancer. The phase II LANDSCAPE trial, a combination therapy with lapatinib and capecitabine resulted in an objective partial response rate of 66% in patients with brain metastases from HER2-positive breast cancer (Bachelot et al., 2013). The phase II BREAK-MB study showed that in patients with V600E BRAF mutant melanoma metastatic to the brain, dabrafenib had an overall objective response rate of 39% in treatment naive patients, and 31% in patients that were previously treated (Long et al., 2012). An open-label pilot study with vemurafenib reported an objective response rate of 42% in patients with non-resectable, symptomatic

brain metastases from BRAFV600 mutation-positive melanoma that were previously treated (Dummer et al., 2014). However, there were no overall survival benefit with these therapeutics, even though there have been partial responses. Lapatinib, dabrafenib and vemurafenib, are all substrates for both P-glycoprotein (P-gp) and breast cancer resistance protein (BCRP), and the observed limited therapeutic responses might be in part due to transporter-mediated efflux and consequential restricted drug delivery to the brain metastases (table 2, 3, and 4). Transporter-mediated efflux and the consequential poor brain penetration across an intact BBB can severely limit the effectiveness of targeted therapies used in the treatment of brain tumors (Agarwal et al., 2011b; Gampa et al., 2017). Also, a heterogeneous brain-tumor barrier permeability can lead to non-uniform drug distribution in various sites of brain metastases adding another level of complexity in the treatment of brain metastases (Fidler et al., 2002; Kienast et al., 2010; Lockman et al., 2010).

### **2.1.3 Barriers to effective treatment**

Limitations in diagnostic imaging for early brain metastases are an obstacle for early detection and diagnosis of the disease. Magnetic resonance imaging (MRI), the most commonly used imaging method, utilizes a hydrophilic contrast dye, gadolinium diethylene-triamine-pentaacetate (Gd-DTPA). However, Gd-DTPA was reported to fail to visualize early-stage brain metastases that have little angiogenesis and BBB disruption, which will be problematic for early diagnosis of brain metastases (On et al., 2013), due to its poor distribution to the brain across an intact BBB. Moreover, a recent study has shown that



repeated exposure to gadolinium-based contrast agents can lead to an increase in gadolinium deposition in the endothelium and neuropil even in the absence of intracranial abnormalities, that can significantly interfere with the MR signal (McDonald et al., 2015; McDonald et al., 2017). Therefore, it is difficult to rely on Gd-DTPA contrast enhancement to identify brain metastases, especially small-volume lesions, or “micro-metastases” (Preusser et al., 2012).

The exclusion of brain tumor patients from clinical trials is yet another barrier to develop effective treatments for brain metastases. Since metastatic brain lesions may be difficult to control, associated with significant morbidity, and are associated with a dire prognosis, clinical trials often specifically exclude patients with known brain metastases. In a meta-analysis of 413 NSCLC clinical trials, only 31% of the industry-sponsored and 16% of university/investigator-sponsored trials allowed inclusion of patients with diagnosed brain metastases (McCoach et al., 2016). For cancer other than NSCLC, the majority of oncology clinical trials have excluded patients with brain metastases. Even those trials that enrolled this patient population, the outcome criteria have not always been clinically relevant. The recent review article by the Neuro-Oncology Brain Metastases (RANO-BM) working group reported in *Lancet Oncology* that many clinical trials for brain metastases utilized inconsistent endpoint criteria across trials that can limit interpretation across these studies (Lin et al., 2015). As a result, patients with brain metastases are often left with limited novel treatment options and are unable to participate in clinical trials testing potentially useful therapeutic treatments. The question that arises is: why are drugs that prove to

be effective against peripheral metastases not as effective against brain metastases?

An important problem with regard to the pharmacological treatment of brain metastases is that many chemotherapeutic agents do not efficiently cross the blood-brain barrier (BBB) and blood-tumor barrier (BTB), and are unable to mount a pharmacodynamic impact on their target of interest (Fidler et al., 2002; Pafundi et al., 2013). The structure of BTB is basically the BBB where the tumor exists, and can have “normal” BBB structure and function, especially in case of brain metastases that grow from small lesion at multiple locations, although the integrity of the barrier, i.e., the BTB, can be variable depending on the size and characteristics of tumor (Fidler et al., 2002; Lockman et al., 2010; Taskar et al., 2012). The desired pharmacodynamic impact (efficacy) cannot be achieved without appropriate pharmacokinetic considerations (exposure). Inaccessibility of potentially effective anti-cancer agents to the parenchymal brain metastases can create a pharmacologic sanctuary where drugs that are otherwise effective against peripheral metastases fail to control brain metastases. Both the BBB and BTB in brain metastases have a unique anatomical barrier comprised of endothelial cells that establish robust tight junction between cells and express a variety of efflux transporters, which are absent in the peripheral microvasculature. P-glycoprotein (P-gp) and Breast cancer resistant protein (BCRP), the two most highly expressed efflux transporters at the BBB, can efflux a wide range of drug molecules and restrict drug delivery to the brain. Numerous studies have shown that many compounds tested in clinical trials are substrates

of P-gp and/or BCRP that have often failed to show clinical efficacy against brain metastases. As this discussion indicates, a thorough knowledge of the BBB and BTB in brain metastases, and how selected agents interact with these barriers, is critical in understanding the success or failure of pharmacological treatments that employ one or more of these targeted therapies.

Heterogeneous BBB and/or BTB integrity is a drug-delivery related challenge in terms of optimizing efficacy of targeted agents for the treatment of brain metastases. Several studies report variable intra-tumoral BBB permeability that results in non-uniform drug distribution and compromised drug efficacy (Pafundi et al., 2013). The study by Lockman et al. evaluated the pharmacodynamic effect resulting from heterogeneous intratumoral drug distribution of doxorubicin or paclitaxel in an experimental brain metastases of breast cancer (Lockman et al., 2010; Taskar et al., 2012). Each of these drugs reached a cytotoxic concentration (i.e., cleaved caspase-3 staining) in the “leaky” BTB regions, but significantly sub-therapeutic concentrations in the areas of intact BTB. In these models, there was no hindrance of drug delivery to the peripheral (non-brain) metastases with drug concentration more than 10-fold higher than the brain metastases. The overall outcome of non-uniform intratumoral distribution in the brain metastases was that each of these drugs failed to reduce tumor burden in *in vivo* animal studies (Lockman et al., 2010).

Besides an anatomical barrier that is unique to the brain, treatment of brain metastases may be further complicated by the oncogenic footprints that are

distinctive to the brain. Brain metastases, sharing a common ancestor with the primary tumor of origin, have evolved independently after reaching the brain, in part, because the brain has a different microenvironment than the rest of the body (Brastianos et al., 2015). A whole exome sequencing study by Brastianos et al. identified mutational signatures that are distinctive to brain metastases compared to their corresponding primary tumors, and 53% of the examined cases displayed such a phenomenon (Brastianos et al., 2015). In this context, analysis of peripheral tumor tissue biopsies could misguide the choice of molecularly-targeted therapies for the treatment of brain metastases. Moreover, a suboptimal drug concentration in the brain metastases could promote emergence of drug resistance, adding to the challenge of treating brain metastases. (Figure 4)

Determination of brain drug exposure, especially in patients, is also challenging when choosing proper therapeutics for the treatment of brain metastases. Cerebral spinal fluid (CSF) is frequently thought to be surrogate of a concentration in the brain drug exposure. However, CSF concentration may not represent brain concentration for many molecularly-targeted agents that are substrates of efflux transporters, such as P-gp and/or BCRP. The CSF concentration is influenced by CSF turnover, extracellular fluid (ECF) bulk flow, and drug transporters at the blood-CSF barrier (BCSFB) (Figure 5) (de Lange and Danhof, 2002; Shen et al., 2004; Liu et al., 2009; de Lange, 2013b). Specifically in contrast to the BBB, drug delivery across the BCSFB is unhindered by P-gp and BCRP, because the blood side of choroid epithelial cells

lack P-gp and BCRP expression (Zhuang et al., 2006; Kodaira et al., 2011). For lipophilic compounds that readily diffuse across the choroid epithelial cells, the CSF concentration can overestimate the actual brain exposure (Kodaira et al., 2011). The study by Kodaira et al. showed that unbound CSF-to-brain concentration ratios of many compounds that are substrates of P-gp and BCRP were lower in *Mdr1a/1b(-/-)Bcrp (-/-)* mice compared to the wild-type, indicating that there can be discrepancies between the unbound CSF concentration and the unbound brain concentration ( $C_{u,brain}$ ) for P-gp and Bcrp substrates (Kodaira et al., 2011). Considering the structural and functional differences in the blood/brain versus the blood/CSF interface, CSF concentrations are often a poor predictor of brain drug exposure.

Microdialysis, a standard method to directly measure unbound brain interstitial fluid concentration ( $C_{u,brain}$ ), currently has limited applications in patients (Ederoth et al., 2004; Hillered et al., 2006; Liu et al., 2009; de Lange, 2013a). Many anticancer agents are often lipophilic, so that practical problems can arise with using microdialysis due to high nonspecific binding (Liu et al., 2009) and poor drug recovery (Liu et al., 2009). In an attempt to bypass such challenges, the brain homogenate and brain slice techniques have been developed to estimate the fraction unbound of drug in the brain. Each of these methods, used in combination with total brain concentrations, has demonstrated to be useful in obtaining surrogates of microdialysis  $C_{u,brain}$ . The study by Friden et al. showed that brain homogenate method predicted the  $C_{u,brain}$  from microdialysis measurements within a 3-fold error for 10 out of 15 compounds

(Friden et al., 2007). In the same study, the brain slice method predicted  $C_{u,brain}$  for 14 out of 15 compounds within a 3-fold error. These findings indicate that, for some compounds, either the brain slice or homogenate method can reasonably estimate the  $C_{u,brain}$ . Recently there was a development in expanding the analysis of the homogenate equilibrium dialysis method to determine unbound fraction of compounds, that might be useful for drug compounds with high protein binding (Kalvass et al., 2018). These techniques can allow determination of “active” free concentrations in different regions of the brain, including important regions of a growing brain tumor, such as the core of the tumor and the growing edge (Laramy et al., 2017).

The application of the brain homogenate method has been readily employed in order to evaluate brain drug distribution in the CNS drug development. Traditionally, the brain-to-plasma ratio ( $K_p$ ), which is the ratio of total brain concentration to total plasma concentration, has been considered to represent the degree of brain drug distribution. However,  $K_{p,uu}$ , the ratio of free brain concentration to free plasma concentration, has recently been introduced as a measurement of brain drug delivery that allows assessment of BBB transport mechanisms, separate from the influence of nonspecific binding in the brain (Liu et al., 2008). According to free drug hypothesis, only unbound drug concentration is considered to be a “pharmacologically active” concentration. The studies that examined brain penetration of molecularly-targeted agents have utilized both  $K_p$  and  $K_{p,uu}$  parameters (Mittapalli et al., 2013; Vaidhyanathan et al., 2014), and are useful in assessing the effect of efflux transporters in brain

drug delivery, but the latter allows differentiation of bound vs. unbound drug and may correlate better with efficacy. This has been recently discussed in the context of brain tumors by Heffron (Heffron, 2016; Heffron, 2018).

The evaluation of brain drug penetration has no single  $K_p$  or  $K_{p,uu}$  value that represents “optimal” brain penetration (Liu et al., 2008). The articles by Doran et al (2005) reported that a set of 32 commonly prescribed CNS drugs have a wide range of  $K_p$  (0.1 to 24), indicative that a compound having  $K_p$  of 0.1 can be still efficacious (Liu et al., 2008). This 240-fold difference in  $K_p$  indicates that  $K_p$  alone is inadequate to characterize brain drug delivery (Liu et al., 2008). On other hand, for the same set of CNS drugs, there is a 34-fold difference for  $K_{p,uu}$  (Maurer et al., 2005), indicating that nonspecific tissue binding can affect assessment of  $K_p$  and brain drug penetration (Liu et al., 2008). Even though there are limited studies that explore a direct relationship between  $K_{p,uu}$  and pharmacodynamic effect for the treatment of brain metastases, higher values of  $K_p$  and/or  $K_{p,uu}$  often serve as parameters to indicate more advantageous delivery of drug across the blood-brain barrier (Heffron, 2016; Heffron, 2018).

#### **2.1.4 Mechanisms that limit drug delivery across the BBB**

The blood-brain barrier (BBB) is a specialized structure of the cerebral microvasculature (Figure 1), comprised of a complex network of cells, extracellular matrix, and proteins that regulate solute and xenobiotic transport into and out of the brain. Given this complexity, and the fact that the BBB is dependent on signaling from the neuronal environment, the BBB is now

frequently referred to as the neurovascular unit (Figure 1). The NVU contains numerous cell types, including vascular endothelial cells, pericytes, glial cells, and neurons (Abbott et al., 2010; Sweeney et al., 2016). Pericytes mainly provide both structural and regulatory support of BBB and also contribute to the regulation of angiogenesis, neuroinflammation and stem cell activity (Sweeney et al., 2016). Astrocytes are cells that play an important role in regulation of BBB tight junctions, expression and localization of transporters and formation of specialized enzymes (Haseloff et al., 2005; Abbott et al., 2006). Unlike the endothelium of many peripheral organs, the endothelial cells forming the capillaries of the brain are held together by tight junctions and adherens junctions that prevent the paracellular transport of most blood-borne substances to the brain (Tietz and Engelhardt, 2015). Adherens junctions are formed between vascular endothelial cadherins and initiate the contact between adjacent endothelial cells (Tietz and Engelhardt, 2015). Tight junctions are consisted of transmembrane proteins such as occludin, claudin, and junctional adhesion molecule (JAM) that interact with cytoskeletal proteins and recruit membrane-associated cytoplasmic proteins (Abbott, 2013). Transporters at the BBB are important in maintaining the brain homeostasis and providing the brain with the necessary nutrients for normal function, while protecting the brain from toxic substances that may be in the systemic circulation (Agarwal et al., 2011a). Solute carriers (SLCs) and ATP-binding cassette transporters (ABC transporters) are two major families of transporters at the BBB (Uchida et al., 2011). These transporters play a crucial role in selectively moving specific substances



(substrates) into or out of the brain depending on their physicochemical and structural properties, and often coordinate (Agarwal et al., 2011a) with each other to efflux potentially toxic compounds out of the brain (Schinkel et al., 1994; Schinkel et al., 1996; Begley, 2004).

The SLC transporters are known to transport many polar compounds, including glucose and amino acids, that are essential nutrients for cell survival. However, this group of transporters is also involved in transporting organic anions (Steeg et al., 2011). Organic anion transporters (OAT) and organic anion transporting polypeptides (OATP) are some members of this family, and are known to be present at the BBB (Uchida et al., 2011). Transporters in this group can be unidirectional or bidirectional and are located in abluminal or luminal side of endothelial cells. Most of them have broad substrate specificity and some of substrates overlap with those of ABC transporters, which may indicate their coordinate function (Miller et al., 2000; Cisternino et al., 2004; Kis et al., 2010).

ABC transporters play a major role as active efflux pumps, consuming ATP, to limit the distribution of toxic substances in the CNS (Schinkel et al., 1996; Begley, 2004; de Lange, 2004). P-gp and BCRP are the examples of efflux pumps which have broad substrate specificity and are able to actively transport substrates back into systemic circulation (Agarwal et al., 2011a). In addition to P-gp and BCRP, multidrug resistance-associate proteins (MRPs) can also be involved in actively limiting the brain delivery of certain drugs (Eilers et al., 2008; Lingineni et al., 2017). In the treatment of brain tumors, the BBB often limits the

brain distribution of therapeutic agents through the efflux activity of ATP binding cassette (ABC) transport proteins (de Vries et al., 2007; Polli et al., 2008; Agarwal et al., 2011a; Elmeliegy et al., 2011; de Vries et al., 2012; Mittapalli et al., 2013; Oberoi et al., 2013; Lin et al., 2014; Tang et al., 2014; Parrish et al., 2015a; Parrish et al., 2015b).

### **2.1.5 Impact of transporters on the treatment of brain metastases**

The transport of a drug from the systemic circulation to the brain parenchyma is often depicted as a multi-step process. Initially, cerebral blood flow carries a drug compound to the brain and the drug is considered to be in equilibrium between the bound and unbound state in plasma, and the unbound drug is available to penetrate across the plasma-tissue barriers. Drug distribution to the brain at the blood-brain interface is regulated by the blood-brain barrier (BBB), blood-cerebrospinal fluid barrier (BCSFB), and other physiological systems in the brain (de Lange, 2013a; Westerhout et al., 2013). Upon successful drug delivery across the relevant anatomical barrier, the unbound (free) drug in the brain interacts with the target site and elicits pharmacological activities (Liu et al., 2009; Kodaira et al., 2011; de Lange, 2013a). Such unbound drug concentration in the brain interstitial fluid ( $C_{u,brain}$ ) is assumed to represent a pharmacologically active concentration. However, if a drug compound has an affinity for efflux transporters, the drug can be “pumped” back into the vasculature before interacting with its intended target (Figure 5) (de Lange, 2013a).

Many molecularly-targeted agents examined in clinical trials for brain cancer have been reported to be substrates of P-gp and/or BCRP (see Table 2) (Agarwal et al., 2011a; Mittapalli et al., 2013; Oberoi et al., 2013; Becker et al., 2015b; Parrish et al., 2015a; Parrish et al., 2015b; Mittapalli et al., 2016). Even though there has been some discussion that class I compounds in the Biopharmaceutics Drug Disposition Classification System (BDDCS) that have high solubility and high permeability may be less affected by efflux transporters (Broccatelli et al., 2012). These active efflux transporters at the BBB are known to prevent anticancer therapeutics from reaching parenchymal tumor cells, especially those from micro-metastases that may reside behind an intact BBB (Heffron, 2016). Genetic knockout mice lacking transporters and transfected cell lines overexpressing transporters (MDCK-II cell line, or Madin-Darby Canine Kidney Epithelial cell line) are widely utilized in vivo and in vitro models to evaluate the substrate status of an investigational compound for P-gp and BCRP in the preclinical setting (Mittapalli et al., 2013; Oberoi et al., 2013; Parrish et al., 2015a; Parrish et al., 2015b).

## **2.2 COMMON TYPES OF BRAIN METASTASES**

### **2.2.1 Lung cancer**

Lung cancer, a prevalent tumor with about 222,500 new cases in 2017 in US, according to the American Cancer society's estimate, is the leading cause of brain metastases. Approximately 20% of lung cancer patients will eventually develop brain metastases (Barnholtz-Sloan et al., 2004). The epidermal growth factor receptor (EGFR) and the anaplastic lymphoma kinase (ALK) are the most

well-known and well-developed drug targets to treat lung cancer, especially in non-small cell lung cancer (NSCLC) patients (Doroshov, 2005; Kwak et al., 2010). Over 45% of the patients with EGFR+ or ALK+ have brain metastases at some stage of disease (Rangachari et al., 2015). The three most commonly-used and studied EGFR tyrosine kinase inhibitors (TKIs) are gefitinib, erlotinib, and afatinib. Gefitinib and erlotinib are first-generation EGFR TKIs and their CNS delivery is reported to be very limited (1.07-3.58% for gefitinib and 2.77% for erlotinib, see Table 2) (Togashi et al., 2010), mainly due to the efflux transporters, P-gp and BCRP (Agarwal et al., 2010; de Vries et al., 2012; Agarwal et al., 2013; Chen et al., 2013). However, despite this low brain penetration, these first-line TKIs seem to modestly reduce the risk of CNS progression when compared to standard chemotherapy (Heon et al., 2012). Therefore, erlotinib and gefitinib may have a prophylactic effect on brain metastases. Afatinib is a second-generation inhibitor, which irreversibly blocks signaling from EGFR, HER2, ErbB3, and ErbB4 (Solca et al., 2012). While the CSF to plasma ratio of afatinib was reported to be extremely low in patients, less than 1%, due to active efflux by P-gp (Hoffknecht et al., 2015), a study showed that response rate to afatinib in the patients with or without CNS metastases were similarly efficacious, possibly due to the high potency of the compound (Hoffknecht et al., 2015). Osimertinib (AZD9291) is a recently approved drug to treat patients with T790M resistant mutant NSCLC showed pre-clinical evidence that it can penetrate the BBB (Ballard et al., 2016). Moreover, in a clinical trial, osimertinib has shown efficacy in patients with EGFR-driven NSCLC lung

metastases in the CNS (Mok et al., 2017). Another EGFR inhibitor, AZD3759, has been specifically designed to penetrate the BBB (Zeng et al., 2015), and efficacy in patients with NSCLC with brain metastases is under current clinical investigation (Yang et al., 2016).

ALK is another potent target that is constitutively active due to gene rearrangements in approximately 2% to 7% of lung cancer patients (Koivunen et al., 2008; Rodig et al., 2009; Wong et al., 2009). Crizotinib, the first ALK targeted TKI, has been reported to have poor brain penetration based on a low CSF-to-plasma ratio (0.26%) in humans (Costa et al., 2011), mainly due to P-gp (Tang et al., 2014). It has been reported that the efficacy of crizotinib in the CNS seems to be limited, even though the overall objective response rate and the median duration of response were significantly improved with crizotinib treatment when compared to standard chemotherapy (2014; Solomon et al., 2014; Costa et al., 2015).

Alectinib and ceritinib are the second generation of ALK inhibitors that demonstrate their activity in crizotinib-resistant patients. Alectinib also inhibits RET, an oncogene involved in the development of several human cancers, including NSCLC (Kodama et al., 2014b). Several clinical studies that include patients with brain metastases at baseline have shown that alectinib has some efficacy in CNS tumors (Gadgeel et al., 2014; Metro et al., 2016), possibly due to the fact that it is not a substrate of major efflux transporters (Kodama et al., 2014a). These efficacy results are in line with its high brain penetration in pre-

clinical rat model (63-94%, Table 2). However, the mean ratio of CSF concentration to the plasma concentration in patients was approximately 0.3% (Metro et al., 2016), which again suggests that concentration measured in CSF may not represent the concentration in brain or at the target site. (Figure 5)

Ceritinib is another potent ALK inhibitor that showed some efficacy with intracranial metastases in a preclinical rat model with a brain to plasma ratio of 15% (Corporation; Friboulet et al., 2014). This brain penetration may seem higher than expected considering ceritinib is a substrate of both P-gp and Bcrp. Nevertheless, the ASCEND study for advanced ALK-positive NSCLC has shown that ceritinib has efficacy against brain metastases, based on both the response and disease control rates (Kim et al., 2016).

Several other therapeutic agents are under clinical investigation to examine their efficacy in lung cancer patients with CNS metastases, including brigatinib, lorlatinib, entrectinib, cabozantinib, and tesevatinib. Brigatinib, a second generation ALK inhibitor, potently inhibits both ALK and EGFR. According to a recently reported phase I/II clinical trial that included patients with CNS metastases, brigatinib has shown efficacy against brain disease (response rate 53% and PFS of 97 weeks).

Recently developed as third generation ALK inhibitors, lorlatinib and entrectinib are specifically designed to improve brain penetration, and a clinical trial is currently recruiting lung cancer patients for their first efficacy evaluation in patients. Lorlatinib is structurally designed to have a low affinity for P-gp

(Johnson et al., 2014). Based on an analysis to examine the influence of physicochemical properties on p-glycoprotein affinity, lorlatinib was intentionally designed to have logD range of 2-3 and minimal introduction of hydrogen bond donors (Johnson et al., 2014). To minimize the hydrogen bond donors, intramolecular hydrogen bonds are introduced in the adjacent ether oxygen in the molecule. This chemical design aimed to have enhanced intrinsic permeability and to avoid efflux transporter liability, allowing lorlatinib to target brain metastases (Johnson et al., 2014). Entrectinib has also been shown to have high brain penetration in nude mice (43% brain concentration to plasma concentration ratio) (Menichincheri et al., 2016). While we await results from the clinical trials regarding improved efficacy, the fact that intentional structure-delivery efforts are being made bodes well for the development of compounds that will be efficacious against brain tumor cells that are behind an intact BBB.

### **2.2.2 Melanoma**

Melanoma is a lethal form of skin cancer with a projected diagnosis of 87,110 patients in the United States for the year 2017, with close to 9,730 deaths expected in the US (American Cancer Society 2017). The most common peripheral sites of melanoma metastases are lung, liver, bones and brain. Melanoma has the second highest prevalence of brain metastasis followed by lung cancer with an overall incidence of 5%-8% (Gavrilovic and Posner, 2005). Metastases in the brain have been identified in 55-75% of melanoma patients at autopsy, indicating a high tropism of melanoma to metastasize to the brain

(McWilliams et al., 2003; Gorantla et al., 2013). Melanoma patients with metastatic disease that has spread to the brain are associated with a poor median overall survival of less than 6 months (Sloan et al., 2009; Damsky et al., 2014). Approximately 40-60% of melanoma patients have a mutation in the serine threonine kinase v-RAF murine sarcoma viral oncogene homolog B1 (BRAF-mu) (Davies et al., 2002). This oncogenic mutation results in sustained activation of the mitogen-activated protein kinase (MAPK) oncogenic signaling pathway (Figure 10) (Flaherty et al., 2010; Capper et al., 2012; Durmus et al., 2012). Therefore, the development of inhibitors specifically targeting BRAF-mu isoform was of significant interest in the treatment of melanoma. Vemurafenib, a FDA approved BRAF-mu inhibitor for the treatment of late-stage melanoma, showed an improvement in the 6-month overall survival rate by 20% when compared to dacarbazine chemotherapy with a response rate of approximately 50% (Luke and Hodi, 2012; Kim and Cohen, 2016). However, the results of preclinical studies show that the brain penetration of vemurafenib is limited due to active efflux by P-glycoprotein and Bcrp (Durmus et al., 2012; Mittapalli et al., 2012). A few patient case studies show that vemurafenib may have a potential efficacy to induce remission of brain metastases (Dummer et al., 2014). This partial efficacy may be related to factors such as the size of the tumor and the degree of disruption of the BBB (Gerstner and Fine, 2007; Narayana et al., 2013). A review of the clinical studies and case reports related to vemurafenib suggests that the effectiveness of vemurafenib seems to be limited in intracranial tumors, but it may provide successful therapeutic outcomes in a subset of patients



depending on the tumor characteristics, the stage of tumor progression and other unknown factors (Rochet et al., 2011; Dummer et al., 2014) (NCT01378975, NCT01781026).

Another BRAF-mu inhibitor, dabrafenib, showed notable benefits in a phase 1 dose-escalation study in V600E BRAF-melanoma patients with untreated brain metastases (Falchook et al., 2012). Nine out of 26 patients with brain metastases showed intracranial tumor size reduction, and four of them had complete tumor regression (Falchook et al., 2012). Another study performed with a total of 23 patients from a single institution has reported that the response rate in intracranial disease was 78% and that in extracranial disease was 90% in BRAF-mutant melanoma patients with brain metastases (Azer et al., 2014). According to the study results, both intracranial and extracranial disease appear to respond similarly to dabrafenib. However, importantly, dabrafenib is known to be a substrate of both P-gp and Bcrp, with a brain to plasma ratio in normal mouse brain of 2%. (Mittapalli et al., 2013). Currently, several clinical studies are ongoing to examine the efficacy of dabrafenib in combination with stereotactic radiosurgery and other therapeutics ([www.clinicaltrials.gov](http://www.clinicaltrials.gov)). As data from these trials become available, it will be critical to establish if the responses are durable and to examine reasons for relapse. Insufficient drug distribution to areas of brain metastases that have an intact BBB replete with efflux transporters, may be related to disease progression.

Another target in the MAPK pathway that is important in metastatic melanoma is MEK (Jiang et al., 2007). Since MEK is a signaling molecule that is downstream of BRAF (Figure 6), MEK inhibitors can overcome the resistance developed against BRAF inhibitors (Flaherty et al., 2012a; Flaherty et al., 2012b). Trametinib and cobimetinib are FDA approved MEK inhibitors for the treatment of melanoma. Combinations of dabrafenib/trametinib and vemurafenib/cobimetinib have also received FDA approval. Dabrafenib/trametinib combination therapy showed an improvement in progression free survival compared to monotherapy in melanoma patients (Flaherty et al., 2012a). Cobimetinib/vemurafenib combination also showed a significant improvement in progression free survival in patients with BRAF V600-mutant metastatic melanoma (Larkin et al., 2014). However, both trametinib and cobimetinib are substrates of p-glycoprotein (Choo et al., 2014; Vaidhyanathan et al., 2014). There are reports that suggest that MEK inhibitors in combination with BRAF inhibitors or RT may improve survival rates in patients with brain metastases, despite the fact that the brain delivery of both trametinib and cobimetinib can be limited due to active drug efflux in areas of metastases with an intact BBB (Patel et al., 2016; Planchard et al., 2016). Currently, clinical trials recruiting patients with brain metastases to examine their clinical efficacy in combination with BRAF inhibitor or RT are underway (NCT02039947, NCT02015117, NCT02537600). Preliminary data from the study in patients with melanoma brain metastases implies that a combination of dabrafenib and trametinib with SRS may show improvements in survival compared to treatment with dabrafenib alone (Long et al., 2016). As stated above

for dabrafenib, durable responses may be limited by progression of tumor in areas with an intact BBB, and if disease progression occurs, it will be important to investigate why.

Immune modulation using monoclonal antibodies (mAbs) directed towards cytotoxic T-lymphocyte-associated antigen 4 (CTLA-4) (e.g, ipilimumab) and programmed cell death receptor (PD-1) (e.g., nivolumab) is an emerging strategy to manage tumors, especially in melanoma. Immune checkpoint inhibitors can cause activation and proliferation of T lymphocytes, which can then attack tumor cells. The rationale for using immune checkpoint inhibitors for the treatment of brain tumors is that the activated T cells are able to gain access to the CNS and show responses (Engelhardt and Coisne, 2011; Di Giacomo and Margolin, 2015). Their efficacy in the treatment of melanoma that has metastasized to the brain is critical to investigate, but there is limited evidence available to prove it in patients with brain metastases, due to the exclusion of patients with brain metastases in many clinical trials. In an open-label phase 2 clinical trial with melanoma and brain metastases study, ipilimumab proved its potency against small and asymptomatic brain metastases (Margolin et al., 2012). In a different clinical study with asymptomatic brain metastases patients, ipilimumab has shown benefits in patients, who had failed or did not tolerate previous treatments (Queirolo et al., 2014). Lately, there are ongoing clinical trials using immune modulation as a single agent or in combination with RT or radiosurgery against brain metastases (NCT01703507, NCT02374242, NCT02696993).

As we noted in the therapeutic agents for other tumors, many treatments for melanoma have limited access to the brain across the BBB due to efflux transporters. (Table 3).

### 2.2.3 Breast cancer

The incidence rate of brain metastases from breast cancer is different depending on the subtype. It is about 20% in triple-negative tumors, i.e., those that do not express hormone receptors, including estrogen and progesterone, and HER2, and increases to 25%-50% in HER2 positive tumors (Aversa et al., 2014). Molecularly targeted therapeutics for HER2 positive breast cancer patients have been significantly improved over the last 2 decades, but the efficacy of these agents in patients with breast cancer brain metastases seems to be limited.

The most frequently prescribed therapeutic agent for HER2 positive breast cancer patients is trastuzumab, an anti-HER2 antibody (Kodack et al., 2015). Trastuzumab has shown to be efficacious for systemic HER2 positive breast cancer, however patients receiving trastuzumab tend to have higher incidence of brain metastases (Clayton et al., 2004). The brain penetration of trastuzumab across an intact BBB is very low, as expected for an antibody drug due to its large molecular weight (Leyland-Jones, 2009). Retrospective research has shown that 50% of patients with CNS metastases responded to the trastuzumab, even though it is difficult to distinguish the systemic efficacy from CNS

metastases specific efficacy, due to the limitations in a retrospective study that simply reports the overall objective response rates (Bendell et al., 2003).

Lapatinib is a small molecule dual tyrosine kinase inhibitor of EGFR and HER2, and interestingly, its percentage brain penetration across the BBB is as low as trastuzumab. The ratio between the patient drug concentration in CSF and plasma averaging 0.11% (see Table 4) (Gori et al., 2014). Preclinical studies in mice have shown that P-gp and Bcrp coordinate with each other to limit the delivery of lapatinib across the BBB (Polli et al., 2008). Consistent with the heterogeneous integrity of the BBB in breast cancer brain metastases, the distribution of lapatinib is highly variable in breast cancer brain metastases (Taskar et al., 2012; Morikawa et al., 2015). The efficacy of lapatinib as a single agent in brain metastases is modest (overall response rate: 21.4%) (Cameron et al., 2008; Lin et al., 2008), but lapatinib in combination with capecitabine showed increased response rate toward CNS metastases (29.2%) (Lin et al., 2009).

The triple negative subtype is also prone to develop brain metastases and there are not many treatment options available for this subtype. Few molecularly targeted drugs are currently being tested for their efficacy in patients with triple negative tumors (Dawood et al., 2009). One possible druggable target for this subtype is poly-adenosine diphosphate ribose polymerase (PARP). There are several PARP inhibitors already approved and additional compounds are being tested in clinical trials, including niraparib, rucaparib, olaparib, veliparib (ABT-888), and talazoparib (BMN 673). Of these, niraparib showed good brain

penetration in an in vivo rat model with brain to plasma ratio of 0.85-0.99 (Mikule and Wilcoxon, 2015). On the other hand, the distribution of rucaparib to the brain is low, due to the effect of the major efflux transporters, P-gp and Bcrp (Parrish et al., 2015a). Veliparib showed significantly improved overall median survival in a phase I study when it was used in conjunction with WBRT (Mehta et al., 2015), even though its brain penetration is reported to be low (less than 5%), due to both P-gp and Bcrp (see Table 4) (Lin et al., 2014).

Vorinostat is the first targeted drug specifically approved to inhibit histone deacetylase (HDAC), a novel target to treat breast cancer, and this compound showed some efficacy in preventing brain metastases in a mouse model with triple negative breast cancer (Palmieri et al., 2009). However the brain delivery of Vorinostat seems to be limited by efflux transport (Hanson et al., 2013).

Because of the limited success in treating breast cancer brain metastases with molecularly targeted agents that have limited delivery across the BBB, there has been an emphasis on developing new brain-penetrant therapies. TPI-287 is a new brain permeable taxane that stabilizes microtubules (Fitzgerald et al., 2012) that is under clinical investigation as a treatment of breast cancer brain metastases and primary brain tumor (NCT01332630, NCT01933815, NCT01582152). There are also several clinical trials evaluating novel compounds for brain metastases including 4-demethyl-4-cholesteryloxycarbonylpenclome (DM-CHOC-PEN) (NCT02038218), eribulin mesylate (NCT02581839), cabozantinib (NCT02260531), abemaciclib (NCT03130439, NCT03220646,

NCT02308020). Neratinib, a recently approved tyrosine kinase inhibitor, has shown some efficacy against breast cancer brain metastases (Freedman et al., 2017).

Even though there were several successful developments of molecularly targeted agents to treat breast cancer, the incidence of patients with brain metastases has increased and have a poor prognosis (Anders et al., 2011), mainly due to resistance development and poor brain penetration of therapeutic agents. Several brain penetrant therapeutics have shown to have promising efficacy on brain metastases in preclinical studies.

#### 2.2.4 Renal cell carcinoma

The incidence rate of renal cell carcinoma (RCC) in adults is 2-3%, and metastases occur in about 50% of these patients. About 8-10% of metastatic renal cell carcinoma (mRCC) patients are known to develop brain metastases (Bianchi et al., 2012). The median overall survival is reported to be less than 13.3 months in the presence of brain metastases when using whole-brain radiotherapy (Bennani et al., 2014). The treatment regimen with molecularly targeted therapeutics has not been established or evaluated for brain metastases, and standard therapy for mRCC has been applied to patients with brain metastases. Several tyrosine kinase inhibitors are approved by FDA for treatment of mRCC, including sorafenib, sunitinib, and axitinib, and have improved survival (Table 4). Sunitinib has some clinical benefit towards brain metastases as a single agent by stabilizing the disease by more than 3 months, but objective response rate was only 12% among 213 patients enrolled (Gore et al., 2011; Dudek et al., 2013). Brain distribution of sunitinib is reported to be high (42%) in a preclinical study, even though sunitinib is found to be substrates of both P-gp and BCRP (Oberoi et al., 2013). According to a few case reports, a newer generation TKI, pazopanib, seems to have good response rate or increase overall survival as a single agent (Roberto et al., 2015). The efficacy of sorafenib has been studied in advanced metastatic renal cell carcinoma, but most of these studies excluded the patients with diagnosed brain metastases. Brain penetration of sorafenib is reported to be modest (9.4%) in mice, probably due to the efflux of both P-gp and BCRP. Recently, novel tyrosine kinase inhibitors, including



cabozantinib and lenvatinib, received FDA approval for mRCC. However, the brain delivery of these agents across the BBB as well as their efficacy against brain metastases have not been reported. Since brain metastases are distinct from other organ metastases, especially in drug delivery, more clinical studies that examine the efficacy of a treatment specifically against brain metastases should be performed.

### **2.3 CONCLUSION**

Several instructive observations can be made from the experience with the use of targeted agents in the context of brain metastases (Box 1.). There is an overall correlation of brain penetration and substrate status of efflux transporters at the BBB, especially P-gp and BCRP (see table 2, 3, and 4). Many molecularly targeted agents are substrates of these efflux transporters, and their accessibility to the brain has been shown to be extremely low when the BBB is intact. This could be one reason why the incidence rate of metastases to the brain has been rising, despite of development of numerous molecularly targeted drugs. Tumors that reside in the brain can be protected from exposure to anticancer therapeutics by the BBB, resulting in limited delivery (Figure 7). Therefore, delivery of therapeutic agents to the brain is critical concern in treating metastatic tumors.

There have been many previous reviews on various methods to improve drug delivery to the brain for the treatment of brain tumors by enhancing the brain penetration of drugs that are systemically available. These methods include

changing formulations of existing compounds by using nanoparticles (Anders et al., 2013; Kreuter, 2014) and using concomitant therapy that inhibits efflux transporters at the BBB to improve brain delivery of substrates (Sandler et al., 2004; Fox and Bates, 2007; Morschhauser et al., 2007). However, it will be even more critical to assess the efflux transporter liability when developing and designing therapeutics, and consider a brain delivery as a key factor in the early phase of discovery and development, especially for the anticancer therapeutics that are often subject to efflux transporters at the BBB. There are examples of using *in silico*-guided drug design to make a brain penetrant anticancer drug by reducing efflux liability, including GNE-317 and lorlatinib (Heffron et al., 2012; Johnson et al., 2014; Salphati et al., 2014).

Another important consideration is that the integrity of BBB in and around the tumor in the brain is heterogeneous (Lockman et al., 2010). The BBB around the tumor core can be relatively permeable to therapeutics, since its structure tends to be disrupted. However, the tumor rim and micro-metastases may have an intact BBB, replete with efflux transporter systems, making these regions more likely to be resistant to therapeutics. Previously, several papers have shown that concentration of drugs in tumor is high enough to result in desirable efficacy in the tumor cells, based on the concentration measured in tumors resected from patients, due to disrupted BBB around tumor (Figures 7). However, since the integrity of BBB is heterogeneous depending on the region, and even within a region, the concentration of drug measured in a resected tumor specimen does represent the concentration throughout the entirety of the

tumor. Given this, it is feasible that variable efficacy of many agents between patients or even amongst metastatic sites is related to inconsistent delivery. There are some drugs that have been shown to have some efficacy against brain metastases, despite of their limited delivery to the brain. In case of erlotinib for lung cancer, even though it has low brain penetration due to P-gp and BCRP, its efficacy against brain metastases patients carrying a specific EGFR mutation was demonstrated (response rate of 82.4%, Table 2). This can be explained by not only improved delivery of a drug through perturbed BBB around tumor core, but also the selectivity and potency of a drug for a particular tumor. Drug may be able to induce desirable efficacy in the brain, if it has sufficient selectivity and potency against its target so that the concentration of a drug required at the site of action can be achieved. This observation indicates that both potency and delivery need to be considered hand-in-hand when evaluating and deciding upon a course of therapy for brain metastases. The potency of a drug against its target is often represented by an inhibitory concentration or efficacious concentration when measured using in vitro experiments. However, that in vitro concentration may not be the same as the efficacious concentration needed at the site of action in patients. Therefore, it is important to consider the concentration of a drug needed at the target, because potency can help overcome limited delivery, when potency is high enough. Since a lack of efficacy of systemic anticancer agents in CNS disease can lead to higher incidence rates of brain metastases (Stegg et al., 2011), the BBB penetration, subsequent distribution into the brain metastatic site, and the potency against a particular

CNS target, of molecularly-targeted agents need to be considered in the early phases of drug development.

**Figure 2.1 The expression and localization of transporters in the brain endothelial cell in the context of the overall composition and structure of the neurovascular unit (NVU). Important drug transporters include: SLC, solute carrier; MRP, multidrug resistance protein; LAT, L-type amino acid transporter; OATP, organic anion transporting polypeptide; MCT, monocarboxylate transporter; ENT, equilibrative nucleoside transporter.**

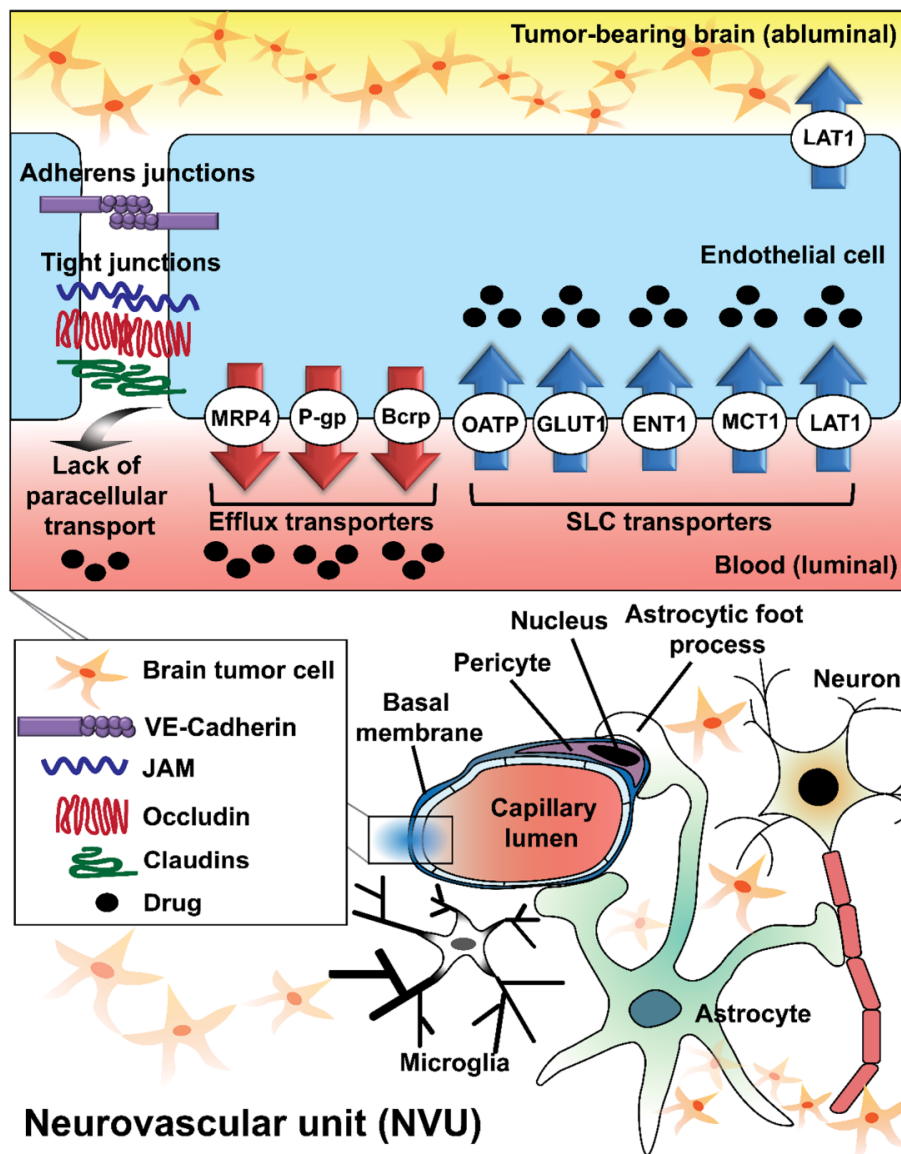


**Figure 2.2 Primary tumors that preferentially metastasize to the brain and the occurrence of brain metastases from each of these primary tumors. Examples of key tumor driving oncogenes are represented for each tumor type.**

Figure 2.

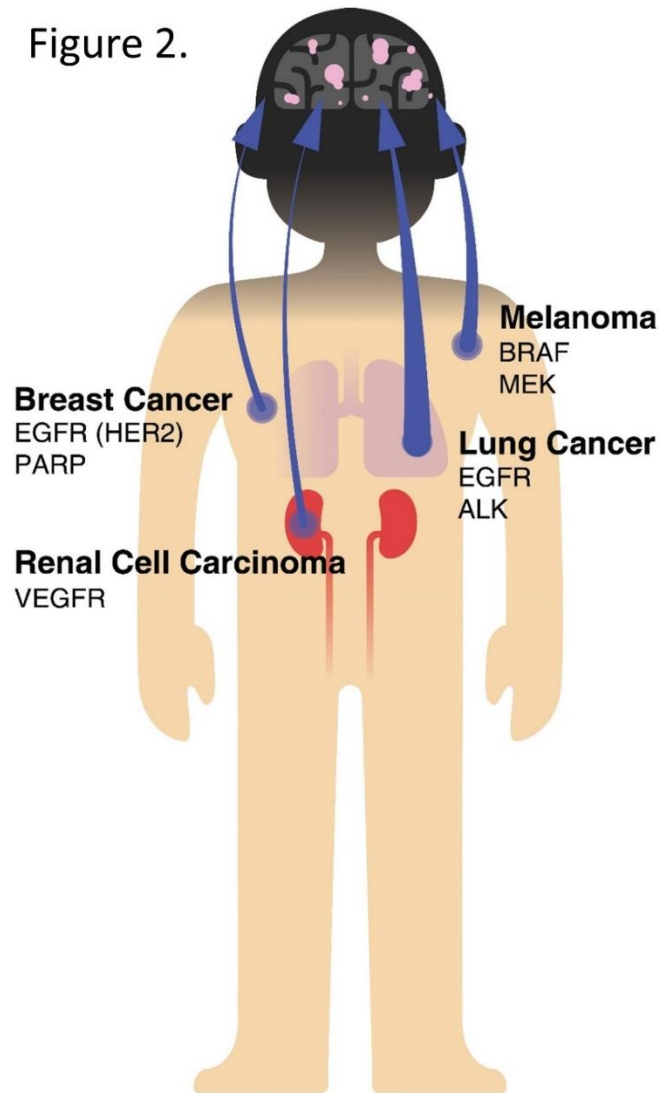


**Figure 2.3 Depiction of the most common treatment options for brain metastases.**

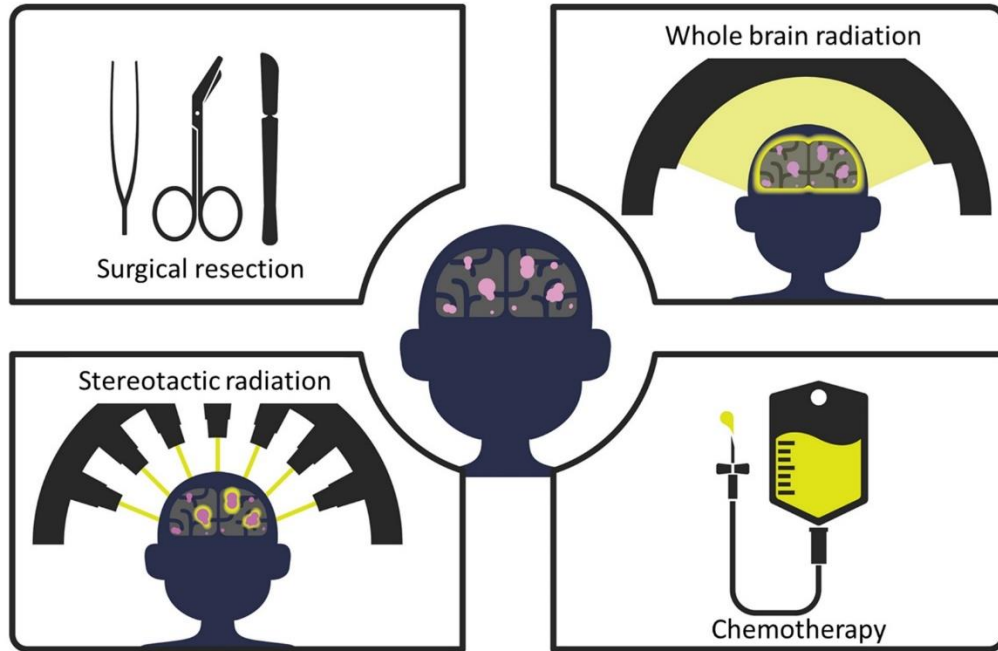


**Figure 2.4 Mechanisms of resistance development against drug in brain metastases due to inherent tumor heterogeneity or acquired resistance.**

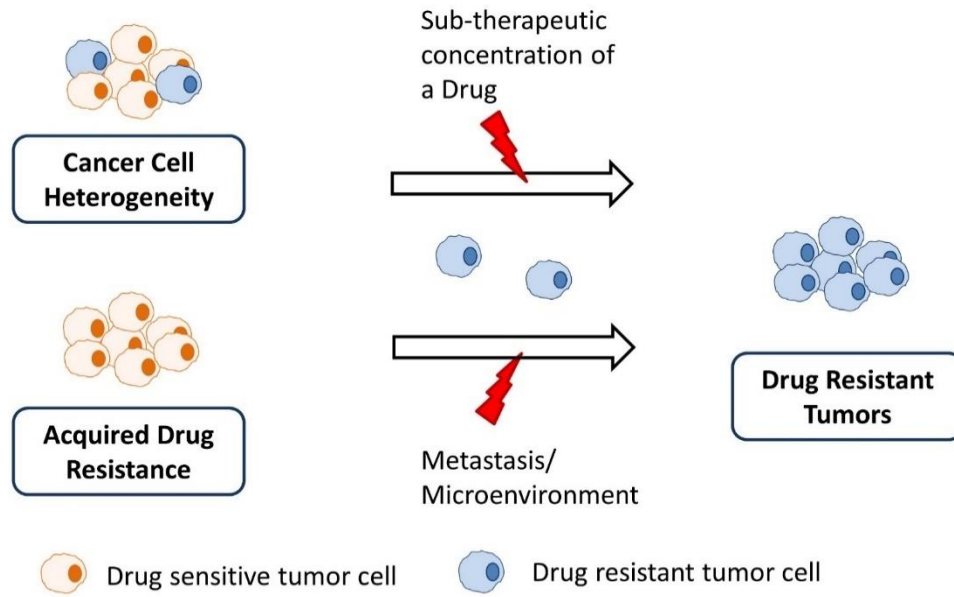




**Figure 2.5 Multiple equilibria in different compartments in the brain, blood, and cerebrospinal fluid.**

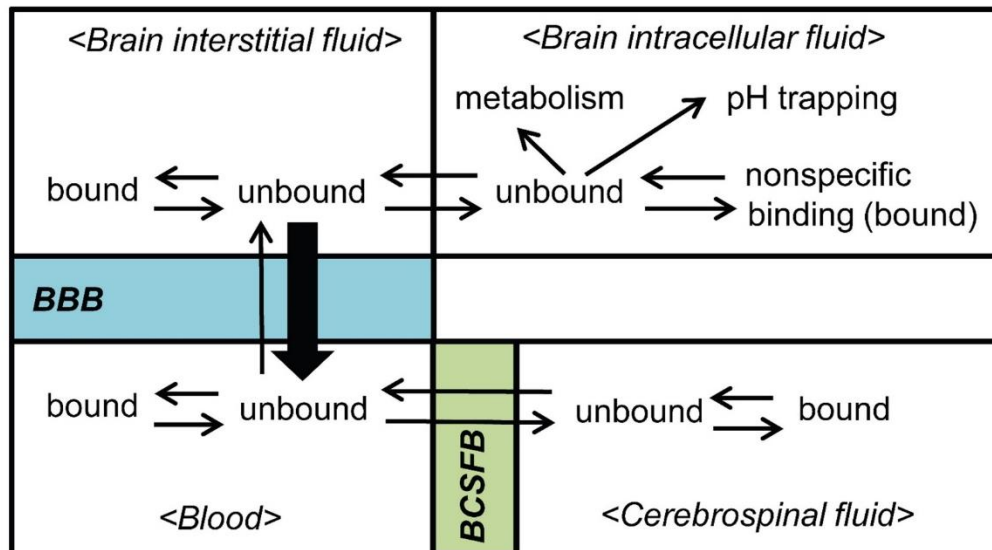


**Figure 2.6 Signaling pathways and oncogenic targets of molecularly-targeted therapeutics for melanoma.**

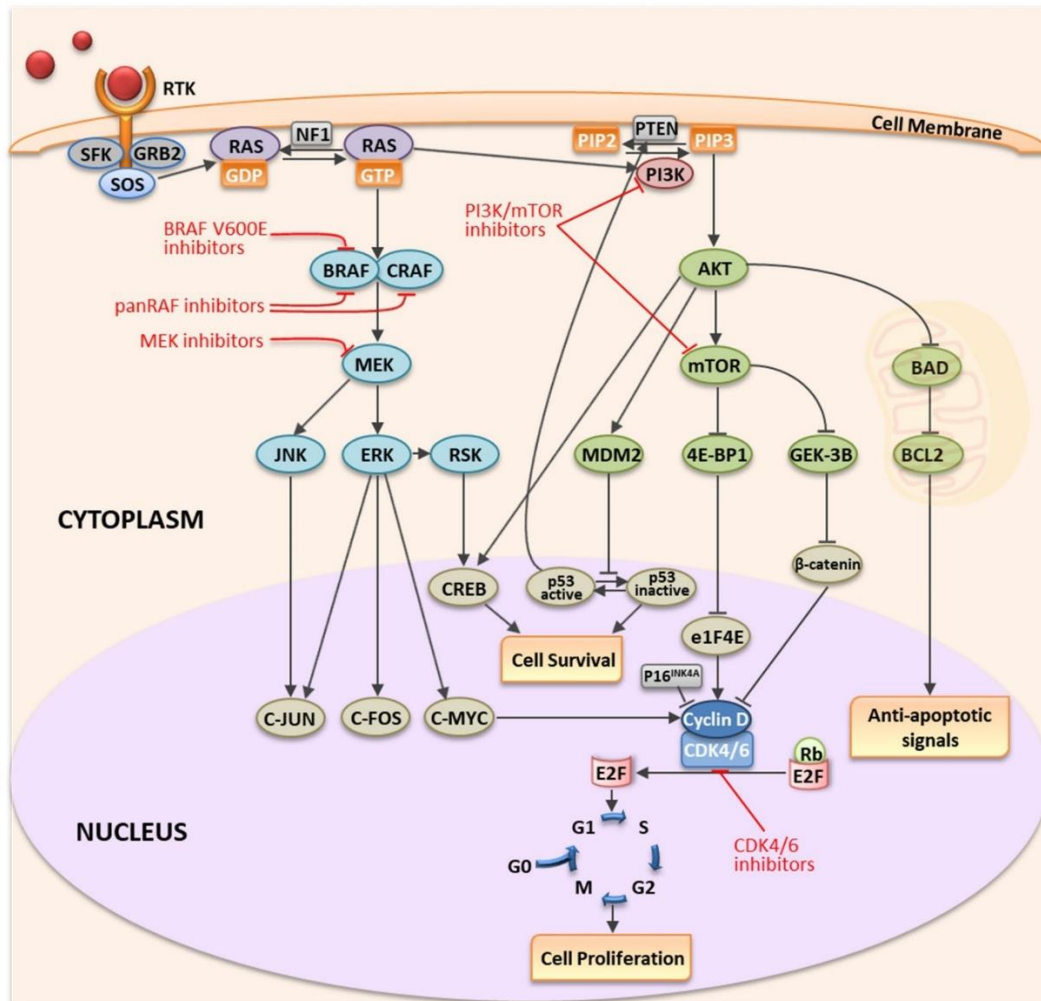


**Figure 2.7 Heterogeneity of blood-brain barrier disruption and drug concentration in the experimental model (mice) of breast cancer brain metastases (from reference (Taskar et al., 2012)). <sup>14</sup>C-lapatinib was measured in normal brain and different brain metastases by quantitative autoradiography at 2 hours (a-c) and 12 hours (d-f) following the oral administration of 100 mg/kg <sup>14</sup>C-lapatinib. Signal from metastatic cells labelled with EGFP (a,d), Texas Red 3kD dextran (b,e), and <sup>14</sup>C-lapatinib (c,f) indicate the location of tumor cells, the integrity of the BBB, and the concentration of drug, respectively. The concentrations of lapatinib, as well as disruption of BBB, were highly variable within and between the metastatic breast cancer lesions in the brain.**

Figure 2.7 continued

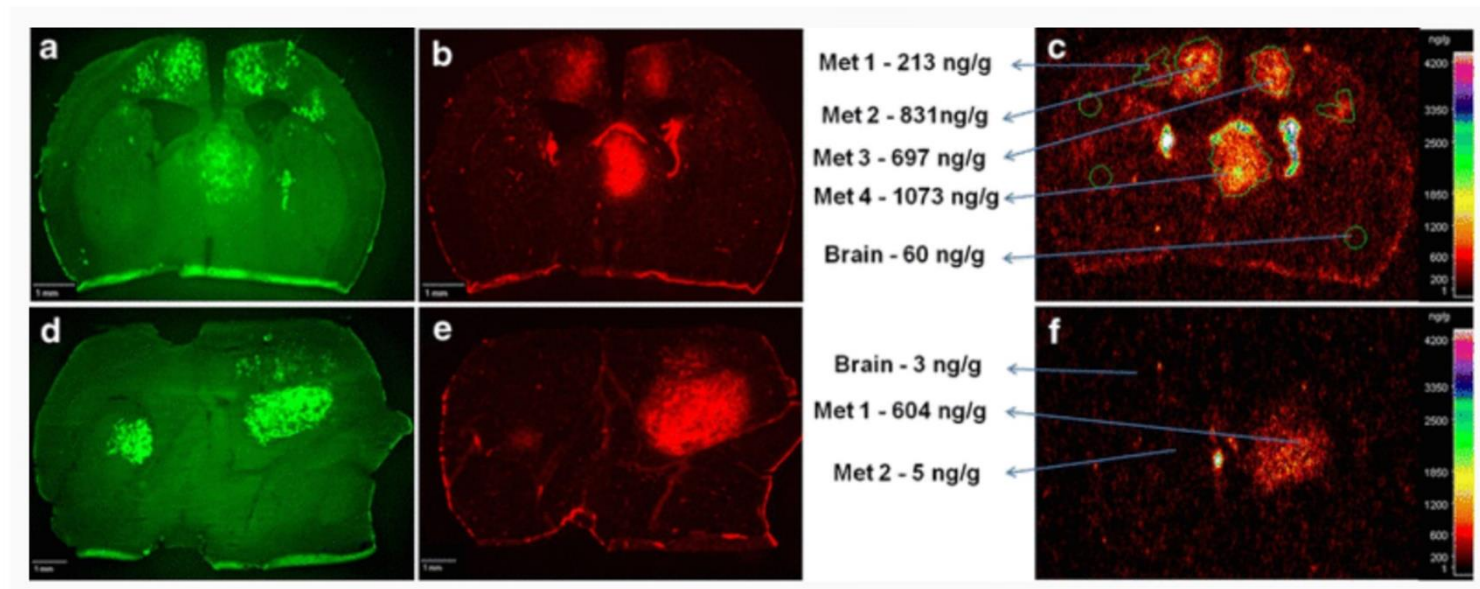


**Table 2.1 Incidence rate of brain metastases**

Primary site	Incidence Rates	References
Lung (overall)	16.3 - 19.9%	(Schouten et al., 2002; Barnholtz-Sloan et al., 2004)
SCLC*	29.7% (at 5 years)	(Schouten et al., 2002; Barnholtz-Sloan et al., 2004)
NSCLC*	12.6% (at 5 years)	(Schouten et al., 2002; Barnholtz-Sloan et al., 2004)
Breast	10-15%	(Schouten et al., 2002; Barnholtz-Sloan et al., 2004)
HER2 positive	25-50%	(Aversa et al., 2014)
Triple negative	20%	(Aversa et al., 2014)
Melanoma	6.9 - 7.4%	(Barnholtz-Sloan et al., 2004)
Renal	6.5 - 9.8%	(Barnholtz-Sloan et al., 2004)
Colorectal	3.0%	(Barnholtz-Sloan et al., 2004)

\* can be up to 50-60% depending on study and disease duration (Newman and Hansen, 1974; Chamberlain et al., 2017)

**Table 2.2 Brain and transporter related features of molecularly targeted therapy for lung cancer. (ND, not determined; NA, not available.)**

Compound	Molecular Target	Dose in patients (mg/day)	Brain penetration (% of CSF to plasma levels) in patient*	Brain penetration (% of brain to plasma ratio) in pre-clinical model*	Response rate in BM patients (%)	Transporter effect	Reference
Gefitinib	EGFR-TKI	750-1000	1.07-3.58	27	27%	P-gp substrate	(Ceresoli et al., 2004; Chen et al., 2013)
Erlotinib	EGFR-TKI	150	2.77- 5.1	13.7	82.4% (EGFR mutation)	P-gp and Bcrp substrate	(Togashi et al., 2010; Porta et al., 2011; de Vries et al., 2012)
Afatinib	EGFR-TKI	50	0.7	ND	35%	P-gp substrate	(Wind et al., 2014; Hoffknecht et al., 2015)
Osimertinib	EGFR-TKI	80	NA	180	ND	P-gp and Bcrp substrate	(Ballard et al., 2016)
AZD3759	EGFR-TKI	100-1000	111	282	83%	ND	(Zeng et al., 2015)
Crizotinib	ALK-TKI	500	0.26	23	18-33 %	P-gp substrate but not Bcrp	(Tang et al., 2014)
Alectinib	ALK-TKI	1200	0.3	63-94	52%	Not a P-gp substrate	(Gadgeel et al., 2014; Kodama et

								al., 2014a; Metro et al., 2016)
Ceritinib	ALK-TKI	400	ND	15	34.5-58.8 %	P-gp and Bcrp substrate	(Crino et al., 2016; Katayama et al., 2016; Kim et al., 2016)	
Brigatinib	ALK and EGFR TKI	300	ND	ND	53%	ND	(Rosell et al., 2016)	
Lorlatinib (PF-06463922)	ALK-TKI	100	ND	64	ND	Not a P-gp substrate	(Johnson et al., 2014)	
Entrectinib	ALK-TKI	ND	ND	43	ND	ND	(Ardini et al., 2016; Menichincheri et al., 2016)	

\* Total drug concentrations are reported

**Table 2.3 Brain and transporter related features of molecularly targeted therapy for melanoma. (ND, not determined; NA, not available.)**

Compound	Molecular Target	Dose in patients (mg/day)	Brain penetration (% of CSF to plasma levels) in patient*	Brain penetration ( % of brain to plasma ratio) in pre-clinical model*	Response rate in BM patients (%)	Transporter effect	Reference
Vemurafenib	BRAF inhibitor	960 (b.i.d.)	0.98	0.012	NA	P-gp and Bcrp substrate	(Mittapalli et al., 2012; Sakji-Dupre et al., 2015)
Dabrafenib	BRAF inhibitor	150 x 2 (b.i.d.)	ND	4.4	71-78	P-gp and Bcrp substrate	(Mittapalli et al., 2013; Azer et al., 2014)
Cobimetinib	MEK inhibitor	60	ND	8	Under investigation (NCT02537600)	P-gp substrate (Not Bcrp)	(Choo et al., 2014)
Trametinib	MEK inhibitor	2	ND	0.28	NA	P-gp substrate, but not Bcrp	(Vaidhyanathan et al., 2014)
E6201	MEK inhibitor		ND	270	NA	Minimal effect with P-gp and Bcrp	(Gampa et al., 2018)

\* Total drug concentrations are reported



Table 2.4 Brain and transporter related features of molecularly targeted therapy for breast cancer and renal cancer cell

(Continued in the next page)

Compound	Molecular Target	Dose in patients (mg/day)	Brain penetration (% of CSF to plasma levels) in patient*	Brain penetration (% of brain to plasma ratio) in pre-clinical model*	Response rate in BM patients (%)	Transporter effect	Reference
Lapatinib	EGFR and HER2	1250	0.11	3	6%	P-gp and Bcrp substrate	(Polli et al., 2008; Lin et al., 2009; Gori et al., 2014)
Trastuzumab	HER2	NA	0.24	ND	0.5	NA	(Stemmler et al., 2007)
Rucaparib	PARP inhibitor	40	ND	11	ND	P-gp and Bcrp substrate	(Parrish et al., 2015a)
Olaparib	PARP inhibitor	400 x 2 (b.i.d.)	ND	1.1 <sup>#</sup>	ND	P-gp substrate	(Lawlor et al., 2014)
Veliparib (ABT-888)	PARP inhibitor	400 x 2 (b.i.d.)	ND	less than 5%	ND	P-gp and Bcrp substrate	(Lin et al., 2014)
Talazoparib (BMN-673)	PARP inhibitor	1	ND	2	ND	P-gp substrate, but not Bcrp	(Kizilbash et al., 2017)
Niraparib	PARP inhibitor	300	10-52 <sup>+</sup>	85-99	ND	NA	(Mikule and Wilcoxon, 2015)
Vorinostat	HDAC inhibitor	360	ND	4	ND	P-gp and Bcrp substrate	(Hanson et al., 2013)
Sunitinib	TKI	50	ND	42	12	P-gp and Bcrp substrate	(Gore et al., 2011; Oberoi et al., 2013)
Sorafenib	Multi-kinase inhibitor	400 x 2 (b.i.d.)	0.02-3.4 <sup>+</sup>	9.4	ND	P-gp and Bcrp substrate	(Agarwal et al., 2011c)
Axitinib	VEGFR inhibitor	5mg x 2 (b.i.d.)	ND	Less than 10%	ND	P-gp and Bcrp substrate	(Poller et al., 2011)

\* Total drug concentrations are reported <sup>#</sup>Unpublished data + in non-human primate

**CHAPTER 3 THE POTENTIAL FOR PROFOUND  
EFFICACY OF THE MDM2 INHIBITOR SAR405838 IN  
GLIOBLASTOMA IS LIMITED BY POOR DISTRIBUTION  
ACROSS THE BLOOD-BRAIN BARRIER**

The content of this chapter has been published in:

Kim, M., Ma, D. J., Calligaris, D., Zhang, S., Feathers, R. W., Vaubel, R. A., ... & Barriere, C. (2018). Efficacy of the MDM2 inhibitor SAR405838 in glioblastoma is limited by poor distribution across the blood-brain barrier. *Molecular cancer therapeutics*, molcanther-0600.

### 3.1 INTRODUCTION

Individualized medicine approaches based on next-generation sequencing (NGS) could significantly improve the dismal outcome for the most common and aggressive primary brain tumor, glioblastoma (GBM). (Vitucci et al., 2011) However, the majority of targeted agents exhibit limited partitioning into the brain, which could limit efficacy, especially given the invasive nature of GBM. (Deeken and Loscher, 2007; Doolittle et al., 2007; Gerstner and Fine, 2007; Agarwal et al., 2011c; Parrish et al., 2015c) While essentially all GBM exhibit some accumulation of radiographic contrast on clinical imaging, whether contrast enhancement translates into meaningful drug accumulation remains uncertain. (Iqbal et al., 2011) Furthermore, image-guided surgical biopsy studies also demonstrate that most patients have significant tumor burden outside of contrast-enhancing regions. (Pafundi et al., 2013) Therefore, the focus of this study was to evaluate the influence of BBB integrity on the efficacy of a molecularly-targeted agent with limited brain penetration.

Disruption of the p53 tumor suppressor pathway occurs in the majority of GBM and is driven by amplification of the *murine double minute 2* (*MDM2*) locus in approximately 14% of patients. (2008) MDM2 is known to be a major regulator of p53, by targeting p53 for degradation mainly through its intrinsic E3 ubiquitin ligase. As a result, high MDM2 expression can effectively suppress p53 expression and activity. (Wade et al., 2013) Reactivation of p53 can be achieved through diverse pharmacologic strategies, including: suppression of MDM2 expression, inhibition of E3 ubiquitin ligase activity, or inhibition of the p53-MDM2-proteasome

interaction, with the latter approach favored by the current generation of MDM2 inhibitors.(Hu et al., 2007; Liu et al., 2010; Villalonga-Planells et al., 2011) Among small molecule MDM2 inhibitors, SAR405838 is clinically advanced in that it is in phase one clinical trials. SAR405838 has a high MDM2 selectivity, with a  $K_i$  of 0.88 nM, and evidence of anti-tumor activity in a variety of tumor types.(Wang et al., 2014) The studies reported herein were designed to assess the potential use of SAR405838 in *MDM2*-amplified GBM to further the clinical development of a precision medicine strategy.

## **3.2 MATERIALS AND METHODS**

### **3.2.1 Cell culture, drugs, and apoptosis**

Short-term explant cultures were obtained from a primary, patient derived glioblastoma panel and were grown in neurobasal media (Life Technologies) as previously described.(Kitange et al., 2012; Nadkarni et al., 2012) Cell authentication was performed using STR profiling last performed on 4/5/2015. Neurosphere formation and Cyquant proliferation assays were performed as previously described.(Kitange et al., 2012) SAR405838 was obtained from Sanofi (Vitry-sur-Seine, France). Annexin-V assays were performed as previously described.(Maddika et al., 2011)

### **3.2.2 TP53 gene Sequencing**

Purified genomic DNA (50 ng) was PCR amplified in a 25  $\mu$ l PCR reaction using primers that were designed to flank exons 4-8 of TP53 gene. Primer sequences are available in Supplemental Materials. The products were then

submitted to Mayo Clinic Sequencing facility for Sanger sequencing. Mutations were detected using Mutation Surveyor software V4.0.9 (Softgenetics, State College, PA).

### 3.2.3 **MDM2 Amplification and RNA expression**

DNA and RNA was extracted from 20 mg of frozen flank tumor using the Qiagen Puregene Core Kit A (Cat# 158667) and the Qiagen RNeasy Mini Kit (Cat# 74106), then quantitated on a Nanodrop 2000. Three tumor samples were used per GBM line. Primer sequences are available in Supplemental Materials.

### 3.2.4 **Real-Time PCR assays**

Total RNA was extracted with the RNeasy kit (Qiagen) according to manufacturer's instructions and cDNA was synthesized using the High Capacity cDNA Reverse Transcription kit (Applied Biosystems). TaqMan gene expression assays were performed by using MDM2 (Hs99999008-m1), p21 (Hs00355782-m1), PUMA (Hs00248075) gene-specific primer/probe sets (Applied Biosystems) for real-time PCR amplification in an Applied Biosystems 7900 thermocycler. RPL37a was used for normalization using probes and primers from Applied Biosystems. Relative quantification of mRNA was calculated by comparative cycle threshold ( $\Delta\Delta C_t$ ) method.

### 3.2.5 **Efficacy studies *in vivo***

All animal studies were approved by the Mayo Institutional Animal Care and Use Committee. Subcutaneous xenografts were established by injecting the flank of athymic nude mice with  $1 \times 10^6$  cells suspended in Matrigel/PBS. When

established tumors reached 150-250 mm<sup>3</sup> in size, mice were randomized and treated by oral gavage with placebo vehicle (98% PEG200 : 2% TPGS) or SAR405838 (50 mg/kg per day). Tumor volume was measured thrice weekly until euthanasia. To prepare cells for orthotopic models, flank tumor xenografts were harvested, mechanically disaggregated, and grown in short-term cell culture (5-14 days) in DMEM supplemented with 2.5% fetal bovine serum, 1% penicillin, and 1% streptomycin. Cells were harvested by trypsinization and injected ( $3 \times 10^5$  or  $1 \times 10^6$  cells per mouse, suspended in 10  $\mu$ L) into the right basal ganglia of anesthetized athymic nude mice (athymic Ncr-nu/nu, National Cancer Institute, Frederick, MD) using a small animal stereotactic frame (ASI Instruments, Houston, TX) as previously described. (Gupta et al., 2014) Mice were observed daily and euthanized upon reaching a moribund state. For pharmacodynamic assessment, tumors were harvested at 24 hours after the last drug dose.

### **3.2.6 Brain-to-plasma ratio for SAR405838.**

*In vivo* brain-to-plasma ratios were determined in Friend leukemia virus strain B (FVB) wild-type mice of either sex from an FVB genetic background (Taconic Farms, Germantown, NY). Five mice in each genotype were orally dosed with 25 mg/kg SAR405838 using the same vehicle as was used in the efficacy studies. Animals were euthanized using a CO<sub>2</sub> chamber 1 hr after dosing. Blood was collected by cardiac puncture in heparinized tubes and plasma was separated after centrifugation at 3500 rpm for 15 min at 4°C. Whole brain was harvested at the same time as the blood collection. Samples were analyzed by a Micromass

Quattro Ultima mass spectrometer coupled with AQUITY UPLC system (Waters, Milford, MA).

### **3.2.7 VEGFA over-expression**

GBM108 cells were transduced with either an empty vector (LV197, Genecopoeia Inc, Cat# EX-NEG-Lv197) or a vector containing VEGFA transcript variant 4 (NM\_001171626.1, Cat# EX-Z0781-Lv197) as previously described.(Cen et al., 2012)

### **3.2.8 VEGFA ELISA**

Cell lysates from GBM108 parental, GBM108 empty vector, and GBM108 VEGFA transfected cells were harvested with 1% Triton X in DPBS (Hyclone®, GE Life Sciences, Logan, Utah) after rinsing with ice cold DPBS. Total cell protein was quantified by the Pierce® BCA protein assay kit (Thermo Scientific). A human VEGF Quantikine ELISA kit (R&D Systems, Minneapolis, MN) was used to quantify VEGFA expression in the culture supernatant. Levels of VEGFA expression were normalized to total cell protein in corresponding wells. The three lines were compared using one-way ANOVA followed by Bonferroni's test for multiple comparisons.

### **3.2.9 TUNEL Staining**

Apoptosis was analyzed by using an ApopTag® Plus peroxidase in situ apoptosis detection kit (S7101, Millipore). GBM108 cells were injected to the mouse flank (n=10). Mice were randomized into 2 groups of 5 mice when the tumor reached 250-400 mm<sup>3</sup>. The placebo group was dosed daily with vehicle,



and treatment group was dosed daily with SAR405838, 50 mg/kg, for 5 days. Tumors were harvested on the fifth day 2 hours after last dose of drug and flash frozen. Tumors were formalin-fixed, paraffin embedded, and sliced at a thickness of 5  $\mu\text{m}$  for staining. Bright field images were acquired using a Leica DMI6000B inverted microscope at 40X. Six images were taken for each tumor and apoptotic cells/bodies were counted blinded with respect to the treatment groups.

### **3.2.10 Texas Red Imaging to Evaluate BBB Integrity**

Tumor-bearing mice were injected with 3kD dextran conjugated with Texas Red (Molecular Probes®, Thermo Fisher Scientific) in the tail vein 10 min before CO<sub>2</sub> euthanasia. Whole brain was harvested after cardiac perfusion with room temperature 4% PFA in saline. The brain was frozen on dry ice and stored at -80°C. Cryostat sections of 20  $\mu\text{m}$  were obtained at -21°C (Leica 3050S), mounted on glass slides and stored at -20°C before imaging. Whole brain slices were imaged using a Nikon AZ100M macroscope at 16X and Nikon software compiled individual images. All slides were imaged on the same day using 400 ms exposure and cresyl violet staining was done to locate the tumor for comparison.

### **3.2.11 Preclinical MRI acquisition and analysis**

MRI was performed using a Bruker DRX-300 (300 MHz 1H) 7 Tesla vertical-bore small animal imaging system (Bruker Biospin, Billerica, MA) according to published protocols.(Renner et al., 2015; Renner et al., 2016) Throughout imaging, mice were anesthetized by inhalation of 3–4% isoflurane in air and their respiratory rate monitored. For T1 weighted imaging, mice were administered

gadolinium contrast (Gadavist 1mM, Bayer, Whippany NJ) intraperitoneally (i.p.) at a dose of 100 mg/kg and imaged after a 15-minute delay.

### 3.2.12 MALDI MSI

Mass spectra of mouse brain tissue sections were acquired using a SolariX XR Fourier transform ion cyclotron resonance mass spectrometer (FT-ICR) (12 T) (Bruker Daltonics, Billerica, USA). MALDI MSI experiments were acquired with a pixel step size for the surface raster set to 80  $\mu$ m in FlexImaging 4.0 software (Bruker Daltonics, Billerica, USA). The analyses were performed in positive ion mode by continuous accumulation of selected ions (CASI) in a mass range comprised between m/z 440-620 and a laser intensity set to 40%. Each mass spectrum is the sum of 250 laser shots randomized over 10 positions within the same spot (25 shots/position) at a laser frequency of 1000 Hz. The MALDI images were displayed using FlexImaging 4.0. The permeability of SAR405838 through the blood vessel was visualized following the signal of the drug (m/z 562.2034  $\pm$  0.001) and a biomarker of vasculature (heme at m/z 616.1768  $\pm$  0.001), as previously described.(Liu et al., 2013) Gadavist was visualized following the signal of one of the isotopologue peaks of the contrast agent at m/z 606.1409  $\pm$  0.001.

### 3.2.13 Immunohistochemistry and quantitative analysis

Staining for human p21 was performed using a rabbit monoclonal antibody 12D1 (Cell Signaling Technology, Danvers, MA) followed by hematoxylin counterstaining. p21 positivity was determined by adapting the Aperio IHC Nuclear

Image Analysis algorithm, which uses color de-convolution to separate the DAB (positive) from hematoxylin (negative) signals, to the nuclei staining patterns and shapes present in these samples. The percent of all stained nuclei that were positive for the DAB chromogen as a marker of p21 was quantitated.

#### 3.2.14 **Statistical analyses**

*In vitro* data presented are the mean  $\pm$  SE from three or more experiments. Two-tailed Student t tests and one-way ANOVA were used to measure statistical differences. *P*-values  $<0.05$  were considered statistically significant. Statistical analysis of animal survival and tumor progression was performed using the log-rank test.

### 3.3 RESULTS

#### 3.3.1 *In vitro* efficacy of SAR405838

The Mayo Clinic has developed a large panel of GBM patient-derived xenograft (PDX) models, and to identify the most relevant models for studying an MDM2 inhibitor, a series of studies were used to select models for further analysis. Initially, 55 PDX models were evaluated for *MDM2* amplification by qPCR, *MDM2* transcript expression by qRT-PCR, and then selected models were evaluated for p53 mutation status by Sanger sequencing (Fig. S1). From these studies, 5 lines were selected for subsequent *in vitro* testing (Fig. 1A): two without *MDM2* transcript over-expression (GBM10, p53 wild-type; GBM12, p53 mutant), one with *MDM2* amplification but without over-expression (GBM102), and two with *MDM2* amplification and over-expression (GBM108, GBM143). The dose response curves for SAR405838 in these tumor lines were obtained by *in vitro* neurosphere formation and CyQuant assay to determine potency. SAR405838 had the best potency in GBM108 (figure S5). Treatment with 100 nM SAR405838 significantly reduced neurosphere formation in all 4 wild-type p53 tumor lines, but the reduction in neurosphere formation was significantly more profound in the *MDM2* amplified/over-expressing GBM108 ( $5.8 \pm 1.2\%$  relative to control) and GBM143 ( $6.4 \pm 6.1\%$ ) lines as compared with GBM10 ( $44.6 \pm 6.2\%$ ) and GBM102 ( $33.6 \pm 17.1\%$ ) lines without *MDM2* transcript over-expression (Fig. 1B). In an evaluation of apoptosis induction, SAR405838 treatment was associated with a significantly increased fraction of Annexin V-positive cells, relative to control, only in GBM108 ( $41.5 \pm 9.4\%$  vs  $9.4 \pm 2.3\%$   $p < 0.0001$ ) and GBM143 ( $23.9 \pm 9.8\%$  vs

9.8±2.0% p=0.003) cells (Fig. 1C). Consistent with robust disruption of MDM2 activity, 24 hour exposure to 100 nM SAR405838 resulted in marked induction of p53 transcriptional targets PUMA and p21 (Fig. 1D). In conjunction with previously published studies, these data support a model in which SAR405838 achieves cytotoxicity in MDM2 over-expressing tumors through restored p53 function and subsequent apoptosis.(Hoffman-Luca et al., 2015)

### 3.3.2 *In vivo* efficacy of SAR405838

The efficacy of SAR405838 was evaluated in a series of flank and intracranial *in vivo* studies. Consistent with the *in vitro* results, SAR405838 induced tumor regression and uniformly suppressed growth of GBM108 flank tumors for over 6 weeks of therapy (50 mg/kg p.o. qd until euthanasia, Fig. 2A), while drug treatment was ineffective in GBM102 flank tumors (Fig. 2B). This regimen was well-tolerated for the entire treatment course. The average weight of the mice at the end of treatment was 106±4% of the beginning weight. In the sensitive GBM108 model, SAR405838 treatment for 5 days resulted in a 21-fold increase in p21 transcript expression and a 7-fold increase in PUMA expression 24 hours after drug treatment (Fig. 2C) and a three-fold increase in apoptosis relative to placebo treatment, as measured by TUNEL-positivity (Fig. S2). In contrast to the profound efficacy observed in flank models, the same SAR405838 dosing regimen was completely ineffective in GBM108 grown as orthotopic tumors (Fig. 2D), which were established at the same time as the GBM108 flank study. Drug delivery to orthotopic tumors might be limited by a partially intact BBB, and consistent with this concept, limited intratumoral accumulation of a BBB-impenetrant Texas Red-

3 kD dextran conjugate was observed in orthotopic GBM108 tumors (Fig. S3). Moreover, measurement of SAR405838 drug distribution into the brain demonstrated the brain-to-plasma ratio for SAR405838 was  $0.01 \pm 0.003$  post 1 hr after single oral dosing in non-tumor bearing mice. Overall, these data suggest that restricted partitioning across a partially intact BBB in orthotopic tumors might limit SAR405838 efficacy in an otherwise highly responsive tumor model.

### 3.3.3 Imaging of BBB integrity

The influence of limited drug delivery across the BBB on treatment efficacy was tested by manipulating the integrity of the tumoral BBB. VEGFA is a pro-angiogenic cytokine that drives the development of an immature, leaky vasculature within GBM, and previous studies have used exogenous delivery of VEGFA to disrupt the BBB.(Dobrogowska et al., 1998; Proescholdt et al., 1999; Argaw et al., 2012) Therefore, we used a lentiviral expression system to over-express VEGFA in GBM108 (GBM108-VEGFA; Fig. S4). Importantly, VEGFA over-expression did not meaningfully change the *in vitro* SAR405838 sensitivity of GBM108-VEGFA cells as compared to empty vector transduced GBM108-Vector cells (Fig. S5). Using these two GBM108 sub-lines, the impact of VEGFA over-expression on BBB integrity was evaluated by injecting mice 10 minutes prior to euthanasia with a TexasRed-3 kD dextran conjugate that only accumulates in brain regions with a physically disrupted BBB. Following sectioning and subsequent processing for fluorescence microscopy, this allows a visual evaluation of BBB integrity that is inversely related to red fluorescent intensity. Consistent with limited disruption of the BBB in the parental PDX model (Fig. S3), faint and heterogeneous red

fluorescence is apparent in GBM108-Vector orthotopic tumors (Fig. 3A). In contrast, the BBB within GBM108-VEGFA tumors was markedly disrupted with brighter and homogeneous red fluorescence across the intra-cranial tumors. Magnetic resonance imaging (MRI) also provides a sensitive measure of BBB deregulation in brain tumors. Even minimal disruptions of the BBB can result in increased fluid accumulation within tissues that can be readily detected on T2-weighted image sequences, and T1-weighted imaging sequences are highly sensitive for detecting accumulation of paramagnetic gadolinium contrast agents, which do not cross an intact BBB. In this context, mice with orthotopic tumors with either GBM108 sub-lines were subjected to MR imaging (Fig. 3B). Consistent with clinical imaging of GBM, orthotopic GBM108-Vector tumors were evident on T2- and T1-post contrast MR images, and consistent with greater disruption of the BBB, the tumor-associated T2- and T1-signals were more evident in the GBM108-VEGFA tumors. Collectively, these data demonstrate that GBM108 tumors have a partially intact BBB that is markedly more disrupted in association with VEGFA over-expression.

The marked disruption of the BBB in GBM108-VEGFA, as compared to the isogenic GBM108-Vector model, provides a platform for evaluating the potential impact of the BBB on imaging, drug delivery, and efficacy in GBM. Accordingly, gadolinium-based contrast (Gadavist) and SAR405838 distribution into orthotopic tumors were evaluated using matrix-assisted laser desorption/ionization mass spectrometric imaging (MALDI MSI) (Fig. 3C). Mice with established GBM108-VEGFA (n=3) or GBM108-Vector (n=3) orthotopic tumors were euthanized after a

single Gadavist and SAR405838 dose and processed for histologic sectioning and MALDI MSI. As suggested by T1-post contrast imaging, both GBM108-Vector and GBM108-VEGFA demonstrated intratumoral Gadavist distribution on MALDI MSI with Gadavist distribution in GBM108-VEGFA being appreciably higher. Consistent with the limited efficacy of SAR405838 in parental GBM108 orthotopic tumors, SAR405838 accumulation within GBM108-Vector was relatively low and highly heterogeneous (Figs. 3C and S6). In contrast, accumulation of SAR405838 in orthotopic GBM108-VEGFA was much higher and more homogeneous throughout the tumor.

#### 3.3.4 Effect of SAR405838 brain penetration on efficacy

Effective suppression of MDM2-p53 interaction should promote p53 signaling, and consistent with this expected pharmacodynamic effect on the p53 transcriptional target p21, daily SAR405838 dosing for 4 days in orthotopic GBM108-VEGFA resulted in an 11.3-fold increase in the fraction of p21-positive nuclei (Fig. 4A, p21-positive nuclei:  $3.2 \pm 0.2\%$  with placebo versus  $34.8 \pm 3.9\%$  with SAR405838 treatment;  $p=0.0002$ ). In comparison, SAR405838 dosing in orthotopic GBM108-Vector only resulted in a 2-fold increase in p21 staining (Fig. 4B,  $13.2 \pm 0.6\%$  versus  $26.1 \pm 6.7\%$ ;  $p=0.006$ , respectively). Finally, the influence of enhanced drug delivery on treatment efficacy was evaluated in both GBM108 sub-lines. SAR405838 treatment had limited impact, even though it was statistically significant ( $p=0.002$ ), on survival in GBM108-Vector tumors with a 7.5 day increase in median survival prolongation when compared to placebo (Figure 4C). In contrast, SAR405838 treatment was markedly more effective in GBM108-



VEGFA tumors with a 45 day prolongation in median survival as compared to placebo treatment ( $p < 0.0001$ ) (Figure 4D). This observed increase in efficacy in the VEGFA-secreting tumors was even more remarkable in light of the fact that the VEGFA tumors had a more aggressive growth pattern (the median survival of GBM108-VEGFA placebo group and GBM108-Vector placebo group were 32 and 45 days, respectively), undoubtedly due to the stimulation of angiogenesis in the tumor. (Claffey and Robinson, 1996; Weathers and de Groot, 2015) While differences in the micro-environment associated with VEGFA expression cannot be completely discounted, these data strongly suggest that limited drug distribution across a relatively intact BBB in the parental GBM108 patient-derived xenograft model critically limits the efficacy of SAR405838

### 3.4 DISCUSSION

The vital role of MDM2 in regulating p53 function makes MDM2 inhibitors an attractive drug class for further exploration and clinical development. MDM2 inhibitors demonstrate efficacy in a variety of cell types and at least seven novel agents are currently undergoing phase I investigation for several solid tumors.(Bill et al., 2015; Deben et al., 2015; Hai et al., 2015) This study joins a growing body of literature suggesting that MDM2 inhibition also represents a promising therapeutic strategy for a sub-population of GBM.(Chen et al., 2015; Verreault et al., 2015; Daniele et al., 2016) Here we demonstrate that the MDM2 inhibitor SAR405838 can induce the expression of downstream p53 targets PUMA and p21 in p53 wild-type/MDM2 over-expressed GBM lines. SAR405838 treatment results in increased apoptosis and a reduction in neurosphere formation in sensitive lines. *In vivo* flank experiments demonstrate both increased apoptosis and profound suppression of tumor volume with SAR405838 treatment in a sensitive line (GBM108), suggesting a cytotoxic mechanism. However, little efficacy was seen in an MDM2-amplified, p53 wild-type line without MDM2 over-expression (GBM102), suggesting that MDM2 amplification is an insufficient biomarker for treatment sensitivity. Further work is required to define biomarkers for treatment sensitivity as this study and others show that the p53 wild-type / MDM2 amplified genotype can have heterogeneity in MDM2 inhibitor sensitivity.(Zhang et al., 2016) This study also highlights the critical role of drug delivery in the successful application of targeted therapy for GBM. We demonstrate that MDM2 inhibition can have profound efficacy in appropriately selected GBM, but limited drug delivery

across the BBB may severely restrict the intracranial efficacy of SAR405838. Disruption of the BBB through VEGFA overexpression results in both markedly increased intra-tumoral accumulation of SAR405838 and increased p21 expression when compared with the empty vector control. Mice with BBB-disrupted tumors also experienced a survival benefit with SAR405838 treatment while mice with mostly BBB-intact tumors derived no benefit from treatment. Considering the fact that G108-VEGFA tumors are intrinsically more virulent compared to G108-Vector due to the effect of VEGFA expression on angiogenesis and hence on glioblastoma growth, the survival benefit that we have seen here is even more pronounced with SAR405838 treatment.(Claffey and Robinson, 1996; Weathers and de Groot, 2015) These data suggest that small-molecule MDM2 inhibitors may have profound efficacy in appropriately selected patients only if a sufficiently brain-penetrant agent can be identified. Similar correlations with limited brain penetration for otherwise highly effective drugs suggest that this may be a generalizable phenomenon.(Vaidhyanathan et al., 2014; Becker et al., 2015a; Parrish et al., 2015a; Parrish et al., 2015b; Pokorny et al., 2015)

Interestingly, relatively BBB-intact tumors in our study maintained visible levels of contrast enhancement on T1-weighted MR imaging despite the lack of significant drug accumulation on MALDI MSI. Though contrast enhancement does indicate a certain degree of BBB disruption, patient biopsy studies of contrast enhancing brain regions following repeated MR scans demonstrate that elemental concentrations of gadolinium as small as 0.3  $\mu\text{g}/\text{mg}$  (1.9 nM) are sufficient to generate T1 signal changes.(McDonald et al., 2015; Radbruch et al., 2015;

Ramalho et al., 2015; Robert et al., 2015; Weberling et al., 2015) Making the assumption that targeted agents have similar CNS distribution characteristics as gadolinium, such low concentrations are often below the threshold required for clinical activity. This work seriously calls into question the likely misguided notion that contrast enhancement as seen on clinical imaging equates with pharmacologically meaningful drug accumulation of brain impenetrant agents, such as SAR405838, in GBM.(Boult et al., 2016) Even in regions of contrast enhancement, drug delivery into GBM may be limited by a heterogeneously intact BBB, significantly limiting the efficacy of drug treatment.

Issues with brain-penetration for targeted therapies also extend to therapy for brain metastases. Individualized medicine approaches based upon targeted therapies have improved systemic disease control in appropriately selected cancer types including melanomas with BRAF V600E mutations, non-small cell lung cancer (NSCLC) with EML4-ALK fusions, and colon cancer with wild-type KRAS. Despite these successes in controlling peripheral disease, CNS metastases remain a substantial problem. Upwards to 60% of NSCLC patients develop CNS metastases while on crizotinib treatment, while treatment with trastuzumab in HER2+ breast cancer is associated with a 35% increase in relative risk of CNS metastases.(Olson et al., 2013; Rangachari et al., 2015) The likely cause of such isolated CNS failure is poor penetration of the BBB by these targeted agents.(Shi and Dicker, 2016) As peripheral disease control improves with new therapies, strategies for decreasing CNS disease burden may become the primary driver for overall survival.

Thus far, no phase III clinical trials utilizing targeted agents in GBM have resulted in improved overall survival. Given that many of these agents have limited BBB permeability(Agarwal et al., 2011b), our results suggest that selection of a drug with optimal brain distribution is a critical consideration in designing and implementing future trials using targeted agents in the context of precision medicine strategies for GBM.

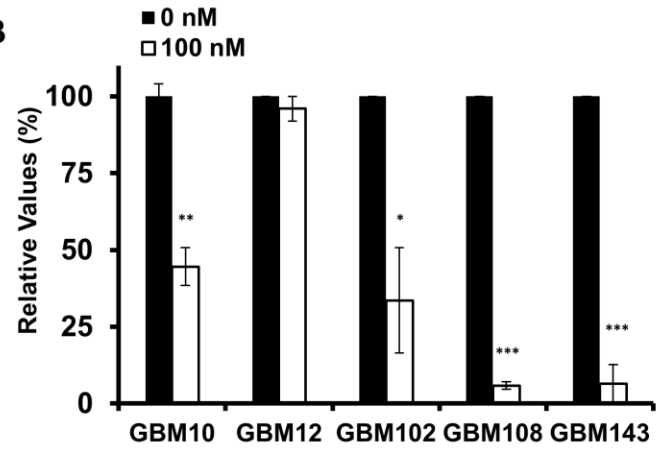
### Figure 3.1 Characteristics of selected PDX GBM lines

**A)** Summary of MDM2 amplification, expression, and p53 status for select xenograft lines. **B)** Relative values of tumor growth with the treatment of SAR405838 (100 nM) compared to controls are measured either neurosphere formation or CyQuant (CyQuant measurement for GBM108). SAR405838 (100 nM) has higher inhibition in MDM2 over-expressed, p53 WT lines (GBM108, GBM143) when compared to MDM2-low lines (GBM10, 12, 102). GBM102 has MDM2-amplification but not over-expression. **C)** SAR405838 (0 nM black, 100 nM grey) induces more apoptosis by Annexin V at 72 hrs in MDM2 over-expressed lines (GBM108, GBM143) when compared to MDM2-low lines (GBM10, GBM102). **D)** Relative transcript expression of p21 and PUMA. Short-term explant cultures were treated with vehicle or 100 nM SAR405838 and then processed for qRT-PCR. Results represent the mean  $\pm$  SE with p-values for p21 (top) and PUMA (bottom). \*  $P < 0.05$ , \*\*  $P < 0.01$ , \*\*\*  $P < 0.001$ .

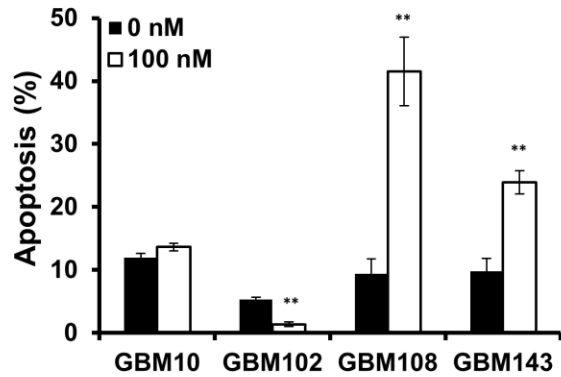
**A**

GBM Line	MDM2 amplification	MDM2 expression	p53 status
10	no	low	wildtype
12	no	low	mutant
102	yes	low	wildtype
108	yes	high	wildtype
143	yes	high	wildtype

**B**



**C**



**D**

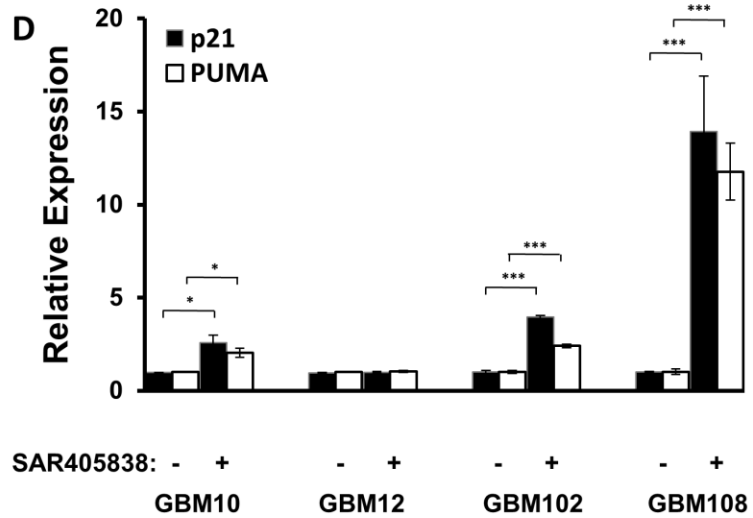


**Figure 3.2 *In vivo* efficacy of SAR405838 in heterotopic and orthotopic models of GBM108**

**A, B)** Average flank tumor volume of surviving mice in placebo (black, n=7) vs. SAR405838 at 50 mg/kg p.o. qd until euthanasia (grey, n=8). Solid arrows at treatment start date. Mice were euthanized once tumor exceeded 1800 mm<sup>3</sup>. **C)** *In vivo* (flank) expression of p21 and PUMA is increased at 24 h after SAR405838 (50 mg/kg) in GBM108 but not GBM102. **D)** SAR405838 at the same dosing regimen does not demonstrate efficacy in an orthotopic model of GBM108. (Placebo : black (n=12), Treated : grey (n=11)) \*  $P < 0.05$ , \*\*  $P < 0.01$ , \*\*\*  $P < 0.001$ .



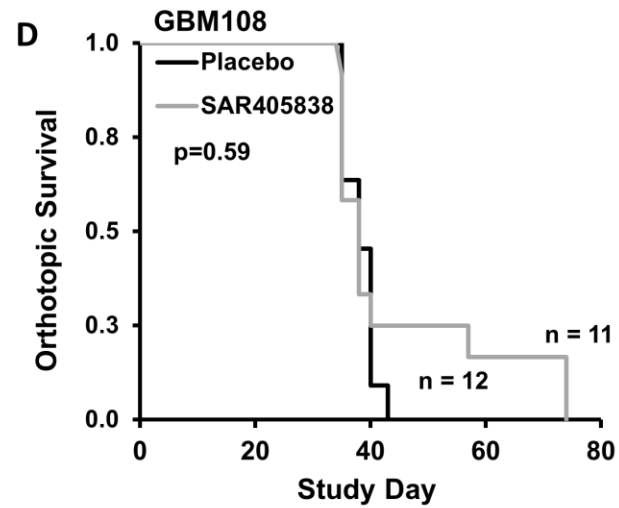
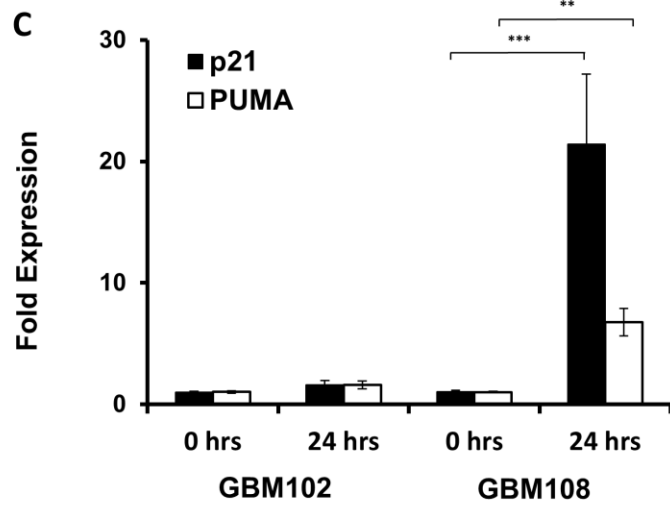
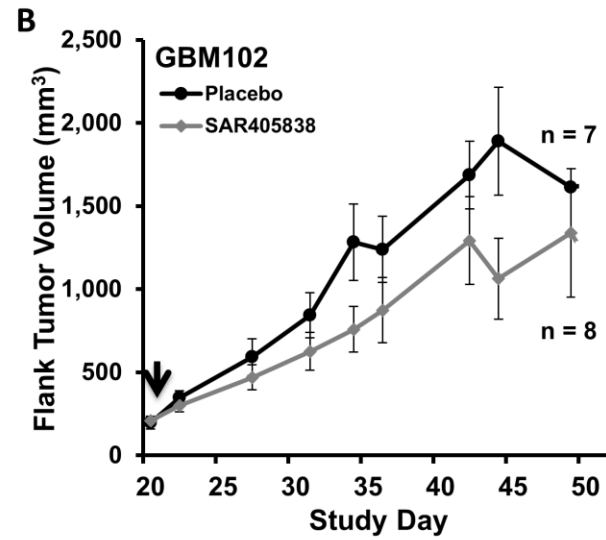
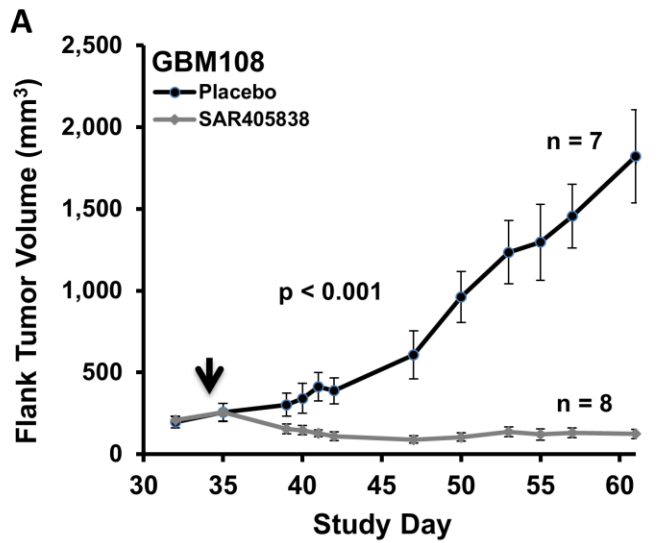
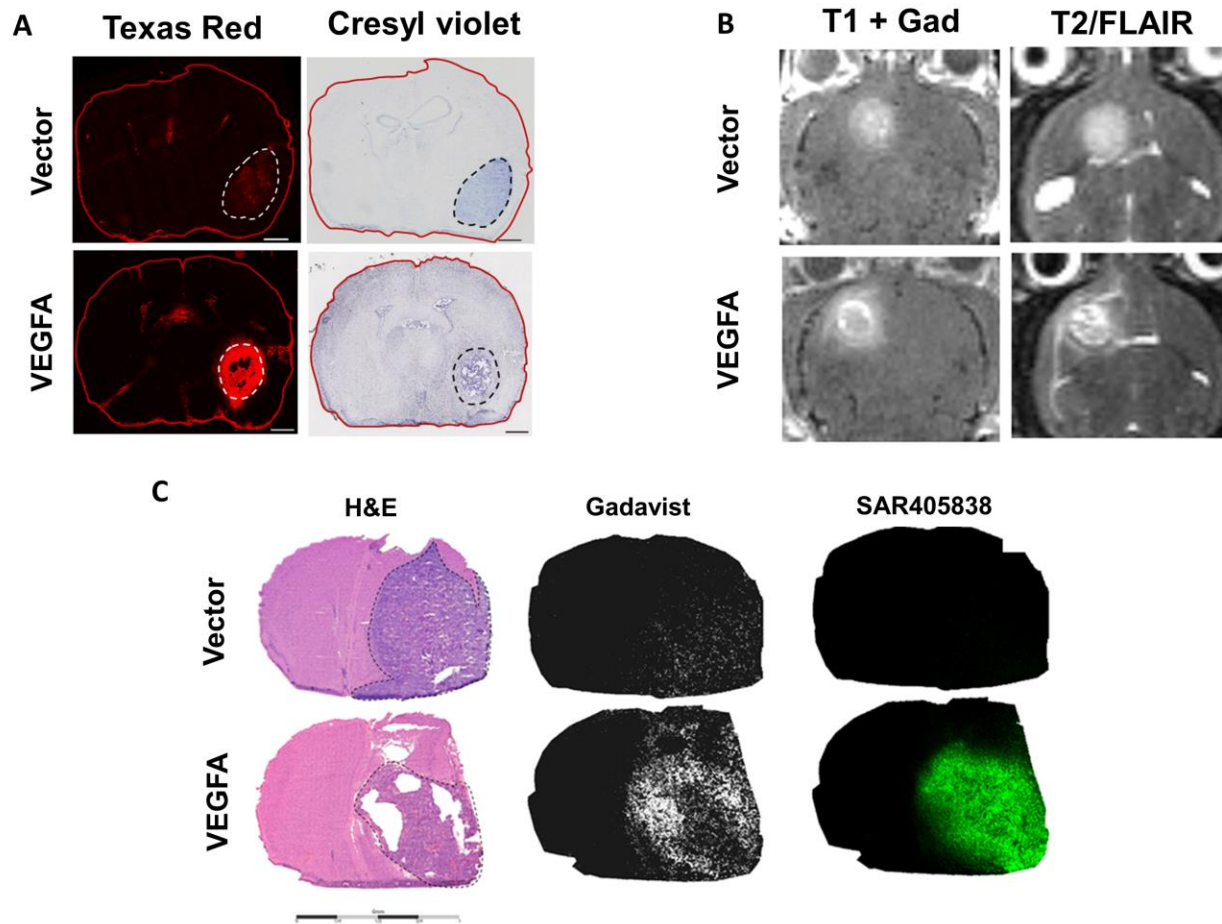


**Figure 3.3 BBB permeability and distribution of SAR405838 in GBM108-Vector and GBM108-VEGFA**

**A)** Comparison of BBB permeability to Texas Red Dextran in GBM108-Vector and GBM108-VEGFA (scale bar = 1000 um) **B)** Contrast enhancement on MRI for GBM108-Vector and GBM108-VEGFA **C)** Comparison of H&E staining in GBM108-Vector and GBM108-VEGFA with MALDI mass spectrometry imaging for Gadavist and SAR405838.

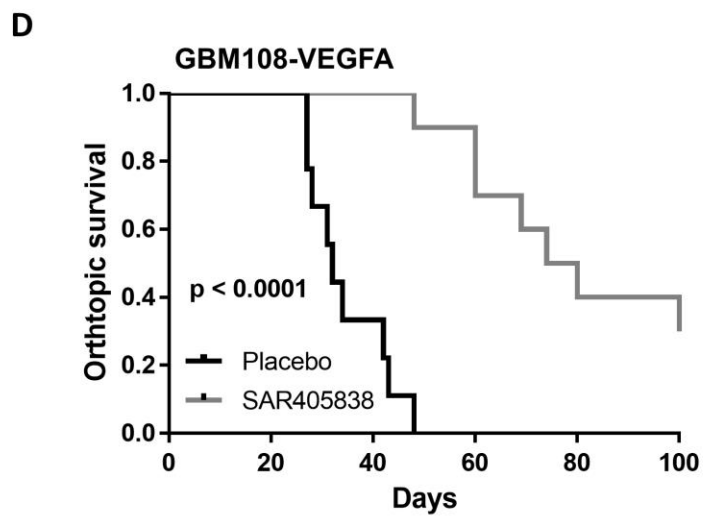
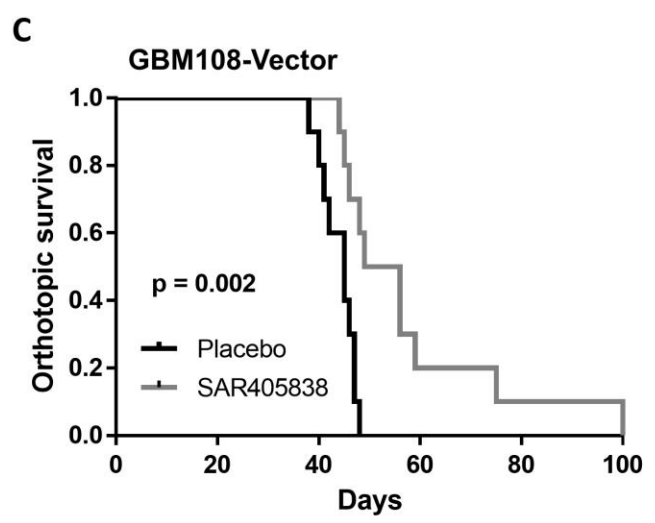
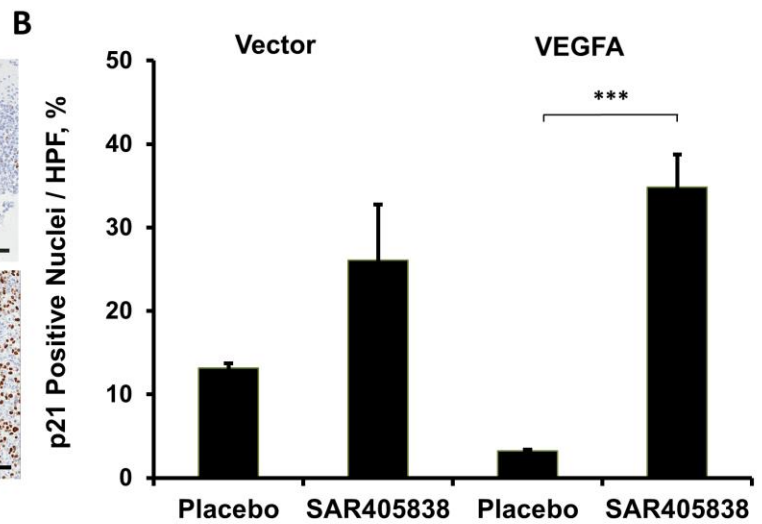
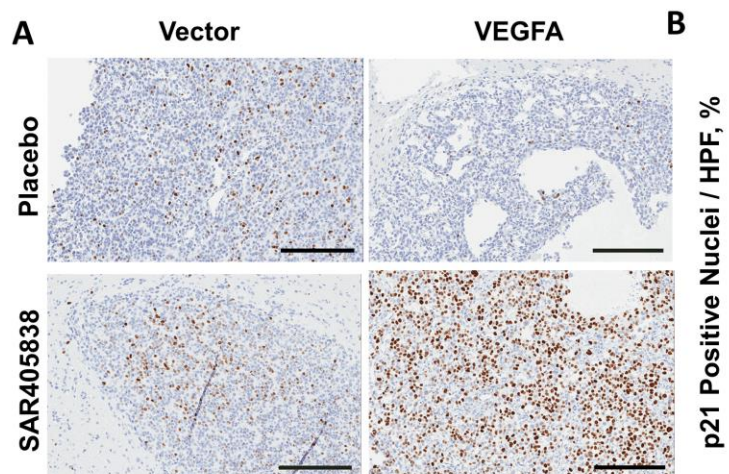
Dotted lines on the H&E stained section images delineate GBM108-Vector and GBM108-VEGFA tumors.

Figure 3.3 continued



### Figure 3.4 Improved pharmacodynamic response and orthotopic survival in GBM108-VEGFA

**A)** p21 expression in GBM108-Vector and GBM108-VEGFA after SAR405838 treatment in orthotopic tumors (scale bar = 200  $\mu$ m). **B)** Quantitation of SAR405838 effect on p53 signaling. Mice with established orthotopic tumors were treated with SAR405838 or placebo and then processed for p21 IHC. The percentage of p21-positive nuclei per high powered field in GBM108-Vector versus GBM108-VEGFA after placebo or SAR405838 (5 mice per group) are presented as mean  $\pm$  standard deviation. **C, D)** Orthotopic survival, GBM108-Vector (n=10 per group) vs GBM108-VEGFA (n=9 for placebo and n=10 for the treatment group). SAR405838 was dosed at 50 mg/kg p.o. qd until moribund. \*  $P<0.05$ , \*\*  $P<0.01$ , \*\*\*  $P<0.001$ .



**CHAPTER 4**

**BRAIN DISTRIBUTIONAL KINETICS OF A NOVEL MDM2**

**INHIBITOR SAR405838: IMPLICATIONS FOR USE IN**

**BRAIN TUMOR THERAPY**

## 4.1 INTRODUCTION

The tumor suppressor p53 has been an attractive target in cancer therapeutics due to its crucial role in tumorigenesis (Hainaut and Hollstein, 2000; Vogelstein et al., 2000). The signaling pathway of p53 is found to be inactivated in various types of human cancers, often without a gene mutation in p53 itself (Wade et al., 2013). Therefore, it was a challenge to find ways to reactivate this protein in tumor cells for therapeutic purposes, until the role of the oncoprotein murine double minute 2 (MDM2) was discovered (Momand et al., 1992; Finlay, 1993). MDM2 has been identified as a major negative regulator of p53 by either direct binding or ubiquitination leading to degradation (Momand et al., 2000; Wade et al., 2013). MDM2 is often amplified or overexpressed in various tumors, which leads to cancer development by downregulating p53 (Wade et al., 2013). Therefore, reactivation of p53 in tumors by the use of small molecule antagonists that target the interaction between MDM2 and p53 has been investigated as a novel molecularly-targeted therapy for various cancers.

Currently there are several small molecule MDM2 antagonists under clinical investigation for various solid tumors. One of these, SAR405838 (Figure 1), is a potent inhibitor that has high selectivity and affinity to MDM2 ( $K_i = 0.88$  nM) (Wang et al., 2014). A previous study from our group has shown that SAR405838 was highly efficacious in a patient-derived xenograft (PDX) model of glioblastoma (GBM) both *in vitro* and in heterotopic tumor implanted subcutaneously in the flank (Kim et al., 2018b). However, SAR405838 showed a lack of efficacy against an orthotopic tumor model, where the tumor was

implanted intracerebrally. We conclude that this is likely due to limited delivery of SAR405838 to the tumor in the brain (Kim et al., 2018b). Interestingly, the *in vivo* orthotopic efficacy of SAR405838 was shown to be significantly increased in a tumor line where the BBB was disrupted by the overexpression of vascular endothelial growth factor A (VEGFA) (Kim et al., 2018b). These data indicate that the brain distribution of this MDM2 inhibitor is a crucial factor in limiting treatment efficacy for infiltrative brain tumors, such as GBM (Sarkaria et al., 2018). Therefore, it is critical to understand the mechanisms that limit SAR405838 entry into the brain at an intact BBB. Clearly, adequate SAR405838 exposure in the brain depends on both systemic pharmacokinetic properties and distribution across the BBB, exemplified by SAR405838 efficacy in the PDX model of GBM dependence on the brain delivery of the compound (Kim et al., 2018b).

Brain distribution of many agents is often limited by the blood-brain barrier (BBB), which is characterized by tight and adherens junctions, that blocks the intercellular pathway for small molecules, and by expression of efflux transporters, that limit transcellular transport. Many of the molecularly targeted anti-cancer therapeutics are not able to penetrate the BBB, and are subject to these active efflux transporters, including P-glycoprotein (P-gp) and breast cancer resistance protein (Bcrp). P-gp and Bcrp are highly expressed active efflux transporters at the BBB of the mouse (Agarwal et al., 2012) and human (Uchida et al., 2011). How these transporters influence the brain delivery of SAR405838 is critical in understanding the delivery and efficacy in the context of



tumors in the brain, whether they be primary tumors, such as GBM (Cancer Genome Atlas Research, 2008), or metastatic brain tumors that may overexpress MDM2 and have areas with an intact BBB (Wade et al., 2013).

The objective of current study was to examine the role of major efflux transporters, P-gp and Bcrp, on the brain distribution of SAR405838 using in vitro and in vivo methods. Moreover, a compartmental model was developed for quantitative and mechanistic understanding of the distributional kinetics of SAR405838 into and out of the brain in the presence and the absence of the major active efflux transporters at the BBB. These studies provide insights on the use of SAR405838 in brain tumor therapy.

## 4.2 MATERIALS AND METHODS

### 4.2.1 Chemicals and reagents

(2'S,3'R,4'S,5'R)-6-Chloro-4'-(3-chloro-2-fluoro-phenyl)-2'-(2,2-dimethylpropyl)-2-oxo-1,2-dihydro-spiro (indole-3,3'-pyrrolidine)-5'-carboxylic acid (trans-4-hydroxy-cyclohexyl)-amide (SAR405838, Figure 1) was obtained from Sanofi Pharmaceutical (Vitry-sur-Seine, France). N-(3-(5-chloro-1H-pyrrolo[2,3-b]pyridine-3-carbonyl)-2,4-difluorophenyl)propane-1-sulfonamide (PLX-4720) was purchased from Chemietek. N-[4-[2-(3,4-dihydro-6,7-dimethoxy-2(1H)isoquinolinyl)ethyl]phenyl]-9,10-dihydro-5-methoxy-9-oxo-4-acridinecarboxamide (elacridar) was purchased from Toronto Research Chemicals (Toronto, ON, Canada). [3H]-Prazosin was purchased from Perkin Elmer Life and Analytical Sciences (Waltham, MA). [3H]-Vinblastine was purchased from Moravek Biochemicals (La Brea, CA). (3S,6S,12aS)1,2,3,4,6,7,12,12a-octahydro-9-methoxy-6-(2-methylpropyl)-1,4-dioxopyrazino(19,29:1,6)pyrido(3,4-b)indole-3-propanoic acid 1,1-dimethylethyl ester (Ko143) was purchased from Tocris Bioscience (Ellisville, MO) and LY335979 (zosuquidar), (R)-4-((1aR,6R,10bS)-1,2-difluoro-1,1a,6,10b-tetrahydrodibenzo-(a,e)cyclopropa(c)cycloheptan-6-yl)-((5-quinoloyloxy)methyl)-1-piperazine ethanol, trihydrochloride (zosuquidar) was kindly provided Eli Lilly and Co. (Indianapolis, IN). All other chemicals and reagents used were high-performance liquid chromatography grade from Thermo Fisher Scientific (Waltham, MA). The rapid equilibrium dialysis (RED) base plate and membrane

inserts (8 kDa molecular weight cut-off cellulose membrane) were purchased from Thermo Fisher Scientific (Waltham, MA).

#### **4.2.2 Animals**

An equal number of female and male Friend Leukemia Virus strain B (FVB) wild-type and transgenic mice lacking either or both efflux transporters, Mdr1 or/and Bcrp1 including Bcrp1(-/-), Mdr1a/b(-/-), and Mdr1a/b(-/-)Bcrp1(-/-) mice (Taconic Biosciences, Inc., Germantown, NY) at the age of 8-14 weeks were used for the experiments. Animal colonies were maintained and housed in Research Animal Resources (RAR) facility located at the Academic Health Center, University of Minnesota, following an established breeding protocol. Animal genotypes were routinely verified by conducting tail snip (TransnetYX, Cordova, TN). All protocols for the animal experiments were approved by University of Minnesota Institutional Animal Care and Use Committee (IACUC) and performed in accordance with the Guide for the Care and Use of Laboratory Animals established by the U.S. National Institutes of Health (Bethesda, MD).

#### **4.2.3 In vitro cell accumulation**

Cell accumulation experiments were performed with Madin-Darby canine kidney II (MDCKII) cells that overexpress either human multidrug resistance protein 1 (P-glycoprotein, MDR1) or murine breast cancer resistance protein (Bcrp1) or vector-controlled cells. Bcrp1 transfected (MDCKII-BCRP1) and P-gp transfected (MDCKII-MDR1) cell lines were kindly provided by Dr. Alfred Schinkel and Dr. Piet Borst (The Netherlands Cancer Institute), respectively. Cells were cultured in Dulbecco's modified Eagle's medium supplemented with 10% (v/v)

fetal bovine serum and antibiotics (penicillin, 100 U/ml; streptomycin, 100 mg/ml; amphotericin B, 250 ng/ml). Cells were seeded in 12-well polystyrene plates with a density of  $4 \times 10^5$  cells/well one day prior to the experiment (over 80% confluent). Cells were washed with serum free cell assay buffer containing 10 mM HEPES and then pre-incubated with either buffer alone or with a selective inhibitor for P-gp (1  $\mu$ M of LY335979) or Bcrp1 (0.2  $\mu$ M of Ko-143) for 30 minutes. Cells were incubated with 2  $\mu$ M of SAR405838 with or without the selective transporter inhibitor for 60 minutes at 37 °C with 60 rpm of agitation in an orbital shaker. At the end of incubation, cells were washed with ice-cold phosphate-buffered saline (PBS) twice to quench transport prior to cell lysis with 1% Triton X-100. The activities of efflux transporters expressed in the cell were validated using positive controls, [3H]-vinblastine for P-gp and [3H]-prazosin for Bcrp. The lysates were stored in -80 °C freezer until the analysis with liquid chromatography coupled with tandem mass spectrometry (LC-MS/MS), and intracellular concentration was normalized to the cellular protein content measured by the BCA assay.

#### **4.2.4 Free fraction in mouse plasma and brain homogenate**

The free fractions of SAR405838 in mouse plasma and brain homogenate were determined by using a rapid equilibrium dialysis (RED) device according to the manufacturer's protocol. Briefly, the brain homogenate was prepared by adding 2 volumes (w/v) of phosphate buffer saline (PBS; pH 7.4) followed by

mechanical homogenization. SAR405838 was added to mouse plasma or brain homogenate to a final concentration of 5  $\mu\text{M}$  containing 0.3% DMSO. The matrix with the drug was loaded into the sample chamber (300  $\mu\text{l}$ ) of the inserts first, and then 500  $\mu\text{l}$  of blank PBS was added into the corresponding buffer chamber. The base plate was sealed with an adhesive lid and incubated at 37  $^{\circ}\text{C}$  for 4 hours in an orbital shaker with a 300 rpm of agitation. At the end of incubation, samples were collected from both chambers, and stored in  $-80^{\circ}\text{C}$  freezer until LC-MS/MS analysis. Undiluted free fraction in the brain was calculated with the equation below reported previously (Kalvass and Maurer, 2002):

$$\text{Free fraction (fu)} = \frac{1/D}{\left(\left(\frac{1}{f_{u,\text{diluted}}}\right)-1\right)+1/D} \quad (1)$$

The dilution factor (D) was 3 in the experiment described above.

The unbound (free) concentration partitioning to the brain was determined as shown below:

$$\text{Free brain partition coefficient (Kp,uu)} = \frac{\text{free brain concentration}}{\text{free plasma concentration}} = K_{p, \text{ brain}} \times \frac{f_{u, \text{ brain}}}{f_{u, \text{ plasma}}} \quad (2),$$

where  $K_{p, \text{ brain}}$  is the ratio of brain-to-plasma areas under the total concentration time profile.

#### 4.2.5 Systemic and distributional pharmacokinetics Concentration-time profile after a single oral or intravenous administration of SAR405838

A single dose of SAR405838 was administered by oral gavage (25 mg/kg) or tail vein injection (5 mg/kg) in a solution to wild-type and genetic knockout FVB mice. The dosing solution was prepared with 98% of PEG200 (v/v) and 2% of TPGS (v/v) for the oral administration, or 10% of PEG400 (v/v), 3% of Cremophor (v/v), and 87% of PBS (v/v) for the intravenous study. Blood and brain samples were collected at the pre-determined time points ranging from 0.5 to 24 hours after oral administration or from 0.167 to 10 hours after intravenous administration ( $N=4$  at each time point). Mouse whole blood was collected via cardiac puncture using heparinized syringes after euthanizing in a carbon dioxide chamber. Plasma was separated by centrifuge at 3500 rpm at 4 °C for 20 minutes. Plasma and brain samples were stored at -80 °C until LC-MS/MS analysis.

#### **4.2.6 Pharmacological inhibition of efflux transporters**

Elacridar (a dual inhibitor of P-glycoprotein and Bcrp) and LY335979 (zosuquidar, a selective P-gp inhibitor) were prepared in a microemulsion formulation as described previously (Sane et al., 2013). Both inhibitors formulated in the microemulsion were diluted with 2 volumes of sterile water to a final concentration of 1 mg/ml. Vehicle control was formulated in the same manner, including all components of the microemulsion, but without any inhibitor. Wild-type FVB mice received either vehicle control or 5 mg/kg of inhibitor, either elacridar or LY335979 (zosuquidar) by tail vein injection. A dose of 25 mg/kg of SAR405838 was administered orally one hour after the administration of either vehicle control or inhibitors. Blood and brain samples were collected as

described in pharmacokinetic experiment, 2 hours following the administration of SAR405838, and stored at -80 °C until LC-MS/MS analysis.

#### **4.2.7 LC-MS/MS bioanalysis**

An LC-MS/MS method was developed by using reverse-phase liquid chromatography (Waters AQUITY ultra performance liquid chromatography system, Waters, Milford, MA) interfaced with a Waters Micromass Quattro Ultima triple quadrupole mass spectrometer (Waters, Milford, MA) with an electrospray interface in negative ion mode. Chromatographic separation was performed by injecting 5 µl of reconstituted sample onto a ZORBAX Eclipse XDB-C18 column (Rapid Resolution HT 4.6x50mm 1.8 µm, Agilent, Santa Clara, CA). Mobile phase was composed of aqueous phase (A) of 55% distilled and filtered water with 0.1% formic acid and organic phase (B) of 45% acetonitrile with 0.1% formic acid using an isocratic method. The total assay run time was 8 minutes, while the retention time for SAR405838 and internal standard (PLX-4720) were 1.95 and 5.45 minutes, respectively. SAR405838 and internal standard were detected with the mass transition of 560>305.9 and 411.9>304.86, respectively. These methods were sensitive and linear over the range of 1 – 5000 ng/mL with coefficient of variation of less than 15% (weighting factor of 1/Y<sup>2</sup>). All the specimen concentrations measured were within the range of calibration curve.

#### **4.2.8 Pharmacokinetic data analysis**

##### **1) Non-compartmental analysis (NCA)**

Concentration-time profiles in plasma and brain after a single oral or intravenous dose of SAR405838 were analyzed by using Phoenix WinNonlin version 6.4 (Certara USA Inc., Princeton, NJ). Pharmacokinetic parameters and metrics were calculated by non-compartmental analysis (NCA). Areas under the curve (AUCs) from time 0 to infinity for plasma and brain were calculated by log-linear trapezoidal integration, and the extrapolation for AUC from last time point to infinite time was calculated by dividing the last concentration measured by the terminal elimination rate constant, determined from the last three to four points in the concentration-time profiles. Other pharmacokinetic parameters, including systemic clearance (CL), volume of distribution (Vd), and  $t_{1/2}$  (half-life), were calculated by using NCA. The brain-to-plasma partition coefficient ( $K_{p, \text{brain}}$ ) was calculated as below:

$$\text{Brain partition coefficient } (K_{p, \text{brain}}) = \frac{\text{AUC}_{\text{brain}}}{\text{AUC}_{\text{plasma}}} \quad (3)$$

Where  $\text{AUC}_{\text{brain}}$  is an area under the curve from time zero to infinity of brain concentration-time profile ( $[\text{AUC}_{0 \rightarrow \infty, \text{brain}}]$ ) and  $\text{AUC}_{\text{plasma}}$  is an area under the curve plasma concentration-time profile ( $[\text{AUC}_{0 \rightarrow \infty, \text{plasma}}]$ ).

The brain partition coefficient of free drug was calculated as described above in methods for free fraction. The distribution advantage (DA) to the brain resulting from lack of P-gp and/or Bcrp mediated efflux at the BBB was determined by the ratio of  $K_{p, \text{knockout}}$  to  $K_{p, \text{wild-type}}$  to understand the magnitude of the role



efflux transporters play in the brain distribution of SAR405838. The oral bioavailability of SAR405838 was calculated by the following equation:

$$\text{Oral bioavailability (F)} = \left\{ \frac{[\text{AUC}_{(0 \rightarrow \infty), \text{plasma}}]_{\text{oral}}}{[\text{AUC}_{(0 \rightarrow \infty), \text{plasma}}]_{\text{IV}}} \right\} \left\{ \frac{\text{Dose}_{\text{IV}}}{\text{Dose}_{\text{oral}}} \right\} \quad (4)$$

Where the  $[\text{AUC}_{(0 \rightarrow \infty), \text{plasma}}]_{\text{oral}}$  is the area under the curve from time zero to infinity of plasma concentration-time profile following a single oral dose and  $[\text{AUC}_{(0 \rightarrow \infty), \text{plasma}}]_{\text{IV}}$  is the area under the curve from time zero to infinity of plasma concentration-time profile following a single intravenous dose.

## 2) Compartmental analysis with a BBB model

A compartmental model that includes a brain compartment (BBB model) was used to quantitatively assess the rate and extent of SAR405838 distribution into and out of the mouse brain (Liu et al., 2005; Laramy et al., 2018). The model was fit to the data in two steps. First, a one-compartment model was fit to WT and TKO mean pooled plasma concentration-time data from a single intravenous bolus (Figure 2A), given that there was no difference between WT and TKO plasma concentration profiles and individual model fits yielded the same disposition parameters for each genotype. These systemic disposition parameters, i.e., clearance (CL), the volume of distribution (Vc), and elimination rate constant from the central compartment (Ke) for wild-type and triple-knockout FVB mice were determined using the one-compartment model fit to the data

obtained following a single intravenous administration. Then, absorption rate constants ( $K_a$ ) for each genotype were estimated from the model fitted to the observed plasma data following a single oral administration. In the second step, a compartmental model that includes a brain compartment was fit to the observed brain concentration-time profile data either from an intravenous bolus or an oral administration (Figure 2B). A forcing function, comprised of the systemic disposition parameters obtained in step 1, including the absorption rate constant when appropriate, was implemented to describe the plasma concentration in the central compartment and used as an input function into the compartmental BBB model. Simulation and model fitting for systemic disposition and brain distribution were performed by using SAAM II (version 2.3; The Epsilon Group, Charlottesville, VA).

The changes in total brain concentration with respect to time were described by using the following differential equation:

$$V_{\text{brain}} * \frac{dC_{\text{brain}}}{dt} = K_{\text{in}} * (V_c * C_{\text{plasma}}) - K_{\text{out}} * (V_{\text{brain}} * C_{\text{brain}}) \quad , \quad (5)$$

where  $V_{\text{brain}}$  is the apparent volume of distribution in the brain,  $K_{\text{in}}$  and  $K_{\text{out}}$  are the first-order rate constants that describe the rates into and out of the brain, and  $V_c$  is the volume of distribution of total drug in the central compartment. In this model,  $C_{\text{plasma}}$  is the predicted total drug concentration in plasma under the model from step 1 and  $C_{\text{brain}}$  is the observed total drug concentrations in brain. Given that the total concentration of drug was measured in the brain as the reference concentration to relate to the total amount in brain, the  $V_{\text{brain}}$  for

SAR405838 was estimated to be the same as the anatomical volume of mouse brain that was obtained from the overall average of our *in vivo* experiments, i.e.,  $0.42 \pm 0.034$  mL/g brain.

The clearances into and out of the brain were calculated with the model estimated  $K_{in}$  and  $K_{out}$  of the brain by using following equation:

$$CL_{in} = K_{in} \times V_c \quad (6)$$

$$CL_{out} = K_{out} \times V_{brain} \quad (7).$$

The exposure of brain tissue to SAR405838 was also quantified by the mean transit time (MTT) using following equation (Kong and Jusko, 1988):

$$\text{Mean transit time in the brain (MTT}_{brain}) = \frac{1}{K_{out}} \quad (8)$$

#### 4.2.9 Statistical analysis

All data are presented as mean  $\pm$  standard deviation (S.D.) or mean  $\pm$  standard error of the estimate (S.E.). Comparison between two groups was tested by using an unpaired two sample t-test with GraphPad Prism version 6.04 (GraphPad, La Jolla, CA) software. A significance level of  $P < 0.05$  was used for the test.

### 4.3 RESULTS

#### 4.3.2 In vitro cell accumulation assay

The role of the two efflux transporters that are highly expressed on the luminal membrane in endothelial cell of brain microvasculature, P-glycoprotein (P-gp, ABCB1) and breast cancer resistance protein (Bcrp, ABCG2), on the brain distribution of SAR405838, was initially examined using an in vitro cell accumulation assay in MDCKII wild-type, MDCKII-MDR1 overexpressing, and MDCKII-BCRP1 overexpressing cell lines. [3H]-Vinblastine and [3H]-prazosin were used as positive controls to check the functionality of P-gp and Bcrp, respectively, in the transfected cell lines. The intracellular accumulation of these positive control substrates was significantly lower in transporter-overexpressing cells when compared to their normalized vector-controlled wild-type cells (Figure 3) [wild-type (MDR1-vector control): 100%  $\pm$  32.18, Mdr1: 36.7%  $\pm$  12.26,  $P < 0.05$ ; wild-type (BCRP-vector control): 100%  $\pm$  11.0, Bcrp1: 29.83%  $\pm$  9.91,  $P < 0.01$ ]. When LY335979, a selective inhibitor of P-gp, and Ko-143, a selective inhibitor of Bcrp, were co-incubated with their respective substrates, the intracellular accumulation was similar to the vector control due to inhibition of the respective efflux transporter (Figure 3) [wild-type (MDR1) + LY335979: 130%  $\pm$  12.2, MDR1 + LY335979: 158.3%  $\pm$  21.81, (*N.S.*); wild-type (BCRP1) + Ko-143: 103.1%  $\pm$  13.7, BCRP1 + Ko-143: 90.8%  $\pm$  19.9, (*N.S.*)]. The accumulation of SAR405838 in MDCKII-MDR1 cells was only 35.2% of the corresponding vector-controlled cells, and this difference was abolished in the presence of the P-gp selective inhibitor, LY335979 (Fig. 3A) [ 139.8%  $\pm$  22.4,  $P < 0.0001$ ]. However, no significant difference was observed in the accumulation of SAR405838 between Bcrp vector control and Bcrp overexpressing cells (Fig. 3B) [Bcrp1:

121.5%  $\pm$  26.6, (N.S.)). These in vitro results indicate that SAR405838 is a substrate of P-gp, but not of Bcrp, suggesting that P-gp may play a significant role in limiting the brain distribution of SAR405838. The use of a selective and potent P-gp inhibitor, such as LY335979, was able to significantly diminish the function of P-gp, and increase the intracellular accumulation of SAR405838 in these in vitro experiments.

#### 4.3.3 SAR405838 disposition following IV dose

The brain and plasma concentration-time profiles were examined at multiple time points up to 10 hours after a single intravenous administration of SAR405838 in wild-type (*WT*) and triple knockout FVB mice (*Mdr1a/1b<sup>-/-</sup>Bcrp1<sup>-/-</sup>*) that lack both *Mdr1a/b* and *Bcrp* (Figure 4A and 4B). Concentrations of SAR405838 in plasma and brain were measured in the specimens that were collected at the pre-determined time points after administration of 5 mg/kg SAR405838 by tail vein injection. The plasma concentrations over time ( $AUC_{(0 \rightarrow t_{last})}$ ) of SAR405838 in *Mdr1a/1b<sup>-/-</sup>Bcrp1<sup>-/-</sup>* were not significantly different than in wild-type FVB mice (Table 1, plasma AUC *WT* = 15851 $\pm$ 542, plasma AUC *Mdr1a/1b<sup>-/-</sup>Bcrp1<sup>-/-</sup>* = 15033 $\pm$ 761, N.S.). Importantly, this was not the case in the distribution of SAR405838 to the brain, where concentrations of SAR405838 in the brain were significantly higher in *Mdr1a/1b<sup>-/-</sup>Bcrp1<sup>-/-</sup>* mice when compared to wild-type mice at all time points ( $P < 0.05$ ). Both plasma and brain concentrations exhibit a mono-exponential decline with respect to time for both wild-type and *Mdr1a/1b<sup>-/-</sup>Bcrp1<sup>-/-</sup>* mice. Brain-to-plasma ratios of SAR405838 were significantly higher in *Mdr1a/1b<sup>-/-</sup>Bcrp1<sup>-/-</sup>* than wild-type, and increased over time in the *Mdr1a/1b<sup>-/-</sup>*

*Bcrp1<sup>-/-</sup>* genotype ( $p < 0.05$ ) but did not increase after the second measurement (30 minutes) in the wild-type (*N.S.*) (Figure 4C). Correspondingly, a plateau in the brain-to-plasma ratio was observed early post dose (30 minutes) in wild-type, but it was not reached in *Mdr1a/1b<sup>-/-</sup>Bcrp1<sup>-/-</sup>* even after 10 hours after the dose. Plasma pharmacokinetic parameters and metrics were calculated in both wild-type and *Mdr1a/1b<sup>-/-</sup>Bcrp1<sup>-/-</sup>* (Table 1). The wild-type and *Mdr1a/1b<sup>-/-</sup>Bcrp1<sup>-/-</sup>* mice had a terminal elimination half-life of 2.25 and 2.76 hours, volume of distribution (*V<sub>d</sub>*) of 973 and 1227 mL/kg, and systemic clearance of 300 and 308 mL/hr/kg, respectively, indicating that there are no differences in the systemic elimination of SAR405838 between these two transporter genotypes. Also, the brain partition coefficient, calculated using  $AUC_{(0 \rightarrow \infty), \text{plasma}}$  and  $AUC_{(0 \rightarrow \infty), \text{brain}}$ , was over 45-fold higher in *Mdr1a/1b<sup>-/-</sup>Bcrp1<sup>-/-</sup>* than wild-type [0.0275 in wild-type and 1.29 in *Mdr1a/1b<sup>-/-</sup>Bcrp1<sup>-/-</sup>*] (Table 1), indicating that P-gp (*Mdr1*) is critical in limiting the BBB permeability and brain distribution of SAR405838.

#### 4.3.4 SAR405838 absorption and disposition following single oral dose

The brain and plasma concentration-time profiles were determined after a single oral dose of SAR405838 (25 mg/kg) in four different genotypes of mice, including wild-type, *Bcrp1<sup>-/-</sup>*, *Mdr1a/b<sup>-/-</sup>*, and *Mdr1a/b<sup>-/-</sup>Bcrp1<sup>-/-</sup>* (Figure 5). The plasma concentration-time profiles of SAR405838 were very similar amongst the different genotypes (Figure 5A), even though there was some variability in  $AUC_{(0 \rightarrow \infty), \text{plasma}}$ . The brain concentrations of SAR405838 in *Mdr1a/b<sup>-/-</sup>* and *Mdr1a/b<sup>-/-</sup>Bcrp1<sup>-/-</sup>* were higher compared to wild-type and *Bcrp1<sup>-/-</sup>* at all time points (Figure 5B,  $P < 0.05$ ). The brain to plasma ratios, shown in Figure 4C, were consistently

greater in *Mdr1a/b*<sup>-/-</sup> and *Mdr1a/b*<sup>-/-</sup>*Bcrp1*<sup>-/-</sup> than wild-type and *Bcrp1*<sup>-/-</sup> (significantly different at all time points in *Mdr1a/b*<sup>-/-</sup> and *Mdr1a/b*<sup>-/-</sup>*Bcrp1*<sup>-/-</sup> compared to wild-type and *Bcrp1*<sup>-/-</sup>,  $P < 0.05$ ). In all four genotypes, the brain to plasma ratio increased over time and reached an early plateau in wild-type and *Bcrp1*<sup>-/-</sup> mice, but the distributional equilibrium plateau was observed at much later times in *Mdr1a/b*<sup>-/-</sup> and *Mdr1a/b*<sup>-/-</sup>*Bcrp1*<sup>-/-</sup> mice. The K<sub>p</sub> values calculated from the brain and plasma AUCs after oral administration were much greater in *Mdr1a/b*<sup>-/-</sup> and *Mdr1a/b*<sup>-/-</sup>*Bcrp1*<sup>-/-</sup> mice (2.35 and 1.53, respectively) than in wild-type and *Bcrp1*<sup>-/-</sup> (0.0218 and 0.0285, respectively), suggesting the dominant influence of P-gp on the brain exposure of SAR405838. The corresponding brain distribution advantage achieved by eliminating the efflux mechanism was calculated in *Bcrp1*<sup>-/-</sup>, *Mdr1a/b*<sup>-/-</sup>, and *Mdr1a/b*<sup>-/-</sup>*Bcrp1*<sup>-/-</sup> mice compared to wild-type mice, and were 1.31, 108, and 70.1, respectively, after a single oral dose (Table 2).

The systemic oral bioavailability was calculated in both wild-type and *Mdr1a/b*<sup>-/-</sup>*Bcrp1*<sup>-/-</sup>, and were 73.2% and 81%, respectively (Table 2). These similar values in bioavailability in these genotypes indicate that P-gp and Bcrp do not have a profound influence on the bioavailability of SAR405838, even though efflux transport significantly changes the brain exposure.

#### 4.3.5 Plasma and brain unbound fraction

The unbound fraction (f<sub>u</sub>) of SAR405838 in plasma and brain homogenate was determined by using rapid equilibrium dialysis after a 4-hour incubation, that was

shown to be adequate time to reach equilibrium in pilot experiments. The  $f_u$  of SAR405838 in the plasma was extremely low, ( $0.059\% \pm 0.034$ ,  $N=9$ ); however, it was approximately 3 times higher ( $P < 0.01$ ) than that in the brain ( $0.015\% \pm 0.0035$ ,  $N=9$ ) (Table 3). The free (unbound) brain-to-plasma ratio ( $K_{p,uu}$ ) values were calculated based on these  $f_u$  values, and are summarized in Table 3. The  $K_{p_{uu}, brain}$  values are 0.006 and 0.007 in wild-type and *Bcrp1*<sup>-/-</sup> after a single oral administration, respectively, indicating that efflux mechanisms play a highly significant role in the brain penetration of SAR405838 in these genotypes. The  $K_{p_{uu}, brain}$  values in *Mdr1a/b*<sup>-/-</sup>, and *Mdr1a/b*<sup>-/-</sup>*Bcrp1*<sup>-/-</sup> (0.598 and 0.389, respectively), were higher than those in wild-type and *Bcrp1*<sup>-/-</sup> due to lack of the dominant efflux transporter, P-gp, at the blood-brain barrier. Even though both P-gp and Bcrp were genetically deleted, the values of  $K_{p_{uu}, brain}$  still did not reach unity, suggesting the possibility that other efflux transporters may be involved in the brain penetration of SAR405838 or other elimination processes may exist in the brain, such as enzymatic degradation or metabolism as well as possible mechanisms of clearance involving bulk flow (Hammarlund-Udenaes et al., 2008).

#### 4.3.6 Pharmacological inhibition of efflux on the brain distribution of SAR405838

We examined the effect of elacridar, a dual inhibitor of both P-gp and Bcrp, and LY335979, a selective inhibitor of P-gp, on the brain distribution of SAR405838 in mice following co-dosing of inhibitors and SAR405838. Concentrations of SAR405838 in plasma with vehicle control were not different from the inhibitor



group at both 2 and 6-hours after the administration of SAR405838 (Figure 6A). However, brain concentrations of SAR405838 were 8.7 times higher at 2-hour and 3.8 times higher at 6-hour with elacridar ( $P < 0.01$  for both) when compared to the corresponding vehicle control at each time point (Figure 6A). Interestingly, brain concentrations of SAR405838 with LY335979 were not different from vehicle control group at 2 and 6 hours after the dosing. The brain to plasma ratio ( $K_{p, \text{brain}}$ ) at 2-hour post SAR405838 dosing, was also significantly higher ( $P < 0.005$ ) than vehicle control with elacridar (dual inhibitor), but there was no difference with LY335979 (selective P-gp inhibitor) (Figure 6B).

#### 4.3.7 Brain distributional kinetics of SAR405838 using BBB modeling

A one-compartment model was fit to mean pooled total plasma concentrations to describe the plasma concentration-time profile following a single intravenous administration and to yield systemic disposition parameters to use as a forcing function in the BBB model. The model predicted plasma concentration-time profiles and the observed plasma concentrations from the experiments for intravenous administration are shown in Figure 7. The systemic volume of distribution was estimated to be 1166 mL/kg, and the elimination rate constant ( $K_e$ ) from the central compartment was estimated to be  $0.269 \text{ hr}^{-1}$  in *Mdr1a/b*<sup>-/-</sup> *Bcrp1*<sup>-/-</sup> animals. Initial models for both wild-type and triple knockout animals were separately fit to the data obtained from each genotype and there were no differences in these systemic parameters between wild-type and triple-knockouts. Therefore, systemic parameters obtained from the mean pooled data were used for all genotypes, and are summarized in Table 4. All parameter estimates were

precisely estimated and had a coefficient of variation (CV) of less than 10%.

Using these parameter estimates, the systemic clearance of SAR405838 (314 mL/hr/kg), half-life ( $t_{1/2}$ ) (2.57 hours), and plasma concentration at time zero ( $C_{p0}$ ) (4288 ng/mL) were calculated (Table 4). These parameter estimates were then used in the plasma concentration-time forcing function to then estimate distribution parameters across the BBB.

One-compartment models for oral administration were individually fit to the total plasma concentration-time data of each genotype following an oral administration of SAR405838 to compare the absorption rate constants in wild-type and transgenic mice. For the models of oral administration, the volume of distribution for the central compartment and the systemic clearance from the central compartment were fixed as described in Table 5. The model predicted plasma concentration-time profiles for each genotype and the observed plasma concentration-time profiles are presented in Figure 8. The absorption rate constants for each genotype were estimated to be 0.265 hr<sup>-1</sup> in wild-type, 0.290 hr<sup>-1</sup> in *Bcrp1*<sup>-/-</sup>, 0.240 hr<sup>-1</sup> in *Mdr1a/b*<sup>-/-</sup>, and 0.258 hr<sup>-1</sup> in *Mdr1a/b*<sup>-/-</sup>*Bcrp1*<sup>-/-</sup> mice (Table 5). All absorption rate constant parameter estimates had a coefficient of variation (CV) of less than 20%. Overall, the model predicted plasma concentration-time profiles for each genotype visually matched well with the observed plasma concentration-time data after both intravenous bolus and oral administration (Figures 7 and 8).

As indicated above, to improve the estimation of the brain distribution parameters, estimated systemic disposition parameters from the one-compartment model were used in a forcing function to create a plasma concentration-time profile in the central compartment for the implementation of a BBB model. The model was fit to the concentration-time data by using the equation 5. The initial results using the BBB model confirmed that the tissue transfer rate constants into the brain ( $K_{in}$ ) of each genotype are not different from one another. Therefore, given the initial results regarding  $K_{in}$  values, and to simplify the model by reducing the number of estimated parameters to improve precision,  $K_{in}$  values were fixed for all four genotypes using the value estimated in *Mdr1a/b*<sup>-/-</sup>*Bcrp1*<sup>-/-</sup> animals. The results from the BBB model were presented in Table 6. The tissue transfer rate constants into the brain ( $K_{in}$ ) were estimated by the BBB model to be  $1.12 \times 10^{-4} \text{ hr}^{-1}$  following intravenous bolus administration and  $1.18 \times 10^{-4} \text{ hr}^{-1}$  following oral administration, and these values were not significantly different ( $P > 0.05$ ). The estimated tissue transfer rate constants out of the brain ( $K_{out}$ ) were much greater, ranging from 0.282 (PKO) to 0.300 (TKO)  $\text{hr}^{-1}$  in the P-gp deficient genotypes, and the transfer rate constants out of brain from wild-type and Bcrp knockout mice were 16.8 and 11.3  $\text{hr}^{-1}$ , respectively, about 40 to 60 times higher than the P-gp deficient mice (Table 6). The resulting clearances into the brain ( $CL_{in}$ ) were estimated by equation (6) to be 0.131 mL/hr/kg in i.v. study and 0.138 mL/hr/kg in p.o. study. The resulting clearances out of the brain ( $CL_{out}$ ), estimated using equation (7), in p-gp deficient mice (PKO and TKO) were similar to the clearance into the brain, however, that

in wild-type and *Bcrp* knockout mice were much higher than the clearance into the brain, as expected, mainly due to the efflux by P-gp (see Table 6).

The mean transit time in the brain (MTT) was calculated by equation (8) to quantify the exposure time of brain to SAR405838. As expected, the brain exposure to SAR405838, as quantified by MTT was significantly longer in *Mdr1a/b*<sup>-/-</sup> and *Mdr1a/b*<sup>-/-</sup>*Bcrp1*<sup>-/-</sup> genotype following both an intravenous bolus (2.32 hours in *Mdr1a/b*<sup>-/-</sup>*Bcrp1*<sup>-/-</sup>) and an oral administration (3.55 and 3.33 hours, respectively) than in wild-type and *Bcrp1*<sup>-/-</sup> (0.082 hours after an i.v. bolus; 0.060 and 0.089 hours after an oral dose) as summarized in Table 6 and 7. In conclusion, the total drug exposure time in the brain is significantly increased in the absence of P-gp (*Mdr1*), the efflux system that plays a leading role at the BBB in preventing SAR405838 access to the brain.

Based on the pharmacokinetic parameters and metrics estimated from the compartmental BBB model; the predicted partition coefficient of the brain ( $K_{p,pred}$ ), distribution advantage ( $DA_{pred}$ ), and the ratio of clearance into the brain to clearance out of the brain were calculated and summarized in Table 7.

The  $K_{p,pred}$  and the ratio of clearances were closely matched with the observed  $K_p$  values calculated with the results from NCA (Table 1 and 2). The ratios of the clearance into and out of the brain were calculated and compared with  $K_p$  values, and clearance ratios and predicted  $K_p$  from the models closely matched with each other in all genotypes. The agreement of the model-based predicted

values to the observed values support the assumptions in the compartmental models and the model described the data well.

#### 4.4 DISCUSSION

Challenges in the successful treatment of primary and metastatic brain tumors include insufficient and heterogeneous distribution of therapeutics across an intact BBB, which can lead to lack of efficacy, as well as acquired drug resistance due to exposure to subtherapeutic concentrations (Lockman et al., 2010; Pafundi et al., 2013). Therefore, it is important when examining innovative therapeutic agents that target novel signaling pathways in brain tumors to understand the pharmacokinetic properties and distributional kinetics of these agents to the brain. SAR405838 has been recently developed to target the p53 and MDM2 interaction, and it has advanced to clinical testing for the treatment of various solid tumors (Wang et al., 2014), but its efficacy in brain tumors has only recently been addressed (Kim et al., 2018b). Given the general mechanism of action of p53 enhancement, and the fact that some glioblastoma and other tumors of the brain overexpress MDM2, there is a great interest in exploring this target in brain tumors. Importantly, the distributional kinetics of this compound to, from and in the brain is critical to its rational use in preclinical efficacy studies, and in eventually informing the clinical use for brain tumors.

Recent studies from our group examined the potential efficacy of SAR405838 in a patient-derived xenograft model of primary brain tumor, glioblastoma (GBM). The overall conclusion of that study was that the limited brain distribution of SAR405838 diminishes its value as an effective treatment for brain tumor (Kim et al., 2018b). However, the specific mechanisms that influence the adequate delivery of an active concentration of SAR405838 to the brain or

brain tumor were not examined. The current study shows that, of the most highly expressed efflux transporters in the BBB, SAR405838 is an avid substrate of p-glycoprotein (P-gp). P-gp and Bcrp are highly expressed in brain endothelial cells of human and mouse (Uchida et al., 2011; Agarwal et al., 2012), therefore it can be expected that P-gp may limit the distribution, hence the efficacy of SAR405838 in both the preclinical and clinical settings of both primary (e.g., GBM) and secondary tumors in the CNS.

In vitro cell accumulation experiments using MDCKII cells transfected with efflux transporter genes have confirmed that SAR405838 is a substrate of human P-gp, but it may not be a substrate of mouse Bcrp. LY335979 (zosuquidar), a selective competitive inhibitor of P-gp, increased the intracellular accumulation of SAR405838. Consistent with the in vitro study results, in vivo studies with wild-type and transporter knockout mice have confirmed that P-gp plays a crucial role in brain distribution of SAR405838. It is valuable to describe the distributional kinetics after an oral administration of SAR405838, because this drug is given by mouth in both preclinical efficacy studies, and in clinical trials. *Mdr1a/b<sup>-/-</sup>Bcrp1<sup>-/-</sup>* FVB mice, after a single intravenous and oral administration of SAR405838, showed enhanced SAR405838 distribution to the brain. The AUCs in the plasma analyzed by NCA in wildtype and *Mdr1a/b<sup>-/-</sup>Bcrp1<sup>-/-</sup>* FVB mice were similar, even though the AUCs in the brain analyzed by NCA were over 30-fold higher in *Mdr1a/b<sup>-/-</sup>Bcrp1<sup>-/-</sup>* when compared to wild-type mice after a tail vein injection. The results from oral dosing were consistent with the IV studies, where SAR405838 achieved significantly high brain distribution in *Mdr1a/b<sup>-/-</sup>* and

*Mdr1a/b<sup>-/-</sup>Bcrp1<sup>-/-</sup>* when compared to wild-type and *Bcrp1<sup>-/-</sup>* mice. Due to the expression of efflux transporters in the intestine, oral absorption and bioavailability can be influenced by the presence or absence of efflux transporters (Kruijtz et al., 2002). In this regard, it is important to note that plasma concentration-time profile following the oral administration of SAR405838 in *Mdr1a/b<sup>-/-</sup>Bcrp1<sup>-/-</sup>* were no different than those of wild-type and *Bcrp1<sup>-/-</sup>*. The oral bioavailability calculated in wild-type and *Mdr1a/b<sup>-/-</sup>Bcrp1<sup>-/-</sup>* mice also confirms that the role of efflux transporters, in the case of SAR405838, does not influence drug absorption in the intestine, unlike the brain. One of the reasons for a lack of effect in the intestine may be that concentrations (especially “free” concentrations that may interact with the transporters) of drug achieved in the intestinal lumen after an oral administration are much higher than in plasma that influence brain distribution, therefore, saturating intestinal transporters (Lin and Yamazaki, 2003). As such, the overall permeability of a drug in the intestine will be governed primarily by passive permeability for drugs that have a favorable intrinsic permeability due to its physicochemical properties, such as SAR405838 (Wang et al., 2014). The AUC<sub>brain</sub> of SAR405838 in *Mdr1a/b<sup>-/-</sup>Bcrp1<sup>-/-</sup>* mice was comparable to that in *Mdr1a/b<sup>-/-</sup>* mice, indicative of, in this case, a lack of “compensation” of one efflux system (Bcrp) for the other (P-gp) (Kodaira et al., 2010; Agarwal et al., 2011a).

The results from compartmental BBB modeling agreed with the results from NCA, which indicated that the results were consistent regardless of the data analysis method. The transporter-mediated SAR405838 efflux at the BBB was



characterized by the fact that the tissue transfer rate constant out of the brain ( $K_{out}$ ) was considerably decreased in transgenic mice that lack P-gp. The simplified compartmental BBB model also gave an additional insight into brain distributional kinetics by calculating mean transit times (MTTs) and mean residence times (MRTs) of SAR405838 in the brain for in wild-type and transgenic mice, that can be translated into a therapeutic exposure time in the brain. The mean residence time in the brain compartment is defined as the average number of times drug molecules visit the brain compartment (N) multiplied by the average time the molecule spends in the brain on one visit, the mean transit time (MTT) (Kong and Jusko, 1988). N is determined by the ratio of  $K_{in}$  and  $K_e$ , or  $CL_{in}$  to  $CL_{sys}$ , that are assumed to be the same across genotypes (Kong and Jusko, 1988). Therefore, the exposure of brain to drug, as exemplified by the mean residence time, will be much higher in the P-gp deficient genotypes than the P-gp intact genotypes.

Nonspecific drug binding to proteins in plasma and tissue is a critical factor to consider for CNS pharmacodynamics as well as distributional kinetics according to the 'free drug hypothesis' (Trainor, 2007). This is especially true for the drugs targeting the CNS, where it is the unbound drug concentrations and unbound AUCs in the brain and plasma that indicate involvement of active efflux processes in CNS delivery of drugs (Kalvass and Maurer, 2002; Hammarlund-Udenaes et al., 2008). With the assumption that the free drug concentrations in the brain and in the plasma are in equilibrium, unbound (free) drug partition coefficient of brain ( $K_{p_{uu, brain}}$ ) is an informative parameter indicating the

contribution of active transport (either influx or efflux) or metabolism in CNS drug distribution (Hammarlund-Udenaes et al., 2008).

There are several ways to experimentally determine the unbound drug concentration in the brain. Recently, the brain homogenate method using rapid equilibrium dialysis (RED) has been suggested as a valid way of determining brain unbound concentration (Waters et al., 2008; Liu et al., 2009). Even though the use of unbound fraction from equilibrium dialysis needs to be carefully evaluated, especially for lipophilic drugs that tend to be highly bound, the RED method is generally accepted as an efficient and practical way to understand tissue binding characteristics (Waters et al., 2008). Therefore, RED was used with brain homogenate and plasma to determine unbound brain and plasma concentrations in the current study. The results show that SAR405838 is more highly bound to components in the brain homogenate than in plasma, consistent with the current understanding about the correlation between lipophilicity and protein binding (Summerfield et al., 2007). As such, the  $K_{p_{uu, \text{brain}}}$  was calculated as 'low', i.e., less than unity, in wild-type and *Bcrp1*<sup>-/-</sup> due to the presence of active efflux transporter, and these values increased in *Mdr1a/b*<sup>-/-</sup> and *Mdr1a/b*<sup>-/-</sup> *Bcrp1*<sup>-/-</sup> mice to 0.5 and 0.3, respectively, when two major efflux transporters are absent. Interestingly,  $K_{p_{uu, \text{brain}}}$  does not reach unity even without the major efflux transporter systems, which leads to the possibility of the presence of other efflux transporters that prevent SAR405838 from entering across the BBB.

The concomitant use of elacridar, a potent dual inhibitor of P-gp and Bcrp, with SAR405838 significantly improves the drug exposure in the brain without increasing the plasma concentration. There have been concerns about using transporter inhibitors with anticancer agents due to possible toxicity related to increased drug systemic exposure, due to drug-drug interactions at the level of the systemic clearance. However, for drugs that do not rely on transporters for their systemic clearance, such as SAR405838, combination therapy with efflux transporter inhibitors may be considered as a potential therapeutic strategy to overcome the BBB, especially with molecularly targeted agents in the treatment of glioblastoma, where only limited therapeutic regimens are available. The dosage and the interlaced schedule of dosing of the two interacting compounds need to be carefully assessed when using such a therapeutic drug-drug interaction strategy in clinical setting. Interestingly, co-administration of LY335979 (zosuquidar), a selective P-gp inhibitor, with SAR405838 did not change the brain delivery of SAR405838 in mice. The inhibitory potencies of elacridar and LY335979 against P-gp are reported to be similar (Jabeen et al., 2012), so the similar in vivo inhibitory efficacy might be expected with the same dose (5 mg/kg) of inhibitors, given similar concentrations. The discrepancies in the results between elacridar and LY335979 might be explained in several ways. One possibility is that the availability of a drug at the site of action, BBB in this case, can be lower with LY335979, so LY335979 may need higher dose to have the similar efficacy as elacridar. Another interesting possibility is that the binding site of SAR405838 to P-gp is different from that of LY335979 in mice, since

LY335979 has been shown to inhibit human P-gp potently in the in vitro study with MDCKII cells transfected with human MDR1 in this study (Fig. 3).

In conclusion, this study has showed that P-glycoprotein, of the major efflux transporters at the blood-brain barrier (P-gp and Bcrp), plays a key role in limiting the brain distribution of a novel MDM2 inhibitor, SAR405838. The distribution to the brain has been shown to be increased significantly in mice that are lacking P-glycoprotein compared to mice that have an intact P-gp at the BBB. Lack of P-gp did not influence the systemic disposition (clearance or volume of distribution) of SAR405838. Both NCA and compartmental analysis resulted in similar estimates of systemic pharmacokinetic parameters and metrics, and the compartmental BBB model provided additional insights into the rate and extent of the delivery of SAR405838 to the brain. The model-estimated tissue transfer rates out of the brain were significantly higher in the presence of P-gp than in the absence of P-gp, even though the tissue transfer rates into the brain were unchanged amongst genotypes. Based on our findings, it may still be of interest to examine the efficacy of brain penetrant MDM2 inhibitors in the GBM patient, as long as the limitations in delivery across an intact BBB can be overcome. Treatments for CNS tumors need to be able to penetrate the intact BBB to have maximal therapeutic efficacy especially for the treatment of infiltrative CNS tumors, such as GBM (Agarwal et al., 2011b). Even though targeting MDM2 is promising for the treatment of GBM (Wade et al., 2013), the ability of therapeutic agents to reach adequate concentration in CNS will limit the potential efficacy due to lack of BBB permeability (Kim et al., 2018b). Moreover, subtherapeutic

concentrations in CNS due to heterogeneous BBB permeability may result in acquired drug resistance (Sacher et al., 2014; Jung et al., 2016; Kim et al., 2018a). Therefore, it is critical to understand the delivery of these agents to the brain and to either find a novel MDM2 inhibitor which can penetrate the intact BBB, modify the structure of SAR405838 to avoid the active efflux by P-gp, or find an additional novel means to improve the delivery of MDM2 inhibitors through the BBB.

#### **AUTHORSHIP CONTRIBUTIONS**

Participated in research design: Kim, Sarkaria, Elmquist

Conducted experiments: Kim, Laramy, Gampa, Parrish

Performed data analysis: Kim, Laramy, Parrish, Brundage, Sarkaria, Elmquist

Wrote or contributed to the writing of the manuscript: Kim, Brundage, Sarkaria, Elmquist

Figure 4.1 Chemical structure of SAR405838.

Figure 1.

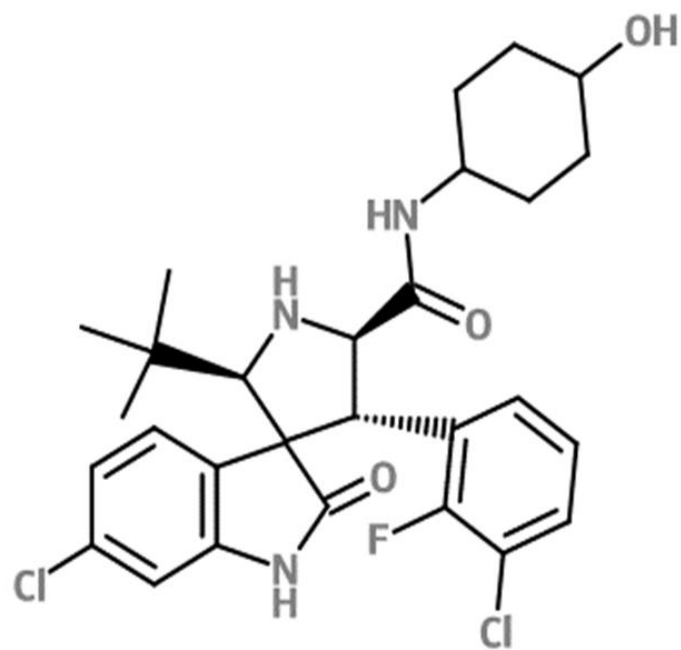
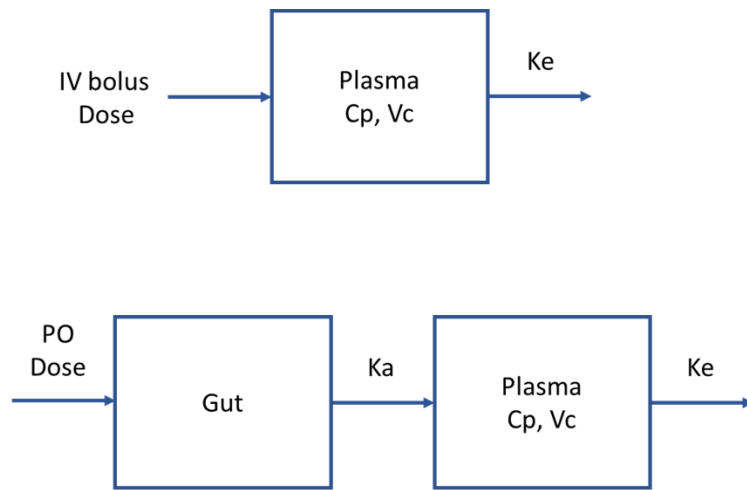


**Figure 4.2 A compartmental blood-brain barrier (BBB) model in order to describe a concentration-time profile in the central (plasma) and brain compartment after a single intravenous bolus or oral dose. (A) A one compartment model to describe the total concentration-time profile in plasma and to get systemic parameters for a forcing function. (B) A compartmental BBB model to describe the total concentration-time profile in brain.  $C_p$ , concentration in plasma;  $V_c$ , the volume of distribution in central compartment;  $K_e$ , the elimination rate constant from the central compartment;  $K_a$ , absorption rate constant;  $K_{in}$ , tissue transfer rate constant into the brain;  $K_{out}$ , tissue transfer rate constant out of the brain;  $C_b$ , concentration in brain;  $V_b$ , the apparent volume of distribution in brain.**

**Figure 2.**

**A**



**B**

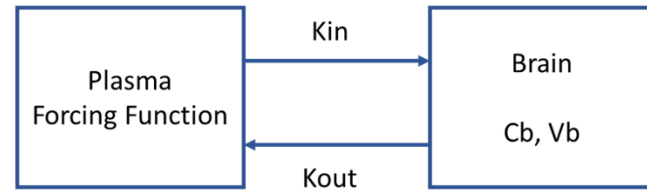




**Figure 4.3 Cell accumulation of SAR405838. (A) The intracellular accumulation of vinblastine (positive control) and SAR405838 in MDCKII vector control and MDR1-transfected cells in the presence and absence of P-gp inhibitor, LY335979 (1  $\mu$ M). (B) The intracellular accumulation of prazosin (positive control) and SAR405838 in MDCKII vector control and Bcrp-transfected cells in the presence and absence of Bcrp inhibitor, Ko-143 (0.2  $\mu$ M). Data presented as mean  $\pm$  standard deviation (S.D.) where  $N = 3$  for all groups. \* $P < 0.05$ , \*\* $P < 0.01$ , \*\*\* $P < 0.005$ , \*\*\*\* $P < 0.001$**

**Figure 3**

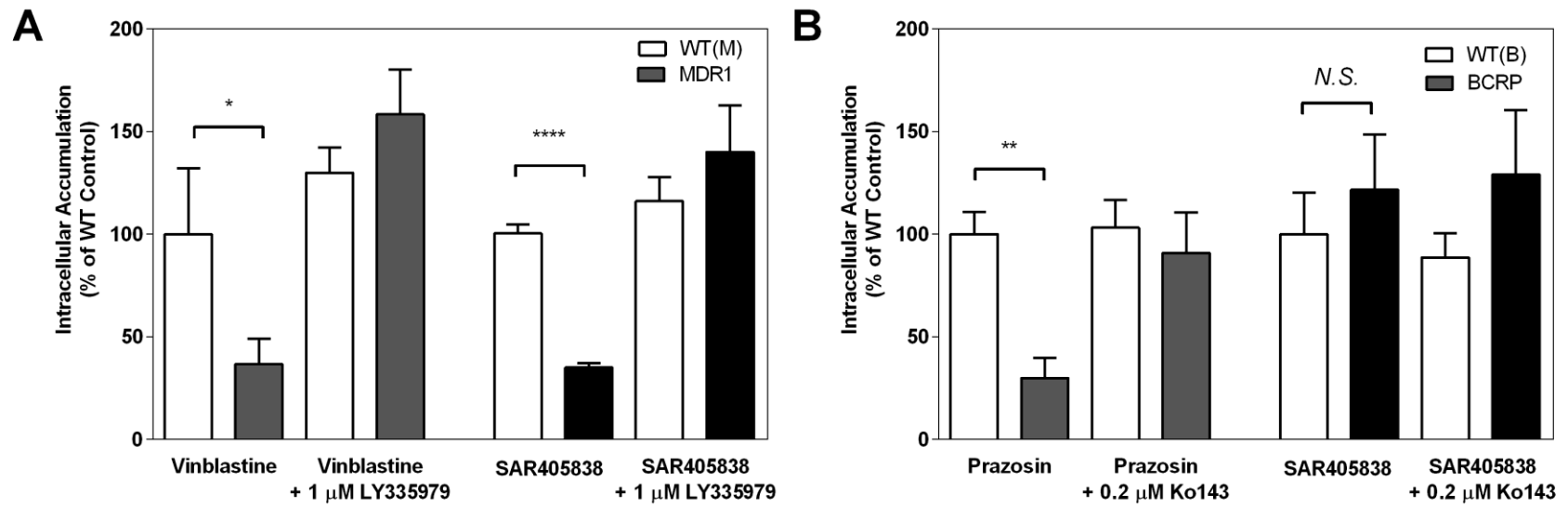


Figure 4.4 Pharmacokinetic profile of SAR405838 following a single intravenous administration. (A) Concentration-over-time in plasma, (B) concentration-over-time in brain, and (C) brain-to-plasma ratio over time in wild-type and *Mdr1a/b*<sup>-/-</sup>*Bcrp1*<sup>-/-</sup> mice. Data presented as mean  $\pm$  standard deviation (S.D.) where *N* = 3 to 5 for each time point.

Figure 4

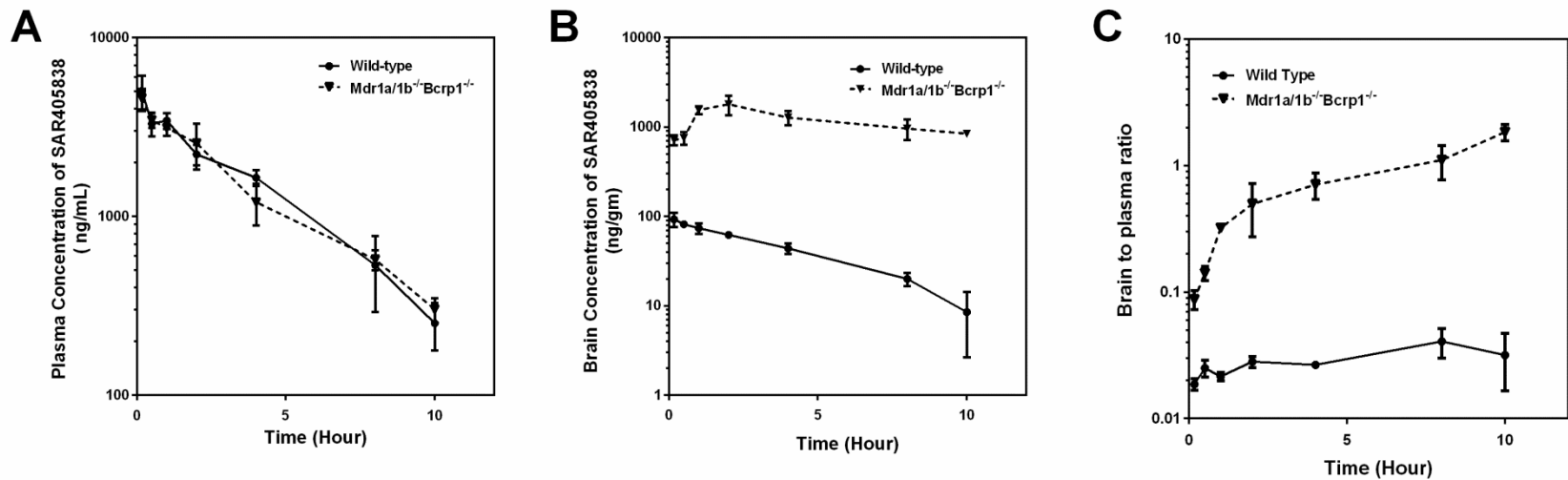
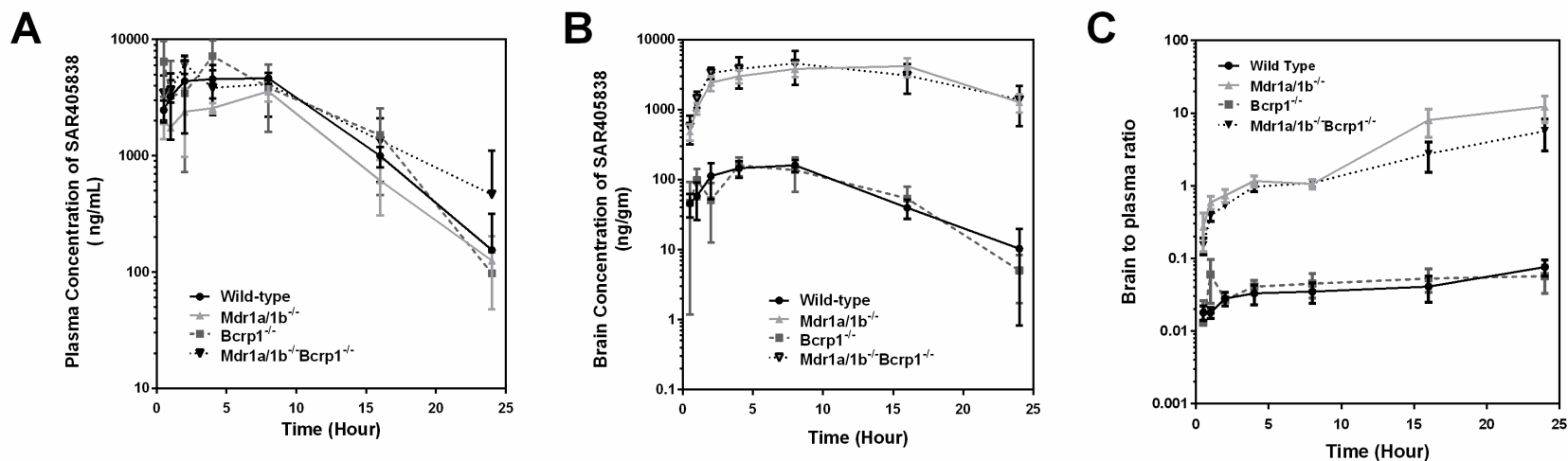


Figure 4.5 Pharmacokinetic profile of SAR405838 following a single oral administration. (A) Concentration-over-time in plasma, (B) concentration-over-time in brain, and (C) brain-to-plasma ratio over time in wild-type, *Mdr1a/b*<sup>-/-</sup>, *Bcrp1*<sup>-/-</sup>, and *Mdr1a/b*<sup>-/-</sup>*Bcrp1*<sup>-/-</sup> FVB mice. Data presented as mean ± standard deviation (S.D.) where *N* = 3 to 5 for each time point.

Figure 5



**Figure 4.6** The effect of a pharmacological inhibitor of efflux transport, elacridar, on the plasma and brain concentration of SAR405838. (A) Concentrations in plasma and brain at 2-hr and 6-hr post dose with co-administration of either vehicle control or inhibitor, either LY335979 or elacridar. (B) Brain-to-plasma ratio at 2-hr and 6-hr post dose. Data presented as mean  $\pm$  standard deviation (S.D.) where  $N = 3$  to 5 for each group. **\*\* $P < 0.01$ , \*\*\* $P < 0.005$**

**Figure 6**

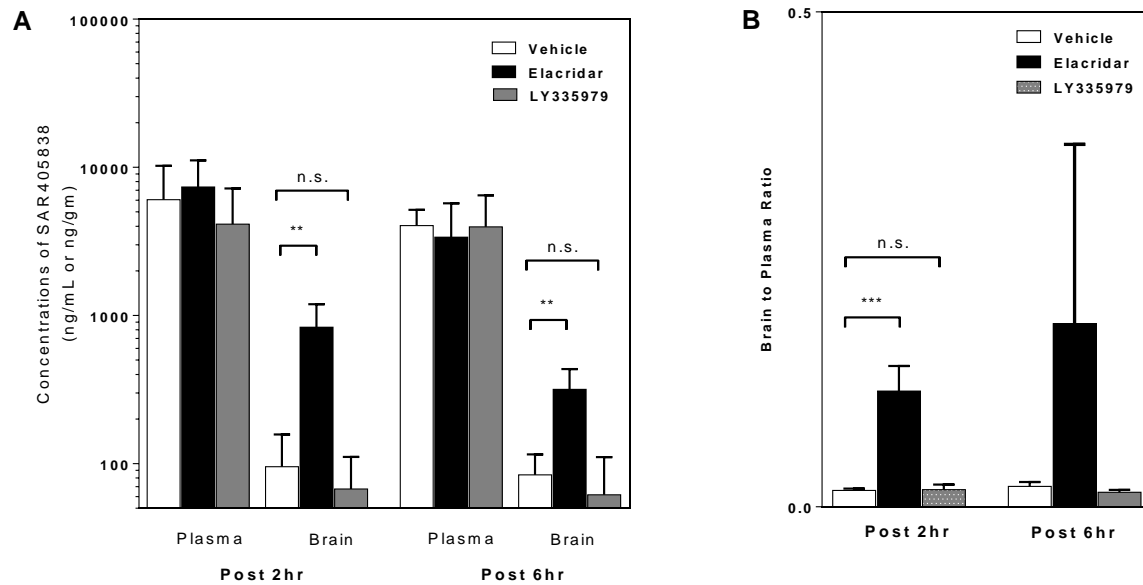
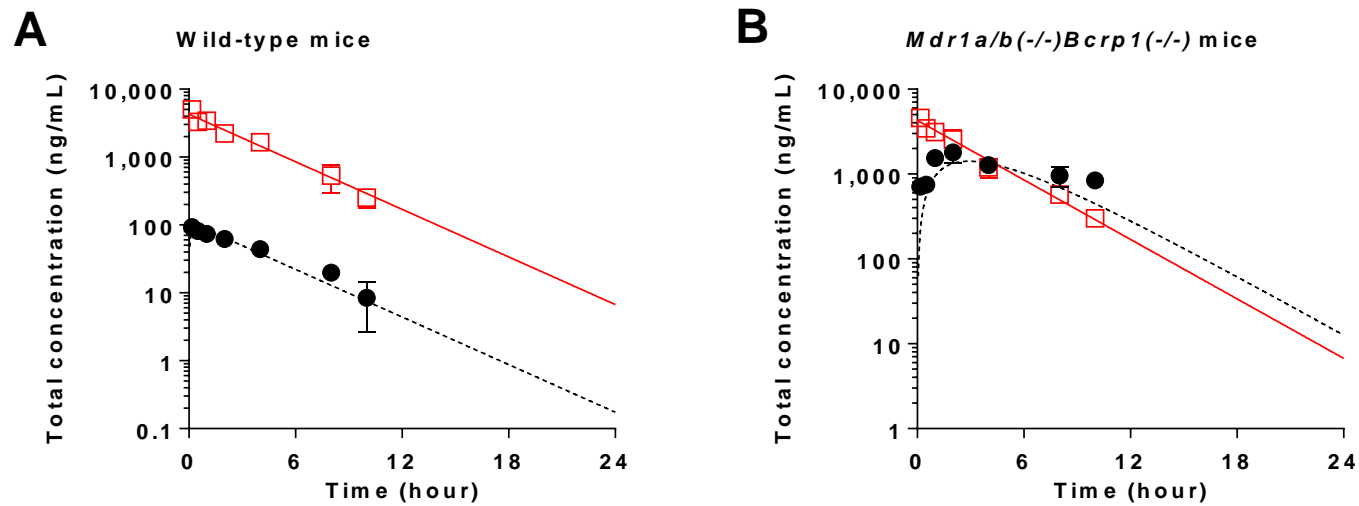


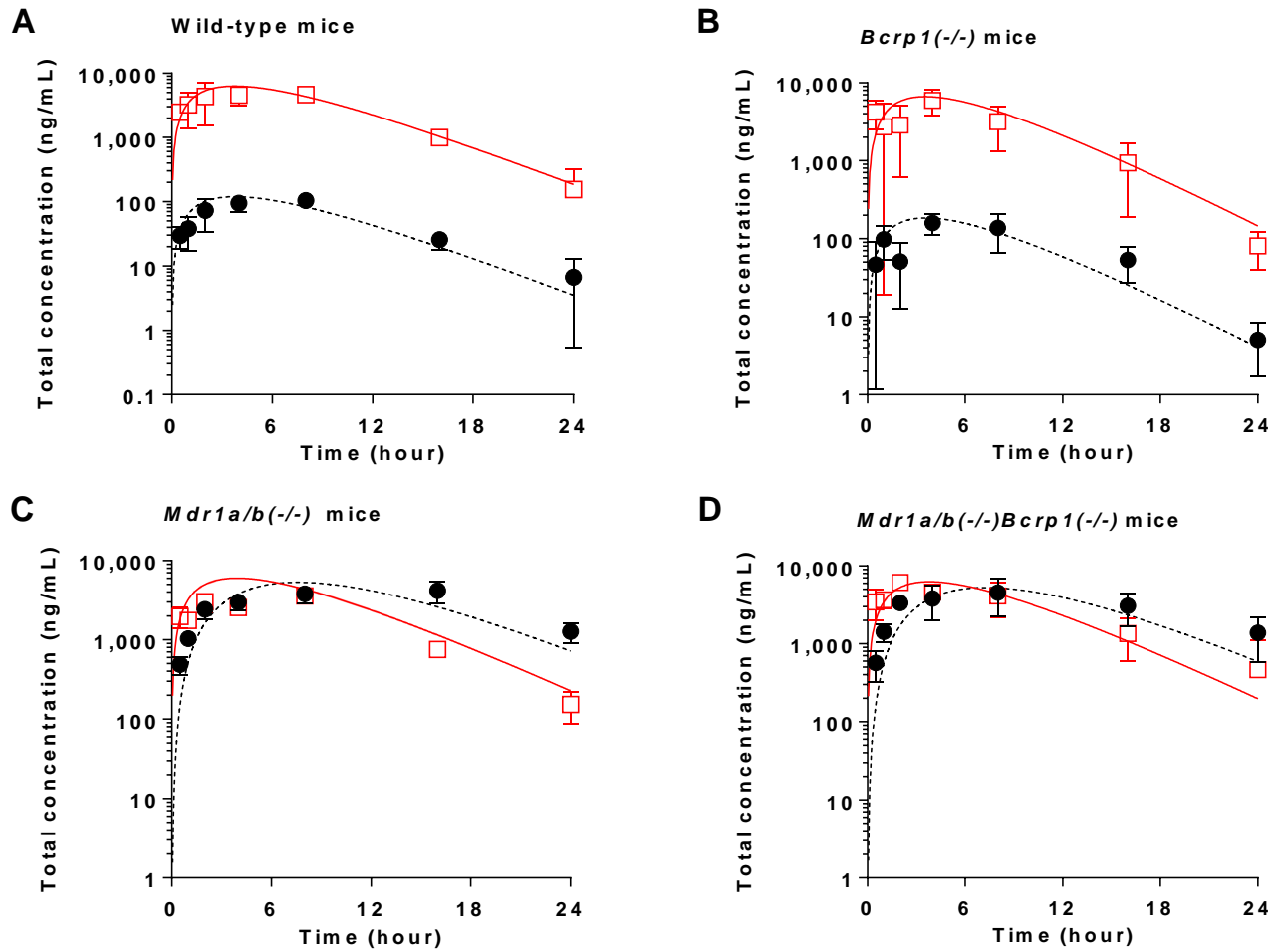
Figure 4.7 Observed (squares and circles) and model predicted (solid line and dotted line) plasma (red) and brain (blank) concentrations of SAR405838 following a single intravenous bolus administration (5 mg/kg) in wild-type (A) and *Mdr1a/b*<sup>-/-</sup>*Bcrp1*<sup>-/-</sup> (B) FVB mice. The observed data are presented as the mean standard deviation (S.D.) where *N* = 3 to 4 for each time point.

Figure 7



**Figure 4.8** Observed (squares and circles) and model predicted (solid line and dotted line) plasma (red) and brain (blank) concentrations of SAR405838 following a single oral administration (25 mg/kg) in wild-type (A), *Bcrp1*<sup>-/-</sup> (B), *Mdr1a/b*<sup>-/-</sup> (C), and *Mdr1a/b*<sup>-/-</sup>*Bcrp1*<sup>-/-</sup> (D) FVB mice. The observed data are presented as the mean standard deviation (S.D.) where *N* = 3 to 4 for each time point.

Figure 8





**Table 4.1 Pharmacokinetic/metric parameters and brain partition coefficients determined by non-compartmental analysis following a single intravenous dose of SAR405838 (5 mg/kg) in wild-type and *Mdr1a/b*<sup>-/-</sup>*Bcrp1*<sup>-/-</sup> FVB mice.**

	Plasma		Brain	
	Wild-type	<i>Mdr1a/b</i> <sup>-/-</sup> <i>Bcrp1</i> <sup>-/-</sup>	Wild-type	<i>Mdr1a/b</i> <sup>-/-</sup> <i>Bcrp1</i> <sup>-/-</sup>
<b>t<sub>1/2</sub> (hour)</b>	2.25	2.76	3.10	7.71*
<b>AUC<sub>0→tlast</sub> (hr*ng/mL)</b>	15851 ± 542.0	15033 ± 761.3	414 ± 11.9	11925 ± 609
<b>AUC<sub>0→∞</sub> (hr*ng/mL)</b>	16715	16280	460	20973
<b>Vd (mL/kg)</b>	973	1227	-	-
<b>CL (mL/hr/kg)</b>	300	308	-	-
<b>K<sub>p,brain</sub></b>	-	-	0.0275	1.29
<b>Distribution Advantage (DA)</b>	-	-	1	46.8

t<sub>1/2</sub> , half-life

AUC<sub>0-tlast</sub>, area under the curve from zero to the time of last measured concentration

AUC<sub>0-∞</sub>, area under the curve from zero to time infinity

CL, clearance

Vd, volume of distribution

K<sub>p,brain</sub> (AUC ratio), the ratio of AUC(0-∞,brain) to AUC(0-∞,plasma) using total drug concentrations

DA (Distribution advantage), the ratio of K<sub>p</sub>knockout to K<sub>p</sub>wild-type

\* half-life was determined by the slope of last four time points in concentration-time profile.

In TKO, equilibrium between plasma and brain has not been reached until the last time point (10 hours)

**Table 4.2 Pharmacokinetic/metric parameters determined by non-compartmental analysis following a single oral dose of SAR405838 (25 mg/kg) in wild-type, *Mdr1a/b*<sup>-/-</sup>, *Bcrp1*<sup>-/-</sup>, and *Mdr1a/b*<sup>-/-</sup>*Bcrp1*<sup>-/-</sup> FVB mice.**

	Plasma				Brain			
	Wild-type	<i>Mdr1a/b</i> <sup>-/-</sup>	<i>Bcrp1</i> <sup>-/-</sup>	<i>Mdr1a/b</i> <sup>-/-</sup> <i>Bcrp1</i> <sup>-/-</sup>	Wild-type	<i>Mdr1a/b</i> <sup>-/-</sup>	<i>Bcrp1</i> <sup>-/-</sup>	<i>Mdr1a/b</i> <sup>-/-</sup> <i>Bcrp1</i> <sup>-/-</sup>
<b>t<sub>1/2</sub> (hour)</b>	3.26	4.18	3.02	5.08	4.03	10.1	3.36	12.1
<b>T<sub>max</sub> (hour)</b>	8	8	4	2	8	16	4	8
<b>C<sub>max</sub> (ng/mL)</b>	4651	3582	7209	6164	161	4176	159	4554
<b>AUC<sub>0→tlast</sub> (hr*ng/mL)</b>	60425 ± 3584	40490 ± 2559	68107 ± 9193	62490 ± 7253	1995 ± 132	74213 ± 5908	1925 ± 249	75281 ± 9392
<b>AUC<sub>0→∞</sub> (hr*ng/mL)</b>	61195	41382	68681	65867	1335	97283	1956	100663
<b>F<sub>oral</sub></b>	0.732	NA	NA	0.809	-	-	-	-
<b>Vd/F (mL/kg)</b>	1922	3642	1585	2778	-	-	-	-
<b>CL/F (mL/kg)</b>	409	604	364	379	-	-	-	-
<b>Kp<sub>brain</sub></b>	-	-	-	-	0.0218	2.35	0.0285	1.53
<b>Distribution Advantage (DA)</b>	-	-	-	-	1	108	1.31	70.1

C<sub>max</sub>, observed maximum concentration

T<sub>max</sub>, time to reach the maximum concentration

AUC<sub>0-tlast</sub>, area under the curve from zero to the time of last measured concentration

AUC<sub>0-∞</sub>, area under the curve from zero to time infinity

F (absolute bioavailability), ratio of the dose corrected AUC(0-∞) following po administration to dose corrected AUC(0-∞) following iv administration

CL/F, apparent clearance

Vd/F, apparent volume of distribution

Kp<sub>brain</sub> (AUC ratio), the ratio of AUC(0-∞,brain) to AUC(0-∞,plasma) using total drug concentrations

DA (Distribution advantage), the ratio of Kp<sub>knockout</sub> to Kp<sub>wild-type</sub>

**Table 4.3 Free fraction ( $f_u$ ) values, partition coefficient of brain ( $K_{p, \text{brain}}$  and  $K_{p_{uu}, \text{brain}}$ ), and distribution advantage. Data presented as mean  $\pm$  standard deviation (S.D.).**

	I.V.		P.O.			
	Wild-type	Mdr1a/1b <sup>-/-</sup> Bcrp1 <sup>-/-</sup>	Wild-type	Mdr1a/1b <sup>-/-</sup>	Bcrp1 <sup>-/-</sup>	Mdr1a/1b <sup>-/-</sup> Bcrp1 <sup>-/-</sup>
$K_{p, \text{brain}}$	0.0275	1.29	0.0218	2.35	0.0285	1.53
$f_{u, \text{plasma}}$	0.00059 $\pm$ 0.00034					
$f_{u, \text{brain}}$	0.00015 $\pm$ 0.000035					
$K_{p_{uu}, \text{brain}}$	0.007	0.328	0.006	0.598	0.007	0.389
$DA_{\text{total}}$	1	46.8	1	108	1.31	70.1

$K_p$  (AUC ratio), the ratio of  $AUC(0-\infty, \text{brain})$  to  $AUC(0-\infty, \text{plasma})$  using total drug concentrations

$f_{u, \text{plasma}}$ , free fraction of SAR405038 in plasma determined by rapid equilibrium dialysis ( $N = 9$ )

$f_{u, \text{brain}}$ , free fraction of SAR405838 in brain homogenate determined by rapid equilibrium dialysis ( $N = 9$ )

$K_{p, uu}$  (AUC ratio), the ratio of  $AUC(0-\infty, \text{brain})$  to  $AUC(0-\infty, \text{plasma})$  using free drug concentrations

DA (Distribution advantage), the ratio of  $K_{p_{\text{knockout}}}$  to  $K_{p_{\text{wild-type}}}$

**Table 4.4 Pharmacokinetic parameters estimated from one-compartment model that describes the total concentration-time profile from each genotype following a single intravenous bolus (5 mg/kg) administration.**

<b>Estimated parameters</b>	<b>Mean</b>	<b>CV (%)</b>	<b>95% Confidence Interval (CI)</b>
V <sub>c</sub> (mL/kg)	1166	6.07	(984.1, 1348.1)
K <sub>e</sub> (hr <sup>-1</sup> )	0.269	4.40	(0.239, 0.300)
<b>Calculated parameters</b>	<b>Mean</b>	<b>CV (%)</b>	<b>95% Confidence Interval (CI)</b>
CL <sub>system</sub> (mL/hr/kg)	314	4.24	(279.8, 348.2)
t <sub>1/2</sub> (hr)	2.57	4.4	(2.28, 2.86)
Cp <sub>0</sub>	4288	6.07	(3619, 4957)

V<sub>c</sub>, volume of distribution of a drug in the central compartment

K<sub>e</sub>, elimination rate constant from the central compartment

CL<sub>system</sub>, clearance from the systemic circulation

t<sub>1/2</sub>, half-life

Cp<sub>0</sub>, initial concentration of SAR405838 in the central compartment at time 0

**Table 4.5 Pharmacokinetic parameters estimated from one-compartment model that describes the total concentration-time profile from each genotype following a single oral (25 mg/kg) administration.**

Estimated parameters	Mean	CV (%)	95% Confidence Interval (CI)
$V_c$ (mL/kg)*	1166		** fixed **
$K_e$ (hr <sup>-1</sup> )*	0.269		** fixed **
$K_{a, WT}$ (hr <sup>-1</sup> )	0.265	6.1	(0.225, 0.304)
$K_{a, BKO}$ (hr <sup>-1</sup> )	0.290	15.7	(0.179, 0.401)
$K_{a, PKO}$ (hr <sup>-1</sup> )	0.240	10.1	(0.177, 0.302)
$K_{a, TKO}$ (hr <sup>-1</sup> )	0.258	14.3	(0.221, 0.460)

$V_c$ , volume of distribution of a drug in the central compartment (obtained value from mean pooled analysis of all genotypes)

$K_e$ , elimination rate constant from the central compartment (obtained value from mean pooled analysis of all genotypes)

$K_a$ , absorption rate constant after oral dosing in different genotypes

WT, wild-type

BKO,  $Bcrp1^{-/-}$

PKO,  $Mdr1a/b^{-/-}$

TKO,  $Mdr1a/b^{-/-} Bcrp1^{-/-}$

**Table 4.6 The changes in tissue transfer rate and clearance values with the total concentration model.**

Route of Administration		I.V.		P.O.			
Genotype		Wild-type	Mdr1a/b <sup>-/-</sup> Bcrp1 <sup>-/-</sup>	Wild-type	Bcrp1 <sup>-/-</sup>	Mdr1a/b <sup>-/-</sup>	Mdr1a/b <sup>-/-</sup> Bcrp1 <sup>-/-</sup>
<b>K<sub>in</sub> (hr<sup>-1</sup>)</b>	Mean	1.12E-04	1.12E-04	1.18E-04	1.18E-04	1.18E-04	1.18E-04
	CV (%)	-	16.5	-	-	-	18.5
<b>K<sub>out</sub> (hr<sup>-1</sup>)</b>	Mean	12.3	0.432	16.8	11.3	0.282	0.300
	CV (%)	7.14	19.0	14.1	10.9	8.25	18.5
<b>CL<sub>in</sub> (mL/hr/kg)</b>	Mean	0.131	0.131	0.138	0.138	0.138	0.138
	CV (%)	-	16.5	-	-	-	17.5
<b>CL<sub>out</sub> (mL/hr/kg)</b>	Mean	5.1	0.181	7.1	4.73	0.118	0.126
	CV (%)	7.14	19.0	14.1	10.9	8.25	18.5
<b>MTT (hr)</b>		0.082	2.315	0.060	0.089	3.55	3.33
<b>CL<sub>in</sub>/CL<sub>out</sub></b>		0.026	0.72	0.019	0.029	1.17	1.10

K<sub>in</sub>, tissue transfer rate constant into the brain

K<sub>out</sub>, tissue transfer rate constant out of the brain

CL<sub>in</sub>, total drug clearance into the brain

CL<sub>out</sub>, total drug clearance out of the brain

MTT, mean transit time in the brain: calculated by 1/K<sub>out</sub>

**Table 4.7 The Kp and Kp,uu values predicted from the compartmental BBB model describing the brain and plasma concentration-time profile following either intravenous or oral administration of SAR405838.**

Route of Administration	I.V.		P.O.			
	Wild-type	Mdr1a/b <sup>-/-</sup> Bcrp1 <sup>-/-</sup>	Wild-type	Bcrp1 <sup>-/-</sup>	Mdr1a/b <sup>-/-</sup>	Mdr1a/b <sup>-/-</sup> Bcrp1 <sup>-/-</sup>
<b>AUC<sub>0→∞, plasma</sub></b>	15915	15915	63748	63955	63503	64165
<b>AUC<sub>0→∞, brain</sub></b>	404	11462	1243	1859	71308	68317
Kp,pred <sup>a</sup>	0.025	0.72	0.019	0.029	1.12	1.06
DA,pred <sup>b</sup>	-	28	-	1.5	58	55
<b>CLin</b>	0.131	0.131	0.138	0.138	0.138	0.138
<b>CLout</b>	5.1	0.181	7.1	4.7	0.118	0.126
CLin/Clout <sup>c</sup>	0.026	0.72	0.019	0.029	1.17	1.10
DA,pred <sup>d</sup>	-	28	-	1.5	60	56

<sup>a</sup> Kp,pred, the ratio of model predicted AUC<sub>0→∞, brain</sub> to model predicted AUC<sub>0→∞, plasma</sub>

<sup>b</sup> DA,pred (distribution advantage), the ratio of Kp<sub>knockout</sub> to Kp<sub>wild-type</sub>

<sup>c</sup> the ratio of model predicted clearance into the brain to model predicted clearance out of the brain compartment

<sup>d</sup> DA,pred (distribution advantage), the ratio of brain clearance ratio in wild-type to brain clearance ratio in transgenic mice

**CHAPTER 5 BRAIN DISTRIBUTION OF A PANEL OF  
EGFR INHIBITORS USING CASSETTE-DOSING IN WILD-  
TYPE AND *ABCB1/ABCG2* DEFICIENT MICE**



## 5.1 INTRODUCTION

The epidermal growth factor receptor (EGFR) has been a useful biomarker and an attractive drug target in the treatment of various tumors (Doroshov, 2005; Seshacharyulu et al., 2012). EGFR is often found to be constitutively activated due to gene mutation and/or amplification, leading to typical oncogenic behavior, including, increased cell survival, proliferation, and invasion (Bertotti et al., 2009; Seshacharyulu et al., 2012). EGFR-tyrosine kinase inhibitors (TKIs) have been developed for use as first-line therapies for patients, especially those with non-small cell lung cancer (NSCLC), and they have shown promising efficacy in patient populations that overexpress EGFR (Doroshov, 2005). Patients with NSCLC have a substantial risk of developing metastases in central nervous system (CNS) (Rangachari et al., 2015; McCoach et al., 2016). CNS metastases often develop even when extracranial disease sites are controlled using standard regimens. First generation of EGFR inhibitors, erlotinib and gefitinib, have shown some success in treating NSCLS patients with peripheral lesions, but these drugs have had limited success in treating brain metastases of NSCLC, potentially due to limited delivery to the CNS (Kawamura et al., 2009; Agarwal et al., 2010; Weber et al., 2011; de Vries et al., 2012; Agarwal et al., 2013). Therefore, there has been a great interest in developing brain penetrant EGFR inhibitors for treating brain metastases.

While there is a clear rationale to use EGFR inhibitors in treating brain metastases, there has also been great interest in treating primary brain tumors with EGFR inhibitors. Approximately 60% of glioblastoma, the most common

and aggressive type of primary brain tumor, is often found to have EGFR overexpression (approximately 60%) (Ohgaki and Kleihues, 2007; Huang et al., 2009; Brennan et al., 2013). Moreover, overexpression of EGFR is closely related to a more aggressive glioblastoma phenotype (Shinojima et al., 2003). In spite of that, EGFR inhibitors have shown no significant benefit in glioblastoma patients (Rich et al., 2004; van den Bent et al., 2009), and have not led to regulatory approval of any EGFR inhibitor for the treatment of glioblastoma. One important factor to consider in examining reasons for the limited efficacy of these drugs in the CNS is that the delivery of many early EGFR inhibitors has shown to be insufficient to elicit a response at the target site in the CNS. Moreover, many of the early generation inhibitors are substrates of the major efflux transporters, p-glycoprotein (P-gp) and breast cancer resistance protein (Bcrp), that at the blood-brain barrier (BBB), may lead to limited brain penetration, especially in intra-tumoral regions that have an intact BBB in metastases (Lockman et al., 2010) and primary tumor (Sarkaria et al., 2018).

In the current study, we examined the distribution to the brain of a set of EGFR inhibitors, including early generation inhibitors, erlotinib, gefitinib and afatinib, and more recently developed inhibitors, osimertinib, vandetanib, AZD3759, dacomitinib, and AEE877 (Figure 1 and Table 1). These eight EGFR inhibitors were chosen based on previous and possible future use in patients with brain tumors. In addition, based on the few preclinical studies with these drugs, this series of EGFR inhibitors was chosen with the intention of having a wide range of BBB permeability.

Brain distributional kinetics were examined by using a cassette-dosing strategy. Cassette-dosing studies are typically performed by co-administering a low dose of multiple compounds to a single animal to calculate pharmacokinetic parameters and metrics of individual compounds from the concentration-time pharmacokinetic profile (Manitpisitkul and White, 2004). As such, multiple concentration-time profiles of individual drugs can be obtained in a single animal. One of the benefits of using cassette dosing strategy is that throughput of the study is significantly increased and the number of animals that are used for the study is significantly reduced. This is especially true in pharmacokinetic and brain distribution studies with mice that are often conducted using a destructive sampling strategy, and may require numerous animals for a single study with a single agent. Another interesting aspect of using cassette dosing to determine the CNS distribution of a series of compounds is that the brain penetration of different compounds can be examined within a single animal under the identical physiological conditions, including blood flow, BBB surface area, tight junction integrity, transporter expression and function. The most common concern with cassette dosing strategy is regarding the possibility of drug-drug interactions due to coadministration of multiple drugs at the same time. However, several studies have reported that drug-drug interactions at the BBB are unlikely to happen in cassette dosing, due to low dosages used in the study (1-2 mg/kg) (Manitpisitkul and White, 2004; Liu et al., 2012) relative to the capacity of the transport systems (Cordon-Cardo et al., 1989; Cooray et al., 2002).

We examined the extent of brain penetration of these 8 EGFR inhibitors by calculating AUC ratios in brain and plasma following cassette dosing. To ensure there were no drug-drug interactions at the BBB, we also performed discrete dosing studies for individual drugs and compared the brain-to-plasma ratios at two time points (1-hr and 8-hr post dose) with the results from the cassette dosing study. Pharmacokinetic parameters and metrics were calculated from concentration-time profiles of each drug from cassette dosing studies. The correlation between the CNS multiparameter optimization (MPO) score (Wager et al., 2010; Wager et al., 2016) and the measured brain penetration of these compounds was examined in order to determine the relationship between various physicochemical properties taken together in a series of EGFR inhibitors.

## **5.2 MATERIALS AND METHODS**

### **5.2.1 Chemicals and reagents**

6-[4-[(4-ethylpiperazin-1-yl)methyl]phenyl]-N-(1-phenylethyl)-7H-pyrrolo[2,3-d]pyrimidin-4-amine (AEE788) and [4-(3-chloro-2-fluoroanilino)-7-methoxyquinazolin-6-yl] (2R)-2,4-dimethylpiperazine-1-carboxylate (AZD3759) were purchased from Selleck Chemicals (Houston, TX). N-[2-[2-(dimethylamino)ethyl-methylamino]-4-methoxy-5-[[4-(1-methylindol-3-yl)pyrimidin-2-yl]amino]phenyl]prop-2-enamide (osimertinib), N-(3-chloro-4-fluorophenyl)-7-methoxy-6-(3-morpholin-4-ylpropoxy)quinazolin-4-amine (gefitinib), N-(4-bromo-2-fluorophenyl)-6-methoxy-7-[(1-methylpiperidin-4-yl)methoxy]quinazolin-4-amine (vandetanib), N-(3-ethynylphenyl)-6,7-bis(2-methoxyethoxy)quinazolin-4-amine;hydrochloride (erlotinib hydrochloride), and

(E)-N-[4-(3-chloro-4-fluoroanilino)-7-methoxyquinazolin-6-yl]-4-piperidin-1-ylbut-2-enamide (dacomitinib) were purchased from LC laboratories (Woburn, MA). (E)-N-[4-(3-chloro-4-fluoroanilino)-7-[(3S)-oxolan-3-yl]oxyquinazolin-6-yl]-4-(dimethylamino)but-2-enamide (Afatinib), [13C, 2H3]-osimertinib, [2H6]-gefitinib, [13C, 2H6]-vandetanib, [2H6]-erlotinib HCL, and [2H6]-afatinib were purchased from Alsachim SAS (Illkirch, France). Analytic-grade reagents were purchased from Fisher Scientific (Waltham, MA). The rapid equilibrium dialysis (RED) device, including a 96-well base plate and membrane inserts (8 kDa molecular weight cut-off cellulose dialysis membrane), was purchased from Thermo Fisher Scientific Inc. (Waltham, MA).

### 5.2.2 Animals

Animals for pharmacokinetic studies and in vitro binding assays utilized both female and male Friend leukemia virus strain B (FVB) wild-type and *Mdr1a*<sup>b<sup>-/-</sup></sup> *Bcrp1*<sup>-/-</sup> mice (Taconic Biosciences, Inc., Germantown, NY) at the age of 8-14 weeks. Animals were bred and maintained in the accredited research animal housing facility at the University of Minnesota. Transgenic mouse colonies were routinely validated by conducting tail snip followed by genotyping (TransnetYX, Cordova, TN). All protocols for the animal experiments were approved by University of Minnesota Institutional Animal Care and Use Committee (IACUC) and performed in accordance with the Guide for the Care and Use of Laboratory Animals by the U.S. National Institutes of Health (Bethesda, MD).

### 5.2.3 Discrete Dosing Pharmacokinetic Study

The dosing suspensions for subcutaneous injection were prepared in 10 % DMSO and 0.25% hydroxypropyl methylcellulose (w/v) in order to achieve a dose of 1 mg/kg for each EGFR inhibitor. A single dose of each EGFR inhibitor was individually dosed in wild-type and triple knockout (*Mdr1a/b*<sup>-/-</sup>*Bcrp1*<sup>-/-</sup>) FVB mice. Blood and brain samples from mice were harvested at 1-hour and 8-hour after discrete drug administration (*N*=3-4 at each time point). Blood was collected by cardiac puncture using heparinized syringes after euthanizing in a carbon dioxide chamber. Plasma was separated by centrifuge at 6500 rpm at 4 °C for 20 minutes. Both plasma and brain samples were stored at -80 °C until LC-MS/MS analysis.

#### **5.2.4 Cassette Dosing Pharmacokinetic Study**

The dosing suspension for cassette dosing was prepared in the final strength of 10% DMSO and 0.25% hydroxypropyl methylcellulose (w/v) the same way for discrete dosing to make the mixture of 8 EGFR inhibitors in the final dosing suspension of 1 mg/kg. A single cocktail of 8 EGFR inhibitors was administered by subcutaneous injection in wild-type and triple knockout (*Mdr1a/b*<sup>-/-</sup>*Bcrp1*<sup>-/-</sup>) FVB mice. Blood and brain samples were harvested at pre-determined time points, including 0.5, 1, 2, 4, 8, and 16 hours after dosing (*N*=3-4 at each time point). Blood and plasma were collected and separated as described in the discrete dosing study.

#### **5.2.5 Protein Binding Study in Plasma and Brain Homogenate**

The free fractions of EGFR inhibitors were determined by using a rapid equilibrium dialysis (RED) device. Mouse plasma was obtained from FVB mice by cardiac puncture. The brain homogenate was prepared from FVB mouse by adding 2 volumes (w/v) of phosphate buffered saline (PBS; pH 7.4) followed by mechanical homogenization. EGFR inhibitor stock solutions are prepared in DMSO, and added to either mouse plasma or brain homogenate to make a final concentration of 5  $\mu$ M containing 0.3% DMSO. Either mouse plasma or brain homogenate containing compounds was loaded to the sample chamber (300  $\mu$ l) of the inserts first, and then blank PBS was loaded to the corresponding buffer chamber (500  $\mu$ l) according to the manufacturer's instruction (N=4). The plate was sealed with an adhesive lid and incubated at 37  $^{\circ}$ C for 4 hours in an orbital shaker at 300 rpm. Samples were collected from both chambers after the incubation, and stored in -80 $^{\circ}$ C freezer until LC-MS/MS analysis.

Unbound free fractions in the brain were calculated according to the following equation:

$$\text{Free fraction (fu)} = \frac{1/D}{\left(\left(\frac{1}{\text{fu, diluted}}\right)-1\right)+1/D} \quad (1).$$

The dilution factor (D) was 3 in the experiment described above.

The unbound (free) concentration partitioning to the brain was determined as below:

$$\text{Free brain partition coefficient (K}_{p,uu}) = \frac{\text{free brain concentration}}{\text{free plasma concentration}} = K_{p, \text{ brain}} \times \frac{f_{u, \text{ brain}}}{f_{u, \text{ plasma}}} \quad (2),$$

where  $K_{p, \text{ brain}}$  is the ratio of brain-to-plasma areas under the total concentration time profile as below:

$$\text{Brain partition coefficient (K}_{p, \text{ brain}}) = \frac{\text{AUC}_{\text{ brain}}}{\text{AUC}_{\text{ plasma}}} \quad (3).$$

The distribution advantage (DA) due to the lack of efflux transporters was calculated as below:

$$\text{Distribution advantage (DA)} = \frac{K_{p, \text{ brain, transporter knockout mice}}}{K_{p, \text{ brain, wild-type mice}}} \quad (4)$$

### 5.2.6 Analytical LC-MS/MS analysis to determine drug concentrations

Concentrations of the 8 EGFR inhibitors in specimens were measured using reverse-phase liquid chromatography (Agilent model 1200 separation system; Agilent Technologies, Santa Clara, CA) coupled with TSQ Quantum triple quadruple mass spectrometer (Thermo Finnigan, San Jose, CA) by operating electrospray in the positive ion mode. For liquid chromatographic separation, either gradient or isocratic elution was performed using Phenomenex Synergi Polar-RP column (75 X 2 mm, 4  $\mu\text{m}$ ; Phenomenex) depending on the compounds. The initial composition of mobile phase for AEE788, AZD3759, afatinib, and gefitinib was comprised of 75% distilled water with 0.1% formic acid (A) and 25% acetonitrile with 0.1% formic acid (B) with a 0.35 ml/min flow rate. The total run time was 7.5 minutes. The retention times for AEE788, AZD3759,



afatinib, and gefitinib were 1.01, 1.30, 1.00, and 1.43 minutes, respectively. The initial mobile phase composition for osimertinib, erlotinib, and vandetanib was comprised of 70% distilled water with 0.1% formic acid (A) and 30% acetonitrile with 0.1% formic acid (B) with a 0.35 ml/min flow rate. The total run time was 8.5 minutes. The retention times for osimertinib, erlotinib, and vandetanib were 1.06, 3.54, and 0.73 minutes, respectively. An isocratic separation was performed to separate dacomitinib with the initial condition of 70% aqueous phase (A) and 30% organic phase (B) for 4 minutes. The retention time for dacomitinib was 0.85 minutes. Mass-to-charge ratio (m/z) transitions were as follows: 500.14 > 72.15 for osimertinib, 504.14 > 72.14 for [<sup>13</sup>C, <sup>2</sup>H<sub>3</sub>]-osimertinib, 460.1 > 141.16 for AZD3759, 447.1 > 128.2 for gefitinib, 455.1 > 136.2 for [<sup>2</sup>H<sub>8</sub>]-gefitinib, 475.1 > 112.1 for vandetanib, 481 > 112.1 for [<sup>13</sup>C, <sup>2</sup>H<sub>6</sub>]-vandetanib, 394.1 > 278 for erlotinib, 400.1 > 284 for [<sup>13</sup>C]-erlotinib, 486.1 > 371.1 for afatinib, 492.1 > 377.1 for [<sup>2</sup>H<sub>6</sub>]-afatinib, 441.27 > 223.05 for AEE788, and 470.2 > 385.0 for dacomitinib.

### 5.2.7 Pharmacokinetic Calculations

Plasma and brain concentration-time data were analyzed with non-compartmental analysis (NCA) using Phoenix WinNonlin version 8.0 (Certara USA, Inc., Princeton, NJ). Areas under the curve (AUCs) for each compound were calculated by the trapezoidal rule to the last time point ( $AUC_{(0 \rightarrow t_{last})}$ ). Other pharmacokinetic parameters/metrics, including clearance (CL), volume of distribution (Vd), and half-life were determined by NCA. Brain-to-plasma ratios (Kp) of each EGFR inhibitor were calculated by the ratio of  $AUC_{(0 \rightarrow t_{last})}$  of brain concentration-time profile ( $AUC_{(0 \rightarrow t_{last}), \text{brain}}$ ) to that of plasma concentration-time

profile ( $AUC_{(0 \rightarrow t_{last}), plasma}$ ). Free partition coefficients of brain ( $K_{p,uu}$ ) were calculated by multiplying the  $K_p$  with the ratio of free fraction in brain homogenate to plasma ( $f_{u,brain}/f_{u,plasma}$ ). A brain distribution advantage (DA) in triple knock-out mice, that are lacking both P-gp and Bcrp (*Mdr1a/b*<sup>-/-</sup>*Bcrp1*<sup>-/-</sup>), compared to wild-type mice was obtained by calculating the ratio of  $K_p$  in triple knock-out to wild-type mice.

### 5.2.8 Statistical Testing

All data are presented as mean  $\pm$  standard deviation (S.D) or standard error of an estimate (S.E.). To compare the brain to plasma ratio in cassette dosing to that in discrete dosing, a parametric analysis unpaired t-test was performed by using GraphPad Prism (version 6; GraphPad Software, La Jolla California USA). A significance level at  $P < 0.05$  was considered as a statistical difference in all statistical testing.

## 5.3 RESULTS

### 5.3.1 Comparison of brain-to-plasma ratios from cassette and discrete dosing studies.

The brain-to-plasma ratios of each drug at a 1-hour and 8-hour following cassette dosing studies were compared with the results from discrete dosing studies at the same times post dose in both wild-type and TKO mice (Figure 2). Figure 2A shows the brain-to-plasma ratios of the 8 EGFR inhibitors from cassette dosing are within two-fold of the ratios from discrete dosing in wild-type mice at 1-hour after dosing, except AEE788, which shows higher brain-to-plasma ratio following

discrete dosing than in cassette dosing (\*  $P < 0.05$ ). Likewise, at 8-hour after dosing in wild-type mice, 5 out of 7 compounds are within two-fold difference in cassette dosing study when compared to discrete dosing study (Figure 2B). The two exceptions, afatinib and osimertinib, show a slightly higher brain-to-plasma ratio in cassette dosing study than in discrete dosing study (afatinib: \*  $P < 0.05$ , osimertinib: *N.S.*). In TKO mice, brain-to-plasma ratios of these drugs from cassette dosing study matched well with the results from discrete dosing study, except AEE788 at 8-hour post dose (Figure 2C and 2D, \*  $P < 0.05$ ). Overall, the results from cassette dosing study show good correlation with those from discrete dosing studies. Even though there were some values that are out of the two-fold range, possibly due to random biological variability, the brain to plasma ratios from cassette and discrete dosing strategy were comparable and support the use of the cassette dosing as a valid strategy to compare brain partition coefficients across the series of compounds.

### **5.3.2 Pharmacokinetic parameters and metrics of 8 EGFR inhibitors following cassette dosing in wild-type and *Mdr1a/b*<sup>-/-</sup>*Bcrp1*<sup>-/-</sup> FVB mice.**

The concentration-time profiles of 8 EGFR inhibitors following a single cassette dosing by subcutaneous injection were used to calculate pharmacokinetic parameters and metrics by using non-compartmental analysis (NCA) in WT and TKO (Table 2 and Table 3). Half-life of inhibitors in plasma were calculated based on the concentrations of plasma at the last three or four time points in the concentration-time profile where the drugs were in elimination phase. Half-life of these drug are ranging from 50 minutes with erlotinib to 13.7 hours with

vandetanib in wild-type FVB mice, and from 50 minutes with erlotinib to 17.6 hours with AEE788 in triple-knockout (*Mdr1a/b*<sup>-/-</sup>*Bcrp1*<sup>-/-</sup>) FVB mice. When the half-life of each drug in wild-type FVB mice is compared to the values in knockout animals, 7 out of 8 inhibitors have shown similar values within a 2-fold difference. Vandetanib showed differences over 2-fold in triple-knockout (TKO) FVB mice (5.74) when compared to wild-type mice (13.7), and the AUC in wild-type FVB mice was significantly higher than that in TKO mice ( $2230 \pm 61.3$  (WT) vs.  $1442 \pm 98.7$  (TKO),  $*P < 0.05$ ). Based on the non-compartmental analysis for vandetanib, the apparent volume of distribution (*Vd/F*) in WT was comparable to TKO (4947 mL/kg (WT) vs. 5085 mL/kg (TKO)), but the apparent clearance (*CL/F*) in TKO was about 2.5-fold higher than the value in WT (250 mL/hr/kg (WT) vs. 614 mL/hr/kg (TKO)). Except vandetanib, all other inhibitors have shown similar plasma AUCs in wild-type when compared to TKO mice. Overall, half-lives of these inhibitors in the brain were close to half-lives observed in plasma. Gefitinib and Afatinib in wild-type mice, and vandetanib in TKO, were the exceptions that showed longer half-life in brain than in plasma. Overall, systemic pharmacokinetic parameters and metrics in WT were similar to the values in TKO, but the AUC in brain were markedly different in WT and TKO across all compounds, following a cassette dosing of a set of EGFR inhibitors (concentration-time profiles of each drug is available in supplemental figure 1 and 2).

### 5.3.3 Brain penetration of EGFR inhibitors within an individual animal

The brain penetration of each EGFR inhibitor following cassette dosing was examined by calculating the brain-to-plasma ratio of each compound at each time point, within individual animal subjects. This allowed these compounds to be rank ordered from the highest penetration (high brain-to-plasma ratio) to the lowest penetration (low brain-to-plasma ratio) within a single animal subject. Ranked values within the same subjects were color-coded depending on their brain penetration in Figure 3, where dark blue was used for a compound with the highest brain penetration and dark red was used for the drugs with the lowest brain penetration. When the measured concentration was lower than the lowest limit of quantitation, the “penetration” color was greyed and marked as LLOQ. This “visual heat-map” of the rank order of the brain penetration of inhibitors was consistent across different subjects at different time points in both wild-type and triple-knockout mice. The overall classification of brain penetration, defined with color, either in the blue group or the red group, was consistent especially at the same time point after dosing. Interestingly, these rank orders within a mouse are more consistent across mice at early time points, until approximately 2 hours after cassette dosing, and less consistent at later time points in both WT and TKO animals.

#### **5.3.4 Determination of $K_p$ and $K_{pu}$ for brain**

The partition coefficients ( $K_p$ ) of brain for this set of EGFR inhibitors were determined in both wild-type and TKO FVB mice from the cassette dosing study (Table 3). The brain partition coefficients were calculated by the ratios of AUC of brain total concentration-time profile to AUC of plasma concentration-time profile

from time zero to the last time point of measured concentrations (16-hour). In wild-type mice that have intact efflux transporters in the BBB, the brain  $K_p$  was the highest for AZD3759 (1.7) and the lowest for erlotinib and AEE788 (0.062 and 0.066, respectively). These  $K_p$  values were increased in TKO mice for all studied compounds when compared to wild-type mice. However, the relative magnitude of increase in  $K_p$  was highly variable, from 1.6-fold for AZD3759 up to 28-fold for AEE788, as quantified by distribution advantage (DA) with equation (4) as shown in Table 3. The free fractions of these compounds were determined in mouse plasma and brain homogenate using rapid equilibrium dialysis. The free partition coefficients of brain ( $K_{p,uu}$ ) are presented in Table 3.  $K_p$  and  $K_{p,uu}$  values were the highest with AZD3759 in wild-type mice.  $K_p$  was the lowest with erlotinib in wild-type, while,  $K_{p,uu}$  was the lowest with AEE788 in wild-type mice. Importantly, in the wild-type mice, most of the  $K_{p,uu}$  values were well below unity, indicating that efflux system(s) play a significant role in limiting the brain penetration of these EGFR inhibitors. AZD3759 was the only compound that showed  $K_{p,uu}$  higher than unity (i.e., 2.96), indicative of a possible involvement of an influx system on modulating the delivery of this compound across the BBB. The rank orders of  $K_p$  and  $K_{p,uu}$  values showed that osimertinib has the highest  $K_p$  in TKO mice (15.7), which is about 16-fold higher than in wild-type mice. Although the rank orders of these values were changing depending on not only the degree of binding in plasma and brain but also the presence and the absence of efflux transporters, AZD3759, osimertinib, vandetanib, and dacomitinib consistently ranked with a comparatively high brain

penetration. On the other hand, the other four compounds in this cassette of eight EGFR inhibitors, including erlotinib, AEE788, afatinib, and gefitinib, categorized in the low brain penetration group.

### **5.3.5 Correlation between physicochemical properties and the brain partition coefficients**

Correlations between physicochemical properties and the brain penetration of this set of EGFR inhibitors were examined. A calculated CNS multiparameter optimization (MPO) score (Wager et al., 2010) and the ratios of cLogD to square root of molecular weight ( $\text{clogD}/\sqrt{\text{MW}}$ ) (Levin, 1980) were compared to  $K_p$  brain and  $K_p,uu$  in wild-type and TKO mice (Table 5 and Figure 4). The suggested CNS MPO scores are typically higher than 4 to predict good CNS penetration (Wager et al., 2016), and the MPO scores for the series of EGFR inhibitors were calculated by the most recent version of MPO score calculation tool (Wager et al., 2016). Importantly, using this tool, dacomitinib, vandetanib, and osimertinib were classified as low brain penetrants according to their MPO scores, but erlotinib and gefitinib as high brain penetrants. On the other hand, the method of predicting brain penetration of compounds by using the ratios of cLogD to square root of molecular weight predicted dacomitinib, vandetanib, and AEE788 as high brain penetrants, and erlotinib as a low brain penetrant. Based on the experimentally-determined brain partition coefficients ( $K_p$ s) reported above from our cassette dosing studies, osimertinib, dacomitinib, and vandetanib were consistently classified as high brain penetrants in wild-type FVB mice, and erlotinib and gefitinib as low brain penetrants. Moreover, compounds with similar

MPO scores, for example, AEE788 (3.3) and vandetanib (3.3), have widely different  $K_p$  values in wild-type mice, ranging from 0.635 for vandetanib, classified as highly brain penetrant, to 0.066 for AEE788, classified as a low brain penetrant (Table 5 and Figure 4C). A similar pattern was observed with  $c\text{LogD}/\sqrt{\text{MW}}$  in AEE788, dacomitinib, and erlotinib, that each have close  $c\text{LogD}/\sqrt{\text{MW}}$  values, but  $K_p$  values that are considerably different from one another. The free partition coefficients of brain ( $K_{p,uu}$ ) were plotted against either  $c\text{LogD}/\sqrt{\text{MW}}$  or MPO scores to understand the influence of binding in these correlations, however, no improved correlation was seen in these parameters (Figure 4). When the effect of major transporters, P-gp and Bcrp, was absent using TKO mice, the  $K_{p,\text{brain}}$  seemed to have a modest correlation with  $c\text{LogD}/\sqrt{\text{MW}}$ , but no correlation with MPO scores (Figure 4B and 4D). In conclusion, both  $c\text{LogD}/\sqrt{\text{MW}}$  and MPO score fail to show a clear predictive correlation with either  $K_{p,\text{brain}}$  or  $K_{p,uu,\text{brain}}$ . About half of compounds show a weak correlation between their physicochemical properties and brain distribution, whereas the other half showed no correlation.

## 5.4 DISCUSSION

Epidermal growth factor receptor (EGFR) has been an attractive target for treatment of primary brain tumors including glioblastoma (GBM), in which EGFR is over-expressed in about 60% of patients (Ohgaki and Kleihues, 2007; Huang et al., 2009; Brennan et al., 2013), as well as brain metastases from various cancers. However, one of the major challenges in developing an efficacious anticancer drug for tumors located in the brain is “delivery” of these agents to the



site of action, the brain tumor across an often intact blood-brain barrier (BBB). A brain-to-blood partition coefficient ( $K_{p, \text{brain}}$ ) is commonly used to experimentally determine and describe the brain distribution of a drug, requiring animal experiments. Recently, other methods, including a cassette dosing strategy (*N*-in-1 dosing), as well as prediction methods based on various physicochemical properties of a compound, have been suggested to determine or predict the brain distribution of therapeutics, which can possibly replace the experimental processes, especially in discovery and development of brain penetrant compounds. The present study shows that the cassette dosing approach can be useful to determine brain penetration of a series of compounds with the same pharmacological target, and to understand a role of efflux transporters at the BBB on the brain distribution of these small molecule therapeutics.

In the current study, we chose 8 EGFR inhibitors that are in different stages of clinical development and varying in their known brain penetration. 5 out of 8 EGFR inhibitors, including afatinib, erlotinib, gefitinib, osimertinib, and vandetanib, are approved anticancer drugs for various solid tumors, including non-small cell lung cancer (NSCLC), a tumor that often metastasizes to the brain. However, none of these approved first and second generation of EGFR inhibitors are effective in patients with primary brain tumors, and have only modest efficacy in patients with metastatic brain tumors (Table 6). Dacomitinib and AZD3759 are third generation of EGFR inhibitors. AZD3759 and osimertinib are reported to be CNS penetrating EGFR inhibitors that are under clinical investigation for the treatment of advanced NSCLC. Clinical studies with AZD3759 demonstrate an

objective response rate in over 80% of patients with NSCLC brain metastases (Ahn et al., 2017). Osimertinib has also shown promise in treating brain metastases (Goss et al., 2018). Dacomitinib has some limited efficacy in patients with metastatic NSCLC brain tumors harboring the T790M mutation (NCT01858389), and its efficacy in GBM is currently under clinical investigation (NSC01112527).

It is possible that irreversible inhibitors, including dacomitinib, afatinib, and osimertinib, may not need as high brain partitioning as for reversible inhibitors in order to achieve the same pharmacodynamic effect. This is predicated on the turnover of the drug-receptor complex. If an EGFR-inhibitor – receptor complex is rapidly turned over, the benefit of being an irreversible inhibitor can be lost. As such, it is still valuable to assess the ability of CNS penetration of all of these drugs, both reversible and irreversible inhibitors, to predict potential efficacy in brain tumor.

The comparison of brain to plasma ratios determined by both cassette and discrete dosing confirms the absence of drug-drug interactions at the BBB in this series of compounds similar to that reported previously by Liu et al (Liu et al., 2012). In the current study, brain to plasma ratios of a series of EGFR inhibitors obtained at 1 and 8 hours after dosing as a cassette were within a 2-fold range of the results from discrete dosing in both wild-type and transgenic mice that are lacking both P-glycoprotein (P-gp) and breast cancer resistance protein (Bcrp) (TKO). The greatest difference in brain to plasma ratio between cassette and

discrete dosing was observed with afatinib at 8 hour after dosing in wild-type mice, where the brain to plasma ratio estimate from the cassette study was about 5 times overestimated than the value from discrete dosing. On the other hand, brain to plasma ratios of AEE788 after cassette dosing underestimated the values after discrete dosing at 1 hour post dose in wild-type mice and at 8 hour post dose in TKO mice. There were no consistent trends between these outliers, and therefore this may represent experimental variability rather than a systematic trend related to the dosing strategies. Although both afatinib and AEE788 seem to be substrates of both P-gp and Bcrp, recognized from the values of the distribution advantage (DA) for these compounds, other compounds that are substrates of P-gp and Bcrp do not show any discrepancy between the results from cassette and discrete studies. In conclusion, overall the results from cassette dosing match well with the results from discrete dosing. Thus, the close correlation between cassette and discrete dosing results confirm that there are no significant drug-drug interactions occurring at the BBB, with the dose of 1 mg/kg, regardless of the efflux transporter liability.

The partition coefficients of brain ( $K_{p,brain}$ ) for each EGFR inhibitor were calculated from the AUC ratios of brain to plasma. In the current study, AUCs from time zero to the last time point were used for both plasma and brain without the extrapolation of AUC from the last time point to infinity, because the complete elimination phase was not reached until 16 hours after the dosing for some compounds. Therefore, AUCs from time zero to the last time point that concentrations were measured (i.e., 4 hours after the dosing for erlotinib, 16

hours after the dosing for all other compounds) were used for both plasma and brain to calculate the  $K_{p,brain}$  for each EGFR inhibitors. When the calculated  $K_{p,brain}$  from this study were compared with previously reported  $K_{p,brain}$  (Table 5), values were within 2-fold, except for vandetanib. Based on a  $K_{p,brain}$  in wild-type mice over 0.5, AZD3759, dacomitinib, osimertinib, and vandetanib can be classified as brain penetrant EGFR inhibitors.

Previous research on the efflux transporter liability of these EGFR inhibitors have shown that afatinib, erlotinib, gefitinib, osimertinib, and vandetanib are substrates of both P-gp and Bcrp (Agarwal et al., 2010; Minocha et al., 2012; Agarwal et al., 2013; Ballard et al., 2016). On the other hand, AZD3759 has been reported to not be a substrate of both P-gp and Bcrp. The  $K_{p,brain}$  calculated in the current study agree with the previous results in that the compounds known to be substrates of efflux transporters showed much higher brain partition coefficient values in  $Mdr1a/b^{-/-}Bcrp1^{-/-}$  mice (TKO) when compared to wild-type mice.

AEE788 and dacomitinib, which have no previous reports regarding their efflux transporter liability, are shown in this study to be substrates of both/either P-gp and/or Bcrp (see the DA values, Table 4). The  $K_{p,brain}$  in TKO for AZD3759 was similar to the value in wild-type with the distribution advantage (DA) of 1.56, that indicates neither P-gp nor Bcrp play a major role in the brain distribution of AZD3759, as has been previously reported (Zeng et al., 2015; Yang et al., 2016).

The brain penetration of each EGFR inhibitor was examined within a single animal to assess the brain penetrability of each drug under the same

physiological conditions by using a “visual heatmap”. Rank orders of brain-to-plasma ratios at a single time point were consistent until 2 hours after dosing in both wild-type and TKO mice. There can be several reasons of having less consistent rank orders after 2 hours. One explanation is that the systemic clearances and the brain distributional clearances, or the combination of the two, that influence the brain-to-plasma ratios may be different in individual animals, and this difference would be accentuated at late times. Another reason can be that some compounds are somewhat excluded from the rank calculation due to low concentration measured near the lowest limit of quantitation. Importantly, the ability of each of these inhibitors to distribute into the brain within a single animal seems to be consistent between animals, even though some physiological conditions may be slightly different in each animal.

The brain distribution, including the BBB permeability of a drug, can be related to the physicochemical properties of a compound when passive diffusion dominates drug transport processes. Importantly, molecular weight, lipophilicity (logP or logD), hydrogen bond donor and acceptor count (HBD), and topological polar surface area (TPSA) of a molecule are considered to be crucial properties to determine the intrinsic permeability and brain distribution (Rankovic, 2015; Heffron, 2016). Among these crucial characteristics of a molecule, clogD and molecular size (weight) were believed to be two key factors that determine the ability to cross the BBB (Oldendorf, 1974; Levin, 1980). It has been shown that there is a reasonable correlation between the calculated ratios of clogD and square root of molecular weight and the permeability in the brain capillaries,

using in situ perfusion as a measure of permeability (Levin, 1980). Recently, the central nervous system multiparameter optimization (CNS MPO) desirability tool has been proposed to predict the CNS penetration and understand the relationship between physicochemical properties and the drug distribution in CNS (Wager et al., 2010; Wager et al., 2016). In the current study, we found that there was a lack of correlation between the brain distribution of a compound defined by  $K_{p,brain}$ , and the physicochemical properties of a set of EGFR inhibitors. Even if non-specific protein binding or the effect of major transporters, P-gp and Bcrp, were considered by using free partition coefficient ( $K_{puu}$ ) or transporter deficient mice, no predictive correlation between brain penetrability and physicochemical properties of these compounds was found (Figure 4).

In conclusion, the current study indicates that cassette dosing can be a useful method to determine the brain distribution of a set of molecularly targeted anticancer therapeutics that share the same target, in this case, EGFR. The concordance of the brain to plasma ratios at a single time point following either cassette dosing or discrete dosing has validated that both methods are comparable, especially for rank order screening. A cassette dosing strategy is useful, not only because of cost and time efficiency, but also because of the ability to directly compare drug brain penetrability among a set of compounds within a single animal. The rank orders of the brain to plasma ratios in a single animal were consistent with the rank orders of  $K_{p,brain}$  calculated by AUC ratios of brain to plasma. Therefore, cassette dosing strategy can be useful for candidate selection with respect to brain distribution. Among this set of EGFR

inhibitors examined in the current study, AZD3759, osimertinib, vandetanib, and dacomitinib have superior brain penetration (over 50% of corresponding plasma concentration). These brain penetrant EGFR inhibitors may have value for the treatment of tumors located in the brain and should be considered for future clinical trials.

### **AUTHORSHIP CONTRIBUTIONS**

Participated in research design: Kim, Laramy, Sarkaria, Elmquist

Conducted experiments: Kim, Laramy, Mohammad, Talele, Fisher

Performed data analysis: Kim, Sarkaria, Elmquist

Wrote or contributed to the writing of the manuscript: Kim, Sarkaria, Elmquist

Figure 5.1 Structures of EGFR inhibitors used in the current study.

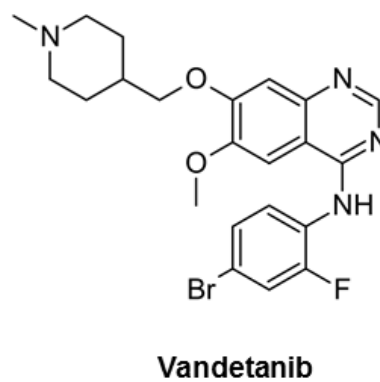
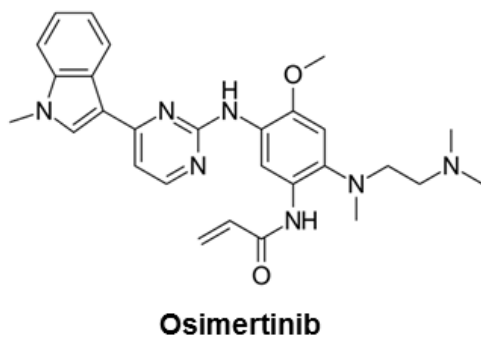
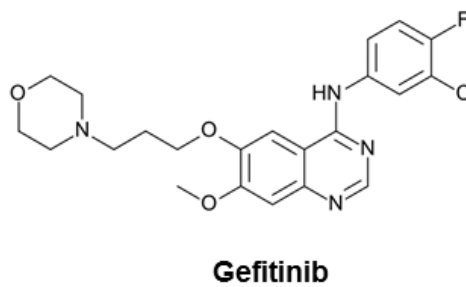
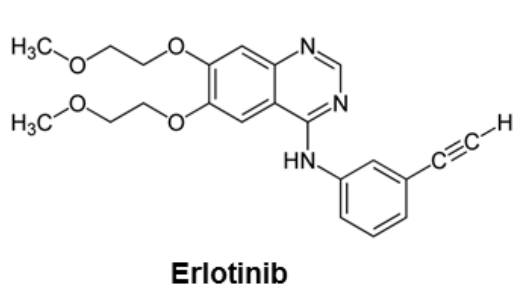
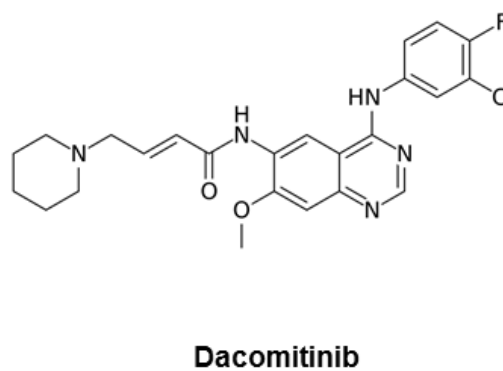
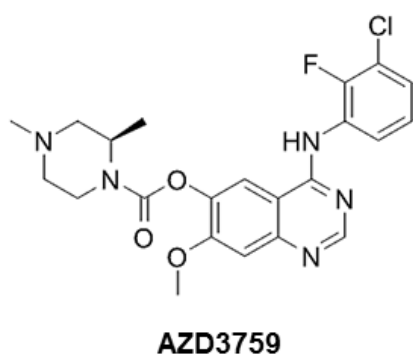
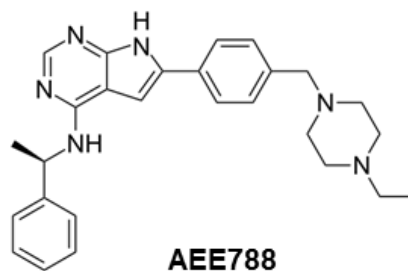
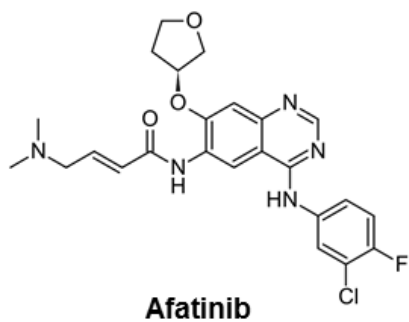




**Figure 5.2 Comparison of brain-to-plasma ratios between cassette and discrete dosing in wild-type and triple-knockout ( $Mdr1a/b^{-/-}Bcrp^{-/-}$ ) FVB mice. (A) Brain-to-plasma ratios at 1-hour post dose in wild-type FVB mice. (B) Brain-to-plasma ratios at 8-hour post dose in wild-type FVB mice. (C) Brain-to-plasma ratios at 1-hour post dose in triple-knockout ( $Mdr1a/b^{-/-}Bcrp^{-/-}$ ) FVB mice. (D) Brain-to-plasma ratios at 8-hour post dose in  $Mdr1a/b^{-/-}Bcrp^{-/-}$  FVB mice.**

Figure 5.2 Continued.

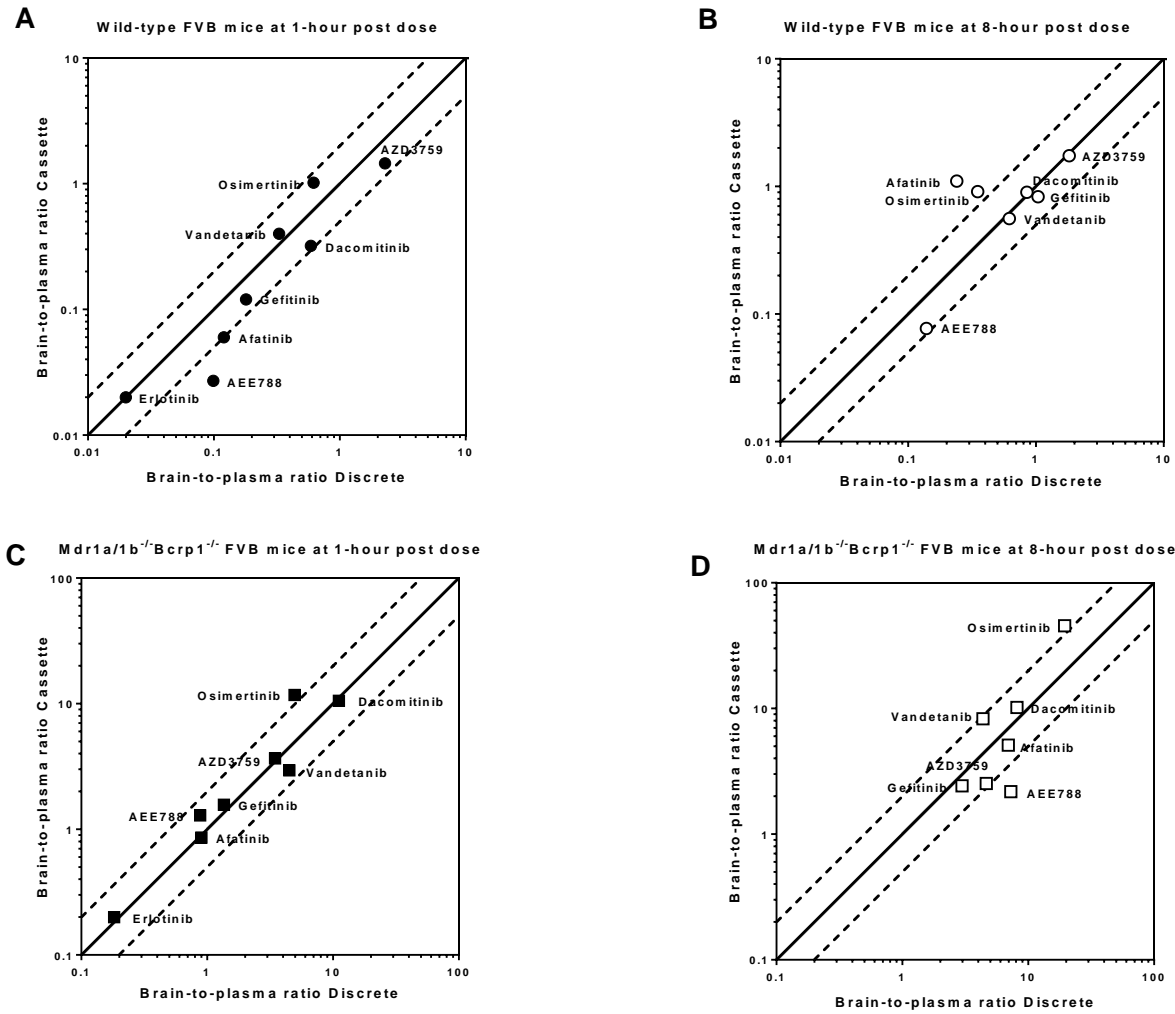


**Figure 5.3 Rank order of the brain distribution of EGFR inhibitors in a single animal. Rank order was based on the brain-to-plasma ratio at a single time point after dosing in individual animal.**

**A. Rank order in wild-type (WT) mice**

Animal ID	Time of Collection	Erlotinib	AEE788	Afatinib	Gefitinib	Dacomitinib	Vandetanib	Osimertinib	AZD3759	Rank
1	0.5h	0.031	0.030	0.121	0.135	0.491	0.302	0.789	0.357	1
2	0.5h	0.027	0.061	0.038	0.130	0.266	0.424	0.566	1.97	2
3	0.5h	0.029	0.031	0.070	0.119	0.174	0.302	0.716	1.67	3
4	0.5h	0.027	0.031	0.032	0.115	0.209	0.295	0.239	1.48	4
5	1h	0.016	0.021	0.022	0.071	0.399	0.355	0.597	1.09	5
6	1h	0.022	0.028	0.059	0.129	0.494	0.333	1.06	1.32	6
7	1h	0.028	0.044	0.070	0.167	0.243	0.607	1.44	2.04	7
8	1h	0.018	0.016	0.044	0.104	0.139	0.314	1.00	1.35	8
9	2h	0.015	0.060	0.147	0.166	1.76	0.347	1.59	1.45	
10	2h	0.028	0.094	0.207	0.216	1.43	0.337	1.73	1.53	
11	2h	0.018	0.046	0.055	0.104	ND	0.739	1.23	1.77	
12	2h	0.017	0.046	0.078	0.128	ND	0.494	0.950	1.08	
13	4h	0.020	0.084	0.165	0.229	0.593	0.816	1.95	1.37	
14	4h	0.027	0.092	0.417	0.195	0.359	0.570	1.80	1.97	
15	4h	2.68	0.084	0.483	0.359	0.435	1.34	1.44	1.95	
16	4h	LLOQ	0.098	0.481	0.658	0.623	1.16	1.14	2.00	
17	8h	LLOQ	0.074	1.03	LLOQ	1.12	0.538	0.485	2.32	
18	8h	LLOQ	0.081	0.970	1.30	1.17	0.509	0.798	1.94	
19	8h	LLOQ	0.070	1.07	0.677	0.361	0.606	1.25	1.54	
20	8h	LLOQ	0.082	1.32	0.498	0.946	0.588	1.10	1.15	
21	16h	LLOQ	0.073	1.11	LLOQ	LLOQ	0.571	0.159	5.45	
22	16h	LLOQ	0.071	LLOQ	3.78	1.01	LLOQ	LLOQ	LLOQ	
23	16h	LLOQ	0.084	1.08	3.97	0.586	0.732	0.050	2.17	
24	16h	LLOQ	0.077	1.34	2.47	0.193	0.793	0.104	21.2	

Figure 5.3 Continued.

**B. Rank order in *Mdr1a/b*<sup>-/-</sup>*Bcrp1*<sup>-/-</sup> (Triple knockout, TKO) mice**

Animal ID	Time of Collection	Erlotinib	Afatinib	AEE788	Gefitinib	AZD3759	Vandetanib	Dacomitinib	Osimertinib
1	0.5h	0.423	0.562	1.85	0.897	1.33	1.74	3.09	5.71
2	0.5h	0.167	0.468	0.574	1.00	2.90	1.64	4.05	5.84
3	0.5h	0.159	0.193	0.658	0.661	2.18	2.45	14.2	8.27
4	0.5h	0.131	0.583	0.621	0.92	2.97	1.81	11.3	3.06
5	1h	0.258	1.14	1.21	1.39	3.10	3.70	ND	17.7
6	1h	0.179	1.15	1.08	1.38	3.04	2.72	5.88	5.55
7	1h	0.217	0.272	1.43	2.01	5.94	3.03	4.19	20.0
8	1h	0.147	0.875	1.45	1.50	2.59	2.37	21.6	3.67
9	2h	0.354	1.94	2.63	2.52	4.39	3.10	12.4	7.66
10	2h	0.164	1.10	4.65	4.73	5.66	7.15	16.4	23.1
11	2h	0.278	1.86	1.53	1.49	2.45	4.66	10.5	3.58
12	2h	0.201	1.16	0.943	1.33	2.11	4.57	4.93	20.0
13	4h	4.18	3.11	2.69	2.39	2.66	8.01	24.1	52.3
14	4h	0.150	3.43	4.20	2.77	2.43	8.29	19.3	19.9
15	4h	0.057	2.55	3.42	3.25	3.48	5.83	23.7	16.3
16	4h	0.915	7.97	2.20	6.65	19.2	7.19	17.1	10.3
17	8h	LLOQ	0.944	1.22	0.96	0.42	13.5	18.5	LLOQ
18	8h	LLOQ	2.11	1.99	2.22	2.28	6.04	11.3	46.7
19	8h	LLOQ	6.71	3.07	3.30	2.65	41.8	28.2	64.5
20	8h	LLOQ	6.51	2.46	3.22	2.67	5.30	12.0	25.3
21	16h	LLOQ	3.21	0.773	2.23	0.766	23.3	6.24	5.18
22	16h	LLOQ	6.41	0.921	3.69	11.4	LLOQ	LLOQ	LLOQ
23	16h	LLOQ	8.59	0.713	11.3	LLOQ	LLOQ	LLOQ	LLOQ

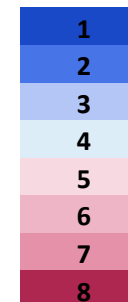


**Figure 5.4 Correlation between Kp and clogD/sqrt(MW) or MPO (multiparameter optimization) scores. (A) Correlation between Kp or Kpuu in wild-type FVB mice and clogD/sqrt(MW) (R square for Kp = 0.04895, R square for Kpuu = 0.224). (B) Correlation between Kp or Kpuu in triple-knockout (*Mdr1a/b*<sup>-/-</sup>*Bcrp*<sup>-/-</sup>) FVB mice and clogD/sqrt(MW) (R square for Kp = 0.137, R square for Kpuu = 0.0386). (C) Correlation between Kp or Kpuu in wild-type FVB mice and MPO score (R square for Kp = 0.108, R square for Kpuu = 0.0000911). (D) Correlation between Kp or Kpuu in triple-knockout (*Mdr1a/b*<sup>-/-</sup>*Bcrp*<sup>-/-</sup>) FVB mice and MPO score (R square for Kp = 0.557, R square for Kpuu = 0.433).**

Figure 5.4 Continued.

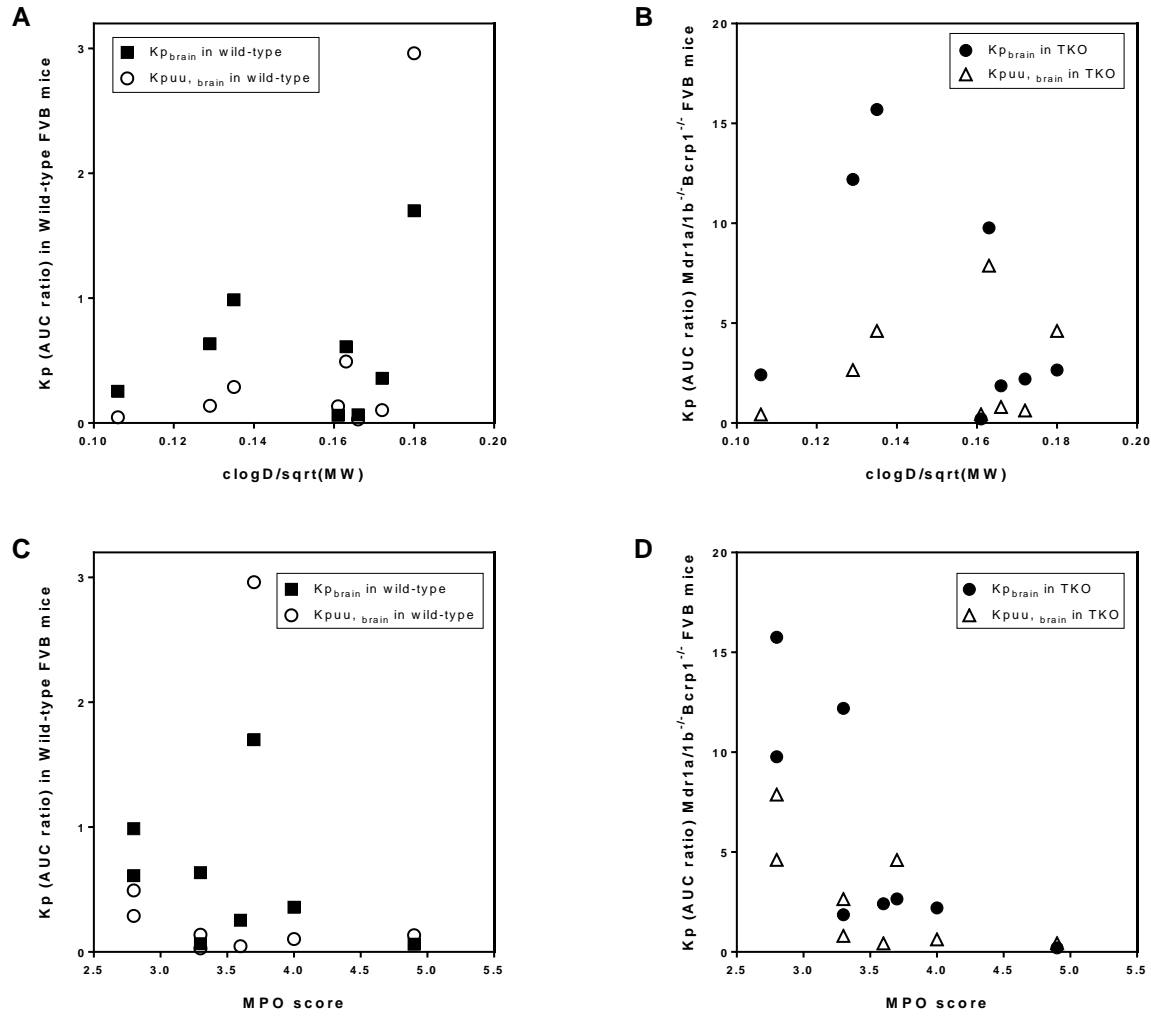


**Table 5.1 Physicochemical properties of EGFR inhibitors used in the study**

Compound	Type	MW <sup>b</sup>	clogP <sup>a</sup>	clogD <sup>a</sup>	TPSA <sup>b</sup>	HBD <sup>b</sup>	pKa <sup>a</sup>	efflux liability
AEE788	Reversible <sup>c</sup>	441	4.44	3.49	60	2	8.24	Not reported
Afatinib	Irreversible <sup>d</sup>	486	3.76	2.34	89	2	8.81	P-gp and Bcrp <sup>h</sup>
AZD3759	NA	460	4.03	3.86	80	1	7.10	Not a substrate <sup>l</sup>
Dacomitinib	Irreversible <sup>e</sup>	470	4.71	3.53	79	2	8.55	Not reported
Erlotinib	Reversible <sup>f</sup>	393	3.20	3.20	75	1	4.62	P-gp and Bcrp <sup>i</sup>
Gefitinib	Reversible <sup>f</sup>	447	3.75	3.64	69	1	6.85	P-gp and Bcrp <sup>j</sup>
Osimertinib	Irreversible <sup>g</sup>	500	4.49	3.01	88	2	8.87	P-gp and Bcrp <sup>h</sup>
Vandetanib	NA	475	4.54	2.81	60	1	9.13	P-gp and Bcrp <sup>k</sup>

<sup>a</sup> obtained from ChemAxon (<https://chemicalize.com/>)

<sup>b</sup> obtained from PubChem (<https://pubchem.ncbi.nlm.nih.gov/>)

<sup>c</sup> (Reardon et al., 2012) <sup>d</sup> (Solca et al., 2012) <sup>e</sup> (Engelman et al., 2007) <sup>f</sup> (Krawczyk et al., 2017)

<sup>g</sup> (Cross et al., 2014) <sup>h</sup> (Ballard et al., 2016) <sup>i</sup> (Agarwal et al., 2013) <sup>j</sup> (Agarwal et al., 2010) <sup>k</sup> (Minocha et al., 2012)

<sup>l</sup> (Zeng et al., 2015)

**Table 5.2 PK parameters in wild-type mice**

	unit	AEE788	Afatinib	AZD3759	Dacomitinib	Erlotinib	Gefitinib	Osimertinib	Vandetanib
$t_{half}$	hr	12.4	7.20	2.37	8.45	0.827	2.66	2.77	13.7
<b>Apparent CL</b>	mL/hr/kg	582	1196	1915	881	961	1706	1407	250
<b>Apparent Vd</b>	mL/kg	10377	12389	6539	10723	1146	6542	5632	4947
$t_{half, brain}$	hr	13.9	25.7*	2.69	10.5	0.75	14.2*	2.27	10.6
$AUC_{last, plasma}$	hr*ng/mL	985	734	486	826	1001	576	645	2230
$SE\_AUC_{last, plasma}$	hr*ng/mL	23.3	80.6	27.7	79.2	39.6	54.6	43.7	61.3
$AUC_{last, brain}$	hr*ng/mL	65.3	186	828	505	62.4	206	638	1416
$SE\_AUC_{last, brain}$	hr*ng/mL	2.20	3.35	60.8	24.0	8.21	3.85	31.9	95.0

$t_{half}$ , half-life of a drug in plasma

Apparent CL, apparent clearance CL/F

Apparent Vd, Apparent volume of distribution, Vd/F

$t_{half, brain}$ , half-life of a drug in brain

$AUC_{last, plasma}$ , area under the curve from zero to the time of last measured concentration in plasma

$SE\_AUC_{last, plasma}$ , standard error of an estimate of area under the curve in plasma

$AUC_{last, brain}$ , area under the curve from zero to the time of last measured concentration in brain

$SE\_AUC_{last, brain}$ , standard error of an estimate of area under the curve in brain

\* the half-life was determined by the slope of last three time points in concentration-time profile.

The values were larger than the half-life in plasma because complete elimination phase has not been captured in the experiments.



**Table 5.3 PK parameters in TKO mice**

	unit	AEE788	Afatinib	AZD3759	Dacomitinib	Erlotinib	Gefitinib	Osimertinib	Vandetanib
<b>t<sub>half</sub></b>	hr	17.6	5.95	2.75	8.99	0.846	4.20	2.24	5.74
<b>Apparent CL</b>	mL/hr/kg	531	679	1598	822	1570	1431	1657	614
<b>Apparent Vd</b>	mL/kg	13502	5827	6349	10667	1916	8680	5353	5085
<b>t<sub>half,brain</sub></b>	hr	5.1	10.5	2.32	16.6	0.95	4.76	3.59	41.8*
<b>AUC<sub>last, plasma</sub></b>	hr*ng/mL	858	1279	617	877	609	658	566	1442
<b>SE_AUC<sub>last, plasma</sub></b>	hr*ng/mL	61.8	234	95.9	135	49.7	95.3	81.6	98.7
<b>AUC<sub>last, brain</sub></b>	hr*ng/mL	1599	3082	1633	8572	124	1449	8913	10773
<b>SE_AUC<sub>last, brain</sub></b>	hr*ng/mL	89.1	174	72.0	307	6.12	57.0	1584	563

t<sub>half</sub>, half-life of a drug in plasma

Apparent CL, apparent clearance CL/F

Apparent Vd, Apparent volume of distribution, Vd/F

t<sub>half, brain</sub>, half-life of a drug in brain

AUC<sub>last, plasma</sub>, area under the curve from zero to the time of last measured concentration in plasma

SE\_AUC<sub>last, plasma</sub>, standard error of an estimate of area under the curve in plasma

AUC<sub>last, brain</sub>, area under the curve from zero to the time of last measured concentration in brain

SE\_AUC<sub>last, brain</sub>, standard error of an estimate of area under the curve in brain

\* the half-life was determined by the slope of last three time points in concentration-time profile.

The values were larger than the half-life in plasma because complete elimination phase has not been captured in the experiments.

**Table 5.4 The partition coefficients and free partition coefficients of brain for EGFR inhibitors.**

	<b>AEE788</b>	<b>Afatinib</b>	<b>AZD3759</b>	<b>Dacomitinib</b>	<b>Erlotinib</b>	<b>Gefitinib</b>	<b>Osimertinib</b>	<b>Vandetanib</b>
Kp,brain, wild-type	0.066	0.254	1.70	0.612	0.062	0.358	0.988	0.635
Kp,brain, TKO	1.86	2.41	2.65	9.77	0.204	2.20	15.7	7.47
f <sub>u,p</sub>	0.068	0.080	0.058	0.008	0.045	0.041	0.005	0.055
f <sub>u,b</sub>	0.029	0.014	0.101	0.007	0.096	0.012	0.001	0.012
Kp,uu, wild-type	0.029	0.046	2.96	0.493	0.134	0.103	0.289	0.138
Kp,uu, TKO	0.804	0.433	4.61	7.88	0.438	0.631	4.61	2.65
DA	28.1	9.49	1.56	16.0	3.27	6.16	15.9	19.1

Kp (AUC ratio), the ratio of AUC<sub>last, brain</sub> to AUC<sub>last, plasma</sub> using total drug concentrations

Kp,uu (AUC ratio), the ratio of AUC<sub>last, brain</sub> to AUC<sub>last, plasma</sub> using free drug concentrations

f<sub>u,p</sub>, free fraction in plasma measured by rapid equilibrium dialysis (n=4)

f<sub>u,b</sub>, free fraction in brain homogenate measured by rapid equilibrium dialysis (n=4)

DA, distribution advantage calculated by the ratios of Kp,brain in transgenic to Kp,brain in wild-type

**Table 5.5 The calculated scores based on physicochemical properties and the partition coefficients of brain**

Compound	CNS MPO Score <sup>a</sup>	cLogD/ sqrt(MW)	K <sub>p</sub> brain in publication	K <sub>p</sub> brain in wild-type	K <sub>p</sub> uu, brain in wild-type	K <sub>p</sub> brain in TKO	K <sub>p</sub> uu, brain in TKO	DA
AEE788	3.3	0.166	NA	0.066	0.029	1.86	0.80	28
Afatinib	3.6	0.106	0.35 <sup>d</sup>	0.268	0.048	2.41	0.43	9
AZD3759	3.7	0.180	0.89 <sup>e</sup>	1.70	2.96	2.65	4.61	2
Dacomitinib	2.8	0.163	NA	0.612	0.493	9.77	7.88	16
Erlotinib	4.9	0.161	0.02 <sup>f</sup> /0.14 <sup>g</sup>	0.060	0.130	0.20	0.44	3
Gefitinib	4.0	0.172	0.21 <sup>h</sup> /0.3 <sup>i</sup>	0.358	0.103	2.20	0.63	6
Osimertinib	2.8	0.135	1.78 <sup>j</sup>	0.988	0.289	15.7	4.61	16
Vandetanib	3.3	0.129	0.21 <sup>k</sup>	0.635	0.138	12.2	2.65	19

<sup>a</sup> MPO, multiparameter optimization score calculated by using the method from (Wager et al., 2016)

<sup>d</sup> reported from (van Hoppe et al., 2017)

<sup>e</sup> reported from (Xiong et al., 2017)

<sup>f</sup> in rat. Reported from (Agarwal et al., 2013)

<sup>g</sup> in mouse. Reported from (de Vries et al., 2012)

<sup>h</sup> in nude mice. Reported from (Ballard et al., 2016)

<sup>i</sup> in FVB mice. Reported from (Agarwal et al., 2010)

<sup>j</sup> in nude mice. Reported from (Ballard et al., 2016)

<sup>k</sup> in FVB mice. Reported from (Minocha et al., 2012)

**Table 5.6 Summary of clinical information on the studied 8 EGFR inhibitors**

Compound	Clinical status	Dose in patients (mg/day)	Brain penetration (% of CSF to plasma levels) in patient	Brain penetration (% of brain to plasma ratio) in pre-clinical model	Response rate in patients with primary brain tumor (%)	Response rate in patients with brain metastases (%)	References
AEE788	Terminated	50 - 800	ND	ND	GBM, stable disease (17%)	ND	(Reardon et al., 2012)
Afatinib	Giotrif	50	0.7	ND	GBM, stable disease (14%)	35%	(Wind et al., 2014; Hoffknecht et al., 2015; Reardon et al., 2015)
AZD3759	Phase I (fast review)	100-1000	111	282	ND	83%	(Zeng et al., 2015; Ahn et al., 2017; Xiong et al., 2017)
Dacomitinib	Phase 2-3	45/60	NA	NA	ND	6.3 % <sup>a</sup>	
Erlotinib	Tarceva	150	2.77- 5.1	13.7	GBM, PFS6 (3%) first-relapse GBM, OR (6.3%)	82.4 (EGFR mutation)	(Raizer et al., 2010; Togashi et al., 2010; Yung et al., 2010; Porta et al., 2011; de Vries et al., 2012)

Gefitinib	Iressa	750-1000	1.07-3.58	27	astrocytoma, overall disease-control rate (17.9%) GBM, overall disease-control rate (12.5%)	27%	(Ceresoli et al., 2004; Franceschi et al., 2007; Chen et al., 2013)
Osimertinib	Tagrisso	80	NA	180	ND	54% (T790M+)	(Ballard et al., 2016; Goss et al., 2018)
Vandetanib	Caprelsa	300	1.2 - 2.4	21	GBM, objective response rate (12.5%)	ND	(Kreisl et al., 2012)

<sup>a</sup> from clinicaltrials.gov (identifier: NCT01858389)

GBM (glioblastoma); ND (not determined); NA (not available); PFS6 (progression-free survival at 6 months); OR (objective rate)

**CHAPTER 6 FACTORS INFLUENCING LUCIFERASE-  
BASED BIOLUMINESCENT IMAGING IN PRECLINICAL  
MODELS OF BRAIN TUMOR.**

## 6.1 INTRODUCTION

Bioluminescent imaging (BLI) is commonly used to visualize gene expression in biomedical research and to measure tumor burden in preclinical cancer research (Thorne et al., 2010). The most common reporter used is firefly luciferase (fLuc) combined with D-luciferin, a natural substrate of firefly luciferase. D-luciferin is oxidized by firefly luciferase in the presence of adenosine triphosphate (ATP) and magnesium cofactors (Kaskova et al., 2016). This enzymatic reaction happens in multiple steps. First, D-luciferin is transformed to luciferyl adenylate, and this central intermediate is then converted through a series of intermediates to ultimately form oxyluciferin in a reaction that releases a photon (bioluminescence). Beyond the fLuc/D-luciferin pair, there are numerous native or sequence-optimized bioluminescent enzymes that can be coupled with natural or synthetic substrates to provide a spectrum of light emission characteristics that are optimized for various uses.

Bioluminescent imaging has various advantages in biomedical research. Light produced by this enzymatic reaction enables various high-throughput screening strategies in multi-well format plates. In addition, substrates of luciferase are non-toxic to animals, so there are no anticipated adverse toxicities associated with standard dosing of animal. Moreover, this non-invasive method to evaluate growth or response to therapy of orthotopic tumors that are not readily measurable by other techniques. Finally, coupled with relevant gene promoters, various luciferase expression constructs can be used to monitor gene expression in real-time without terminal processing of cell culture or animal samples.

Because in all of these use scenarios, the concentration of luciferin substrate ultimately can affect the photon flux associated with luciferase-mediated metabolism, definition of the physical and biological factors that influence luciferin concentrations at the site of action inside cells is critically important.

There are several factors that affect the light signal measurements (Figure 1) when whole animal BLI is performed. (1) Pharmacokinetics and biodistribution of luciferase substrates are crucial in the eventual production of the light signal in animal. Luciferase substrates, often given to the animal by intraperitoneal injection, need to be adequately delivered to the tissue where the luciferase enzyme is expressed. (2) Even though these substrates may be extensively distributed to a specific tissue, they need proper membrane permeability to diffuse into the cell where the luciferase enzyme is present. (3) The physico-chemical parameters, such as enzyme affinity for the substrate,  $K_m$ , and activity of the enzyme at the location critically affect the rate of reaction (light signal intensity) according to Michaelis-Menten kinetics. (4) Attenuation of light intensity between the location of photon production and the photon detection device, such a CCD camera. This is especially important for in vivo imaging where photon wavelength can dramatically affect attenuation in biological tissues; longer or red-shifted wavelengths penetrate tissue better with less attenuation. (Dawson et al., 1980; Weissleder and Ntziachristos, 2003; Jathoul et al., 2014). (5) The sensitivity of a detector or camera to measure the light signal can also be closely related to signal intensities. In this context, significant research is devoted to identifying novel synthetic or natural luciferase/luciferin



pairings that produce intense, red-shifted photon emissions that maximize utility for in vivo imaging.

D-luciferin have been used extensively as a substrate for non-invasive imaging in neuroscience research despite limitations on distribution across the blood-brain barrier (Berger et al., 2008). This limited distribution to the brain is possibly due to activity of the breast cancer resistance protein (Bcrp) efflux transporter in the luminal membrane of brain capillary endothelial cells (Zhang et al., 2007; Bakhsheshian et al., 2013). BCRP is one of several efflux transporters that translocate xenobiotics from the intracellular compartment of endothelial cells back into the capillary lumen, and previous mouse studies demonstrated enhanced bioluminescent signal from the brain when mice were co-dosed with a pharmacologic Bcrp inhibitor (Bakhsheshian et al., 2013). Recently, a synthetic analogue of D-luciferin, CycLuc1, was reported as an alternative substrate for firefly luciferase that may be more suitable for use in neuroscience (Evans et al., 2014). The structure and physicochemical properties of CycLuc1 are similar to D-luciferin and are summarized in Supplementary Table 1 with the main difference being higher lipophilicity of CycLuc1 (XLogP 2.6) as compared to D-luciferin (XLogP 0.9). Another distinctive and important characteristic of CycLuc1 is the much lower  $K_m$  with firefly luciferase ( $K_m$  for D-luciferin and CycLuc1, 6.76  $\mu$ M and 0.1  $\mu$ M, respectively) (Harwood et al., 2011). Consistent with these metrics, CycLuc1 provided a much brighter signal at a significantly lower dose than D-luciferin in a mouse imaging model in which an fLuc-expressing virus was injected into a deep brain structure. In light of the known limitations of D-luciferin

distribution into brain and enhanced lipophilicity of CycLuc1, these results were interpreted as consistent with superior distribution of CycLuc1 across the BBB. The focus of the present study is to critically evaluate this hypothesis or otherwise explain the superior neuro-imaging characteristics of CycLuc1.

The distributional and pharmacokinetic properties of these luciferase substrates were compared by directly measuring the concentrations of both D-luciferin and CycLuc1 by liquid chromatography coupled with mass spectrometry (LC-MS) in brain and plasma. This is a novel approach, since concentrations of luciferase substrates have been predicted in many previous publications solely based on their bioluminescent light signal intensities. However, the signal intensity of light can be influenced by various factors (Figure 1) other than the concentration or the amount of substrates at the site of action, as previously described.

Therefore, the direct determination of substrate concentrations by using LC-MS provides a more robust and direct determination of the biodistribution and pharmacokinetics of luciferase substrates, which then critically informs their use as reporter systems in neuroscience.

In the current study, several specific questions were examined to understand the role of efflux transporters on the distribution of luciferase substrates and the possible reasons for the enhanced light signal from CycLuc1. First, the intensity of bioluminescent signal with D-luciferin and CycLuc1 were compared in heterotopic and orthotopic models of patient-derived glioblastoma (GBM). Second, the permeability of substrates across a cell monolayer and

substrate liabilities of both compounds with respect to Bcrp-mediated transport were examined by using *in vitro* experiments in Bcrp-transfected cells. Third, the role of Bcrp on the brain distribution of D-luciferin and CycLuc1 was studied *in vivo* using Bcrp knockout mice. Fourth, the influence of efflux transporter inhibitors was investigated in both *in vitro* and *in vivo* GBM models to examine the role of transporters on D-luciferin and CycLuc1 biodistribution. The answers to these specific questions, as discussed in the current study, provide a better understanding and interpretation of the use of bioluminescent markers and give more general guidance when choosing substrate for luciferase-based reporter systems for *in vivo* imaging.

## **6.2 MATERIALS AND METHODS**

### **6.2.1 Chemicals and reagents**

(S)-2-(6-Hydroxy-2-benzothiazolyl)-2-thiazoline-4-carboxylic acid, 4,5-Dihydro-2-(6-hydroxy-2-benzothiazolyl)-4-thiazolecarboxylic acid (D-luciferin) was purchased from Thermo Fisher Scientific (Waltham, MA). (4R)-2-(6,7-dihydro-5H-pyrrolo[3,2-f][1,3]benzothiazol-2-yl)-4,5-dihydro-1,3-thiazole-4-carboxylic acid (CycLuc1) was purchased from Millipore (Burlington, MA). 17-(Cyclopropylmethyl)-6,7-dehydro-4,5 $\alpha$ -epoxy-3,14-dihydroxy-6,7-2',3'-indolomorphinan hydrochloride (Naltrindole) was purchased from Tocris Bioscience (Ellisville, MO). All other chemicals and reagents used were high-performance liquid chromatography grade from Thermo Fisher Scientific

(Waltham, MA). The rapid equilibrium dialysis (RED) base plate and membrane inserts (8 kDa molecular weight cut-off cellulose membrane) were purchased from Thermo Fisher Scientific (Waltham, MA).

### **6.2.2 *Lentiviral vector and cell transduction***

A modified lentivirus vector, pGIPZ-Luc2 5 tdT, was developed by replacing turbo green fluorescent protein tag of pGIPZ with a fusion of firefly luciferase (Luc2) and tandem tomato (tdT) red fluorescent protein excised from pcDNA3.1(+)/Luc2-tdT. Lentiviral particles were packaged in HEK293T cells, and transduction to primary GBM6 cells was performed in the presence of 5 mg/ml polybrene (MilliporeSigma, Jaffrey, NH) as previously described (Laramy et al., 2017). Stable transduction expressing Luc2-tdT fusion gene (GBM6-Luc2-tdT) were selected in 5 mg/ml puromycin, and subsequently propagated as flank tumors.

### **6.2.3 *In vivo tumor xenograft mouse model***

All animals were approved by the Mayo Institutional Animal Care and Use Committee. For subcutaneous xenograft model, GBM6-Luc2=tdTomato cells were suspended in Matrigel/PBS and injected on the flank of athymic nude mice with  $2 \times 10^6$  cells. For orthotopic models, flank tumor xenografts were harvested and cultured for 5-14 days for intracranial injection. Tumor cells were harvested and injected  $3 \times 10^5$  cells to the right basal ganglia of anesthetized athymic nude mice (athymic Ncr-nu/nu, National Cancer Institute, Frederick, MD) using a small animal stereotactic frame (ASI Instruments, Houston, TX).

#### 6.2.4 *In vivo* bioluminescent tumor imaging

GBM12 fLUC2-tdTomato cells from explant cultures were injected orthotopically as described above. Animals were anesthetized by isoflurane inhalation and maintained under anesthesia by continuous inhalation of isoflurane until imaging was complete. Bioluminescent signal from the tumor was measured twice weekly with either D-luciferin or CycLuc1 (Glix Laboratories, Hopkinton, MA), ten minutes after a single i.p. injection of these substrates by IVIS Spectrum. The conditions for BLI acquisition were open emission filter, exposure time 60 seconds, binning medium for 8, field of view 12.9 cm, and f/stop as 1. Images were analyzed with Living Image 4.3 software (PerkinElmer).

#### 6.2.5 Pharmacokinetic studies in vivo

##### *Animals*

Friend leukemia virus strain B (FVB) wild-type (WT) and Bcrp knockout (*Bcrp1<sup>-/-</sup>*, BKO) mice were used for in vivo studies (Taconic Farms, Germantown, NY). Mice used for the experiments were in between 8 to 16 week-old with approximate weight of 15 to 35 g at the time of experiments and balanced for sex. For all animals for pharmacokinetic and inhibitor studies were maintained and housed in Research Animal Resources (RAR) facility located at the Academic Health Center, University of Minnesota, following an approved breeding protocol.

#### 6.2.6 *Full time course pharmacokinetic studies*

A single dose of either D-luciferin or CycLuc1 was administered by either intraperitoneal injection or tail vein injection with designated dose in wild-type and Bcrp knockout FVB mice. The dosing solutions for both compounds were prepared in sterile water with 1% DMSO. Blood and brain samples were collected at the pre-determined time points ranging from 2 minutes to 180 minutes after either a single intraperitoneal or intravenous injection (N=3-5 at each time point). Mouse whole blood was collected by cardiac puncture using heparinized syringes. Plasma was separated by centrifuge at 6500 rpm at 4 °C for 20 minutes. Plasma and brain were stored at -80 °C until LC-MS/MS analysis.

#### **6.2.7 Transporter inhibitor studies**

Transporter inhibitors, either Ko-143 or probenecid, were dosed by intravenous bolus injection either 10 minutes for Ko-143 or 30 minutes for probenecid prior to the administration of D-luciferin or CycLuc1. Doses used for the inhibitor studies were as follows; 16 mg/kg for Ko-143, 150 mg/kg for probenecid, 50 mg/kg for D-luciferin, and 10 mg/kg for CycLuc1. Blood and brain samples were collected at 10 minutes and 60 minutes after the dose of D-luciferin and CycLuc1. Mouse whole blood was collected by cardiac puncture using heparinized syringes. Plasma was separated by centrifuge at 6500 rpm at 4 °C for 20 minutes. Plasma and brain were stored at -80 °C until LC-MS/MS analysis.

#### **6.2.8 In vitro trans-well permeability assay**

In vitro bi-directional flux assay was performed with Madin-Darby Canine Kidney II (MDCKII) cells that overexpress murine breast cancer resistance protein (Bcrp1) or vector-controlled cells. Both cell lines were kindly provided by Dr. Alfred Schinkel. Cells were cultured by using Dulbecco's modified Eagle's medium supplemented with 10% (v/v) fetal bovine serum and antibiotics (penicillin, 100 U/ml; streptomycin, 100 mg/ml; amphotericin B, 250 ng/ml). Cells were seeded on the permeable polyester membrane inserts in 12-well plate (Corning™, Corning, NY) with a density of  $1 \times 10^5$  cells/well, and cultured for 7 days. The average values of transepithelial electrical resistance (TEER) on day 7 were about  $280 \Omega/\text{cm}^2$ . On the day of experiment, cells were washed with serum free cell assay buffer twice and pre-incubated with or without inhibitor, ko-143, for 30 minutes. Buffer with specified concentrations of either D-luciferin or CycLuc1 was added to a donor compartment. For apical to basolateral transport, 0.4 ml of drug containing buffers were added to the apical (top) compartment, and for basolateral to apical transport, 1.2 ml of drug containing buffers were added to the basolateral (bottom) compartment. Drug free buffers were added to the receiver compartments. Immediately after the incubation starts, 10  $\mu\text{l}$  of buffer were collected from the donor compartments. Plates were incubated in orbital shaker at  $37^\circ\text{C}$ , and 50  $\mu\text{l}$  of buffer samples were collected from the receiver compartments at 60, 90, 120 minutes after incubation, and drug free buffer was added to the receiver compartments at each time point. After 120 minutes, the integrity of cell monolayer has been confirmed with lucifer yellow. All samples were store at  $-80^\circ\text{C}$  until the analyses by using LC-MS/MS.

Apparent permeabilities of D-luciferin and CycLuc1 were determined by the following equation;

$$\text{Apparent permeability (Papp)} = \frac{dQ/dt}{C_0 \times A} \quad (\text{Equation 1})$$

where  $dQ/dt$  is mass transported across the cell monolayer over time,  $C_0$  is a concentration in the donor compartment at time zero, and  $A$  is a surface area for the cell monolayer.

Efflux ratios of D-luciferin and CycLuc1 were calculated by the following equation;

$$\text{Efflux ratio (ER)} = \frac{\text{Papp from basolateral to apical compartment}}{\text{Papp from apical to basolateral compartment}} \quad (\text{Equation 2})$$

### 6.2.9 Free fraction in mouse plasma and brain homogenate

The free fractions of D-luciferin and CycLuc1 in mouse plasma and mouse brain homogenate were examined by using a rapid equilibrium dialysis (RED).

The free fractions of D-luciferin and CycLuc1 in mouse plasma and mouse brain homogenate were examined by using a rapid equilibrium dialysis (RED). The brain homogenate was prepared by using mechanical homogenization after adding 2 volumes (w/v) of phosphate buffer saline (PBS; pH 7.4). Either mouse plasma or brain homogenate with 5  $\mu\text{M}$  of either D-luciferin or CycLuc1 was loaded into the samples chamber of the cellulose membrane inserts that has 8000 Da cut off, and then drug free PBS was loaded into the corresponding



chamber ( $N=5$ ). The apparatus was sealed and incubated at 37°C for 4 hours in an orbital shaker with a 300 rpm agitation. Samples were collected at the end of incubation from both chambers. All samples were stored at at -80°C until LC-MS/MS analysis. Undiluted free fraction in the brain was extrapolated with the equation below reported previously (Kalvass and Maurer, 2002):

$$\text{Free fraction (fu)} = \frac{1/D}{\left(\left(\frac{1}{f_{u,\text{diluted}}}\right)-1\right)+1/D} \quad (\text{Equation 3})$$

The dilution factor (D) was 3 in the current experiment.

The unbound (free) concentration partitioning to the brain was determined by the equation below:

$$\text{Free brain partition coefficient (Kp,uu)} = \frac{\text{free brain concentration}}{\text{free plasma concentration}} = K_{p, \text{ brain}} \times \frac{f_{u,\text{brain}}}{f_{u,\text{plasma}}} \quad (\text{Equation 4}),$$

where  $K_{p, \text{ brain}}$  is the ratio of brain-to-plasma areas under the total concentration time profile.

The brain homogenate was prepared by using mechanical homogenization after adding 2 volumes (w/v) of phosphate buffer saline (PBS; pH 7.4). Either mouse plasma or brain homogenate with 5 μM of either D-luciferin or CycLuc1 was loaded into the samples chamber of the cellulose membrane inserts that has 8000 Da cut off, and then drug free PBS was loaded into the corresponding chamber ( $N=5$ ). The apparatus was sealed and incubated at 37°C for 4 hours in an orbital shaker with a 300 rpm agitation. Samples were

collected at the end of incubation from both chambers. All samples were stored at at -80°C until LC-MS/MS analysis. Undiluted free fraction in the brain was extrapolated with the equation below reported previously (Kalvass and Maurer, 2002):

$$\text{Free fraction (fu)} = \frac{1/D}{\left(\left(\frac{1}{f_{u,\text{diluted}}}\right)-1\right)+1/D} \quad (\text{Equation 3})$$

The dilution factor (D) was 3 in the current experiment.

The unbound (free) concentration partitioning to the brain was determined by the equation below:

$$\text{Free brain partition coefficient (Kp,uu)} = \frac{\text{free brain concentration}}{\text{free plasma concentration}} = K_{p, \text{ brain}} \times \frac{f_{u, \text{ brain}}}{f_{u, \text{ plasma}}} \quad (\text{Equation 4}),$$

where  $K_{p, \text{ brain}}$  is the ratio of brain-to-plasma areas under the total concentration time profile.

#### 6.2.10 Analytical LC-MS/MS bioanalysis

Total concentrations of both D-luciferin and CycLuc1 in samples were determined by using high performance liquid chromatography (Agilent model 1200 separation system; Agilent Technologies, Santa Clara, CA) coupled with TSQ Quantum triple quadrupole mass spectrometer (Thermo Finnigan, San Jose, CA). For liquid chromatographic separation, gradient elution was implemented using Phenomenex Synergi Polar-RP column (75 X 2 mm, 4 μm).

The initial composition of mobile phase was comprised of 75% distilled water with

0.1% formic acid (A) and 25% acetonitrile with 0.1% formic acid (B) with a 0.2 ml/min flow rate. The total run time was 11 minutes, and retention times for D-luciferin, CycLuc1, and naltrindole (internal standards) were 1.5, 1.8, and 4.62, respectively. Mass-to-charge (m/z) transitions were as follows: 281.0 > 234.91 (D-luciferin), 306.03 > 259.98 (CycLuc1), 415.097 > 254.10 (Naltrindole). All compounds were extracted from biological samples by using protein precipitation method with ice cold acetonitrile. All samples were stored in the dark and sample preparations were done with the minimal exposure to the light, because D-luciferin and CycLuc1 are unstable with a light exposure.

#### 6.2.11 Pharmacokinetic data analysis

Concentration-time profiles of D-luciferin and CycLuc1 were analyzed by using Phoenix WinNonlin version 6.4 (Certara USA Inc., Princeton, NJ), and pharmacokinetic parameters and metrics were calculated by non-compartmental analysis (NCA). The terminal elimination rate constants were determined by using the last three to four points in the concentration-time profiles. The brain-to-plasma partition coefficients ( $K_{p,brain}$ ) were calculated as below:

$$\text{Brain partition coefficient } (K_{p,brain}) = \frac{AUC_{brain}}{AUC_{plasma}} \quad (\text{Equation 5}),$$

where  $AUC_{brain}$  is an area under the curve from time zero to infinity of brain concentration-time profile ( $[AUC_{(0 \rightarrow \infty), brain}]$ ) and  $AUC_{plasma}$  is an area under the curve plasma concentration-time profile ( $[AUC_{(0 \rightarrow \infty), plasma}]$ ). The distribution advantages (DA) of brain in Bcrp knockout mice were determined by the ratio of brain partition coefficients in knockout mice to that in wild-type mice.

The bioavailability of D-luciferin and CycLuc1 following an intraperitoneal injection was calculated as below:

$$\text{Intraperitoneal bioavailability (F)} = \left\{ \frac{[\text{AUC}_{(0 \rightarrow \infty), \text{plasma}}]_{\text{IP}}}{[\text{AUC}_{(0 \rightarrow \infty), \text{plasma}}]_{\text{IV}}} \right\} \quad (\text{Equation 6})$$

where the  $[\text{AUC}_{(0 \rightarrow \infty), \text{plasma}}]_{\text{IP}}$  is the area under the curve from time zero to infinity of plasma concentration-time profile following a single intraperitoneal dose and  $[\text{AUC}_{(0 \rightarrow \infty), \text{plasma}}]_{\text{IV}}$  is the area under the curve from time zero to infinity of plasma concentration-time profile following a single intravenous dose.

#### 6.2.12 Statistical analysis

Data were presented as mean  $\pm$  standard deviation (S.D.) or mean  $\pm$  standard error of the estimate (S.E.) for the area under the curves. An unpaired two sample t-test was used to compare two groups in GraphPad Prism version 6.04 (GraphPad, La Jolla, CA) software with a significance level of  $P < 0.05$ .

### 6.3 RESULTS

#### 6.3.1 Comparisons of bioluminescence imaging with D-luciferin and CycLuc1 in flank and intracranial tumors

Total flux of bioluminescent light was compared using D-luciferin and CycLuc1 in the tumors implanted either on the flank (heterotopic model) or in the brain (orthotopic model) (Figure 2). GBM6, a GBM patient-derived xenograft (PDX), was stably transduced with a lentivirus expressing both Td-tomato and a

sequence optimized fLuc2 firefly luciferase gene. To enable a direct comparison between D-luciferin and CycLuc1, cross-over imaging was performed in the same mice on consecutive days for the flank and two-day intervals for the brain. In the preliminary experiments, the order of imaging, i.e., either D-luciferin first or CycLuc1 first, was found not to affect the intensities of bioluminescence signal for either compound, likely due to their short half-lives (less than 1 hour) (Supplementary Figure 1). Therefore, cross-over imaging was done on days 15, 21, and 28 for D-luciferin and on days 16, 22, and 29 for CycLuc1 after flank tumor implantation ( $N=5$ ). In intracranial tumor models, bioluminescence imaging was performed on days 13, 19, and 26 for D-luciferin and on days 15, 21, and 28 for CycLuc1 after intracranial tumor injection ( $N=4$ ). Two different doses of substrates were used for imaging: 30 and 150 mg/kg for D-luciferin and 5 and 25 mg/kg for CycLuc1. Bioluminescence images taken approximately 2 weeks after tumor implantation are presented in Figure 2A and 2B. Overall intensities of the bioluminescence signal were stronger in flank tumors when compared to intracranial tumors. When the signal intensity from CycLuc1 was compared to D-luciferin in the flank model, there was no significant difference between substrates when compared after low-dose administration or high-dose administration, respectively (Figure 2C and 2D). However, the signal intensity from CycLuc1 was significantly higher than D-luciferin in intracranial tumor model at either dose level (Figure 2E and 2F). To determine if these differences in signal intensity are because of differences in D-luciferin and CycLuc1 distribution in and around intracranial tumors, the concentrations of these compounds were

determined in different regions in the brain (Supplementary Figure 2). The concentrations of both D-luciferin and CycLuc1 in the tumor core, defined by robust Td-tomato signal, were more variable and higher compared to those in brain around tumor (BAT) and in normal brain (NB), even though the average tissue to plasma ratios in all regions were below 2% of their plasma concentrations for both D-luciferin and CycLuc1 (Supplementary Figure 2). Therefore, there is a potential advantage of using CycLuc1 compared to D-luciferin for intracranial tumor imaging with a higher photon flux, even though there is no such advantage with CycLuc1 for flank tumor imaging. In the context of factors that can affect in vivo bioluminescence signal intensity (see Figure 1), these data, all based on light production, would initially suggest that distribution across the BBB into the brain may be a critical factor affecting the superiority of CycLuc1 imaging.

### **6.3.2 Apparent permeability and efflux ratios of D-luciferin and CycLuc1**

Previous data suggest that D-luciferin is an efflux substrate for Bcrp, and therefore the efflux liability for D-luciferin was compared to CycLuc1 in a standard bi-directional flux assay. Apparent permeabilities ( $P_{app}$ ) of both D-luciferin and CycLuc1 were measured in both apical-to-basolateral (A-to-B) and basolateral-to-apical (B-to-A) directions using MDCKII wild-type vector control cells and MDCKII-Bcrp overexpressing cells in a Transwell™ plate (Figure 3A). With wild-type vector control cells, there were no significant differences in the apparent permeabilities from apical to basolateral compartment when compared to those from basolateral to apical compartment with either D-luciferin or CycLuc1 (*N.S.*,

$P > 0.05$ ). However, the Papp from basolateral to apical compartments for both D-luciferin and CycLuc1 were significantly higher in Bcrp-overexpressing MDCKII cells than those from apical to basolateral compartments, indicative of a possible role of Bcrp on the biodistribution of these compounds ( $P < 0.05$ ). The efflux ratios calculated for D-luciferin and CycLuc1 were 2.74 and 2.48, respectively, which demonstrated that both compounds were relatively low affinity substrates of the BBB efflux transporter, Bcrp. The effect of using Bcrp inhibitor, Ko-143, was examined in MDCKII-Bcrp overexpressing cells. The apparent permeability coefficients (Papp) from basolateral to apical compartments were measured in the presence of varying concentrations of Ko-143 from 0 to 100  $\mu$ M. The results show that the B-to-A Papp of both D-luciferin and CycLuc1 were decreased with increasing concentrations of the selective Bcrp inhibitor, Ko-143 (Figure 3B). The B-to-A Papp were significantly less in the presence of an inhibitor from that in the absence of an inhibitor ( $*P < 0.05$ ).

### **6.3.3 Comparisons of pharmacokinetic parameters and metrics of D-luciferin and CycLuc1 in wild-type and *Bcrp1*<sup>-/-</sup> FVB mice following a single intravenous dose**

The plasma and brain concentration-time profiles of D-luciferin and CycLuc1 were obtained in both wild-type (WT) and *Bcrp1*<sup>-/-</sup> knockout (BKO) FVB mice following a single intravenous bolus administration (Figure 4A and 4B). Blood and brain were collected by serial sacrifice at 5 time points up to 60 minutes for D-luciferin, and 7 time points up to 180 minutes for CycLuc1, based on their previously-determined plasma half-lives. The concentrations of both D-

luciferin and CycLuc1 in the BKO mice were higher at all time points when compared to the concentrations in WT for both plasma and brain. The pharmacokinetic parameters and metrics of both D-luciferin and CycLuc1 were calculated by non-compartmental analysis and are summarized in Table 1. The half-lives of D-luciferin in WT and BKO were 9.0 and 9.6 minutes, respectively. The half-lives of CycLuc1 in WT and BKO were 29.0 and 21.1 minutes, respectively; 2-3 times longer when compared to D-luciferin in both genotypes. The volumes of distribution of D-luciferin in both WT and BKO were much smaller (348 and 261 mL/kg in WT and BKO, respectively) than those of CycLuc1 (3430 and 2684 mL/kg in WT and BKO, respectively). The clearance of D-luciferin in WT (26.7 mL/min/kg) was higher than that in BKO (18.8 mL/min/kg), which possibly could be due to lack of efflux transporter in the elimination process of D-luciferin. Similarly, the clearance of CycLuc1 in WT (82 mL/min/kg) was higher than that in BKO (61.3 mL/min/kg). As expected from the concentration-time profiles, the areas under the curve (AUCs) from time zero to the last time point of D-luciferin in the BKO plasma and BKO brain were significantly higher than those in WT (plasma: 1860 min\* $\mu$ g/mL in WT and 2608 min\*  $\mu$ g/mL in BKO, \* $P$  < 0.05; brain: 9.19 min\* $\mu$ g/mL in WT and 19.2 min\*  $\mu$ g/mL in BKO, \* $P$  < 0.05). CycLuc1 also showed the similar results as D-luciferin, where the areas under the curve (AUCs) of both plasma and brain in WT were significantly higher than those in BKO (plasma: 607 min\* $\mu$ g/mL in WT and 810 min\*  $\mu$ g/mL in BKO, \* $P$  < 0.05; brain: 1.87 min\* $\mu$ g/mL in WT and 2.80 min\*  $\mu$ g/mL in BKO, \* $P$  < 0.05). The partition coefficients of brain to plasma for both luciferase substrates were



calculated by the ratios of AUCs from time zero to infinity in the brain to that in the plasma. For both D-luciferin and CycLuc1, the partition coefficients in BKO were slightly higher when compared to WT, but both values were extremely low; i.e., about 0.5 % for D-luciferin and 0.3% for CycLuc1. The free brain partition coefficients values were determined from the free fraction obtained by using rapid equilibrium dialysis (RED). The free brain partition coefficients of D-luciferin and CycLuc1 in both WT and BKO were also lower than unity. The calculated distribution advantages in BKO were less than 1.5 for both D-luciferin and CycLuc1, suggesting that the role of efflux transporter, Bcrp, in the brain distribution of these compounds is limited.

#### **6.3.4 Pharmacokinetic parameters and metrics of D-luciferin and CycLuc1 following a single intraperitoneal dose**

Because most laboratories use intraperitoneal administration of luciferin substrates, the concentrations in brain and plasma over time were examined following a single intraperitoneal administration of either 150 mg/kg of D-luciferin or 20 mg/kg of CycLuc1 in wild-type (WT) FVB mice (Figure 4C and 4D). The elimination phase of D-luciferin has a mono-exponential decline, while the elimination phase of CycLuc1 has more of a bi-exponential decline.

Pharmacokinetic parameters and metrics for both compounds were calculated by non-compartmental analysis (Table 2). Similar to the results from intravenous administration, the half-lives of CycLuc1 in the plasma and the brain were about 3 times higher (31.4 minutes in the plasma and 38.8 minutes in the brain) than those of D-luciferin (10.9 minutes in plasma and 12.6 minutes in brain). The

apparent volumes of distribution ( $V_d/F$ ) were 240 and 334 mL/min/kg for D-luciferin and CycLuc1, respectively. The apparent clearances ( $CL/F$ ) of D-luciferin and CycLuc1 seem to be similar, 15.3 and 18.9 mL/min/kg, respectively. The brain partition coefficients of D-luciferin and CycLuc1 were calculated by using the ratio of AUCs from time zero to infinity, and those were 0.5% for D-luciferin and 1.1% for CycLuc1. Similar to the results following an intravenous bolus dosing, the free brain partition coefficients were much lower than unity for both D-luciferin and CycLuc1. In conclusion, the brain distribution of both D-luciferin and CycLuc1 is similarly limited following an intraperitoneal administration in wild-type mice.

### **6.3.5 Tissue distribution of D-luciferin and CycLuc1 following a single intraperitoneal dose**

Distributions of D-luciferin and CycLuc1 in different tissues were examined following an intraperitoneal injection with either substrate, 150 mg/kg for D-luciferin and 25 mg/kg for CycLuc1 (Figure 4E and 4F). Each tissue was harvested at six pre-determined time points to obtain the concentration-time profiles for each tissue. The tissue partition coefficients ( $K_{ps}$ ) were calculated using the AUCs of each tissue obtained from non-compartmental analysis of the concentration-time profiles (Figure 4E and 4F). The partition coefficient was the highest in liver (10.3) for D-luciferin. On the contrary, for CycLuc1, the kidney has the highest tissue partition coefficient (7.5) (Table 3). The partition coefficient of brain for both D-luciferin and CycLuc1 were the lowest among these tissues and different from other  $K_{ps}$ . Most of  $K_{ps}$  for D-luciferin and CycLuc1 were higher

than or close to 1 except the partition coefficients of brain for both D-luciferin and CycLuc1 and the partition coefficient of heart for CycLuc1. Therefore, the distribution of both D-luciferin and CycLuc1 was not restricted in most tissues, except for the brain.

### **6.3.6 Influence of co-administration of transporter inhibitors on the systemic clearance and the brain partition coefficients of D-luciferin and CycLuc1**

Efflux transporter inhibitors, either Ko-143 (Bcrp selective) or probenecid (organic acid transporters), were co-administered with D-luciferin and CycLuc1 in wild-type FVB mice to understand the role of selected efflux transporters on the brain distribution of these compounds. Plasma and brain concentrations and brain-to-plasma ratios of D-luciferin and CycLuc1 following a co-administration of either Ko-143 or probenecid are presented in Figure 5. The concentrations of D-luciferin and CycLuc1 in both plasma and brain with the co-administration of Ko-143 were significantly increased at 60 minutes after dosing when compared to a vehicle control group (Figure 5A, 5B, and 5C). However, there were no significant changes at a more typical experimental imaging time-frame of 10 minutes after dosing, with or without an inhibitor (Figure 5A and 5B). Importantly, ratio of substrate in brain relative to plasma is not altered with or without Ko-143 at either time point (Figure 5C). Similarly, the co-administration of probenecid, the inhibitor of organic anion transporters, with either D-luciferin or CycLuc1

significantly increased the concentrations of both compounds in the plasma at 60 minutes, but not 10 minutes, after the dosing (Figure 5D, 5E, and 5F), while brain concentrations were unaffected at either time-point. As a result, the brain to plasma ratios of D-luciferin and CycLuc1 were significantly decreased with a co-administration of probenecid due to significant increases in plasma concentrations at 60 minutes after the dosing. In conclusion, co-administration of the Bcrp inhibitor and the inhibitor of organic anion transporters with either D-luciferin or CycLuc1 influenced the systemic clearance of these luciferase substrates.

#### **6.4 DISCUSSION**

Bioluminescent imaging (BLI) is a powerful noninvasive tool to determine the longitudinal growth of a tumor located in deep tissues or organs in preclinical cancer research (Lewis et al., 2002; Mook et al., 2003; Zeamari et al., 2004; Lyons, 2005). It is the most common method of measuring tumor size in orthotopic models, and often used as a guide to determine a drug efficacy (Vassileva et al., 2008; Xi et al., 2012; Textor et al., 2014; Li et al., 2018). However, there have been concerns and difficulties of using BLI in brain tumor models, due to the limited brain delivery of luciferase substrate, D-luciferin (Genevois et al., 2016). A synthetic luciferase substrate, CycLuc1, has recently been described and has shown to produce a much stronger signal than D-luciferin from the brain at a dramatically lower dose (Evans et al., 2014). This

novel BL imaging agent, CycLuc1, has been reported to have a greater potency than D-luciferin, based on its low  $K_m$  for firefly luciferase (about 70-fold higher than D-luciferin), but the brain distribution and pharmacokinetic properties of CycLuc1 have not been investigated (Harwood et al., 2011). The main goal of current study is to compare the bio-distribution of D-luciferin and CycLuc1 and understand the role of efflux transporters on the distribution and pharmacokinetics, and resultant efficacy as BLI agents in the brain. The current study shows that both D-luciferin and CycLuc1 are weak substrates of Bcrp. However, the role of Bcrp on the brain distribution of both substrates is limited based on our findings in both *in vitro* and *in vivo* experiments using transporter transfected cell lines and transporter knockout mice. In particular, this conclusion was drawn based on concentrations of both D-luciferin and CycLuc1 that were not inferred from the intensity of BL signal, but rather by a stability-indicating highly quantitative LC-MS assay, to avoid possible additional confounding factors affecting the light signal (see Figure 1).

Comparison of BL signal with D-luciferin and CycLuc1 showed that the light signal from luciferase transfected brain tumors from CycLuc1 was significantly stronger (at practical and routine IP doses) than the signal given by D-luciferin from tumors growing in the brain. This difference between substrates was particularly important and highlighted by the fact there was no significant difference when the same tumors were growing in the flank, according to the cross-over imaging results. The stronger light signal with CycLuc1 from the brain has been reported in luciferase expressing mice by Evans et al. However, this

study did not elucidate the reason for the stronger BL signal from CycLuc1 (Evans et al., 2014). It is possible that CycLuc1, as speculated by Evans et al., may have better accessibility or distribution to the brain than D-luciferin. No significant changes in the BLI signal with CycLuc1 in flank tumors implies that the distributional barrier for D-luciferin and CycLuc1 is less in the flank tumor as compared to tumors placed in the brain. It is possible that the higher affinity of firefly luciferase for CycLuc1, i.e., a lower  $K_m$ , is the main reason that leads to a stronger BLI signal, even if there is no distributional advantage to the brain with CycLuc1 as compared to D-luciferin. To understand the mechanism of the more intense BLI signal with CycLuc1 in the brain, the current study examined the possibility that CycLuc1 has a higher brain distribution coefficient as compared to D-luciferin, possibly due to a different substrate affinity to efflux transporters at the BBB, resulting in an enhanced permeability across the BBB.

Apparent permeabilities of both D-luciferin and CycLuc1 were determined to be lower than  $1 \times 10^{-6}$  cm/s, a common lower limit that indicates low intrinsic permeability (Artursson et al., 2001; Hubatsch et al., 2007), from apical to basolateral direction by using *in vitro* experiments with MDCKII wild-type and Bcrp overexpressing cell lines. Efflux ratios of D-luciferin and CycLuc1 using MDCKII Bcrp overexpressing cells indicate that Bcrp plays a role in the permeabilities of these compounds, even though the change in permeability was minor when compared to the underlying intrinsic permeability. Consistent with the conclusion from the efflux ratios, the inhibition of Bcrp by Ko143 decreases apparent permeabilities of both D-luciferin and CycLuc1 from basolateral to

apical compartment. However, even though the same concentration of Ko-143 decreases the permeability of D-luciferin more than that of CycLuc1 (1.7-fold decrease in D-luciferin, 1.1-fold decrease in CycLuc1 with 0.01  $\mu$ M of Ko143 compared to the absence of an inhibitor), both reductions were minor, yet statistically significant (\*  $P < 0.05$ ). Interestingly, the transcellular permeabilities of both D-luciferin and CycLuc1 were found to be extremely low based on the results from in vitro cell uptake assay (results not shown), consistent with a previous report with D-luciferin (Lee et al., 2003). Therefore, the major distributional mechanism of D-luciferin and CycLuc1 to the organs and tissues is likely through a paracellular pathway of transport, similar to other hydrophilic compounds, and not a transcellular pathway affected by active transport. This is likely a primary reason why these compounds lack significant distribution into the brain and not peripheral organs and tissues (Figure 4E, 4F and Table 3), because the paracellular pathway of molecular transport is extremely limited at the blood-brain barrier, mainly due to the high expression of tight and adherens junctions that is confirmed by a high electrical resistance (Butt et al., 1990). Bcrp, expressed on the luminal side of brain endothelial cell, transports compounds from inside the brain capillary endothelial cells or from within the lipid bilayer of luminal cell membrane (Kubo et al., 2015). These findings may explain why Bcrp has a limited role in the distribution of both D-luciferin and CycLuc1 to the brain. Moreover, since polar compounds like D-luciferin and CycLuc1 have a low intrinsic permeability, the substrate concentration accessible to the transporter will be limited, and in conjunction with a low transporter affinity for

each compound, the Bcrp-mediated transport rate could be low irrespective of the transport capacity at the BBB.

In vivo experiments using wild-type (WT) and Bcrp knockout (BKO) FVB mice showed the limited role of Bcrp at the BBB on the brain distribution of D-luciferin and CycLuc1. The brain partition coefficients of D-luciferin and CycLuc1 in BKO did not show significant changes from those in WT. However, the areas under the curve (AUCs) of both plasma and brain concentrations for D-luciferin and CycLuc1 were significantly higher in BKO when compared to WT. The genetic deletion of Bcrp changed the overall systemic exposure to D-luciferin and CycLuc1 by decreasing the systemic clearances (Table 1). It has been reported that D-luciferin is eliminated mainly by both kidney and hepato-biliary system, based on the biodistribution of radiolabeled D-luciferin (Lee et al., 2003; Berger et al., 2008). Therefore, the results from BKO and WT indicate that Bcrp plays a significant role in how the kidney and liver eliminate luciferin, likely through active secretory processes at the kidney tubule and bile canaliculus, but not in the distribution to the brain. There can be several possible reasons to explain why the lack of Bcrp does not change the brain partition coefficient in mice. First, there may be some other efflux transporters besides Bcrp, possibly multidrug resistance-associated proteins (Mrps) or organic anion transporters (Oats) known to transport organic anions. It has been reported that D-luciferin is a substrate of MRP4 (Cheung et al., 2015). Considering that both D-luciferin and CycLuc1 have a carboxylic acid group, which has an anionic charge at physiological pH, these organic anion transporters may be involved in the brain distribution of



these luciferase substrates at the BBB. Either Mrps and/or Oats, given the results of the probenecid inhibition studies (Figure 5D-5F), are involved in the transport of both D-luciferin and CycLuc1, even though inhibition of organic anion transport by probenecid does not lead to an increase in brain partition coefficients. Second, the role of Bcrp may be limited in this case, especially at the BBB, due to low intrinsic permeability of the substrates to cross the BBB, as outlined above by the in vitro permeability experiments. Intrinsic permeability, driven by diffusion, may consist of a transcellular pathway and a paracellular pathway of molecular transport. As previously mentioned, the transcellular diffusive pathway minimally contributes to the overall molecular transport for the polar substrates, D-luciferin and CycLuc1. Due to lack of paracellular transport, limited by intact tight junctions, across the BBB, transport of polar molecules such as D-luciferin and CycLuc1 into the brain is limited. Therefore, overall permeabilities of D-luciferin and CycLuc1 across the BBB are extremely low regardless of the activity of Bcrp. This is consistent with the general understanding that substrates of active efflux transporters are mostly lipophilic compounds (Golden and Pollack, 2003). Hydrophilic compounds like D-luciferin and CycLuc1 are reported to be much less influenced by active efflux transporters (Abbott, 2013). On the other hand, the activity of Bcrp becomes more pronounced in other tissues, such as the eliminating organs (kidney and liver), because permeabilities are great enough to allow the substrates ready access to the transporter, and as such the efflux activity of Bcrp is important. Moreover, the activity of Bcrp is reported to be dependent upon the pH by

changing the effective ionization state of its substrates (Li et al., 2011). The ionization of carboxylic acid on D-luciferin and CycLuc1 at physiological pH influences the activity of Bcrp on these substrates. Similar phenomena have been observed with methotrexate, pemetrexed, and fluorescein, which are all hydrophilic compounds with low permeabilities (Sun et al., 2001; Li et al., 2013; Sane et al., 2014). Methotrexate is a hydrophilic compound with low XLogP of -1.8 and a substrate of Bcrp (Sane et al., 2014), and its apparent permeability is reported to be  $1.2 \times 10^6$  cm/sec in Caco-2 cells, that is similar to D-luciferin and CycLuc1 (Yee, 1997). According to Sane et al., the absence of Bcrp in *Abcg2*<sup>-/-</sup> mice increases both the plasma and brain exposure of methotrexate, which results in minor (statistically not significant) increase in brain to plasma ratios. Interestingly, methotrexate is a substrate of both Bcrp and Mrp4, so there was a statistically significant increase in  $K_p$ ,brain with double knockout mice that are lacking both Bcrp and Mrp4, even though it was still only 2-fold higher. Therefore, it is also possible that other efflux transporters are involved in the brain distribution of D-luciferin and CycLuc1, as an example of methotrexate.

D-luciferin has been previously reported to be a substrate of Bcrp (Zhang et al., 2007; Bakhsheshian et al., 2013). Bakhsheshian et al., have shown that co-administration of the Bcrp inhibitor, Ko-143, increased the bioluminescence light output from the brain in mice without significant changes in the concentration of D-luciferin in plasma at 10-minutes after dosing (Bakhsheshian et al., 2013). The results from the current study are not fully consistent with the conclusions of Bakhsheshain et al., since the co-administration of Ko-143 was

not able to significantly increase the concentration of D-luciferin in the brain at 10-minute after the dosing with the same dose and dosing schedule as used by Bakhsheshian et al. However, there was a significant increase in both plasma and brain concentrations of D-luciferin at 60-minute after the dosing, even though the brain to plasma ratios of the inhibitor treated group were not significantly different from the ones of vehicle control group (Figure 5). These results prompted us to ask what would be the reasons that may lead to a discrepancy between these two experiments. The only difference between these experiments is the method of “estimating” the D-luciferin concentrations in the brain and plasma specimens. The concentrations of both D-luciferin and CycLuc1 were determined by mass spectrometry coupled with high performance liquid chromatography (LC-MS) in the current study. In Bakhsheshian et al., the concentrations of D-luciferin in the brain and plasma were assumed to be directly proportional to the measured bioluminescence light intensity (Bakhsheshian et al., 2013). As discussed earlier, the intensity of light signal can be affected by several factors other than the concentration of substrate itself (Figure 1). Moreover, the intensity of bioluminescent light signal that is the product of enzyme reaction does not always have a direct linear correlation with the concentration of substrates. According to the Michaelis-Menten kinetics on the enzyme reaction, small changes in the substrate concentration can be resulted in large changes in the response depending on the affinity of enzyme to a substrate. Therefore, it is not possible to make a direct correlation between the light signal intensity and the concentration of D-luciferin. Even though there is no

question that both D-luciferin and CycLuc1 are substrates of Bcrp, the question arises if the activity of Bcrp influences the brain distribution of these compounds. Consistent with the results from BKO mice, the role of efflux transporter, Bcrp, at the BBB is limited, due to their low intrinsic permeability across BBB at the beginning. Therefore, the inhibition of Bcrp increased the systemic exposure, and as such, increased the driving force for distribution to the brain of these compounds, a result not necessarily due to the role of efflux transporters, such as Bcrp, at the BBB.

Unlike D-luciferin, there are limited data available regarding the biodistribution and substrate status of CycLuc1 to understand the mechanism of enhanced bioluminescent light signal (Evans et al., 2014). There was speculation on the brain distribution and intrinsic permeability of CycLuc1 to be better than D-luciferin, based on the higher XLogP value of CycLuc1 when compared to D-luciferin. However, the current study has clarified that the biodistribution, especially the brain distribution, of both D-luciferin and CycLuc1 are similar. Moreover, both compounds are weak substrates of Bcrp. The reason that CycLuc1 does not have any advantage on the permeability and brain distribution over D-luciferin is likely due to a free carboxylate of both compounds which is ionized at physiological pH, thus resulting in the similar cLogD. The presence of ionized carboxylate is required to be a substrate of firefly luciferase, but it is a major limiting factor for their cell permeability and brain penetration. There has been an interesting study of making a pro-drug of luciferin to avoid the problem with carboxylic acid (Mofford and Miller, 2015). Mofford et al. have

reported that luciferin amides improve brain bioluminescence in live mice over their parent luciferins (Mofford and Miller, 2015). The current study, combined with the previous findings, yields answers to a series of questions that includes why CycLuc1 has a more robust bioluminescent signal and how it can be further improved.

In summary, the present study examined the pharmacokinetics, brain distribution, and the role of active efflux transporters on luciferase substrates, D-luciferin and CycLuc1, to understand the factors influencing the bioluminescent light signal. D-luciferin and CycLuc1 have similar physicochemical properties as well as similar chemical structure. In conclusion, CycLuc1 would be a better substrate of firefly luciferase for an intracranial tumor imaging, mainly due to its superior affinity to firefly luciferase. Even though further investigation is needed to find the involvement of other transporters on the biodistribution of D-luciferin and CycLuc1, the current paper suggests that the role of Bcrp is limited on the brain distribution of both D-luciferin and CycLuc1. Not only substrate status of compounds for efflux transporters but also intrinsic permeability needs to be considered to understand the influence of various transporters on the tissue distribution.

Figure 6.1 Schematic depiction of factors influencing bioluminescence light signal.

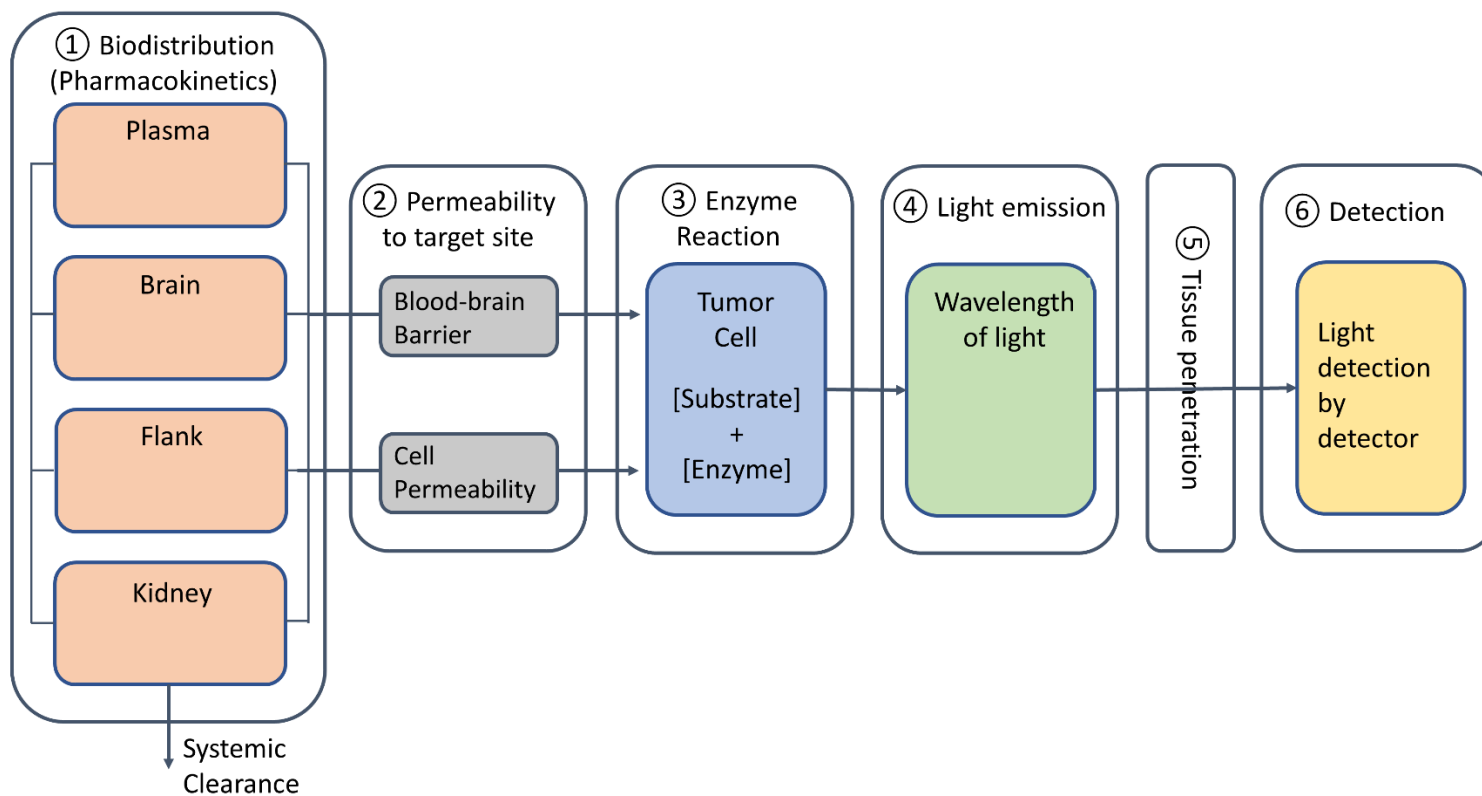
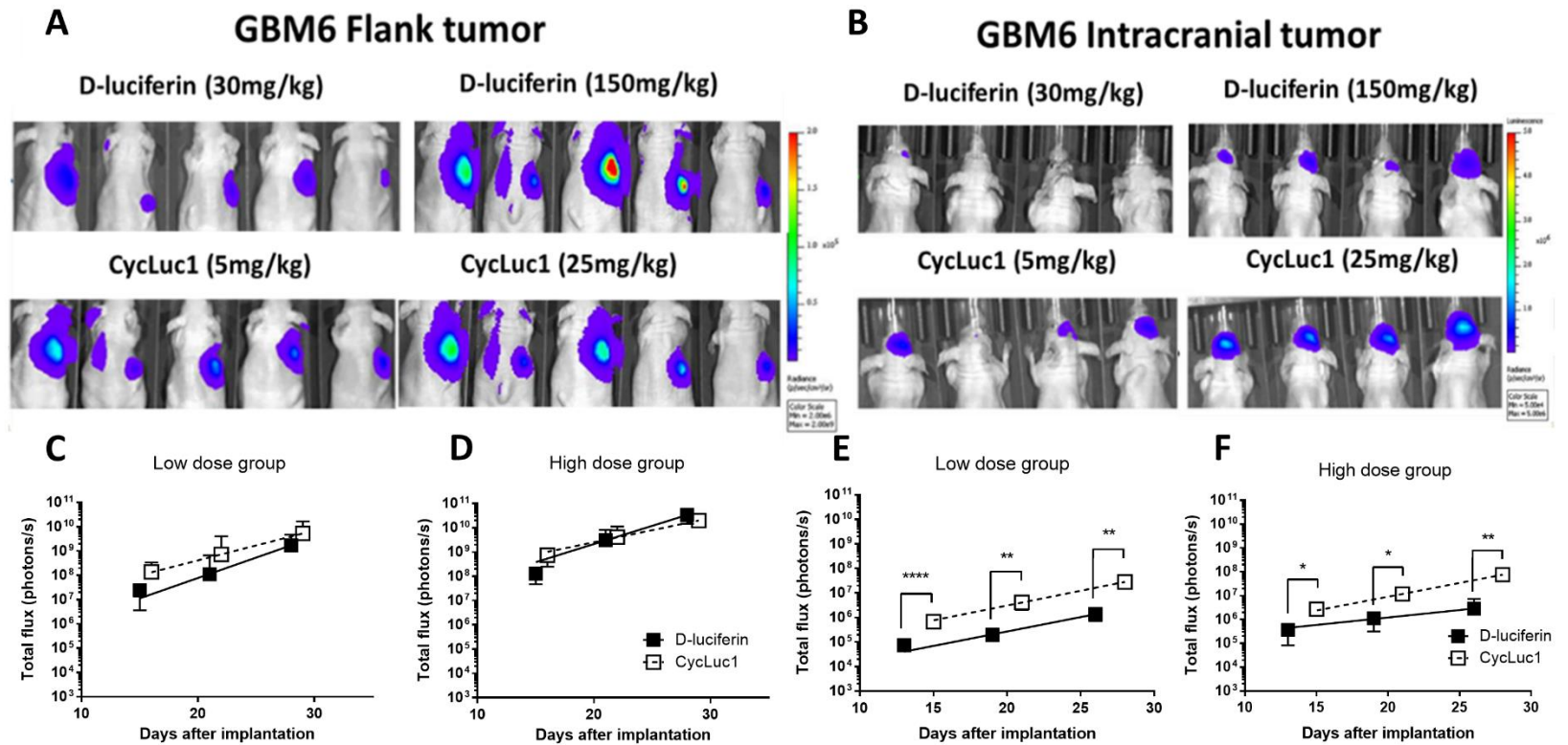
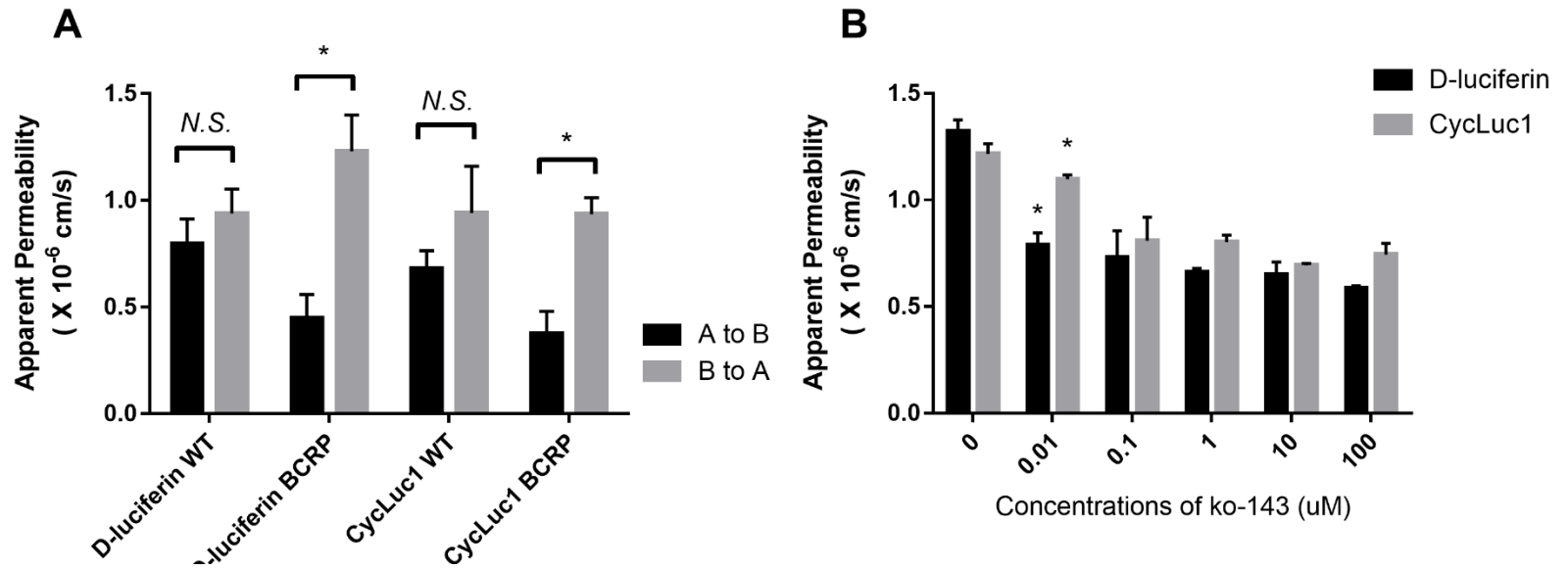


Figure 6.2 Bioluminescent imaging of GBM6 in flank tumor (A) and intracranial tumor (B) models. Cross-over imaging was performed for both substrate D-luciferin and CycLuc1 on different days.



**Figure 6.3** *In vitro* trans-well experiment results to examine the apparent permeability of D-luciferin and CycLuc1 with MDCKII-wildtype vector control and Bcrp overexpressing cell lines in the absence of Ko-143 (A) or in the presence of Ko-143 (B).





**Figure 6.4 Concentration-time profiles of D-luciferin and CycLuc1 in plasma and brain following a single intravenous dose in wild-type and Bcrp knockout FVB mice (A and B) or following a single intraperitoneal dose in wild-type FVB mice (C and D). Concentration-time profiles of D-luciferin and CycLuc1 in different tissues following an intraperitoneal injection (E and F).**

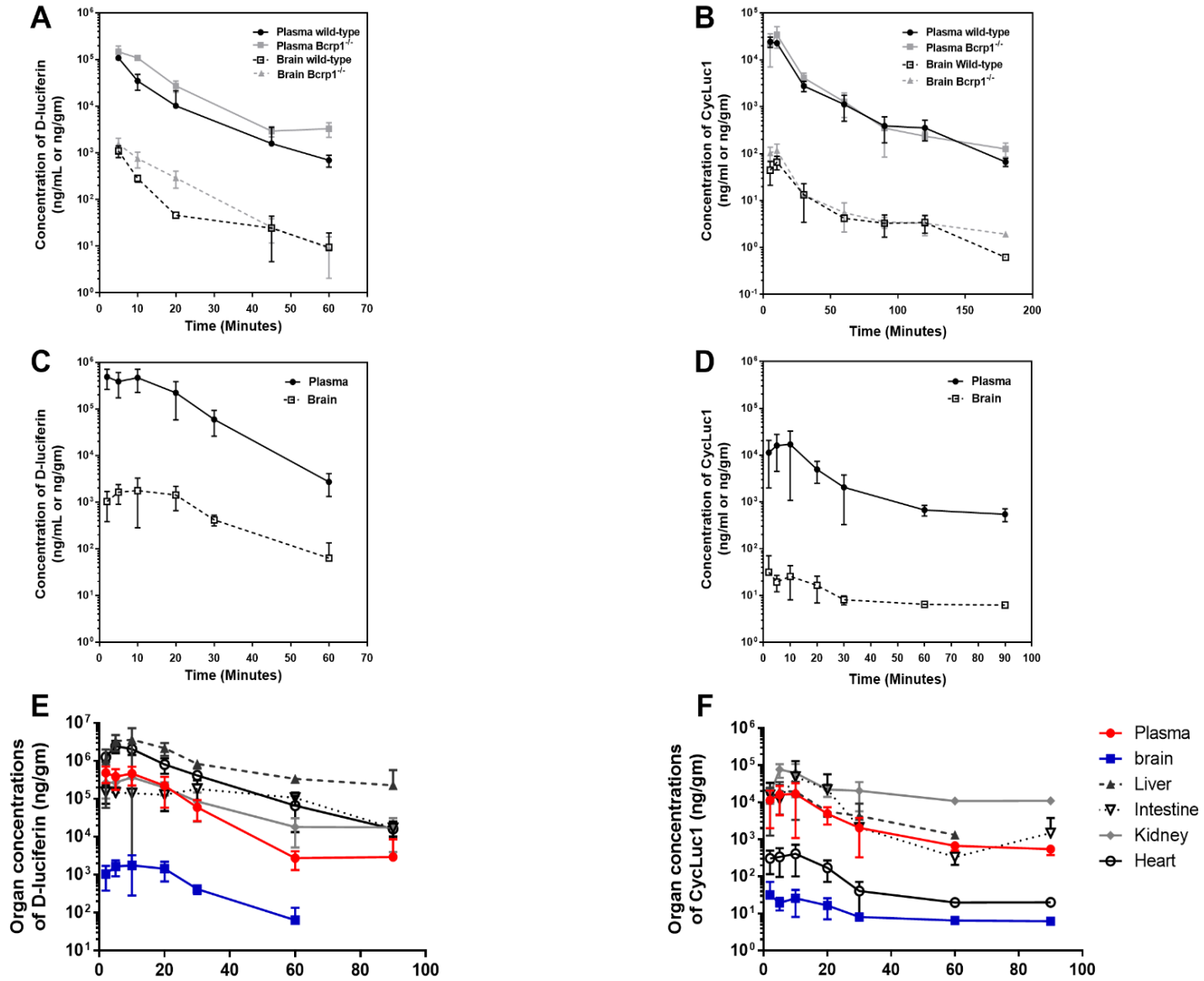


**Figure 6.5 Plasma and brain concentrations and brain-to-plasma ratios of D-luciferin and CycLuc1 at two time points with a co-administration of either Ko-143 (A-C) or probenecid (D-F).**

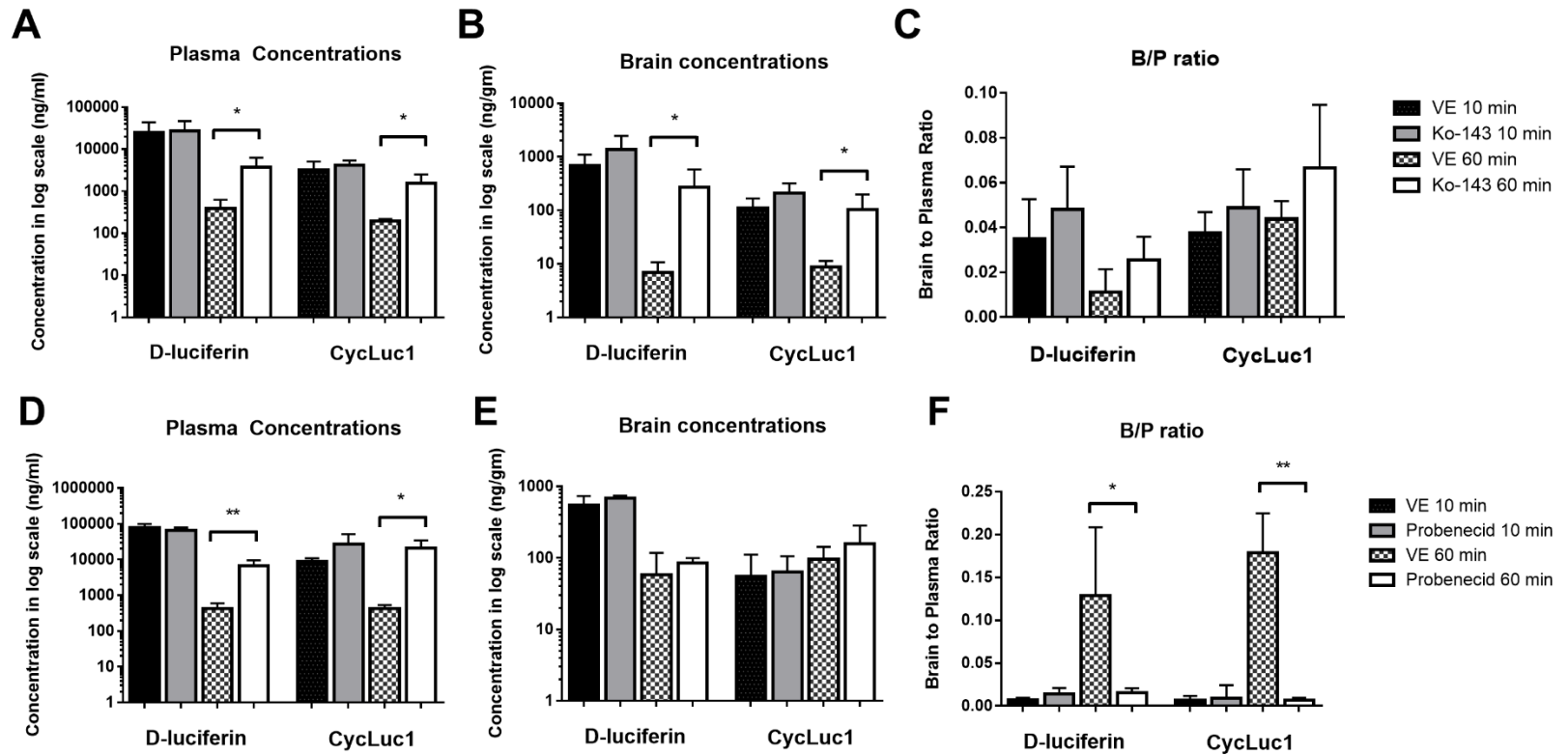


**Table 6.1 Summary of pharmacokinetic parameters and metrics following a single intravenous dose of either D-luciferin or CycLuc1 in wild-type and Bcrp knockout FVB mice.**

**Table 1.**

	D-luciferin				CycLuc1			
	Plasma		Brain		Plasma		Brain	
	Wild-type	Bcrp1 <sup>-/-</sup>	Wild-type	Bcrp1 <sup>-/-</sup>	Wild-type	Bcrp1 <sup>-/-</sup>	Wild-type	Bcrp1 <sup>-/-</sup>
t <sub>1/2</sub> (minutes)	9.01	9.59	11.8	7.69	29.0	21.1	38.3	23.8
Dose (mg/kg)	50	50	-	-	20	20	-	-
AUC <sub>0→last</sub> (min*ug/mL)	1860 ± 117	2608 ± 139 (*)	9.03 ± 0.819	9.1 ± 1.97 (*)	607 ± 25.2	810 ± 106 (*)	1.84 ± 0.199	2.80 ± 0.298 (*)
AUC <sub>0→∞</sub> (min*ug/mL)	1869	2653	9.19	19.2	610	815	1.87	2.97
Vd (mL/kg)	348	261	-	-	3430	2684	-	-
CL (mL/min/kg)	26.7	18.8	-	-	82.0	61.3	-	-
K <sub>p,brain</sub>	-	-	0.0049	0.0072	-	-	0.0031	0.0036
K <sub>puu,brain</sub>			0.0029	0.0043			0.0013	0.0015
Distribution Advantage (DA)	-	-	1	1.5	-	-	1	1.2

t<sub>1/2</sub>, half-life

AUC<sub>0→last</sub>, area under the curve from zero to the time of last measured concentration

AUC<sub>0→∞</sub>, area under the curve from zero to time infinity

CL, clearance

Vd, volume of distribution

K<sub>p,brain</sub> (AUC ratio), the ratio of AUC(0→∞,brain) to AUC(0→∞,plasma) using total drug concentrations

DA (Distribution advantage), the ratio of K<sub>p, knockout</sub> to K<sub>p, wild-type</sub>

**Table 6.2 Summary of pharmacokinetic parameters and metrics following a single intraperitoneal dose of either D-luciferin or CycLuc1 in wild-type FVB mice.**

**Table 2.**

	Plasma		Brain	
	D-luciferin	CycLuc1	D-luciferin	CycLuc1
<b>t<sub>1/2</sub> (minutes)</b>	10.9	31.4	12.6	38.8
<b>Dose (mg/kg)</b>	150	20	-	-
<b>AUC<sub>0→tlast</sub> (min*ug/mL)</b>	9784 ± 1362	339 ± 68.3	47.5 ± 7.17	2.72 + 0.221
<b>AUC<sub>0→∞</sub> (min*ug/mL)</b>	9830	364	48.13	3.97
<b>F (%)</b>	176	60	-	-
<b>Vd/F (mL/kg)</b>	240	334	-	-
<b>CL/F (mL/min/kg)</b>	15.3	18.9	-	-
<b>Kp<sub>brain</sub></b>	-	-	0.00490	0.0109
<b>fu</b>	0.512	0.360	0.307	0.152
<b>Kp<sub>uu,brain</sub></b>	-	-	0.00294	0.00461

t<sub>1/2</sub> , half-life

AUC<sub>0-tlast</sub>, area under the curve from zero to the time of last measured concentration

AUC<sub>0-∞</sub>, area under the curve from zero to time infinity

CL/F, apparent clearance

F, bioavailability

Vd/F, apparent volume of distribution

Kp<sub>brain</sub> (AUC ratio), the ratio of AUC(0-∞,brain) to AUC(0-∞,plasma) using total drug concentrations

DA (Distribution advantage), the ratio of Kp<sub>knockout</sub> to Kp<sub>wild-type</sub>

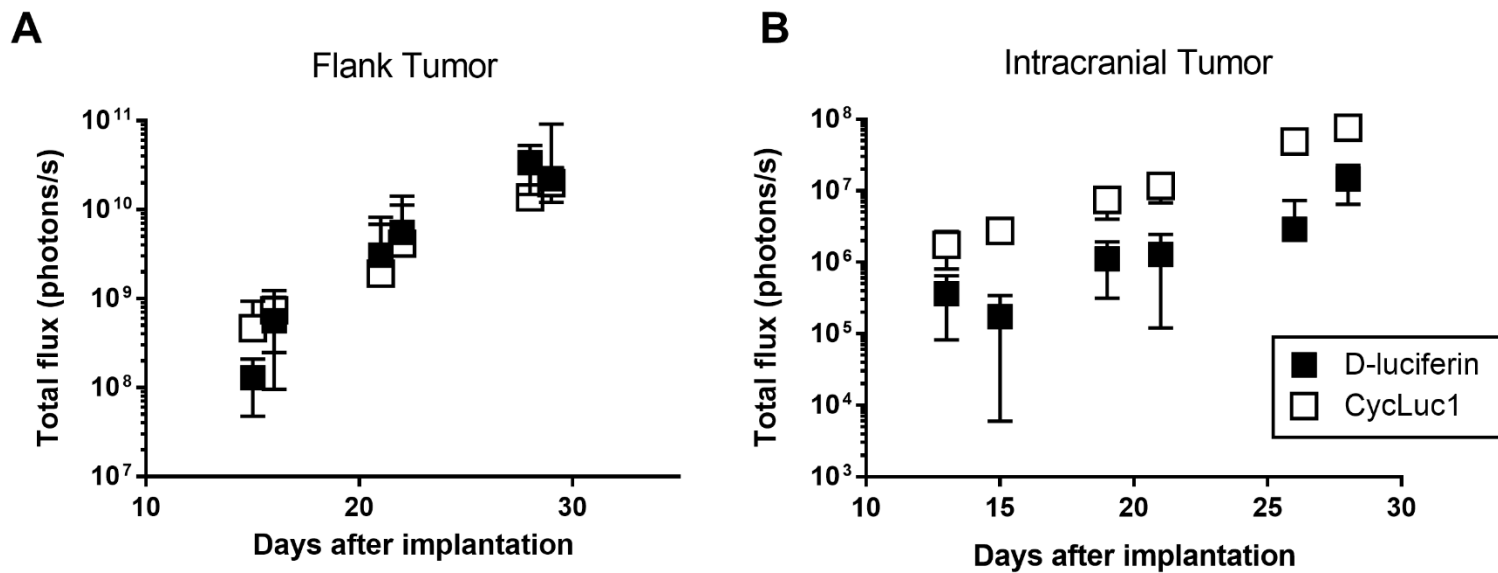
**Table 6.3** The areas under the curve (AUCs) and calculated partition coefficients (Kp) of tissues following a single intraperitoneal dose of D-luciferin and CycLuc1.

**Table 3.**

		Plasma	Brain	Heart	Liver	Kidney	Intestine
<b>D-luciferin</b>	AUC <sub>0→∞</sub> (min*ug/mL)	9830	48	47332	101666	9687	11335
	<b>Kp</b>	-	<b>0.00490</b>	<b>4.82</b>	<b>10.3</b>	<b>0.985</b>	<b>1.15</b>
<b>CycLuc1</b>	AUC <sub>0→∞</sub> (min*ug/mL)	364	3.97	9.38	458	2722	271
	<b>Kp</b>	-	<b>0.0109</b>	<b>0.0258</b>	<b>1.26</b>	<b>7.48</b>	<b>0.745</b>

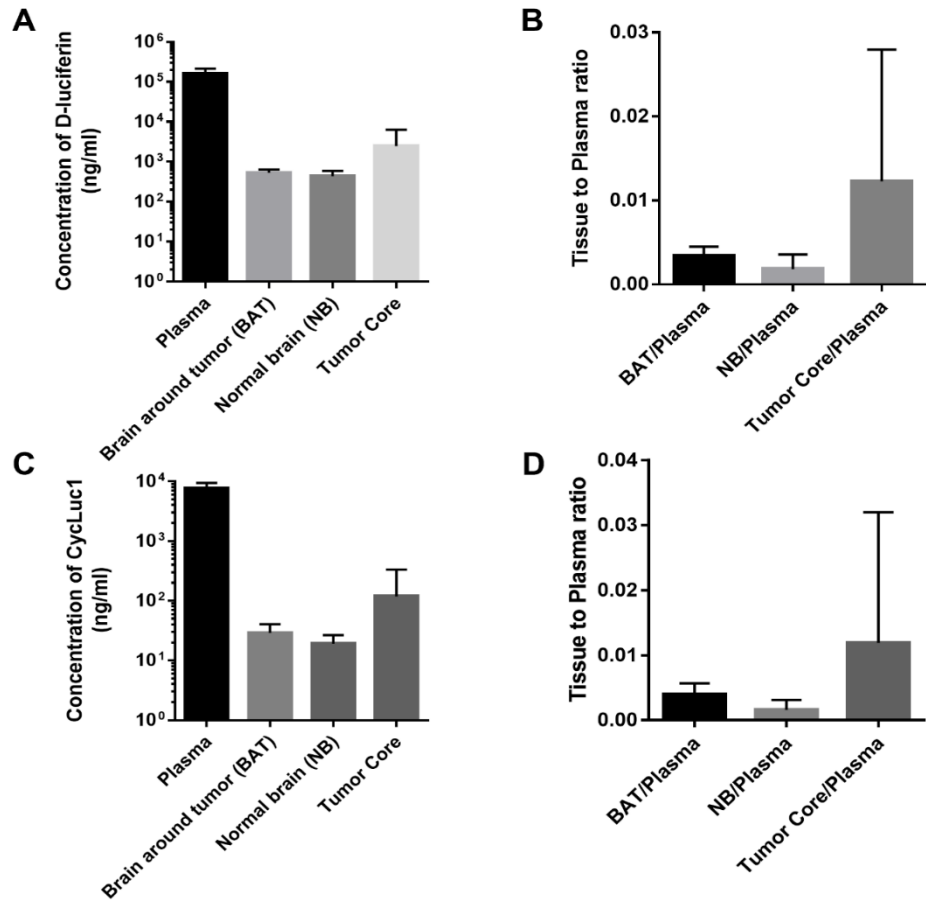
Supplementary Figure 1. The intensity of bioluminescent light signal from D-luciferin and CycLuc1 with different orders of cross-over imaging with GBM6 implanted on the different locations, flank and brain.

### Supplementary Figure 1.



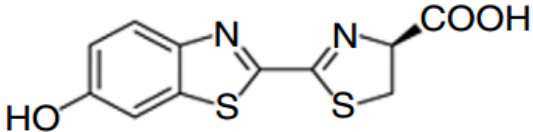
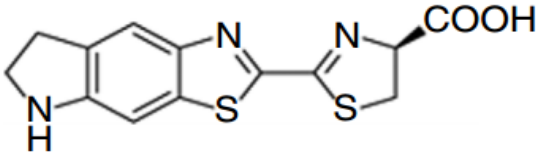
Supplementary Figure 2. The concentration of D-luciferin and CycLuc1 measured by LC-MS in and around the brain tumor.

### Supplementary Figure 2.





**Supplementary table 1. Summary of physicochemical properties of D-luciferin and CycLuc1**

	D-luciferin	CycLuc1
Structure		
Molecular Weight <sup>1</sup>	280.32	305.37
XLogP <sup>1</sup>	0.9	2.6
Hydrogen bond donor count <sup>1</sup>	2	2
Hydrogen bond acceptor count <sup>1</sup>	7	7
Polar surface area (Å <sup>2</sup> ) <sup>1</sup>	129	128
Emission wavelength (nm) <sup>2</sup>	553	603
Km (uM) <sup>2</sup>	6.76 ± 0.3	0.1 ± 0.01

<sup>1</sup>Pubchem (<https://pubchem.ncbi.nlm.nih.gov/>)

<sup>2</sup>Harwood, Katelyn R., et al. "Identification of mutant firefly luciferases that efficiently utilize aminoluciferins." *Chemistry & biology* 18.12 (2011): 1649-1657.

## **RECAPITULATION**

Chapter 1 provides a literature overview of glioblastoma (GBM) and unresolved challenges for the treatment of GBM. This dissertation aimed to gain insight on the manifold drug delivery challenges of a tyrosine kinase inhibitor, through a case example of ponatinib, a multi-kinase inhibitor, which was selected based on the proteomic profile (oncogenic target expression) of a drug-resistant GBM line (GBM6).

Chapter 2 provides a literature overview of metastatic brain tumors and role of efflux transporters on the treatment of them. The treatment of metastatic lesions in the brain represents a serious unmet medical need in the field of neuro-oncology. Even though many effective compounds have demonstrated success in treating peripheral (non-CNS) tumors with targeted agents, one aspect of this lack of success in the brain may be related to poor delivery of otherwise effective compounds. Many factors can influence the brain delivery of these agents, but one key barrier is a heterogeneously “leaky” BBB that expresses efflux transporters that limit the BBB permeability for many targeted agents. Future success in therapeutics for brain metastases must take into account the adequate delivery of “active, free drug” to the target, and may include combinations of targeted drugs that are appropriate to address each individual patient’s tumor type. This review discusses some issues that are pertinent to precision medicine for brain metastases, using specific examples of tumor types that have a high incidence of brain metastases.

In Chapter 3, Controversy exists surrounding whether heterogeneous disruption of the blood-brain barrier (BBB), as seen in glioblastoma (GBM), leads to adequate drug delivery sufficient for efficacy in GBM. This question is especially important when using potent, targeted agents that have a poor penetration across an intact BBB. Efficacy of the murine double minute-2 (MDM2) inhibitor SAR405838 was tested in patient-derived xenograft (PDX) models of GBM. In vitro efficacy of SAR405838 was evaluated in PDX models with varying MDM2-expression and those with high (GBM108) and low (GBM102) expression were evaluated for flank and orthotopic efficacy. BBB permeability, evaluated using TexasRed-3kDa dextran, was significantly increased in GBM108 through VEGFA over-expression. Drug delivery, magnetic resonance imaging (MRI), and orthotopic survival were compared between BBB-intact (GBM108-vector) and BBB-disrupted (GBM108-VEGFA) models. MDM2-amplified PDX lines with high MDM2 expression were sensitive to SAR405838 in comparison to MDM2 control lines in both in vitro and heterotopic models. In contrast to profound efficacy observed in flank xenografts, SAR405838 was ineffective in orthotopic tumors. Although both GBM108-vector and GBM108-VEGFA readily imaged on MRI following gadolinium contrast administration, GBM108-VEGFA tumors had a significantly enhanced drug and gadolinium accumulation, as determined by MALDI-MSI. Enhanced drug delivery in GBM108-VEGFA translated into a marked improvement in orthotopic efficacy. This study clearly shows that limited drug distribution across a partially intact BBB may limit the efficacy of targeted

agents in GBM. Brain penetration of targeted agents is a critical consideration in any precision medicine strategy for GBM.

Chapter 4 examine the mechanism of the limited brain delivery of a novel MDM2 inhibitor, SAR405838, by using in vitro, in vivo, and in silico methods. Achieving an effective drug concentration in the brain is as important as targeting the right pathway when developing targeted agents for brain tumors. SAR405838 is a novel molecularly-targeted agent that is in clinical trials for various solid tumors. Its application for tumors in the brain has not yet been examined, even though the target, the MDM2-p53 interaction, is attractive for tumors that could occur in the brain, including glioblastoma (GBM) and brain metastases. In vitro and in vivo studies indicate that SAR405838 is an avid substrate of P-glycoprotein (P-gp). P-gp mediated active efflux at the blood-brain barrier plays a dominant role in limiting SAR405838 brain distribution. Even though the absence of P-gp significantly increases the drug exposure in the brain; the systemic exposure, including absorption and clearance processes, were unaffected by P-gp deletion. Model-based parameters of SAR405838 distribution across the BBB indicate the CL<sub>out</sub> of the brain was approximately 40-fold greater than the CL<sub>in</sub>. The free fraction of SAR405838 in plasma and brain were found to be low, and subsequent K<sub>p,uu</sub> values were less than unity, even in P-gp/Bcrp knockout mice. These results indicate additional efflux transporters other than P-gp and Bcrp may be limiting distribution of SAR405838 to the brain. Concomitant administration of elacridar significantly increased brain exposure, also without

affecting the systemic exposure. This study characterized the brain distributional kinetics of SAR405838, a novel MDM2 inhibitor, to evaluate its potential in the treatment of primary and metastatic brain tumors.

Chapter 5 investigated the brain distributional kinetics of 8 EGFR inhibitors by using cassette-dosing in wild-type and efflux transporter deficient mice. Tyrosine kinase inhibitors that target the epidermal growth factor receptor (EGFR) have had success in treating EGFR positive tumors, including non-small cell lung cancer (NSCLC). However, developing EGFR inhibitors that can be delivered to the brain remains a challenge. To identify optimal compounds for brain delivery, a panel of EGFR inhibitors was evaluated for distributional kinetics using cassette dosing with the ultimate goal of understanding the brain penetrability of compounds that share the same molecular target in an important oncogenic signaling pathway for both primary brain tumors (glioblastoma) and brain metastases (e.g., NSCLC). Cassette dosing was validated by comparing the brain-to-plasma ratios obtained from cassette dosing to discrete dosing studies. The brain to blood partition coefficients ( $K_{p,brain}$ ) were calculated following cassette dosing of the 8 EGFR inhibitors. The comparison of  $K_{p,brain}$  in wild-type and transporter-deficient mice confirmed that two major efflux transporters at the BBB, p-glycoprotein (P-gp) and breast cancer resistance protein (Bcrp), play a crucial role in the brain distribution of 7 out of 8 EGFR inhibitors. Results show that the prediction of brain distribution based on physicochemical properties of a drug can be misleading, especially for compounds subject to

extensive efflux transport. Moreover, this study informs the choice of EGFR inhibitors, i.e., determining BBB permeability combined with a known target potency, that may be effective in future clinical trials for brain tumors.

Chapter 6 examine the factors influencing the bioluminescent imaging signal and the mechanism of limited brain delivery of luciferase substrates. The partition coefficients of brain for D-luciferin and CycLuc1 were extremely low in both wild-type and Bcrp knockout FVB mice when compared to other tissues. In the absence of Bcrp, both the systemic and brain exposure to D-luciferin and CycLuc1 were significantly increased. However, the brain partition coefficients did not show significant changes. In vitro trans-well assay results showed that the apparent permeabilities of both D-luciferin and CycLuc1 were extremely low, and both compounds were weak substrates of Bcrp. The stronger light signal with CycLuc1 from intracranial tumor is likely to be due to its low  $K_m$  to firefly luciferase but not due to its better brain penetration when compared to D-luciferin.

## **BIBLIOGRAPHY**



- (2008) Comprehensive genomic characterization defines human glioblastoma genes and core pathways. *Nature* **455**:1061-1068.
- (2014) A Clinical Trial Testing The Efficacy Of Crizotinib Versus Standard Chemotherapy Pemetrexed Plus Cisplatin Or Carboplatin In Patients With ALK Positive Non Squamous Cancer Of The Lung (PROFILE 1014), [clinicaltrials.gov](http://clinicaltrials.gov).
- Abbott NJ (2013) Blood-brain barrier structure and function and the challenges for CNS drug delivery. *J Inherit Metab Dis* **36**:437-449.
- Abbott NJ, Patabendige AA, Dolman DE, Yusof SR, and Begley DJ (2010) Structure and function of the blood-brain barrier. *Neurobiol Dis* **37**:13-25.
- Abbott NJ, Ronnback L, and Hansson E (2006) Astrocyte-endothelial interactions at the blood-brain barrier. *Nat Rev Neurosci* **7**:41-53.
- Agarwal S, Hartz AM, Elmquist WF, and Bauer B (2011a) Breast cancer resistance protein and P-glycoprotein in brain cancer: two gatekeepers team up. *Curr Pharm Des* **17**:2793-2802.
- Agarwal S, Manchanda P, Vogelbaum MA, Ohlfest JR, and Elmquist WF (2013) Function of the blood-brain barrier and restriction of drug delivery to invasive glioma cells: findings in an orthotopic rat xenograft model of glioma. *Drug Metab Dispos* **41**:33-39.
- Agarwal S, Sane R, Gallardo JL, Ohlfest JR, and Elmquist WF (2010) Distribution of gefitinib to the brain is limited by P-glycoprotein (ABCB1) and breast cancer resistance protein (ABCG2)-mediated active efflux. *J Pharmacol Exp Ther* **334**:147-155.
- Agarwal S, Sane R, Oberoi R, Ohlfest JR, and Elmquist WF (2011b) Delivery of molecularly targeted therapy to malignant glioma, a disease of the whole brain. *Expert Rev Mol Med* **13**:e17.
- Agarwal S, Sane R, Ohlfest JR, and Elmquist WF (2011c) The role of the breast cancer resistance protein (ABCG2) in the distribution of sorafenib to the brain. *J Pharmacol Exp Ther* **336**:223-233.
- Agarwal S, Uchida Y, Mittapalli RK, Sane R, Terasaki T, and Elmquist WF (2012) Quantitative proteomics of transporter expression in brain capillary endothelial cells isolated from P-glycoprotein (P-gp), breast cancer resistance protein (Bcrp), and P-gp/Bcrp knockout mice. *Drug Metab Dispos* **40**:1164-1169.
- Ahn MJ, Kim DW, Cho BC, Kim SW, Lee JS, Ahn JS, Kim TM, Lin CC, Kim HR, John T, Kao S, Goldman JW, Su WC, Natale R, Rabbie S, Harrop B, Overend P, Yang Z, and Yang JC (2017) Activity and safety of AZD3759 in EGFR-mutant non-small-cell lung cancer with CNS metastases (BLOOM): a phase 1, open-label, dose-escalation and dose-expansion study. *Lancet Respir Med* **5**:891-902.
- Anders CK, Adamo B, Karginova O, Deal AM, Rawal S, Darr D, Schorzman A, Santos C, Bash R, Kafri T, Carey L, Miller CR, Perou CM, Sharpless N, and Zamboni WC (2013) Pharmacokinetics and efficacy of PEGylated liposomal doxorubicin in an intracranial model of breast cancer. *PLoS One* **8**:e61359.
- Anders CK, Deal AM, Miller CR, Khorram C, Meng H, Burrows E, Livasy C, Fritchie K, Ewend MG, Perou CM, and Carey LA (2011) The prognostic contribution of clinical breast cancer

- subtype, age, and race among patients with breast cancer brain metastases. *Cancer* **117**:1602-1611.
- Ardini E, Menichincheri M, Banfi P, Bosotti R, De Ponti C, Pulci R, Ballinari D, Ciomei M, Texido G, Degrassi A, Avanzi N, Amboldi N, Saccardo MB, Casero D, Orsini P, Bandiera T, Mologni L, Anderson D, Wei G, Harris J, Vernier JM, Li G, Felder E, Donati D, Isacchi A, Pesenti E, Magnaghi P, and Galvani A (2016) Entrectinib, a Pan-TRK, ROS1, and ALK Inhibitor with Activity in Multiple Molecularly Defined Cancer Indications. *Mol Cancer Ther* **15**:628-639.
- Argaw AT, Asp L, Zhang J, Navrazhina K, Pham T, Mariani JN, Mahase S, Dutta DJ, Seto J, Kramer EG, Ferrara N, Sofroniew MV, and John GR (2012) Astrocyte-derived VEGF-A drives blood-brain barrier disruption in CNS inflammatory disease. *J Clin Invest* **122**:2454-2468.
- Artursson P, Palm K, and Luthman K (2001) Caco-2 monolayers in experimental and theoretical predictions of drug transport. *Adv Drug Deliv Rev* **46**:27-43.
- Auperin A, Arriagada R, Pignon JP, Le Pechoux C, Gregor A, Stephens RJ, Kristjansen PE, Johnson BE, Ueoka H, Wagner H, and Aisner J (1999) Prophylactic cranial irradiation for patients with small-cell lung cancer in complete remission. Prophylactic Cranial Irradiation Overview Collaborative Group. *N Engl J Med* **341**:476-484.
- Aversa C, Rossi V, Geuna E, Martinello R, Milani A, Redana S, Valabrega G, Aglietta M, and Montemurro F (2014) Metastatic breast cancer subtypes and central nervous system metastases. *Breast* **23**:623-628.
- Azer MW, Menzies AM, Haydu LE, Kefford RF, and Long GV (2014) Patterns of response and progression in patients with BRAF-mutant melanoma metastatic to the brain who were treated with dabrafenib. *Cancer* **120**:530-536.
- Bachelot T, Romieu G, Campone M, Dieras V, Cropet C, Dalenc F, Jimenez M, Le Rhun E, Pierga JY, Goncalves A, Leheurteur M, Domont J, Gutierrez M, Cure H, Ferrero JM, and Labbe-Devilliers C (2013) Lapatinib plus capecitabine in patients with previously untreated brain metastases from HER2-positive metastatic breast cancer (LANDSCAPE): a single-group phase 2 study. *Lancet Oncol* **14**:64-71.
- Bailon O, Chouahnia K, Augier A, Bouillet T, Billot S, Coman I, Ursu R, Belin C, Zelek L, Des Guetz G, Levy C, Carpentier AF, and Morere JF (2012) Upfront association of carboplatin plus pemetrexed in patients with brain metastases of lung adenocarcinoma. *Neuro Oncol* **14**:491-495.
- Bakhsheshian J, Wei BR, Chang KE, Shukla S, Ambudkar SV, Simpson RM, Gottesman MM, and Hall MD (2013) Bioluminescent imaging of drug efflux at the blood-brain barrier mediated by the transporter ABCG2. *Proc Natl Acad Sci U S A* **110**:20801-20806.
- Ballard P, Yates JW, Yang Z, Kim DW, Yang JC, Cantarini M, Pickup K, Jordan A, Hickey M, Grist M, Box M, Johnstrom P, Varnas K, Malmquist J, Thress KS, Janne PA, and Cross D (2016) Preclinical Comparison of Osimertinib with Other EGFR-TKIs in EGFR-Mutant NSCLC Brain Metastases Models, and Early Evidence of Clinical Brain Metastases Activity. *Clin Cancer Res* **22**:5130-5140.
- Barnholtz-Sloan JS, Sloan AE, Davis FG, Vignea FD, Lai P, and Sawaya RE (2004) Incidence proportions of brain metastases in patients diagnosed (1973 to 2001) in the Metropolitan Detroit Cancer Surveillance System. *J Clin Oncol* **22**:2865-2872.

- Bayraktar S and Gluck S (2013) Molecularly targeted therapies for metastatic triple-negative breast cancer. *Breast Cancer Res Treat* **138**:21-35.
- Becker CM, Oberoi RK, McFarren SJ, Muldoon DM, Pafundi DH, Pokorny JL, Brinkmann DH, Ohlfest JR, Sarkaria JN, Largaespada DA, and Elmquist WF (2015a) Decreased affinity for efflux transporters increases brain penetrance and molecular targeting of a PI3K/mTOR inhibitor in a mouse model of glioblastoma. *Neuro Oncol*.
- Becker CM, Oberoi RK, McFarren SJ, Muldoon DM, Pafundi DH, Pokorny JL, Brinkmann DH, Ohlfest JR, Sarkaria JN, Largaespada DA, and Elmquist WF (2015b) Decreased affinity for efflux transporters increases brain penetrance and molecular targeting of a PI3K/mTOR inhibitor in a mouse model of glioblastoma. *Neuro Oncol* **17**:1210-1219.
- Becker JC, Kirkwood JM, Agarwala SS, Dummer R, Schrama D, and Hauschild A (2006) Molecularly targeted therapy for melanoma: current reality and future options. *Cancer* **107**:2317-2327.
- Begley DJ (2004) ABC transporters and the blood-brain barrier. *Curr Pharm Des* **10**:1295-1312.
- Bendell JC, Domchek SM, Burstein HJ, Harris L, Younger J, Kuter I, Bunnell C, Rue M, Gelman R, and Winer E (2003) Central nervous system metastases in women who receive trastuzumab-based therapy for metastatic breast carcinoma. *Cancer* **97**:2972-2977.
- Bennani O, Derrey S, Langlois O, Castel H, Laquerriere A, Freger P, and Proust F (2014) Brain metastasis from renal cell carcinoma. *Neurochirurgie* **60**:12-16.
- Berger F, Paulmurugan R, Bhaumik S, and Gambhir SS (2008) Uptake kinetics and biodistribution of <sup>14</sup>C-D-luciferin--a radiolabeled substrate for the firefly luciferase catalyzed bioluminescence reaction: impact on bioluminescence based reporter gene imaging. *Eur J Nucl Med Mol Imaging* **35**:2275-2285.
- Bertotti A, Burbridge MF, Gastaldi S, Galimi F, Torti D, Medico E, Giordano S, Corso S, Rolland-Valognes G, Lockhart BP, Hickman JA, Comoglio PM, and Trusolino L (2009) Only a subset of Met-activated pathways are required to sustain oncogene addiction. *Sci Signal* **2**:ra80.
- Bianchi M, Sun M, Jeldres C, Shariat SF, Trinh QD, Briganti A, Tian Z, Schmitges J, Graefen M, Perrotte P, Menon M, Montorsi F, and Karakiewicz PI (2012) Distribution of metastatic sites in renal cell carcinoma: a population-based analysis. *Ann Oncol* **23**:973-980.
- Bill KL, Garnett J, Meaux I, Ma X, Creighton CJ, Bolshakov S, Barriere C, Debussche L, Lazar AJ, Prudner BC, Casadei L, Braggio D, Lopez G, Zewdu A, Bid H, Lev D, and Pollock RE (2015) SAR405838: A Novel and Potent Inhibitor of the MDM2:p53 Axis for the Treatment of Dedifferentiated Liposarcoma. *Clin Cancer Res*.
- Boult JK, Borri M, Jury A, Popov S, Box G, Perryman L, Eccles SA, Jones C, and Robinson SP (2016) Investigating intracranial tumour growth patterns with multiparametric MRI incorporating Gd-DTPA and USPIO-enhanced imaging. *NMR Biomed* **29**:1608-1617.
- Brastianos PK, Carter SL, Santagata S, Cahill DP, Taylor-Weiner A, Jones RT, Van Allen EM, Lawrence MS, Horowitz PM, Cibulskis K, Ligon KL, Tabernero J, Seoane J, Martinez-Saez E, Curry WT, Dunn IF, Paek SH, Park SH, McKenna A, Chevalier A, Rosenberg M, Barker FG, 2nd, Gill CM, Van Hummelen P, Thorner AR, Johnson BE, Hoang MP, Choueiri TK, Signoretti S, Sougnez C, Rabin MS, Lin NU, Winer EP, Stemmer-Rachamimov A, Meyerson M, Garraway L, Gabriel S, Lander ES, Beroukhim R, Batchelor TT, Baselga J, Louis DN, Getz G, and Hahn WC (2015) Genomic Characterization of Brain Metastases

- Reveals Branched Evolution and Potential Therapeutic Targets. *Cancer Discov* **5**:1164-1177.
- Brennan CW, Verhaak RG, McKenna A, Campos B, Nounshmehr H, Salama SR, Zheng S, Chakravarty D, Sanborn JZ, Berman SH, Beroukhir R, Bernard B, Wu CJ, Genovese G, Shmulevich I, Barnholtz-Sloan J, Zou L, Vegesna R, Shukla SA, Ciriello G, Yung WK, Zhang W, Sougnez C, Mikkelsen T, Aldape K, Bigner DD, Van Meir EG, Prados M, Sloan A, Black KL, Eschbacher J, Finocchiaro G, Friedman W, Andrews DW, Guha A, Iacocca M, O'Neill BP, Foltz G, Myers J, Weisenberger DJ, Penny R, Kucherlapati R, Perou CM, Hayes DN, Gibbs R, Marra M, Mills GB, Lander E, Spellman P, Wilson R, Sander C, Weinstein J, Meyerson M, Gabriel S, Laird PW, Haussler D, Getz G, Chin L, and Network TR (2013) The somatic genomic landscape of glioblastoma. *Cell* **155**:462-477.
- Broccatelli F, Larregieu CA, Cruciani G, Oprea TI, and Benet LZ (2012) Improving the prediction of the brain disposition for orally administered drugs using BDDCS. *Adv Drug Deliv Rev* **64**:95-109.
- Brown PD, Buckner JC, Uhm JH, and Shaw EG (2003) The neurocognitive effects of radiation in adult low-grade glioma patients. *Neuro Oncol* **5**:161-167.
- Brown PD, Pugh S, Laack NN, Wefel JS, Khuntia D, Meyers C, Choucair A, Fox S, Suh JH, Roberge D, Kavadi V, Bentzen SM, Mehta MP, Watkins-Bruner D, and Radiation Therapy Oncology G (2013) Memantine for the prevention of cognitive dysfunction in patients receiving whole-brain radiotherapy: a randomized, double-blind, placebo-controlled trial. *Neuro Oncol* **15**:1429-1437.
- Bruzzone MG, D'Incerti L, Farina LL, Cuccarini V, and Finocchiaro G (2012) CT and MRI of brain tumors. *Q J Nucl Med Mol Imaging* **56**:112-137.
- Butt AM, Jones HC, and Abbott NJ (1990) Electrical resistance across the blood-brain barrier in anaesthetized rats: a developmental study. *J Physiol* **429**:47-62.
- Cameron D, Casey M, Press M, Lindquist D, Pienkowski T, Romieu CG, Chan S, Jagiello-Gruszfeld A, Kaufman B, Crown J, Chan A, Campone M, Viens P, Davidson N, Gorbounova V, Raats JI, Skarlos D, Newstat B, Roychowdhury D, Paoletti P, Oliva C, Rubin S, Stein S, and Geyer CE (2008) A phase III randomized comparison of lapatinib plus capecitabine versus capecitabine alone in women with advanced breast cancer that has progressed on trastuzumab: updated efficacy and biomarker analyses. *Breast Cancer Res Treat* **112**:533-543.
- Cancer Genome Atlas Research N (2008) Comprehensive genomic characterization defines human glioblastoma genes and core pathways. *Nature* **455**:1061-1068.
- Capper D, Berghoff AS, Magerle M, Ilhan A, Wohrer A, Hackl M, Pichler J, Pusch S, Meyer J, Habel A, Petzelbauer P, Birner P, von Deimling A, and Preusser M (2012) Immunohistochemical testing of BRAF V600E status in 1,120 tumor tissue samples of patients with brain metastases. *Acta Neuropathol* **123**:223-233.
- Cen L, Carlson BL, Schroeder MA, Ostrem JL, Kitange GJ, Mladek AC, Fink SR, Decker PA, Wu W, Kim JS, Waldman T, Jenkins RB, and Sarkaria JN (2012) p16-Cdk4-Rb axis controls sensitivity to a cyclin-dependent kinase inhibitor PD0332991 in glioblastoma xenograft cells. *Neuro Oncol* **14**:870-881.

- Ceresoli GL, Cappuzzo F, Gregorc V, Bartolini S, Crino L, and Villa E (2004) Gefitinib in patients with brain metastases from non-small-cell lung cancer: a prospective trial. *Ann Oncol* **15**:1042-1047.
- Chamberlain MC, Baik CS, Gadi VK, Bhatia S, and Chow LQ (2017) Systemic therapy of brain metastases: non-small cell lung cancer, breast cancer, and melanoma. *Neuro Oncol* **19**:i1-i24.
- Chen X, Tai L, Gao J, Qian J, Zhang M, Li B, Xie C, Lu L, and Lu W (2015) A stapled peptide antagonist of MDM2 carried by polymeric micelles sensitizes glioblastoma to temozolomide treatment through p53 activation. *J Control Release* **218**:29-35.
- Chen Y, Wang M, Zhong W, and Zhao J (2013) Pharmacokinetic and pharmacodynamic study of Gefitinib in a mouse model of non-small-cell lung carcinoma with brain metastasis. *Lung Cancer* **82**:313-318.
- Cheung L, Yu DM, Neiron Z, Failes TW, Arndt GM, and Fletcher JI (2015) Identification of new MRP4 inhibitors from a library of FDA approved drugs using a high-throughput bioluminescence screen. *Biochem Pharmacol* **93**:380-388.
- Cheung YT, Yap KY, Chui WK, and Chan A (2010) Drug-drug interactions between oral antiepileptics and oral anticancer drugs: implications to clinicians. *Eur Neurol* **64**:88-94.
- Choo EF, Ly J, Chan J, Shahidi-Latham SK, Messick K, Plise E, Quiason CM, and Yang L (2014) Role of P-glycoprotein on the brain penetration and brain pharmacodynamic activity of the MEK inhibitor cobimetinib. *Mol Pharm* **11**:4199-4207.
- Cisternino S, Mercier C, Bourasset F, Roux F, and Scherrmann JM (2004) Expression, up-regulation, and transport activity of the multidrug-resistance protein Abcg2 at the mouse blood-brain barrier. *Cancer Res* **64**:3296-3301.
- Claffey KP and Robinson GS (1996) Regulation of VEGF/VPF expression in tumor cells: consequences for tumor growth and metastasis. *Cancer Metastasis Rev* **15**:165-176.
- Clayton AJ, Danson S, Jolly S, Ryder WD, Burt PA, Stewart AL, Wilkinson PM, Welch RS, Magee B, Wilson G, Howell A, and Wardley AM (2004) Incidence of cerebral metastases in patients treated with trastuzumab for metastatic breast cancer. *Br J Cancer* **91**:639-643.
- Cooray HC, Blackmore CG, Maskell L, and Barrand MA (2002) Localisation of breast cancer resistance protein in microvessel endothelium of human brain. *Neuroreport* **13**:2059-2063.
- Cordon-Cardo C, O'Brien JP, Casals D, Rittman-Grauer L, Biedler JL, Melamed MR, and Bertino JR (1989) Multidrug-resistance gene (P-glycoprotein) is expressed by endothelial cells at blood-brain barrier sites. *Proc Natl Acad Sci U S A* **86**:695-698.
- Corporation NP Zykadia. *Product insert*.
- Costa DB, Kobayashi S, Pandya SS, Yeo WL, Shen Z, Tan W, and Wilner KD (2011) CSF concentration of the anaplastic lymphoma kinase inhibitor crizotinib. *J Clin Oncol* **29**:e443-445.
- Costa DB, Shaw AT, Ou SH, Solomon BJ, Riely GJ, Ahn MJ, Zhou C, Shreeve SM, Selaru P, Polli A, Schnell P, Wilner KD, Wiltshire R, Camidge DR, and Crino L (2015) Clinical Experience With Crizotinib in Patients With Advanced ALK-Rearranged Non-Small-Cell Lung Cancer and Brain Metastases. *J Clin Oncol* **33**:1881-1888.
- Crino L, Ahn MJ, De Marinis F, Groen HJ, Wakelee H, Hida T, Mok T, Spigel D, Felip E, Nishio M, Scagliotti G, Branle F, Emeremni C, Quadrigli M, Zhang J, and Shaw AT (2016)

- Multicenter Phase II Study of Whole-Body and Intracranial Activity With Ceritinib in Patients With ALK-Rearranged Non-Small-Cell Lung Cancer Previously Treated With Chemotherapy and Crizotinib: Results From ASCEND-2. *J Clin Oncol* **34**:2866-2873.
- Cross DA, Ashton SE, Giorghiu S, Eberlein C, Nebhan CA, Spitzler PJ, Orme JP, Finlay MR, Ward RA, Mellor MJ, Hughes G, Rahi A, Jacobs VN, Red Brewer M, Ichihara E, Sun J, Jin H, Ballard P, Al-Kadhimi K, Rowlinson R, Klinowska T, Richmond GH, Cantarini M, Kim DW, Ranson MR, and Pao W (2014) AZD9291, an irreversible EGFR TKI, overcomes T790M-mediated resistance to EGFR inhibitors in lung cancer. *Cancer Discov* **4**:1046-1061.
- Damsky WE, Theodosakis N, and Bosenberg M (2014) Melanoma metastasis: new concepts and evolving paradigms. *Oncogene* **33**:2413-2422.
- Daniele S, Barresi E, Zappelli E, Marinelli L, Novellino E, Da Settimo F, Taliani S, Trincavelli ML, and Martini C (2016) Long lasting MDM2/Translocator protein modulator: a new strategy for irreversible apoptosis of human glioblastoma cells. *Oncotarget*.
- Davies H, Bignell GR, Cox C, Stephens P, Edkins S, Clegg S, Teague J, Woffendin H, Garnett MJ, Bottomley W, Davis N, Dicks E, Ewing R, Floyd Y, Gray K, Hall S, Hawes R, Hughes J, Kosmidou V, Menzies A, Mould C, Parker A, Stevens C, Watt S, Hooper S, Wilson R, Jayatilake H, Gusterson BA, Cooper C, Shipley J, Hargrave D, Pritchard-Jones K, Maitland N, Chenevix-Trench G, Riggins GJ, Bigner DD, Palmieri G, Cossu A, Flanagan A, Nicholson A, Ho JW, Leung SY, Yuen ST, Weber BL, Seigler HF, Darrow TL, Paterson H, Marais R, Marshall CJ, Wooster R, Stratton MR, and Futreal PA (2002) Mutations of the BRAF gene in human cancer. *Nature* **417**:949-954.
- Davis FG, Dolecek TA, McCarthy BJ, and Villano JL (2012) Toward determining the lifetime occurrence of metastatic brain tumors estimated from 2007 United States cancer incidence data. *Neuro Oncol* **14**:1171-1177.
- Dawood S, Broglio K, Esteva FJ, Yang W, Kau SW, Islam R, Albarracin C, Yu TK, Green M, Hortobagyi GN, and Gonzalez-Angulo AM (2009) Survival among women with triple receptor-negative breast cancer and brain metastases. *Ann Oncol* **20**:621-627.
- Dawson JB, Barker DJ, Ellis DJ, Grassam E, Cotterill JA, Fisher GW, and Feather JW (1980) A theoretical and experimental study of light absorption and scattering by in vivo skin. *Phys Med Biol* **25**:695-709.
- de Lange EC (2004) Potential role of ABC transporters as a detoxification system at the blood-CSF barrier. *Adv Drug Deliv Rev* **56**:1793-1809.
- de Lange EC (2013a) The mastermind approach to CNS drug therapy: translational prediction of human brain distribution, target site kinetics, and therapeutic effects. *Fluids Barriers CNS* **10**:12.
- de Lange EC (2013b) Utility of CSF in translational neuroscience. *J Pharmacokinet Pharmacodyn* **40**:315-326.
- de Lange EC and Danhof M (2002) Considerations in the use of cerebrospinal fluid pharmacokinetics to predict brain target concentrations in the clinical setting: implications of the barriers between blood and brain. *Clin Pharmacokinet* **41**:691-703.
- de Vries NA, Buckle T, Zhao J, Beijnen JH, Schellens JH, and van Tellingen O (2012) Restricted brain penetration of the tyrosine kinase inhibitor erlotinib due to the drug transporters P-gp and BCRP. *Invest New Drugs* **30**:443-449.

- de Vries NA, Zhao J, Kroon E, Buckle T, Beijnen JH, and van Tellingen O (2007) P-glycoprotein and breast cancer resistance protein: two dominant transporters working together in limiting the brain penetration of topotecan. *Clin Cancer Res* **13**:6440-6449.
- Deben C, Wouters A, Op de Beeck K, van Den Bossche J, Jacobs J, Zwaenepoel K, Peeters M, Van Meerbeeck J, Lardon F, Rolfo C, Deschoolmeester V, and Pauwels P (2015) The MDM2-inhibitor Nutlin-3 synergizes with cisplatin to induce p53 dependent tumor cell apoptosis in non-small cell lung cancer. *Oncotarget* **6**:22666-22679.
- Deeken JF and Loscher W (2007) The blood-brain barrier and cancer: transporters, treatment, and Trojan horses. *Clin Cancer Res* **13**:1663-1674.
- Delattre JY, Krol G, Thaler HT, and Posner JB (1988) Distribution of brain metastases. *Arch Neurol* **45**:741-744.
- Di Giacomo AM and Margolin K (2015) Immune checkpoint blockade in patients with melanoma metastatic to the brain. *Semin Oncol* **42**:459-465.
- Dobrogowska DH, Lossinsky AS, Tarnawski M, and Vorbrodtt AW (1998) Increased blood-brain barrier permeability and endothelial abnormalities induced by vascular endothelial growth factor. *J Neurocytol* **27**:163-173.
- Doolittle ND, Peereboom DM, Christoforidis GA, Hall WA, Palmieri D, Brock PR, Campbell KC, Dickey DT, Muldoon LL, O'Neill BP, Peterson DR, Pollock B, Soussain C, Smith Q, Tyson RM, and Neuwelt EA (2007) Delivery of chemotherapy and antibodies across the blood-brain barrier and the role of chemoprotection, in primary and metastatic brain tumors: report of the Eleventh Annual Blood-Brain Barrier Consortium meeting. *J Neurooncol* **81**:81-91.
- Doroshov JH (2005) Targeting EGFR in non-small-cell lung cancer. *N Engl J Med* **353**:200-202.
- Druker BJ (2002) Perspectives on the development of a molecularly targeted agent. *Cancer Cell* **1**:31-36.
- Dudek AZ, Raza A, Chi M, Singhal M, Oberoi R, Mittapalli RK, Agarwal S, and Elmquist WF (2013) Brain metastases from renal cell carcinoma in the era of tyrosine kinase inhibitors. *Clin Genitourin Cancer* **11**:155-160.
- Dummer R, Goldinger SM, Turttschi CP, Eggmann NB, Michielin O, Mitchell L, Veronese L, Hilfiker PR, Felderer L, and Rinderknecht JD (2014) Vemurafenib in patients with BRAF(V600) mutation-positive melanoma with symptomatic brain metastases: final results of an open-label pilot study. *Eur J Cancer* **50**:611-621.
- Durmus S, Sparidans RW, Wagenaar E, Beijnen JH, and Schinkel AH (2012) Oral availability and brain penetration of the B-RAFV600E inhibitor vemurafenib can be enhanced by the P-GLYCOPROTEIN (ABCB1) and breast cancer resistance protein (ABCG2) inhibitor elacridar. *Mol Pharm* **9**:3236-3245.
- Ederoth P, Tunblad K, Bouw R, Lundberg CJ, Ungerstedt U, Nordstrom CH, and Hammarlund-Udenaes M (2004) Blood-brain barrier transport of morphine in patients with severe brain trauma. *Br J Clin Pharmacol* **57**:427-435.
- Eilers M, Roy U, and Mondal D (2008) MRP (ABCC) transporters-mediated efflux of anti-HIV drugs, saquinavir and zidovudine, from human endothelial cells. *Exp Biol Med (Maywood)* **233**:1149-1160.

- Elmeliegy MA, Carcaboso AM, Tagen M, Bai F, and Stewart CF (2011) Role of ATP-binding cassette and solute carrier transporters in erlotinib CNS penetration and intracellular accumulation. *Clin Cancer Res* **17**:89-99.
- Engelhardt B and Coisne C (2011) Fluids and barriers of the CNS establish immune privilege by confining immune surveillance to a two-walled castle moat surrounding the CNS castle. *Fluids Barriers CNS* **8**:4.
- Engelman JA, Zejnullahu K, Gale CM, Lifshits E, Gonzales AJ, Shimamura T, Zhao F, Vincent PW, Naumov GN, Bradner JE, Althaus IW, Gandhi L, Shapiro GI, Nelson JM, Heymach JV, Meyerson M, Wong KK, and Janne PA (2007) PF00299804, an irreversible pan-ERBB inhibitor, is effective in lung cancer models with EGFR and ERBB2 mutations that are resistant to gefitinib. *Cancer Res* **67**:11924-11932.
- Essig M, Weber MA, von Tengg-Koblighk H, Knopp MV, Yuh WT, and Giesel FL (2006) Contrast-enhanced magnetic resonance imaging of central nervous system tumors: agents, mechanisms, and applications. *Top Magn Reson Imaging* **17**:89-106.
- Evans MS, Chaurette JP, Adams ST, Jr., Reddy GR, Paley MA, Aronin N, Prescher JA, and Miller SC (2014) A synthetic luciferin improves bioluminescence imaging in live mice. *Nat Methods* **11**:393-395.
- Falchook GS, Long GV, Kurzrock R, Kim KB, Arkenau TH, Brown MP, Hamid O, Infante JR, Millward M, Pavlick AC, O'Day SJ, Blackman SC, Curtis CM, Lebowitz P, Ma B, Ouellet D, and Kefford RF (2012) Dabrafenib in patients with melanoma, untreated brain metastases, and other solid tumours: a phase 1 dose-escalation trial. *The Lancet* **379**:1893-1901.
- Fidler IJ, Yano S, Zhang RD, Fujimaki T, and Bucana CD (2002) The seed and soil hypothesis: vascularisation and brain metastases. *Lancet Oncol* **3**:53-57.
- Finlay CA (1993) The mdm-2 oncogene can overcome wild-type p53 suppression of transformed cell growth. *Mol Cell Biol* **13**:301-306.
- Fitzgerald DP, Emerson DL, Qian Y, Anwar T, Liewehr DJ, Steinberg SM, Silberman S, Palmieri D, and Steeg PS (2012) TPI-287, a new taxane family member, reduces the brain metastatic colonization of breast cancer cells. *Mol Cancer Ther* **11**:1959-1967.
- Flaherty KT, Infante JR, Daud A, Gonzalez R, Kefford RF, Sosman J, Hamid O, Schuchter L, Cebon J, Ibrahim N, Kudchadkar R, Burris HA, 3rd, Falchook G, Algazi A, Lewis K, Long GV, Puzanov I, Lebowitz P, Singh A, Little S, Sun P, Allred A, Ouellet D, Kim KB, Patel K, and Weber J (2012a) Combined BRAF and MEK inhibition in melanoma with BRAF V600 mutations. *N Engl J Med* **367**:1694-1703.
- Flaherty KT, Puzanov I, Kim KB, Ribas A, McArthur GA, Sosman JA, O'Dwyer PJ, Lee RJ, Grippo JF, Nolop K, and Chapman PB (2010) Inhibition of mutated, activated BRAF in metastatic melanoma. *N Engl J Med* **363**:809-819.
- Flaherty KT, Robert C, Hersey P, Nathan P, Garbe C, Milhem M, Demidov LV, Hassel JC, Rutkowski P, Mohr P, Dummer R, Trefzer U, Larkin JM, Utikal J, Dreno B, Nyakas M, Middleton MR, Becker JC, Casey M, Sherman LJ, Wu FS, Ouellet D, Martin AM, Patel K, Schadendorf D, and Group MS (2012b) Improved survival with MEK inhibition in BRAF-mutated melanoma. *N Engl J Med* **367**:107-114.
- Fox E and Bates SE (2007) Tariquidar (XR9576): a P-glycoprotein drug efflux pump inhibitor. *Expert Rev Anticancer Ther* **7**:447-459.



- Franceschi E, Cavallo G, Lonardi S, Magrini E, Tosoni A, Grosso D, Scopece L, Blatt V, Urbini B, Pession A, Tallini G, Crino L, and Brandes AA (2007) Gefitinib in patients with progressive high-grade gliomas: a multicentre phase II study by Gruppo Italiano Cooperativo di Neuro-Oncologia (GICNO). *Br J Cancer* **96**:1047-1051.
- Franciosi V, Cocconi G, Michiara M, Di Costanzo F, Fosser V, Tonato M, Carlini P, Boni C, and Di Sarra S (1999) Front-line chemotherapy with cisplatin and etoposide for patients with brain metastases from breast carcinoma, nonsmall cell lung carcinoma, or malignant melanoma: a prospective study. *Cancer* **85**:1599-1605.
- Freedman RA, Gelman RS, Melisko ME, Anders CK, Moy B, Blackwell KL, Connolly RM, Niravath PA, Poznak CHV, Puhalla S, Farooq S, Cropp A, Cotter CM, Liu MC, Krop IE, Nangia JR, Tung NM, Wolff AC, Winer EP, and Lin NU (2017) TBCRC 022: Phase II trial of neratinib + capecitabine for patients (Pts) with human epidermal growth factor receptor 2 (HER2+) breast cancer brain metastases (BCBM). *Journal of Clinical Oncology* **35**:1005-1005.
- Friboulet L, Li N, Katayama R, Lee CC, Gainor JF, Crystal AS, Michellys PY, Awad MM, Yanagitani N, Kim S, Pferdekamper AC, Li J, Kasibhatla S, Sun F, Sun X, Hua S, McNamara P, Mahmood S, Lockerman EL, Fujita N, Nishio M, Harris JL, Shaw AT, and Engelman JA (2014) The ALK inhibitor ceritinib overcomes crizotinib resistance in non-small cell lung cancer. *Cancer Discov* **4**:662-673.
- Friden M, Gupta A, Antonsson M, Bredberg U, and Hammarlund-Udenaes M (2007) In vitro methods for estimating unbound drug concentrations in the brain interstitial and intracellular fluids. *Drug Metab Dispos* **35**:1711-1719.
- Furnari FB, Fenton T, Bachoo RM, Mukasa A, Stommel JM, Stegh A, Hahn WC, Ligon KL, Louis DN, Brennan C, Chin L, DePinho RA, and Cavenee WK (2007) Malignant astrocytic glioma: genetics, biology, and paths to treatment. *Genes Dev* **21**:2683-2710.
- Gadgeel SM, Gandhi L, Riely GJ, Chiappori AA, West HL, Azada MC, Morcos PN, Lee RM, Garcia L, Yu L, Boisserie F, Di Laurenzio L, Golding S, Sato J, Yokoyama S, Tanaka T, and Ou SH (2014) Safety and activity of alectinib against systemic disease and brain metastases in patients with crizotinib-resistant ALK-rearranged non-small-cell lung cancer (AF-002JG): results from the dose-finding portion of a phase 1/2 study. *Lancet Oncol* **15**:1119-1128.
- Gampa G, Kim M, Cook-Rostie N, Laramy JK, Sarkaria JN, Paradiso L, DePalatis L, and Elmquist WF (2018) Brain Distribution of a Novel MEK Inhibitor E6201: Implications in the Treatment of Melanoma Brain Metastases. *Drug Metab Dispos* **46**:658-666.
- Gampa G, Vaidhyanathan S, Sarkaria JN, and Elmquist WF (2017) Drug delivery to melanoma brain metastases: Can current challenges lead to new opportunities? *Pharmacol Res* **123**:10-25.
- Gaspar L, Scott C, Rotman M, Asbell S, Phillips T, Wasserman T, McKenna WG, and Byhardt R (1997) Recursive partitioning analysis (RPA) of prognostic factors in three Radiation Therapy Oncology Group (RTOG) brain metastases trials. *Int J Radiat Oncol Biol Phys* **37**:745-751.
- Gavrilovic IT and Posner JB (2005) Brain metastases: epidemiology and pathophysiology. *J Neurooncol* **75**:5-14.
- Genevois C, Loiseau H, and Couillaud F (2016) In Vivo Follow-up of Brain Tumor Growth via Bioluminescence Imaging and Fluorescence Tomography. *Int J Mol Sci* **17**.

- Gerstner ER and Fine RL (2007) Increased permeability of the blood-brain barrier to chemotherapy in metastatic brain tumors: establishing a treatment paradigm. *J Clin Oncol* **25**:2306-2312.
- Golden PL and Pollack GM (2003) Blood-brain barrier efflux transport. *J Pharm Sci* **92**:1739-1753.
- Gorantla V, Kirkwood JM, and Tawbi HA (2013) Melanoma brain metastases: an unmet challenge in the era of active therapy. *Curr Oncol Rep* **15**:483-491.
- Gore ME, Hariharan S, Porta C, Bracarda S, Hawkins R, Bjarnason GA, Oudard S, Lee SH, Carteni G, Nieto A, Yuan J, and Szczylik C (2011) Sunitinib in metastatic renal cell carcinoma patients with brain metastases. *Cancer* **117**:501-509.
- Gori S, Lunardi G, Inno A, Foglietta J, Cardinali B, Del Mastro L, and Crino L (2014) Lapatinib concentration in cerebrospinal fluid in two patients with HER2-positive metastatic breast cancer and brain metastases. *Ann Oncol* **25**:912-913.
- Goss G, Tsai CM, Shepherd FA, Ahn MJ, Bazhenova L, Crino L, de Marinis F, Felip E, Morabito A, Hodge R, Cantarini M, Johnson M, Mitsudomi T, Janne PA, and Yang JC (2018) CNS response to osimertinib in patients with T790M-positive advanced NSCLC: pooled data from two phase II trials. *Ann Oncol* **29**:687-693.
- Gupta SK, Mladek AC, Carlson BL, Boakye-Agyeman F, Bakken KK, Kizilbash SH, Schroeder MA, Reid J, and Sarkaria JN (2014) Discordant in vitro and in vivo chemopotentiating effects of the PARP inhibitor veliparib in temozolomide-sensitive versus -resistant glioblastoma multiforme xenografts. *Clin Cancer Res* **20**:3730-3741.
- Hai J, Sakashita S, Allo G, Ludkovski O, Ng C, Shepherd FA, and Tsao MS (2015) Inhibiting MDM2-p53 Interaction Suppresses Tumor Growth in Patient-Derived Non-Small Cell Lung Cancer Xenograft Models. *J Thorac Oncol* **10**:1172-1180.
- Hainaut P and Hollstein M (2000) p53 and human cancer: the first ten thousand mutations. *Adv Cancer Res* **77**:81-137.
- Hammarlund-Udenaes M, Friden M, Syvanen S, and Gupta A (2008) On the rate and extent of drug delivery to the brain. *Pharm Res* **25**:1737-1750.
- Hanson JE, La H, Plise E, Chen YH, Ding X, Hanania T, Sabath EV, Alexandrov V, Brunner D, Leahy E, Steiner P, Liu L, Scearce-Levie K, and Zhou Q (2013) SAHA enhances synaptic function and plasticity in vitro but has limited brain availability in vivo and does not impact cognition. *PLoS One* **8**:e69964.
- Harwood KR, Mofford DM, Reddy GR, and Miller SC (2011) Identification of mutant firefly luciferases that efficiently utilize aminoluciferins. *Chem Biol* **18**:1649-1657.
- Haseloff RF, Blasig IE, Bauer HC, and Bauer H (2005) In search of the astrocytic factor(s) modulating blood-brain barrier functions in brain capillary endothelial cells in vitro. *Cell Mol Neurobiol* **25**:25-39.
- Heffron TP (2016) Small Molecule Kinase Inhibitors for the Treatment of Brain Cancer. *J Med Chem* **59**:10030-10066.
- Heffron TP (2018) Challenges of developing small-molecule kinase inhibitors for brain tumors and the need for emphasis on free drug levels. *Neuro Oncol* **20**:307-312.
- Heffron TP, Salphati L, Alick B, Cheong J, Dotson J, Edgar K, Goldsmith R, Gould SE, Lee LB, Lesnick JD, Lewis C, Ndubaku C, Nonomiya J, Olivero AG, Pang J, Plise EG, Sideris S, Trapp S, Wallin J, Wang L, and Zhang X (2012) The design and identification of brain penetrant inhibitors of phosphoinositide 3-kinase alpha. *J Med Chem* **55**:8007-8020.

- Heon S, Yeap BY, Lindeman NI, Joshi VA, Butaney M, Britt GJ, Costa DB, Rabin MS, Jackman DM, and Johnson BE (2012) The impact of initial gefitinib or erlotinib versus chemotherapy on central nervous system progression in advanced non-small cell lung cancer with EGFR mutations. *Clin Cancer Res* **18**:4406-4414.
- Hillered L, Persson L, Nilsson P, Ronne-Engstrom E, and Enblad P (2006) Continuous monitoring of cerebral metabolism in traumatic brain injury: a focus on cerebral microdialysis. *Curr Opin Crit Care* **12**:112-118.
- Hoffknecht P, Tufman A, Wehler T, Pelzer T, Wiewrodt R, Schutz M, Serke M, Stohlmacher-Williams J, Marten A, Maria Huber R, Dickgreber NJ, and Afatinib Compassionate Use C (2015) Efficacy of the irreversible ErbB family blocker afatinib in epidermal growth factor receptor (EGFR) tyrosine kinase inhibitor (TKI)-pretreated non-small-cell lung cancer patients with brain metastases or leptomeningeal disease. *J Thorac Oncol* **10**:156-163.
- Hoffman-Luca CG, Yang CY, Lu J, Ziazadeh D, McEachern D, Debussche L, and Wang S (2015) Significant Differences in the Development of Acquired Resistance to the MDM2 Inhibitor SAR405838 between In Vitro and In Vivo Drug Treatment. *PLoS One* **10**:e0128807.
- Hu B, Gilkes DM, and Chen J (2007) Efficient p53 activation and apoptosis by simultaneous disruption of binding to MDM2 and MDMX. *Cancer Res* **67**:8810-8817.
- Huang PH, Xu AM, and White FM (2009) Oncogenic EGFR signaling networks in glioma. *Sci Signal* **2**:re6.
- Hubatsch I, Ragnarsson EG, and Artursson P (2007) Determination of drug permeability and prediction of drug absorption in Caco-2 monolayers. *Nat Protoc* **2**:2111-2119.
- Iqbal U, Abulrob A, and Stanimirovic DB (2011) Integrated platform for brain imaging and drug delivery across the blood-brain barrier. *Methods Mol Biol* **686**:465-481.
- Jabeen I, Pleban K, Rinner U, Chiba P, and Ecker GF (2012) Structure-activity relationships, ligand efficiency, and lipophilic efficiency profiles of benzophenone-type inhibitors of the multidrug transporter P-glycoprotein. *J Med Chem* **55**:3261-3273.
- Jathoul AP, Grounds H, Anderson JC, and Pule MA (2014) A dual-color far-red to near-infrared firefly luciferin analogue designed for multiparametric bioluminescence imaging. *Angew Chem Int Ed Engl* **53**:13059-13063.
- Jiang CC, Chen LH, Gillespie S, Wang YF, Kiejda KA, Zhang XD, and Hersey P (2007) Inhibition of MEK sensitizes human melanoma cells to endoplasmic reticulum stress-induced apoptosis. *Cancer Res* **67**:9750-9761.
- Johnson TW, Richardson PF, Bailey S, Brooun A, Burke BJ, Collins MR, Cui JJ, Deal JG, Deng YL, Dinh D, Engstrom LD, He M, Hoffman J, Hoffman RL, Huang Q, Kania RS, Kath JC, Lam H, Lam JL, Le PT, Lingardo L, Liu W, McTigue M, Palmer CL, Sach NW, Smeal T, Smith GL, Stewart AE, Timofeevski S, Zhu H, Zhu J, Zou HY, and Edwards MP (2014) Discovery of (10R)-7-amino-12-fluoro-2,10,16-trimethyl-15-oxo-10,15,16,17-tetrahydro-2H-8,4-(metheno)pyrazolo[4,3-h][2,5,11]-benzoxadiazacyclotetradecine-3-carbonitrile (PF-06463922), a macrocyclic inhibitor of anaplastic lymphoma kinase (ALK) and c-ros oncogene 1 (ROS1) with preclinical brain exposure and broad-spectrum potency against ALK-resistant mutations. *J Med Chem* **57**:4720-4744.
- Jovcevska I, Kocevar N, and Komel R (2013) Glioma and glioblastoma - how much do we (not) know? *Mol Clin Oncol* **1**:935-941.

- Jung J, Lee JS, Dickson MA, Schwartz GK, Le Cesne A, Varga A, Bahleda R, Wagner AJ, Choy E, de Jonge MJ, Light M, Rowley S, Mace S, and Watters J (2016) TP53 mutations emerge with HDM2 inhibitor SAR405838 treatment in de-differentiated liposarcoma. *Nat Commun* **7**:12609.
- Kalvass JC and Maurer TS (2002) Influence of nonspecific brain and plasma binding on CNS exposure: implications for rational drug discovery. *Biopharm Drug Dispos* **23**:327-338.
- Kalvass JC, Phipps C, Jenkins GJ, Stuart P, Zhang X, Heinle L, Nijsen M, and Fischer V (2018) Mathematical and Experimental Validation of Flux Dialysis Method: An Improved Approach to Measure Unbound Fraction for Compounds with High Protein Binding and Other Challenging Properties. *Drug Metab Dispos* **46**:458-469.
- Kaskova ZM, Tsarkova AS, and Yampolsky IV (2016) 1001 lights: luciferins, luciferases, their mechanisms of action and applications in chemical analysis, biology and medicine. *Chem Soc Rev* **45**:6048-6077.
- Katayama R, Sakashita T, Yanagitani N, Ninomiya H, Horiike A, Friboulet L, Gainor JF, Motoi N, Dobashi A, Sakata S, Tambo Y, Kitazono S, Sato S, Koike S, John lafrate A, Mino-Kenudson M, Ishikawa Y, Shaw AT, Engelman JA, Takeuchi K, Nishio M, and Fujita N (2016) P-glycoprotein Mediates Ceritinib Resistance in Anaplastic Lymphoma Kinase-rearranged Non-small Cell Lung Cancer. *EBioMedicine* **3**:54-66.
- Kawamura K, Yamasaki T, Yui J, Hatori A, Konno F, Kumata K, Irie T, Fukumura T, Suzuki K, Kanno I, and Zhang MR (2009) In vivo evaluation of P-glycoprotein and breast cancer resistance protein modulation in the brain using [(11)C]gefitinib. *Nucl Med Biol* **36**:239-246.
- Kienast Y, von Baumgarten L, Fuhrmann M, Klinkert WE, Goldbrunner R, Herms J, and Winkler F (2010) Real-time imaging reveals the single steps of brain metastasis formation. *Nat Med* **16**:116-122.
- Kim A and Cohen MS (2016) The discovery of vemurafenib for the treatment of BRAF-mutated metastatic melanoma. *Expert Opin Drug Discov* **11**:907-916.
- Kim DW, Mehra R, Tan DS, Filip E, Chow LQ, Camidge DR, Vansteenkiste J, Sharma S, De Pas T, Riely GJ, Solomon BJ, Wolf J, Thomas M, Schuler M, Liu G, Santoro A, Sutradhar S, Li S, Szczudlo T, Yovine A, and Shaw AT (2016) Activity and safety of ceritinib in patients with ALK-rearranged non-small-cell lung cancer (ASCEND-1): updated results from the multicentre, open-label, phase 1 trial. *Lancet Oncol* **17**:452-463.
- Kim M, Kizilbash SH, Laramy JK, Gampa G, Parrish KE, Sarkaria JN, and Elmquist WF (2018a) Barriers to Effective Drug Treatment for Brain Metastases: A Multifactorial Problem in the Delivery of Precision Medicine. *Pharm Res* **35**:177.
- Kim M, Ma DJ, Calligaris D, Zhang S, Feathers RW, Vaubel RA, Meaux I, Mladek AC, Parrish KE, Jin F, Barriere C, Debussche L, Watters J, Tian S, Decker PA, Eckel-Passow JE, Kitange GJ, Johnson AJ, Parney IF, Anastasiadis PZ, Agar NYR, Elmquist WF, and Sarkaria JN (2018b) Efficacy of the MDM2 inhibitor SAR405838 in glioblastoma is limited by poor distribution across the blood-brain barrier. *Mol Cancer Ther*.
- Kis O, Robillard K, Chan GN, and Bendayan R (2010) The complexities of antiretroviral drug-drug interactions: role of ABC and SLC transporters. *Trends Pharmacol Sci* **31**:22-35.
- Kitange GJ, Mladek AC, Carlson BL, Schroeder MA, Pokorny JL, Cen L, Decker PA, Wu W, Lomberk GA, Gupta SK, Urrutia RA, and Sarkaria JN (2012) Inhibition of histone deacetylation

- potentiates the evolution of acquired temozolomide resistance linked to MGMT upregulation in glioblastoma xenografts. *Clin Cancer Res* **18**:4070-4079.
- Kizilbash SH, Gupta SK, Chang K, Kawashima R, Parrish KE, Carlson BL, Bakken KK, Mladek AC, Schroeder MA, Decker PA, Kitange GJ, Shen Y, Feng Y, Protter AA, Elmquist WF, and Sarkaria JN (2017) Restricted Delivery of Talazoparib Across the Blood-Brain Barrier Limits the Sensitizing Effects of PARP Inhibition on Temozolomide Therapy in Glioblastoma. *Mol Cancer Ther* **16**:2735-2746.
- Kocher M, Soffiatti R, Abacioglu U, Villa S, Fauchon F, Baumert BG, Fariselli L, Tzuk-Shina T, Kortmann RD, Carrie C, Ben Hassel M, Kouri M, Valeinis E, van den Berge D, Collette S, Collette L, and Mueller RP (2011) Adjuvant whole-brain radiotherapy versus observation after radiosurgery or surgical resection of one to three cerebral metastases: results of the EORTC 22952-26001 study. *J Clin Oncol* **29**:134-141.
- Kodack DP, Askoxylakis V, Ferraro GB, Fukumura D, and Jain RK (2015) Emerging strategies for treating brain metastases from breast cancer. *Cancer Cell* **27**:163-175.
- Kodaira H, Kusuhara H, Fujita T, Ushiki J, Fuse E, and Sugiyama Y (2011) Quantitative evaluation of the impact of active efflux by p-glycoprotein and breast cancer resistance protein at the blood-brain barrier on the predictability of the unbound concentrations of drugs in the brain using cerebrospinal fluid concentration as a surrogate. *J Pharmacol Exp Ther* **339**:935-944.
- Kodaira H, Kusuhara H, Ushiki J, Fuse E, and Sugiyama Y (2010) Kinetic analysis of the cooperation of P-glycoprotein (P-gp/Abcb1) and breast cancer resistance protein (Bcrp/Abcg2) in limiting the brain and testis penetration of erlotinib, flavopiridol, and mitoxantrone. *J Pharmacol Exp Ther* **333**:788-796.
- Kodama T, Hasegawa M, Takanashi K, Sakurai Y, Kondoh O, and Sakamoto H (2014a) Antitumor activity of the selective ALK inhibitor alectinib in models of intracranial metastases. *Cancer Chemother Pharmacol* **74**:1023-1028.
- Kodama T, Tsukaguchi T, Satoh Y, Yoshida M, Watanabe Y, Kondoh O, and Sakamoto H (2014b) Alectinib shows potent antitumor activity against RET-rearranged non-small cell lung cancer. *Mol Cancer Ther* **13**:2910-2918.
- Koivunen JP, Mermel C, Zejnullahu K, Murphy C, Lifshits E, Holmes AJ, Choi HG, Kim J, Chiang D, Thomas R, Lee J, Richards WG, Sugarbaker DJ, Ducko C, Lindeman N, Marcoux JP, Engelman JA, Gray NS, Lee C, Meyerson M, and Janne PA (2008) EML4-ALK fusion gene and efficacy of an ALK kinase inhibitor in lung cancer. *Clin Cancer Res* **14**:4275-4283.
- Kong AN and Jusko WJ (1988) Definitions and applications of mean transit and residence times in reference to the two-compartment mammillary plasma clearance model. *J Pharm Sci* **77**:157-165.
- Krawczyk P, Kowalski DM, Ramlau R, Kalinka-Warzocho E, Winiarczyk K, Stencel K, Powrozek T, Reszka K, Wojas-Krawczyk K, Bryl M, Wojcik-Superczynska M, Glogowski M, Barinow-Wojewodzki A, Milanowski J, and Krzakowski M (2017) Comparison of the effectiveness of erlotinib, gefitinib, and afatinib for treatment of non-small cell lung cancer in patients with common and rare EGFR gene mutations. *Oncol Lett* **13**:4433-4444.
- Kreisl TN, McNeill KA, Sul J, Iwamoto FM, Shih J, and Fine HA (2012) A phase I/II trial of vandetanib for patients with recurrent malignant glioma. *Neuro Oncol* **14**:1519-1526.

- Kreuter J (2014) Drug delivery to the central nervous system by polymeric nanoparticles: what do we know? *Adv Drug Deliv Rev* **71**:2-14.
- Kromer C, Xu J, Ostrom QT, Gittleman H, Kruchko C, Sawaya R, and Barnholtz-Sloan JS (2017) Estimating the annual frequency of synchronous brain metastasis in the United States 2010-2013: a population-based study. *J Neurooncol* **134**:55-64.
- Kruijtzter CM, Beijnen JH, Rosing H, ten Bokkel Huinink WW, Schot M, Jewell RC, Paul EM, and Schellens JH (2002) Increased oral bioavailability of topotecan in combination with the breast cancer resistance protein and P-glycoprotein inhibitor GF120918. *J Clin Oncol* **20**:2943-2950.
- Kubo Y, Ohtsuki S, Uchida Y, and Terasaki T (2015) Quantitative Determination of Luminal and Abluminal Membrane Distributions of Transporters in Porcine Brain Capillaries by Plasma Membrane Fractionation and Quantitative Targeted Proteomics. *J Pharm Sci* **104**:3060-3068.
- Kwak EL, Bang YJ, Camidge DR, Shaw AT, Solomon B, Maki RG, Ou SH, Dezube BJ, Janne PA, Costa DB, Varella-Garcia M, Kim WH, Lynch TJ, Fidias P, Stubbs H, Engelman JA, Sequist LV, Tan W, Gandhi L, Mino-Kenudson M, Wei GC, Shreeve SM, Ratain MJ, Settleman J, Christensen JG, Haber DA, Wilner K, Salgia R, Shapiro GI, Clark JW, and Iafrate AJ (2010) Anaplastic lymphoma kinase inhibition in non-small-cell lung cancer. *N Engl J Med* **363**:1693-1703.
- Laramy JK, Kim M, Gupta SK, Parrish KE, Zhang S, Bakken KK, Carlson BL, Mladek AC, Ma DJ, Sarkaria JN, and Elmquist WF (2017) Heterogeneous Binding and Central Nervous System Distribution of the Multitargeted Kinase Inhibitor Ponatinib Restrict Orthotopic Efficacy in a Patient-Derived Xenograft Model of Glioblastoma. *J Pharmacol Exp Ther* **363**:136-147.
- Laramy JK, Kim M, Parrish KE, Sarkaria JN, and Elmquist WF (2018) Pharmacokinetic Assessment of Cooperative Efflux of the Multitargeted Kinase Inhibitor Ponatinib Across the Blood-Brain Barrier. *J Pharmacol Exp Ther* **365**:249-261.
- Larkin J, Ascierto PA, Dreno B, Atkinson V, Liszkay G, Maio M, Mandala M, Demidov L, Stroyakovskiy D, Thomas L, de la Cruz-Merino L, Dutriaux C, Garbe C, Sovak MA, Chang J, Choong N, Hack SP, McArthur GA, and Ribas A (2014) Combined vemurafenib and cobimetinib in BRAF-mutated melanoma. *N Engl J Med* **371**:1867-1876.
- Lawlor D, Martin P, Busschots S, Thery J, O'Leary JJ, Hennessy BT, and Stordal B (2014) PARP Inhibitors as P-glycoprotein Substrates. *J Pharm Sci* **103**:1913-1920.
- Lee KH, Byun SS, Paik JY, Lee SY, Song SH, Choe YS, and Kim BT (2003) Cell uptake and tissue distribution of radioiodine labelled D-luciferin: implications for luciferase based gene imaging. *Nucl Med Commun* **24**:1003-1009.
- Levin VA (1980) Relationship of octanol/water partition coefficient and molecular weight to rat brain capillary permeability. *J Med Chem* **23**:682-684.
- Lewis JS, Achilefu S, Garbow JR, Laforest R, and Welch MJ (2002) Small animal imaging. current technology and perspectives for oncological imaging. *Eur J Cancer* **38**:2173-2188.
- Leyland-Jones B (2009) Human epidermal growth factor receptor 2-positive breast cancer and central nervous system metastases. *J Clin Oncol* **27**:5278-5286.

- Li L, Agarwal S, and Elmquist WF (2013) Brain efflux index to investigate the influence of active efflux on brain distribution of pemetrexed and methotrexate. *Drug Metab Dispos* **41**:659-667.
- Li L, Sham YY, Bikadi Z, and Elmquist WF (2011) pH-Dependent transport of pemetrexed by breast cancer resistance protein. *Drug Metab Dispos* **39**:1478-1485.
- Li Y, Du Y, Sun T, Xue H, Jin Z, and Tian J (2018) PD-1 blockade in combination with zoledronic acid to enhance the antitumor efficacy in the breast cancer mouse model. *BMC Cancer* **18**:669.
- Lin F, de Gooijer MC, Roig EM, Buil LC, Christner SM, Beumer JH, Wurdinger T, Beijnen JH, and van Tellingen O (2014) ABCB1, ABCG2, and PTEN determine the response of glioblastoma to temozolomide and ABT-888 therapy. *Clin Cancer Res* **20**:2703-2713.
- Lin JH and Yamazaki M (2003) Role of P-glycoprotein in pharmacokinetics: clinical implications. *Clin Pharmacokinet* **42**:59-98.
- Lin NU, Bellon JR, and Winer EP (2004) CNS metastases in breast cancer. *J Clin Oncol* **22**:3608-3617.
- Lin NU, Carey LA, Liu MC, Younger J, Come SE, Ewend M, Harris GJ, Bullitt E, Van den Abbeele AD, Henson JW, Li X, Gelman R, Burstein HJ, Kasparian E, Kirsch DG, Crawford A, Hochberg F, and Winer EP (2008) Phase II trial of lapatinib for brain metastases in patients with human epidermal growth factor receptor 2-positive breast cancer. *J Clin Oncol* **26**:1993-1999.
- Lin NU, Dieras V, Paul D, Lossignol D, Christodoulou C, Stemmler HJ, Roche H, Liu MC, Greil R, Ciruelos E, Loibl S, Gori S, Wardley A, Yardley D, Brufsky A, Blum JL, Rubin SD, Dharan B, Steplewski K, Zembryki D, Oliva C, Roychowdhury D, Paoletti P, and Winer EP (2009) Multicenter phase II study of lapatinib in patients with brain metastases from HER2-positive breast cancer. *Clin Cancer Res* **15**:1452-1459.
- Lin NU, Lee EQ, Aoyama H, Barani IJ, Barboriak DP, Baumert BG, Bendszus M, Brown PD, Camidge DR, Chang SM, Dancey J, de Vries EG, Gaspar LE, Harris GJ, Hodi FS, Kalkanis SN, Linskey ME, Macdonald DR, Margolin K, Mehta MP, Schiff D, Soffiatti R, Suh JH, van den Bent MJ, Vogelbaum MA, Wen PY, and Response Assessment in Neuro-Oncology g (2015) Response assessment criteria for brain metastases: proposal from the RANO group. *Lancet Oncol* **16**:e270-278.
- Lingineni K, Belekar V, Tangadpalliwar SR, and Garg P (2017) The role of multidrug resistance protein (MRP-1) as an active efflux transporter on blood-brain barrier (BBB) permeability. *Mol Divers*.
- Liu M, Li C, Pazgier M, Mao Y, Lv Y, Gu B, Wei G, Yuan W, Zhan C, Lu WY, and Lu W (2010) D-peptide inhibitors of the p53-MDM2 interaction for targeted molecular therapy of malignant neoplasms. *Proc Natl Acad Sci U S A* **107**:14321-14326.
- Liu X, Chen C, and Smith BJ (2008) Progress in brain penetration evaluation in drug discovery and development. *J Pharmacol Exp Ther* **325**:349-356.
- Liu X, Ding X, Deshmukh G, Liederer BM, and Hop CE (2012) Use of the cassette-dosing approach to assess brain penetration in drug discovery. *Drug Metab Dispos* **40**:963-969.
- Liu X, Ide JL, Norton I, Marchionni MA, Ebling MC, Wang LY, Davis E, Sauvageot CM, Kesari S, Kellersberger KA, Easterling ML, Santagata S, Stuart DD, Alberta J, Agar JN, Stiles CD, and

- Agar NY (2013) Molecular imaging of drug transit through the blood-brain barrier with MALDI mass spectrometry imaging. *Sci Rep* **3**:2859.
- Liu X, Smith BJ, Chen C, Callegari E, Becker SL, Chen X, Cianfrogna J, Doran AC, Doran SD, Gibbs JP, Hosea N, Liu J, Nelson FR, Szewc MA, and Van Deusen J (2005) Use of a physiologically based pharmacokinetic model to study the time to reach brain equilibrium: an experimental analysis of the role of blood-brain barrier permeability, plasma protein binding, and brain tissue binding. *J Pharmacol Exp Ther* **313**:1254-1262.
- Liu X, Van Natta K, Yeo H, Vilenski O, Weller PE, Worboys PD, and Monshouwer M (2009) Unbound drug concentration in brain homogenate and cerebral spinal fluid at steady state as a surrogate for unbound concentration in brain interstitial fluid. *Drug Metab Dispos* **37**:787-793.
- Lockman PR, Mittapalli RK, Taskar KS, Rudraraju V, Gril B, Bohn KA, Adkins CE, Roberts A, Thorsheim HR, Gaasch JA, Huang S, Palmieri D, Steeg PS, and Smith QR (2010) Heterogeneous blood-tumor barrier permeability determines drug efficacy in experimental brain metastases of breast cancer. *Clin Cancer Res* **16**:5664-5678.
- Long GV, Trefzer U, Davies MA, Kefford RF, Ascierto PA, Chapman PB, Puzanov I, Hauschild A, Robert C, Algazi A, Mortier L, Tawbi H, Wilhelm T, Zimmer L, Switzky J, Swann S, Martin AM, Guckert M, Goodman V, Streit M, Kirkwood JM, and Schadendorf D (2012) Dabrafenib in patients with Val600Glu or Val600Lys BRAF-mutant melanoma metastatic to the brain (BREAK-MB): a multicentre, open-label, phase 2 trial. *Lancet Oncol* **13**:1087-1095.
- Long GV, Weber JS, Infante JR, Kim KB, Daud A, Gonzalez R, Sosman JA, Hamid O, Schuchter L, Cebon J, Kefford RF, Lawrence D, Kudchadkar R, Burris HA, 3rd, Falchook GS, Algazi A, Lewis K, Puzanov I, Ibrahim N, Sun P, Cunningham E, Kline AS, Del Buono H, McDowell DO, Patel K, and Flaherty KT (2016) Overall Survival and Durable Responses in Patients With BRAF V600-Mutant Metastatic Melanoma Receiving Dabrafenib Combined With Trametinib. *J Clin Oncol* **34**:871-878.
- Luke JJ and Hodi FS (2012) Vemurafenib and BRAF inhibition: a new class of treatment for metastatic melanoma. *Clin Cancer Res* **18**:9-14.
- Lyons SK (2005) Advances in imaging mouse tumour models in vivo. *J Pathol* **205**:194-205.
- Maddika S, Kavela S, Rani N, Palicharla VR, Pokorny JL, Sarkaria JN, and Chen J (2011) WWP2 is an E3 ubiquitin ligase for PTEN. *Nat Cell Biol* **13**:728-733.
- Manitpisitkul P and White RE (2004) Whatever happened to cassette-dosing pharmacokinetics? *Drug Discov Today* **9**:652-658.
- Margolin K, Ernstoff MS, Hamid O, Lawrence D, McDermott D, Puzanov I, Wolchok JD, Clark JI, Sznol M, Logan TF, Richards J, Michener T, Balogh A, Heller KN, and Hodi FS (2012) Ipilimumab in patients with melanoma and brain metastases: an open-label, phase 2 trial. *The Lancet Oncology* **13**:459-465.
- Maurer TS, DeBartolo DB, Tess DA, and Scott DO (2005) Relationship between exposure and nonspecific binding of thirty-three central nervous system drugs in mice. *Drug Metab Dispos* **33**:175-181.
- McCoach CE, Berge EM, Lu X, Baron AE, and Camidge DR (2016) A Brief Report of the Status of Central Nervous System Metastasis Enrollment Criteria for Advanced Non-Small Cell



- Lung Cancer Clinical Trials: A Review of the ClinicalTrials.gov Trial Registry. *J Thorac Oncol* **11**:407-413.
- McDonald RJ, McDonald JS, Kallmes DF, Jentoft ME, Murray DL, Thielen KR, Williamson EE, and Eckel LJ (2015) Intracranial Gadolinium Deposition after Contrast-enhanced MR Imaging. *Radiology* **275**:772-782.
- McDonald RJ, McDonald JS, Kallmes DF, Jentoft ME, Paolini MA, Murray DL, Williamson EE, and Eckel LJ (2017) Gadolinium Deposition in Human Brain Tissues after Contrast-enhanced MR Imaging in Adult Patients without Intracranial Abnormalities. *Radiology* **285**:546-554.
- McWilliams RR, Brown PD, Buckner JC, Link MJ, and Markovic SN (2003) Treatment of brain metastases from melanoma. *Mayo Clin Proc* **78**:1529-1536.
- Mehta MP, Wang D, Wang F, Kleinberg L, Brade A, Robins HI, Turaka A, Leahy T, Medina D, Xiong H, Mostafa NM, Dunbar M, Zhu M, Qian J, Holen K, Giranda V, and Curran WJ (2015) Veliparib in combination with whole brain radiation therapy in patients with brain metastases: results of a phase 1 study. *J Neurooncol* **122**:409-417.
- Menichincheri M, Ardini E, Magnaghi P, Avanzi N, Banfi P, Bossi R, Buffa L, Canevari G, Ceriani L, Colombo M, Corti L, Donati D, Fasolini M, Felder E, Fiorelli C, Fiorentini F, Galvani A, Isacchi A, Borgia AL, Marchionni C, Nesi M, Orrenius C, Panzeri A, Pesenti E, Rusconi L, Saccardo MB, Vanotti E, Perrone E, and Orsini P (2016) Discovery of Entrectinib: A New 3-Aminoindazole As a Potent Anaplastic Lymphoma Kinase (ALK), c-ros Oncogene 1 Kinase (ROS1), and Pan-Tropomyosin Receptor Kinases (Pan-TRKs) inhibitor. *J Med Chem* **59**:3392-3408.
- Metro G, Lunardi G, Bennati C, Chiarini P, Sperduti I, Ricciuti B, Marcomigni L, Costa C, Crino L, Floridi P, Gori S, and Chiari R (2016) Alectinib's activity against CNS metastases from ALK-positive non-small cell lung cancer: a single institution case series. *J Neurooncol* **129**:355-361.
- Mikule K and Wilcoxon K (2015) The PARP inhibitor, niraparib, crosses the blood brain barrier in rodents and is efficacious in a BRCA2-mutant intracranial tumor model. [abstract]. in: *In: Proceedings of the AACR-NCI-EORTC International Conference: Molecular Targets and Cancer Therapeutics*, Philadelphia (PA).
- Miller DS, Nobmann SN, Gutmann H, Toeroek M, Drewe J, and Fricker G (2000) Xenobiotic transport across isolated brain microvessels studied by confocal microscopy. *Mol Pharmacol* **58**:1357-1367.
- Minniti G, Muni R, Lanzetta G, Marchetti P, and Enrici RM (2009) Chemotherapy for glioblastoma: current treatment and future perspectives for cytotoxic and targeted agents. *Anticancer Res* **29**:5171-5184.
- Minocha M, Khurana V, Qin B, Pal D, and Mitra AK (2012) Co-administration strategy to enhance brain accumulation of vandetanib by modulating P-glycoprotein (P-gp/Abcb1) and breast cancer resistance protein (Bcrp1/Abcg2) mediated efflux with m-TOR inhibitors. *Int J Pharm* **434**:306-314.
- Mittapalli RK, Chung AH, Parrish KE, Crabtree D, Halvorson KG, Hu G, Elmquist WF, and Becher OJ (2016) ABCG2 and ABCB1 Limit the Efficacy of Dasatinib in a PDGF-B-Driven Brainstem Glioma Model. *Mol Cancer Ther* **15**:819-829.

- Mittapalli RK, Vaidhyanathan S, Dudek AZ, and Elmquist WF (2013) Mechanisms limiting distribution of the threonine-protein kinase B-RaF(V600E) inhibitor dabrafenib to the brain: implications for the treatment of melanoma brain metastases. *J Pharmacol Exp Ther* **344**:655-664.
- Mittapalli RK, Vaidhyanathan S, Sane R, and Elmquist WF (2012) Impact of P-glycoprotein (ABCB1) and breast cancer resistance protein (ABCG2) on the brain distribution of a novel BRAF inhibitor: vemurafenib (PLX4032). *J Pharmacol Exp Ther* **342**:33-40.
- Mofford DM and Miller SC (2015) Luciferins behave like drugs. *ACS Chem Neurosci* **6**:1273-1275.
- Mok TS, Wu YL, Ahn MJ, Garassino MC, Kim HR, Ramalingam SS, Shepherd FA, He Y, Akamatsu H, Theelen WS, Lee CK, Sebastian M, Templeton A, Mann H, Marotti M, Ghiorghiu S, Papadimitrakopoulou VA, and Investigators A (2017) Osimertinib or Platinum-Pemetrexed in EGFR T790M-Positive Lung Cancer. *N Engl J Med* **376**:629-640.
- Momand J, Wu HH, and Dasgupta G (2000) MDM2--master regulator of the p53 tumor suppressor protein. *Gene* **242**:15-29.
- Momand J, Zambetti GP, Olson DC, George D, and Levine AJ (1992) The mdm-2 oncogene product forms a complex with the p53 protein and inhibits p53-mediated transactivation. *Cell* **69**:1237-1245.
- Mook OR, Van Marle J, Vreeling-Sindelarova H, Jonges R, Frederiks WM, and Van Noorden CJ (2003) Visualization of early events in tumor formation of eGFP-transfected rat colon cancer cells in liver. *Hepatology* **38**:295-304.
- Morikawa A, Peereboom DM, Thorsheim HR, Samala R, Balyan R, Murphy CG, Lockman PR, Simmons A, Weil RJ, Tabar V, Steeg PS, Smith QR, and Seidman AD (2015) Capecitabine and lapatinib uptake in surgically resected brain metastases from metastatic breast cancer patients: a prospective study. *Neuro Oncol* **17**:289-295.
- Morschhauser F, Zinzani PL, Burgess M, Sloots L, Bouafia F, and Dumontet C (2007) Phase I/II trial of a P-glycoprotein inhibitor, Zosuquidar.3HCl trihydrochloride (LY335979), given orally in combination with the CHOP regimen in patients with non-Hodgkin's lymphoma. *Leuk Lymphoma* **48**:708-715.
- Nadkarni A, Shrivastav M, Mladek AC, Schwingler PM, Grogan PT, Chen J, and Sarkaria JN (2012) ATM inhibitor KU-55933 increases the TMZ responsiveness of only inherently TMZ sensitive GBM cells. *J Neurooncol* **110**:349-357.
- Narayana A, Mathew M, Tam M, Kannan R, Madden KM, Golfinos JG, Parker EC, Ott PA, and Pavlick AC (2013) Vemurafenib and radiation therapy in melanoma brain metastases. *J Neurooncol* **113**:411-416.
- Nayak L, Lee EQ, and Wen PY (2012) Epidemiology of brain metastases. *Curr Oncol Rep* **14**:48-54.
- Newman SJ and Hansen HH (1974) Proceedings: Frequency, diagnosis, and treatment of brain metastases in 247 consecutive patients with bronchogenic carcinoma. *Cancer* **33**:492-496.
- Oberoi RK, Mittapalli RK, and Elmquist WF (2013) Pharmacokinetic assessment of efflux transport in sunitinib distribution to the brain. *J Pharmacol Exp Ther* **347**:755-764.
- Ohgaki H and Kleihues P (2007) Genetic pathways to primary and secondary glioblastoma. *Am J Pathol* **170**:1445-1453.
- Oldendorf WH (1974) Lipid solubility and drug penetration of the blood brain barrier. *Proc Soc Exp Biol Med* **147**:813-815.

- Olson EM, Abdel-Rasoul M, Maly J, Wu CS, Lin NU, and Shapiro CL (2013) Incidence and risk of central nervous system metastases as site of first recurrence in patients with HER2-positive breast cancer treated with adjuvant trastuzumab. *Ann Oncol* **24**:1526-1533.
- On NH, Mitchell R, Savant SD, Bachmeier CJ, Hatch GM, and Miller DW (2013) Examination of blood-brain barrier (BBB) integrity in a mouse brain tumor model. *J Neurooncol* **111**:133-143.
- Osswald M, Blaes J, Liao Y, Solecki G, Gommel M, Berghoff AS, Salphati L, Wallin JJ, Phillips HS, Wick W, and Winkler F (2016) Impact of Blood-Brain Barrier Integrity on Tumor Growth and Therapy Response in Brain Metastases. *Clin Cancer Res* **22**:6078-6087.
- Pafundi DH, Laack NN, Youland RS, Parney IF, Lowe VJ, Giannini C, Kemp BJ, Grams MP, Morris JM, Hoover JM, Hu LS, Sarkaria JN, and Brinkmann DH (2013) Biopsy validation of 18F-DOPA PET and biodistribution in gliomas for neurosurgical planning and radiotherapy target delineation: results of a prospective pilot study. *Neuro Oncol* **15**:1058-1067.
- Palmieri D, Lockman PR, Thomas FC, Hua E, Herring J, Hargrave E, Johnson M, Flores N, Qian Y, Vega-Valle E, Taskar KS, Rudraraju V, Mittapalli RK, Gaasch JA, Bohn KA, Thorsheim HR, Liewehr DJ, Davis S, Reilly JF, Walker R, Bronder JL, Feigenbaum L, Steinberg SM, Camphausen K, Meltzer PS, Richon VM, Smith QR, and Steeg PS (2009) Vorinostat inhibits brain metastatic colonization in a model of triple-negative breast cancer and induces DNA double-strand breaks. *Clin Cancer Res* **15**:6148-6157.
- Pang KS, Maeng HJ, and Fan J (2009) Interplay of transporters and enzymes in drug and metabolite processing. *Mol Pharm* **6**:1734-1755.
- Parrish KE, Cen L, Murray J, Calligaris D, Kizilbash S, Mittapalli RK, Carlson BL, Schroeder MA, Sludden J, Boddy AV, Agar NY, Curtin NJ, Elmquist WF, and Sarkaria JN (2015a) Efficacy of PARP Inhibitor Rucaparib in Orthotopic Glioblastoma Xenografts Is Limited by Ineffective Drug Penetration into the Central Nervous System. *Mol Cancer Ther* **14**:2735-2743.
- Parrish KE, Pokorny J, Mittapalli RK, Bakken K, Sarkaria JN, and Elmquist WF (2015b) Efflux transporters at the blood-brain barrier limit delivery and efficacy of cyclin-dependent kinase 4/6 inhibitor palbociclib (PD-0332991) in an orthotopic brain tumor model. *J Pharmacol Exp Ther* **355**:264-271.
- Parrish KE, Sarkaria JN, and Elmquist WF (2015c) Improving drug delivery to primary and metastatic brain tumors: strategies to overcome the blood-brain barrier. *Clin Pharmacol Ther* **97**:336-346.
- Patchell RA, Tibbs PA, Walsh JW, Dempsey RJ, Maruyama Y, Kryscio RJ, Markesbery WR, Macdonald JS, and Young B (1990) A randomized trial of surgery in the treatment of single metastases to the brain. *N Engl J Med* **322**:494-500.
- Patel BG, Ahmed KA, Johnstone PA, Yu HH, and Etame AB (2016) Initial experience with combined BRAF and MEK inhibition with stereotactic radiosurgery for BRAF mutant melanoma brain metastases. *Melanoma Res* **26**:382-386.
- Planchard D, Besse B, Groen HJ, Souquet PJ, Quoix E, Baik CS, Barlesi F, Kim TM, Mazieres J, Novello S, Rigas JR, Upalawanna A, D'Amelio AM, Jr., Zhang P, Mookerjee B, and Johnson BE (2016) Dabrafenib plus trametinib in patients with previously treated BRAF(V600E)-mutant metastatic non-small cell lung cancer: an open-label, multicentre phase 2 trial. *Lancet Oncol* **17**:984-993.

- Pokorny JL, Calligaris D, Gupta SK, Iyekegbe DO, Jr., Mueller D, Bakken KK, Carlson BL, Schroeder MA, Evans DL, Lou Z, Decker PA, Eckel-Passow JE, Pucci V, Ma B, Shumway SD, Elmquist WF, Agar NY, and Sarkaria JN (2015) The Efficacy of the Wee1 Inhibitor MK-1775 Combined with Temozolomide Is Limited by Heterogeneous Distribution across the Blood-Brain Barrier in Glioblastoma. *Clin Cancer Res* **21**:1916-1924.
- Poller B, Iusuf D, Sparidans RW, Wagenaar E, Beijnen JH, and Schinkel AH (2011) Differential impact of P-glycoprotein (ABCB1) and breast cancer resistance protein (ABCG2) on axitinib brain accumulation and oral plasma pharmacokinetics. *Drug Metab Dispos* **39**:729-735.
- Polli JW, Humphreys JE, Harmon KA, Castellino S, O'Mara MJ, Olson KL, John-Williams LS, Koch KM, and Serabjit-Singh CJ (2008) The role of efflux and uptake transporters in [N-(3-chloro-4-[(3-fluorobenzyl)oxy]phenyl)-6-[5-[[2-(methylsulfonyl)ethyl]amino]methyl]-2-furyl]-4-quinazolinamine (GW572016, lapatinib) disposition and drug interactions. *Drug Metab Dispos* **36**:695-701.
- Porta R, Sanchez-Torres JM, Paz-Ares L, Massuti B, Reguart N, Mayo C, Lianes P, Queralt C, Guillem V, Salinas P, Catot S, Isla D, Pradas A, Gurrpide A, de Castro J, Polo E, Puig T, Taron M, Colomer R, and Rosell R (2011) Brain metastases from lung cancer responding to erlotinib: the importance of EGFR mutation. *Eur Respir J* **37**:624-631.
- Preusser M, Capper D, Ilhan-Mutlu A, Berghoff AS, Birner P, Bartsch R, Marosi C, Zielinski C, Mehta MP, Winkler F, Wick W, and von Deimling A (2012) Brain metastases: pathobiology and emerging targeted therapies. *Acta Neuropathol* **123**:205-222.
- Proescholdt MA, Heiss JD, Walbridge S, Muhlhauser J, Capogrossi MC, Oldfield EH, and Merrill MJ (1999) Vascular endothelial growth factor (VEGF) modulates vascular permeability and inflammation in rat brain. *J Neuropathol Exp Neurol* **58**:613-627.
- Queirolo P, Spagnolo F, Ascierto PA, Simeone E, Marchetti P, Scoppola A, Del Vecchio M, Di Guardo L, Maio M, Di Giacomo AM, Antonuzzo A, Cognetti F, Ferraresi V, Ridolfi L, Guidoboni M, Guida M, Pigozzo J, and Chiarion Sileni V (2014) Efficacy and safety of ipilimumab in patients with advanced melanoma and brain metastases. *J Neurooncol* **118**:109-116.
- Radbruch A, Weberling LD, Kieslich PJ, Eidel O, Burth S, Kickingereeder P, Heiland S, Wick W, Schlemmer HP, and Bendszus M (2015) Gadolinium retention in the dentate nucleus and globus pallidus is dependent on the class of contrast agent. *Radiology* **275**:783-791.
- Raizer JJ, Abrey LE, Lassman AB, Chang SM, Lamborn KR, Kuhn JG, Yung WK, Gilbert MR, Aldape KD, Wen PY, Fine HA, Mehta M, Deangelis LM, Lieberman F, Cloughesy TF, Robins HI, Dancey J, Prados MD, and North American Brain Tumor C (2010) A phase I trial of erlotinib in patients with nonprogressive glioblastoma multiforme postirradiation therapy, and recurrent malignant gliomas and meningiomas. *Neuro Oncol* **12**:87-94.
- Ramalho J, Castillo M, AlObaidy M, Nunes RH, Ramalho M, Dale BM, and Semelka RC (2015) High Signal Intensity in Globus Pallidus and Dentate Nucleus on Unenhanced T1-weighted MR Images: Evaluation of Two Linear Gadolinium-based Contrast Agents. *Radiology* **276**:836-844.
- Rangachari D, Yamaguchi N, VanderLaan PA, Folch E, Mahadevan A, Floyd SR, Uhlmann EJ, Wong ET, Dahlberg SE, Huberman MS, and Costa DB (2015) Brain metastases in patients with EGFR-mutated or ALK-rearranged non-small-cell lung cancers. *Lung Cancer* **88**:108-111.

- Rankovic Z (2015) CNS drug design: balancing physicochemical properties for optimal brain exposure. *J Med Chem* **58**:2584-2608.
- Reardon DA, Conrad CA, Cloughesy T, Prados MD, Friedman HS, Aldape KD, Mischel P, Xia J, DiLea C, Huang J, Mietlowski W, Dugan M, Chen W, and Yung WK (2012) Phase I study of AEE788, a novel multitarget inhibitor of ErbB- and VEGF-receptor-family tyrosine kinases, in recurrent glioblastoma patients. *Cancer Chemother Pharmacol* **69**:1507-1518.
- Reardon DA, Nabors LB, Mason WP, Perry JR, Shapiro W, Kavan P, Mathieu D, Phuphanich S, Cseh A, Fu Y, Cong J, Wind S, Eisenstat DD, Group BIT, and the Canadian Brain Tumour C (2015) Phase I/randomized phase II study of afatinib, an irreversible ErbB family blocker, with or without protracted temozolomide in adults with recurrent glioblastoma. *Neuro Oncol* **17**:430-439.
- Renner DN, Jin F, Litterman AJ, Balgeman AJ, Hanson LM, Gamez JD, Chae M, Carlson BL, Sarkaria JN, Parney IF, Ohlfest JR, Pirko I, Pavelko KD, and Johnson AJ (2015) Effective Treatment of Established GL261 Murine Gliomas through Picornavirus Vaccination-Enhanced Tumor Antigen-Specific CD8+ T Cell Responses. *PLoS One* **10**:e0125565.
- Renner DN, Malo CS, Jin F, Parney IF, Pavelko KD, and Johnson AJ (2016) Improved Treatment Efficacy of Antiangiogenic Therapy when Combined with Picornavirus Vaccination in the GL261 Glioma Model. *Neurotherapeutics* **13**:226-236.
- Reungwetwattana T, Weroha SJ, and Molina JR (2012) Oncogenic pathways, molecularly targeted therapies, and highlighted clinical trials in non-small-cell lung cancer (NSCLC). *Clin Lung Cancer* **13**:252-266.
- Rich JN, Reardon DA, Peery T, Dowell JM, Quinn JA, Penne KL, Wikstrand CJ, Van Duyn LB, Dancey JE, McLendon RE, Kao JC, Stenzel TT, Ahmed Rasheed BK, Tourt-Uhlig SE, Herndon JE, 2nd, Vredenburgh JJ, Sampson JH, Friedman AH, Bigner DD, and Friedman HS (2004) Phase II trial of gefitinib in recurrent glioblastoma. *J Clin Oncol* **22**:133-142.
- Robert P, Lehericy S, Grand S, Violas X, Fretellier N, Idee JM, Ballet S, and Corot C (2015) T1-Weighted Hypersignal in the Deep Cerebellar Nuclei After Repeated Administrations of Gadolinium-Based Contrast Agents in Healthy Rats: Difference Between Linear and Macrocyclic Agents. *Invest Radiol* **50**:473-480.
- Roberto M, Bassanelli M, Iannicelli E, Giacinti S, D'Antonio C, Aschelter AM, and Marchetti P (2015) Clinical Outcome of Third-Line Pazopanib in a Patient with Metastatic Renal Cell Carcinoma. *Case Rep Oncol Med* **2015**:629046.
- Rochet NM, Kottschade LA, and Markovic SN (2011) Vemurafenib for melanoma metastases to the brain. *N Engl J Med* **365**:2439-2441.
- Rodig SJ, Mino-Kenudson M, Dacic S, Yeap BY, Shaw A, Barletta JA, Stubbs H, Law K, Lindeman N, Mark E, Janne PA, Lynch T, Johnson BE, Iafrate AJ, and Chirieac LR (2009) Unique clinicopathologic features characterize ALK-rearranged lung adenocarcinoma in the western population. *Clin Cancer Res* **15**:5216-5223.
- Rosell R, Gettinger SN, Bazhenova LA, Langer CJ, Salgia R, Shaw AT, Narasimhan NI, Dorer DJ, Kerstein D, and Camidge DR (2016) 1330: Brigatinib efficacy and safety in patients (Pts) with anaplastic lymphoma kinase (ALK)-positive (ALK+) non-small cell lung cancer (NSCLC) in a phase 1/2 trial. *J Thorac Oncol* **11**:S114.
- Rostami R, Mittal S, Rostami P, Tavassoli F, and Jabbari B (2016) Brain metastasis in breast cancer: a comprehensive literature review. *J Neurooncol* **127**:407-414.

- Sacher AG, Janne PA, and Oxnard GR (2014) Management of acquired resistance to epidermal growth factor receptor kinase inhibitors in patients with advanced non-small cell lung cancer. *Cancer* **120**:2289-2298.
- Sakji-Dupre L, Le Rhun E, Templier C, Desmedt E, Blanchet B, and Mortier L (2015) Cerebrospinal fluid concentrations of vemurafenib in patients treated for brain metastatic BRAF-V600 mutated melanoma. *Melanoma Res* **25**:302-305.
- Salphati L, Shahidi-Latham S, Quiason C, Barck K, Nishimura M, Alicke B, Pang J, Carano RA, Olivero AG, and Phillips HS (2014) Distribution of the phosphatidylinositol 3-kinase inhibitors Pictilisib (GDC-0941) and GNE-317 in U87 and GS2 intracranial glioblastoma models-assessment by matrix-assisted laser desorption ionization imaging. *Drug Metab Dispos* **42**:1110-1116.
- Sampson JH, Carter JH, Jr., Friedman AH, and Seigler HF (1998) Demographics, prognosis, and therapy in 702 patients with brain metastases from malignant melanoma. *J Neurosurg* **88**:11-20.
- Sandler A, Gordon M, De Alwis DP, Pouliquen I, Green L, Marder P, Chaudhary A, Fife K, Battiato L, Sweeney C, Jordan C, Burgess M, and Slapak CA (2004) A Phase I trial of a potent P-glycoprotein inhibitor, zosuquidar trihydrochloride (LY335979), administered intravenously in combination with doxorubicin in patients with advanced malignancy. *Clin Cancer Res* **10**:3265-3272.
- Sane R, Mittapalli RK, and Elmquist WF (2013) Development and evaluation of a novel microemulsion formulation of elacridar to improve its bioavailability. *J Pharm Sci* **102**:1343-1354.
- Sane R, Wu SP, Zhang R, and Gallo JM (2014) The effect of ABCG2 and ABCC4 on the pharmacokinetics of methotrexate in the brain. *Drug Metab Dispos* **42**:537-540.
- Sarkaria JN, Hu LS, Parney IF, Pafundi DH, Brinkmann DH, Laack NN, Giannini C, Burns TC, Kizilbash SH, Laramy JK, Swanson KR, Kaufmann TJ, Brown PD, Agar NYR, Galanis E, Buckner JC, and Elmquist WF (2018) Is the blood-brain barrier really disrupted in all glioblastomas? A critical assessment of existing clinical data. *Neuro Oncol* **20**:184-191.
- Schinkel AH, Smit JJ, van Tellingen O, Beijnen JH, Wagenaar E, van Deemter L, Mol CA, van der Valk MA, Robanus-Maandag EC, te Riele HP, and et al. (1994) Disruption of the mouse *mdr1a* P-glycoprotein gene leads to a deficiency in the blood-brain barrier and to increased sensitivity to drugs. *Cell* **77**:491-502.
- Schinkel AH, Wagenaar E, Mol CA, and van Deemter L (1996) P-glycoprotein in the blood-brain barrier of mice influences the brain penetration and pharmacological activity of many drugs. *J Clin Invest* **97**:2517-2524.
- Schouten LJ, Rutten J, Huvneers HAM, and Twijnstra A (2002) Incidence of brain metastases in a cohort of patients with carcinoma of the breast, colon, kidney, and lung and melanoma. *Cancer* **94**:2698-2705.
- Scott AM, Wolchok JD, and Old LJ (2012) Antibody therapy of cancer. *Nat Rev Cancer* **12**:278-287.
- Seshacharyulu P, Ponnusamy MP, Haridas D, Jain M, Ganti AK, and Batra SK (2012) Targeting the EGFR signaling pathway in cancer therapy. *Expert Opin Ther Targets* **16**:15-31.

- Shen DD, Artru AA, and Adkison KK (2004) Principles and applicability of CSF sampling for the assessment of CNS drug delivery and pharmacodynamics. *Adv Drug Deliv Rev* **56**:1825-1857.
- Shi S and Li Y (2014) Interplay of Drug-Metabolizing Enzymes and Transporters in Drug Absorption and Disposition. *Curr Drug Metab* **15**:915-941.
- Shi W and Dicker AP (2016) CNS Metastases in Patients With Non-Small-Cell Lung Cancer and ALK Gene Rearrangement. *J Clin Oncol* **34**:107-109.
- Shinojima N, Tada K, Shiraishi S, Kamiryo T, Kochi M, Nakamura H, Makino K, Saya H, Hirano H, Kuratsu J, Oka K, Ishimaru Y, and Ushio Y (2003) Prognostic value of epidermal growth factor receptor in patients with glioblastoma multiforme. *Cancer Res* **63**:6962-6970.
- Siegel RL, Miller KD, and Jemal A (2016) Cancer statistics, 2016. *CA Cancer J Clin* **66**:7-30.
- Sloan AE, Nock CJ, and Einstein DB (2009) Diagnosis and treatment of melanoma brain metastasis: a literature review. *Cancer Control* **16**:248-255.
- Solca F, Dahl G, Zoephel A, Bader G, Sanderson M, Klein C, Kraemer O, Himmelsbach F, Haakma E, and Adolf GR (2012) Target binding properties and cellular activity of afatinib (BIBW 2992), an irreversible ErbB family blocker. *J Pharmacol Exp Ther* **343**:342-350.
- Solomon BJ, Mok T, Kim DW, Wu YL, Nakagawa K, Mekhail T, Felip E, Cappuzzo F, Paolini J, Usari T, Iyer S, Reisman A, Wilner KD, Tursi J, Blackhall F, and Investigators P (2014) First-line crizotinib versus chemotherapy in ALK-positive lung cancer. *N Engl J Med* **371**:2167-2177.
- Sperduto PW, Kased N, Roberge D, Xu Z, Shanley R, Luo X, Sneed PK, Chao ST, Weil RJ, Suh J, Bhatt A, Jensen AW, Brown PD, Shih HA, Kirkpatrick J, Gaspar LE, Fiveash JB, Chiang V, Knisely JP, Sperduto CM, Lin N, and Mehta M (2012) Summary report on the graded prognostic assessment: an accurate and facile diagnosis-specific tool to estimate survival for patients with brain metastases. *J Clin Oncol* **30**:419-425.
- Steeg PS, Camphausen KA, and Smith QR (2011) Brain metastases as preventive and therapeutic targets. *Nat Rev Cancer* **11**:352-363.
- Stemmler HJ, Schmitt M, Willems A, Bernhard H, Harbeck N, and Heinemann V (2007) Ratio of trastuzumab levels in serum and cerebrospinal fluid is altered in HER2-positive breast cancer patients with brain metastases and impairment of blood-brain barrier. *Anticancer Drugs* **18**:23-28.
- Summerfield SG, Read K, Begley DJ, Obradovic T, Hidalgo IJ, Coggon S, Lewis AV, Porter RA, and Jeffrey P (2007) Central nervous system drug disposition: the relationship between in situ brain permeability and brain free fraction. *J Pharmacol Exp Ther* **322**:205-213.
- Sun H, Miller DW, and Elmquist WF (2001) Effect of probenecid on fluorescein transport in the central nervous system using in vitro and in vivo models. *Pharm Res* **18**:1542-1549.
- Sweeney MD, Ayyadurai S, and Zlokovic BV (2016) Pericytes of the neurovascular unit: key functions and signaling pathways. *Nat Neurosci* **19**:771-783.
- Tang SC, Nguyen LN, Sparidans RW, Wagenaar E, Beijnen JH, and Schinkel AH (2014) Increased oral availability and brain accumulation of the ALK inhibitor crizotinib by coadministration of the P-glycoprotein (ABCB1) and breast cancer resistance protein (ABCG2) inhibitor elacridar. *Int J Cancer* **134**:1484-1494.
- Taskar KS, Rudraraju V, Mittapalli RK, Samala R, Thorsheim HR, Lockman J, Gril B, Hua E, Palmieri D, Polli JW, Castellino S, Rubin SD, Lockman PR, Steeg PS, and Smith QR (2012) Lapatinib

- distribution in HER2 overexpressing experimental brain metastases of breast cancer. *Pharm Res* **29**:770-781.
- Textor A, Listopad JJ, Wuhrmann LL, Perez C, Kruschinski A, Chmielewski M, Abken H, Blankenstein T, and Charo J (2014) Efficacy of CAR T-cell therapy in large tumors relies upon stromal targeting by IFN $\gamma$ . *Cancer Res* **74**:6796-6805.
- Thakkar JP, Dolecek TA, Horbinski C, Ostrom QT, Lightner DD, Barnholtz-Sloan JS, and Villano JL (2014) Epidemiologic and molecular prognostic review of glioblastoma. *Cancer Epidemiol Biomarkers Prev* **23**:1985-1996.
- Thorne N, Inglese J, and Auld DS (2010) Illuminating insights into firefly luciferase and other bioluminescent reporters used in chemical biology. *Chem Biol* **17**:646-657.
- Tietz S and Engelhardt B (2015) Brain barriers: Crosstalk between complex tight junctions and adherens junctions. *J Cell Biol* **209**:493-506.
- Togashi Y, Masago K, Fukudo M, Terada T, Fujita S, Irida K, Sakamori Y, Kim YH, Mio T, Inui K, and Mishima M (2010) Cerebrospinal fluid concentration of erlotinib and its active metabolite OSI-420 in patients with central nervous system metastases of non-small cell lung cancer. *J Thorac Oncol* **5**:950-955.
- Trainor GL (2007) The importance of plasma protein binding in drug discovery. *Expert Opin Drug Discov* **2**:51-64.
- Uchida Y, Ohtsuki S, Katsukura Y, Ikeda C, Suzuki T, Kamiie J, and Terasaki T (2011) Quantitative targeted absolute proteomics of human blood-brain barrier transporters and receptors. *J Neurochem* **117**:333-345.
- Vaidhyanathan S, Mittapalli RK, Sarkaria JN, and Elmquist WF (2014) Factors influencing the CNS distribution of a novel MEK-1/2 inhibitor: implications for combination therapy for melanoma brain metastases. *Drug Metab Dispos* **42**:1292-1300.
- van den Bent MJ, Brandes AA, Rampling R, Kouwenhoven MC, Kros JM, Carpentier AF, Clement PM, Frenay M, Campone M, Baurain JF, Armand JP, Taphoorn MJ, Tosoni A, Kletzl H, Klughammer B, Lacombe D, and Gorlia T (2009) Randomized phase II trial of erlotinib versus temozolomide or carmustine in recurrent glioblastoma: EORTC brain tumor group study 26034. *J Clin Oncol* **27**:1268-1274.
- van Hoppe S, Sparidans RW, Wagenaar E, Beijnen JH, and Schinkel AH (2017) Breast cancer resistance protein (BCRP/ABCG2) and P-glycoprotein (P-gp/ABCB1) transport afatinib and restrict its oral availability and brain accumulation. *Pharmacol Res* **120**:43-50.
- Vassileva V, Moriyama EH, De Souza R, Grant J, Allen CJ, Wilson BC, and Piquette-Miller M (2008) Efficacy assessment of sustained intraperitoneal paclitaxel therapy in a murine model of ovarian cancer using bioluminescent imaging. *Br J Cancer* **99**:2037-2043.
- Verreault M, Schmitt C, Goldwirt L, Pelton K, Haidar S, Levasseur C, Guehenne C, Knoff D, Labussiere M, Marie Y, Ligon AH, Mokhtari K, Hoang-Xuan K, Sanson M, Alexander BM, Wen PY, Delattre JY, Ligon KL, and Idubai A (2015) Preclinical Efficacy of the MDM2 Inhibitor RG7112 in MDM2-Amplified and TP53 Wild-type Glioblastomas. *Clin Cancer Res*.
- Villalonga-Planells R, Coll-Mulet L, Martinez-Soler F, Castano E, Acebes JJ, Gimenez-Bonafe P, Gil J, and Tortosa A (2011) Activation of p53 by nutlin-3a induces apoptosis and cellular senescence in human glioblastoma multiforme. *PLoS One* **6**:e18588.



- Vitucci M, Hayes DN, and Miller CR (2011) Gene expression profiling of gliomas: merging genomic and histopathological classification for personalised therapy. *Br J Cancer* **104**:545-553.
- Vogelstein B, Lane D, and Levine AJ (2000) Surfing the p53 network. *Nature* **408**:307-310.
- Wade M, Li YC, and Wahl GM (2013) MDM2, MDMX and p53 in oncogenesis and cancer therapy. *Nat Rev Cancer* **13**:83-96.
- Wager TT, Hou X, Verhoest PR, and Villalobos A (2010) Moving beyond rules: the development of a central nervous system multiparameter optimization (CNS MPO) approach to enable alignment of druglike properties. *ACS Chem Neurosci* **1**:435-449.
- Wager TT, Hou X, Verhoest PR, and Villalobos A (2016) Central Nervous System Multiparameter Optimization Desirability: Application in Drug Discovery. *ACS Chem Neurosci* **7**:767-775.
- Wang S, Sun W, Zhao Y, McEachern D, Meaux I, Barriere C, Stuckey JA, Meagher JL, Bai L, Liu L, Hoffman-Luca CG, Lu J, Shangary S, Yu S, Bernard D, Aguilar A, Dos-Santos O, Besret L, Guerif S, Pannier P, Gorge-Bernat D, and Debussche L (2014) SAR405838: an optimized inhibitor of MDM2-p53 interaction that induces complete and durable tumor regression. *Cancer Res* **74**:5855-5865.
- Waters NJ, Jones R, Williams G, and Sohal B (2008) Validation of a rapid equilibrium dialysis approach for the measurement of plasma protein binding. *J Pharm Sci* **97**:4586-4595.
- Weathers SP and de Groot J (2015) VEGF Manipulation in Glioblastoma. *Oncology (Williston Park)* **29**:720-727.
- Weber B, Winterdahl M, Memon A, Sorensen BS, Keiding S, Sorensen L, Nexø E, and Meldgaard P (2011) Erlotinib accumulation in brain metastases from non-small cell lung cancer: visualization by positron emission tomography in a patient harboring a mutation in the epidermal growth factor receptor. *J Thorac Oncol* **6**:1287-1289.
- Weberling LD, Kieslich PJ, Kickingereider P, Wick W, Bendszus M, Schlemmer HP, and Radbruch A (2015) Increased Signal Intensity in the Dentate Nucleus on Unenhanced T1-Weighted Images After Gadobenate Dimeglumine Administration. *Invest Radiol* **50**:743-748.
- Weil RJ, Palmieri DC, Bronder JL, Stark AM, and Steeg PS (2005) Breast cancer metastasis to the central nervous system. *Am J Pathol* **167**:913-920.
- Weissleder R and Ntziachristos V (2003) Shedding light onto live molecular targets. *Nat Med* **9**:123-128.
- Westerhout J, Smeets J, Danhof M, and de Lange EC (2013) The impact of P-gp functionality on non-steady state relationships between CSF and brain extracellular fluid. *J Pharmacokinet Pharmacodyn* **40**:327-342.
- Wind S, Giessmann T, Jungnik A, Brand T, Marzin K, Bertulis J, Hocke J, Gansser D, and Stopfer P (2014) Pharmacokinetic drug interactions of afatinib with rifampicin and ritonavir. *Clin Drug Investig* **34**:173-182.
- Wong DW, Leung EL, So KK, Tam IY, Sihoe AD, Cheng LC, Ho KK, Au JS, Chung LP, Pik Wong M, and University of Hong Kong Lung Cancer Study G (2009) The EML4-ALK fusion gene is involved in various histologic types of lung cancers from nonsmokers with wild-type EGFR and KRAS. *Cancer* **115**:1723-1733.
- Xi G, Rajaram V, Mania-Farnell B, Mayanil CS, Soares MB, Tomita T, and Goldman S (2012) Efficacy of vincristine administered via convection-enhanced delivery in a rodent

- brainstem tumor model documented by bioluminescence imaging. *Childs Nerv Syst* **28**:565-574.
- Xiong S, Xue M, Mu Y, Deng Z, Sun P, and Zhou R (2017) Determination of AZD3759 in rat plasma and brain tissue by LC-MS/MS and its application in pharmacokinetic and brain distribution studies. *J Pharm Biomed Anal* **140**:362-366.
- Yang Z, Guo Q, Wang Y, Chen K, Zhang L, Cheng Z, Xu Y, Yin X, Bai Y, Rabbie S, Kim DW, Ahn MJ, Yang JC, and Zhang X (2016) AZD3759, a BBB-penetrating EGFR inhibitor for the treatment of EGFR mutant NSCLC with CNS metastases. *Sci Transl Med* **8**:368ra172.
- Yap KY, Chui WK, and Chan A (2008) Drug interactions between chemotherapeutic regimens and antiepileptics. *Clin Ther* **30**:1385-1407.
- Yee S (1997) In vitro permeability across Caco-2 cells (colonic) can predict in vivo (small intestinal) absorption in man--fact or myth. *Pharm Res* **14**:763-766.
- Yung WK, Vredenburgh JJ, Cloughesy TF, Nghiemphu P, Klencke B, Gilbert MR, Reardon DA, and Prados MD (2010) Safety and efficacy of erlotinib in first-relapse glioblastoma: a phase II open-label study. *Neuro Oncol* **12**:1061-1070.
- Zakrzewski J, Geraghty LN, Rose AE, Christos PJ, Mazumdar M, Polsky D, Shapiro R, Berman R, Darvishian F, Hernando E, Pavlick A, and Osman I (2011) Clinical variables and primary tumor characteristics predictive of the development of melanoma brain metastases and post-brain metastases survival. *Cancer* **117**:1711-1720.
- Zeamari S, Rumping G, Floot B, Lyons S, and Stewart FA (2004) In vivo bioluminescence imaging of locally disseminated colon carcinoma in rats. *Br J Cancer* **90**:1259-1264.
- Zeng Q, Wang J, Cheng Z, Chen K, Johnstrom P, Varnas K, Li DY, Yang ZF, and Zhang X (2015) Discovery and Evaluation of Clinical Candidate AZD3759, a Potent, Oral Active, Central Nervous System-Penetrant, Epidermal Growth Factor Receptor Tyrosine Kinase Inhibitor. *J Med Chem* **58**:8200-8215.
- Zhang C, Liu J, Tan C, Yue X, Zhao Y, Peng J, Wang X, Laddha SV, Chan CS, Zheng S, Hu W, and Feng Z (2016) microRNA-1827 represses MDM2 to positively regulate tumor suppressor p53 and suppress tumorigenesis. *Oncotarget*.
- Zhang W, Jiang W, Luan L, Wang L, Zheng X, and Wang G (2014) Prophylactic cranial irradiation for patients with small-cell lung cancer: a systematic review of the literature with meta-analysis. *BMC Cancer* **14**:793.
- Zhang Y, Bressler JP, Neal J, Lal B, Bhang HE, Laterra J, and Pomper MG (2007) ABCG2/BCRP expression modulates D-Luciferin based bioluminescence imaging. *Cancer Res* **67**:9389-9397.
- Zhuang Y, Fraga CH, Hubbard KE, Hagedorn N, Panetta JC, Waters CM, and Stewart CF (2006) Topotecan central nervous system penetration is altered by a tyrosine kinase inhibitor. *Cancer Res* **66**:11305-11313.